

IMAGING DETECTORS FOR X-RAY ASTRONOMY.

A thesis submitted to the University of Leicester
by Richard Gott, B.Sc. for the Degree of Doctor of
Philosophy. 1970.

"The brilliant stars are the beauty of the sky,
a glittering array in the heights of the Lord."

Ecclesiasticus 43, 9.

UMI Number: U376678

All rights reserved

INFORMATION TO ALL USERS

The quality of this reproduction is dependent upon the quality of the copy submitted.

In the unlikely event that the author did not send a complete manuscript and there are missing pages, these will be noted. Also, if material had to be removed, a note will indicate the deletion.



UMI U376678

Published by ProQuest LLC 2015. Copyright in the Dissertation held by the Author.
Microform Edition © ProQuest LLC.

All rights reserved. This work is protected against
unauthorized copying under Title 17, United States Code.



ProQuest LLC
789 East Eisenhower Parkway
P.O. Box 1346
Ann Arbor, MI 48106-1346

X753044268

THESIS

387369

9.11.71

DECLARATION.

I declare that this thesis is my own work and is based on investigations carried out by myself at the University of Leicester, except where otherwise stated. This work has not been presented as a thesis to any other university.

Richard Gott.

ACKNOWLEDGEMENTS.

This work has been carried out as part of the research programme of the X-ray Astronomy Group in the Department of Physics. I would like to record my thanks to the group for their financial and technical support.

Special thanks go to my supervisor Dr.K.A.Pounds, to Dr.A.F.Janes for his continued help and interest, to Mr.J.Spragg for his technical support, and to Mr. W.Parkes for his invaluable assistance during the later stages of the work.

The work was carried out with the support of a Science Research Council Studentship.

I would also like to thank my wife and family for their support and encouragement over the past three years and for their help in the production stages of this thesis.

ABSTRACT.

This work is concerned with the development of imaging detectors and was undertaken as part of a laboratory investigation into requirements for future experiments by the X-ray astronomy group of this university in its programme of study of solar and non-solar X-ray emission. Much of the work is concerned with the establishment of the operating characteristics of a new detector, the channel multiplier array, and its use as an imaging device.

As a result of the investigations, new methods of one and two dimensional image dissection have been developed giving a spatial resolution comparable to that of photographic film. Together with recent advances in X-ray imaging optics, these methods are of considerable interest in the rapidly expanding field of X-ray astronomy.

In addition to work on channel arrays, a brief account is given of a spectroheliograph which is operating successfully on the 5th Orbiting Solar Observatory and which has been designed by Leicester University and University College, London.

CONTENTS.

Page no.

Declaration.

Acknowledgements.

Abstract.

Chapter 1. X-ray astronomy.

1.1	Introduction.	1.1
1.2	The detection and location of sources.	1.2
1.3	Energy spectra of known sources.	1.9
1.4	The diffuse X-ray background.	1.12
1.5	Solar X-ray studies.	1.14
1.6	A summary of future detector requirements.	1.20

Chapter 2. Position sensitive particle and photon detectors.

2.1	Introduction.	2.1
2.2	The photographic method.	2.1
2.3	Gaseous ionisation methods.	2.3
2.4	Scintillation detectors.	2.11
2.5	Semiconductor detectors.	2.12
2.6	Photo-electric detectors.	2.16
2.7	Electro-imaging detectors.	2.17

Chapter 3. Experimental techniques and apparatus.

3.1	Introduction.	3.1
3.2	The plane crystal spectrometer.	3.1
3.3	The collimated X-ray source.	3.6
3.4	The ultra-high vacuum system.	3.9

Page no.

3.5	The electronics.	3.9
3.6	General experimental techniques.	3.12

Chapter 4. The operating characteristics of channel multiplier arrays.

4.1	Introduction.	4.1
4.2	The detector mounts.	4.3
4.3	The pulse height distributions of the arrays.	4.5
4.4	The detection efficiency of array B.	4.9
4.5	The uniformity of response across array B.	4.11
4.6	Lifetests of array A in high vacuum conditions.	4.14
4.7	Further work.	4.16

Chapter 5. The use of the channel multiplier array as an imaging detector.

5.1	Introduction.	5.1
5.2	One dimensional imaging.	5.1
5.3	The extension of the method to two dimensions.	5.15
5.4	A comparison with other imaging detectors.	5.18
5.5	Further work.	5.23

Chapter 6. The Leicester experiment on the OSO-5
satellite.

6.1	Introduction.	6.1
6.2	The proportional counters.	6.2
6.3	Some results.	6.7

Appendix.

References.

CHAPTER 1. X-RAY ASTRONOMY.

1.1 Introduction.

X-ray astronomy is the study of the radiation in the energy range $0.1 \frac{\text{K}\cdot\text{V}}{\text{\AA}}$ to 1 Mev. originating in and beyond the solar system. Contrary to the accepted practice in the laboratory of classifying radiation into X and γ according to its origin, the distinction between X and γ -ray astronomy is one of photon energy, the dividing line being drawn usually at 1 Mev.

X-ray astronomy originated in 1948 with the discovery of solar X-radiation above the earth's atmosphere.* In 1962 the first cosmic X-ray source was discovered and since then the sensitivity of instruments has increased considerably and with it the number of reported sources .

Owing to the opacity of the earth's atmosphere to wavelengths below about 3000 \AA , observations have to be made from a suitable platform above the atmosphere. The height at which this platform must be for adequate transmission of X-rays through the remaining material is dependent on energy. For photon energies greater than about 15 kev. a balloon will reach a sufficient altitude but below this, sounding rockets or satellites are necessary. Recently the use of the moon as a laboratory has become feasible, but will probably not be exploited for astronomy for some years, however, due to the low priority placed on scientific experiments in the Apollo programme.

* See chapter 2 for references and details of exper's.

This chapter is devoted to a review of the present state of X-ray astronomy and to a consideration of future requirements in the field of detectors. The following three sections are concerned with cosmic X-ray astronomy while the final section deals with the more sophisticated instrumentation used for the special case of the sun.

Frequent reference has been made to review papers by Friedman (1969), Sciama (1969), Pounds (1969) and Boyd (1969).

1.2 The detection and location of sources.

The most widely used method for the detection of new sources is the unstabilised sounding rocket. The detector is allowed to randomly scan the sky, and examination of the count rate profile, together with an aspect determination obtained using rigid body dynamics leads to approximate positioning of the sources.

After the initial sky surveys, stabilised rockets have been used in which the detector scans a limited region of the sky in which sources are either known or expected to be found.

To put the energy spectra of the sources into context, an optical identification is of paramount importance and this has led to a third class of experiment. Once the source has been approximately located, experiments on stabilised rockets can then be specifically designed for accurate location of the source.

Greatly increased stability and pointing accuracy

has been achieved using sun pointing and star pointing rockets. The attitude control system of the rocket allows an initial stabilisation using magnetometers after which photocells are used to view either the sun or a bright star and give a platform stable to better than thirty arc seconds. Satellites have not been used extensively in cosmic X-ray astronomy experiments due principally to the long period between the design and flight of an experiment.

1.2.1 Detection.

The detectability of an X-ray source is dependent principally on the viewing time and the detector area, efficiency and background counting rate. For a source giving S photons/cm²/sec. incident on the earth's atmosphere resulting in a source count S_1 , the limit of detectability is usually defined as:

$$S_1 \gg 3 \times (\text{background counting rate})^{\frac{1}{2}} \dots\dots(1.1)$$

The background counting rate consists of two separate components. Cosmic ray induced counts are produced in the volume of the detector either by high energy minimum ionising particles, protons or electrons, or by low energy electrons produced by γ rays in Compton interactions. The rate of production is dependent on the volume of the detector. The other source of background is the diffuse cosmic X-ray flux with a rate in the detector dependent not only on the efficiency and area of the detector as in the case of a point source, but also on the

field of view.

The source counting rate S_1 is given by:

$S_1 = S.A.E.T.t$ and equation (1) can be written; (after Pounds 1969)

$$S \geq 3 \times \frac{(B_1.A'.t.k) + (B_2.A.t.T.\Omega.E)}{A.E.T.t} \dots (1.2)$$

where A is the effective detection area for X-rays,
 $A' \approx 1.3A$ is the effective area for the cosmic ray induced background.

B_1 and B_2 are the cosmic ray and diffuse cosmic X-ray background rates respectively.

E is the photon detection efficiency,

$(1-k)$ is the efficiency of rejection of cosmic background events,

T represents the transmission of any auxiliary optics and is typically 0.5 to 0.7,

t is the time spent viewing the source S and

Ω is the field of view for the diffuse X-rays in steradians.

By considering this equation, the various parameters can be optimised for the best sensitivity for a particular experiment.

Observing time.

From equation (1.2) it is clear that the sensitivity increases as the square root of the observing time. The observing time depends on the method used to get the instruments above the atmosphere. Sounding rockets have provided most of the information on X-ray sources even

though the observing time is only a few minutes. A considerable increase can be achieved using balloons, but the energy range is then restricted to greater than 15 kev. Observing times of several hours are possible and heavier payloads can be used.

Satellites have not been used extensively in X-ray astronomy even though the observing time is limited only by the lifetime of the instrument itself. Several payloads are in an advanced state of preparation, however, with projected launch dates in 1970 and 1971.

Improvements in detectors.

In 1962 the first cosmic X-ray source was discovered in an experiment in which a Geiger counter, of area 20 cm^2 , was launched on a sounding rocket. Since the sensitivity of detectors is proportional to the square root of the area much of the development of detectors has been concentrated on increasing the area. The largest detector used to date has been a proportional counter with an area of 3000 cm^2 . It should be noted that although the area is 150 times that of the early detectors, the increase in sensitivity is only a factor of 12. With the sounding rockets and satellites at present available no further comparable increase in detector area can be expected in the near future and improvements in instrument sensitivity by other means are now beginning to be used.

Background reduction.

Referring again to equation (1.2) it is apparent that an increase in sensitivity can be achieved by reducing

the background counting rate. This background is made up of two components; that due to the cosmic X-ray flux and that due to cosmic rays. The X-ray background can be reduced by having a smaller field of view, but at the same time this will reduce the observing time on the source. Thus, for an unstabilised rocket, there is no net increase in sensitivity, indeed for very small fields of view of less than 10^{-3} sr. giving an X-ray background comparable to that of cosmic rays, there is a loss in sensitivity.

The cosmic ray background can be reduced in three ways. The simplest and most commonly used method is that of a scintillation or proportional guard detector in anticoincidence with the detector (see for example Seward et.al.(1967)). A similar method has been under development in this department involving the use of a multi-wire proportional counter and this is described in more detail in chapter 2.

Alternatively rise time discrimination can be used for proportional counters in which cosmic rays give a pulse with a longer risetime than an X-ray pulse.(see for example Gorenstein et.al. 1968).

Using either or both of these methods a background rejection of 80% can be readily achieved with a consequent increase in sensitivity. A third method of background reduction is by the use of grazing incidence optics in which the large collecting area of the telescope focusses the X-rays onto a small detector which has only a small interception area for cosmic rays (Giacconi et.al.1969).

1.2.2 The location of known sources.

In a recent article Oda (1968) has demonstrated the need for accurate location of known sources in order that an optical identification can be made. At present optical identifications have been made of only a handful of sources including Sco X-1, Cyg X-2, Cen X-2 and the Crab nebula.

For completely objective identifications the position of a source must be known to a few tens of seconds of arc for sources in the plane of the galaxy, and to about a degree for sources at high galactic latitudes. To date the best that has been achieved is only of the order of a minute of arc. Thus the identifications mentioned above are subjective, with the exception of the Crab (vide infra), in the sense that observers have looked for peculiar objects within the error box of the X-ray observations.

The most widely used method for the location of sources is that of passive collimation of the detector. The error $d\theta$ in the measurement of position depends on the f.w.h.m. of the collimator and the strength of the source where;

$$d\theta = \frac{(\text{f.w.h.m. of collimator}) \times (\text{noise count})^{\frac{1}{2}}}{\text{signal count}}$$

(after Pounds 1969)

The collimator is usually a rectangular 'egg box' type in which the field of view in one direction is very narrow, typically 2° to 3° , while in the other a field of view as large as possible, typically 20° or 30° , is used to

increase the area of the sky covered. The limits of this type of experiment are in the mechanical difficulties of constructing the collimators and the time of observation, and hence the signal count. An accuracy of location of a source of strength $0.5 \text{ ph./cm}^2/\text{sec}$ to about 0.5° is possible. The position of the source can then be fixed in celestial co-ordinates using a star camera to an accuracy of one minute of arc, adding a negligible further error. Clearly similar experiments on satellites would extend such survey data to much weaker sources.

Improved accuracy can be obtained with a wire grid collimator of the type described by Oda (1965). Sets of two or more parallel wire grids are used to impose a series of transmission bands on the sky (Moiré fringes) and either rotation of the collimator or separation of the grids produces for any source a periodic fluctuation in count rate at a frequency dependent on the position of the source. Improvements in the accuracy of location of the source is achieved since the f.w.h.m. of the collimators can be reduced and the signal count is increased, the source being viewed for half the time. A collimator of this type was used in the optical identification of Sco X-1 by Gursky et.al. (1966).

Occasionally a source will be occulted by the moon, in which case an accurate location and indication of its size is possible. This occurs only rarely, however, and has only been used for the Crab nebula by Bowyer et. al. (1964).

The accuracy of location can now be limited by the accuracy of determination of the aspect of the rocket or satellite. A novel way of improving aspect data has been described by Pounds (1969) in which the star field is not only photographed but also viewed through the wire grid collimator by a photocell. In this way location of a source to 30 arc seconds or so should be possible.

With the advent of the grazing incidence telescope having excellent spatial resolution over a narrow field of view, the size and structure of a single source can be studied. Such telescopes have been constructed with angular resolutions of 2 arc seconds but as yet have only been used successfully in solar experiments (Giacconi et.al. 1969).

With sufficient sensitivity and such high resolution the structure of sources such as the Crab nebula and the extra galactic source M-87, both of which show evidence of being extended sources, can be determined. The strength of these sources is such, however, that photographic film, the obvious choice for recording the data, is not sufficiently sensitive. This fact has led to renewed interest in imaging detectors where an improvement in sensitivity by a factor of 10 can be achieved. Chapter 2 of this thesis contains a review of imaging detectors of the types suitable for this application.

1.3 Energy spectra of known sources.

The best spectral information obtained to date has been with proportional and scintillation counters

with an energy resolution of about 10. A very recent flight (Griffiths, 1970) using a crystal spectrometer has failed to reveal any clear evidence of line emission from Sco X - 1.

The two most likely mechanisms giving rise to discrete X-ray sources are thermal bremsstrahlung and the synchrotron process. (See for example Burbidge, 1969). On the simplest assumptions the bremsstrahlung spectrum will be exponential while synchrotron radiation will exhibit a power law spectrum with negative index.

Most of the spectral information obtained so far has been in the energy range 2 to 15 keV and with rather poor energy resolution. The X-ray data on all detected sources is inconclusive as to the nature of the source of radiation. The spectrum of Sco X-1 which has been measured by a number of groups and which is the best so far obtained for any source can be fitted well by an exponential. This exponential spectrum, characteristic of an optically thin source, when extrapolated to lower energies falls well above the observed fluxes. The visible flux is a factor of five lower, while infra red measurements follow an $(\text{energy})^2$ distribution characteristic of a black body.

The Crab nebula, which was expected to be a synchrotron source because of its output at visible and radio wavelengths, cannot be said to have a simple power law spectrum. Although the X-ray measurements appeared to fit to a power law there was some argument in favour of bremsstrahlung. (Sartori and Morrison (1967)).

Recently Fritz et.al.(1969) and others have reported the discovery in the X-radiation from the Crab a pulsating component with the frequency of the radio pulsar NP 0532. About 10% of the energy emitted as X-rays by the Crab is in this pulsating component. It has been shown by Bowyer et.al.(1964) that the Crab is an extended object in X-rays but pulsars are thought to be highly condensed objects. Thus it seems that the non-pulsating component is being emitted from an extended region, presumably around the pulsar. The Crab is a very interesting object and a study of the structure and energy spectrum is of some importance.

The data on other sources is even less conclusive than for these two. It is clear from the preceding that in order to determine the source mechanism, spectral information with higher energy resolution and over a more extended energy range is required. Of particular interest is the extension of measurements below 1 kev.

Results taken to date below this energy have been confined to measurements at 0.25 kev, beyond the carbon K edge. The reason for this is apparent in the transmission of the plastic windows of proportional counters used in the experiments (see fig. 2.1 in chapter 2). No results are available in the region 0.25 to 0.7 kev and due to problems in operation the results at 0.25 kev are difficult to obtain and subject to large errors.

This region of the spectrum is of considerable interest. Accurate measurements of the flux at low energies

coupled with optical identifications, the only way of estimating the distance of the source, will lead to an independent determination of the column density of hydrogen to the source from the low energy cut-off of the spectrum. Similarly the sensitivity of separation of bremsstrahlung from synchrotron spectra is increased with increased bandwidth of the observations. Comparison of cut-offs for different sources may also lead to information on internal absorption in the source itself.

Improvements in energy resolution may soon be possible using the slitless X-ray spectrograph described in chapter 2. Resolutions of E/dE of 100 are possible using this system which requires an imaging detector at the focus of a grazing incidence telescope.

1.4 The diffuse X-ray background.

Measurements of the diffuse X-ray background have been made by several groups and the results have shown that for energies at which galactic absorption is negligible the flux is isotropic to within 10%, while for lower energies the flux is more intense at high galactic latitudes. On the basis of this evidence the background flux has been assumed to have an extra-galactic origin. A recent high sensitivity survey however, has shown that there is an enhancement of the background radiation in the plane of the galaxy, (Cooke et.al., 1969) indicating a component of galactic origin. Several explanations of this increase are postulated by the authors, the most likely explanations being either inverse Compton scattering by cosmic rays of the

high flux of infra-red radiation reported by Shivanandan (1968) or of starlight in the galactic disc, or of the effect of unresolved sources. The energy spectrum obtained is not sufficiently accurate ^{to distinguish} between any of the proposed mechanisms.

In a recent review article, Sciama (1969) has discussed the possible origins of the extra-galactic component and indicated the experimental information necessary to identify the source. The origin of the background flux at energies greater than 1 kev has been attributed to two mechanisms, either a) Compton scattering of starlight or the cosmic black body radiation by intergalactic relativistic electrons or b) the integrated contribution of unresolved discrete sources. For hypothesis b) a later suggestion by several authors is that Compton scattering of black body radiation by electrons from discrete radio sources may be the mechanism. This is an attractive proposition because, since the radiation may be coming from the edge of the observable universe, the radio sources may have been in a more energetic state of evolution and the black body radiation would have been more intense.

Of even greater interest cosmologically is the origin of the low energy flux at about 0.25 kev. Measurements of the flux at high galactic latitudes by Bowyer et. al. (1968) and Henry et. al. (1968) are subject to different interpretations. The high observed flux may be due either to a lower opacity for the galaxy than that inferred from

21 cm. observations or to an additional source of soft X-rays. The source proposed by Henry et.al. is a hot intergalactic gas with a present particle density of $10/m^3$. This question arises because several cosmological theories predict such a large mass of gas over and above that in localised sources. Another factor in the absorption of soft X-rays is intergalactic absorption.

If the X-rays originate at the limits of the observable universe there is a severe limitation on the amount of neutral hydrogen and helium allowable in the line of sight. ^{Alternatively} the abundance of the elements carbon and nitrogen cannot be more than about 2% of their normal 'cosmical' abundances.

In conclusion it can be said that the X-ray background contains a considerable amount of information about our galaxy, other galaxies and the universe as a whole. An accurate and extended energy spectrum is needed for a variety of directions in order that the information can be extracted in a reliable way.

1.5 Solar X-ray studies.

1.5.1 Introduction.

Although the sun is a very ordinary main sequence star, it is often treated as a separate subject for study because the high flux of X-rays, due to its proximity to earth, allows for a range of specialised experiments not yet possible with weak cosmic sources. The X-ray flux from the sun varies from about 10^3 to 10^5 photons/cm²/sec in the wavelength range from 2 to 8 Å, while the strongest

cosmic X-ray source, Sco X-1, gives a flux of only about 20 ph./cm²/sec. in the same energy interval.

The main advantages gained from this high flux are that relatively small area dispersive systems can be used for spectral studies, and variations in flux over periods of a few seconds can be measured with broad band spectrometers. The development of solar X-ray astronomy until recently has been along two lines, the use of broad-band spectrometers to obtain good time resolution studies of active regions and flares, and plane crystal spectrometers for high resolution studies of their associated spectra. With the use of grazing incidence optics these two branches have developed into new experiments involving good spatial, and spectral or temporal resolution.

In the following sections these three general trends, which are not necessarily in strict chronological order, are discussed and again, consideration is given to future detector requirements.

1.5.2 Broadband spectrometers and the importance of good time resolution.

Much of the early work in X-ray astronomy of the sun was done using broadband spectrometers such as film, gas counters and scintillation counters in which the energy resolution is at best of the order of 10. Early work using pinhole cameras flown on sounding rockets gave fairly good spatial resolution and interesting correlations with observations in other spectral regions.

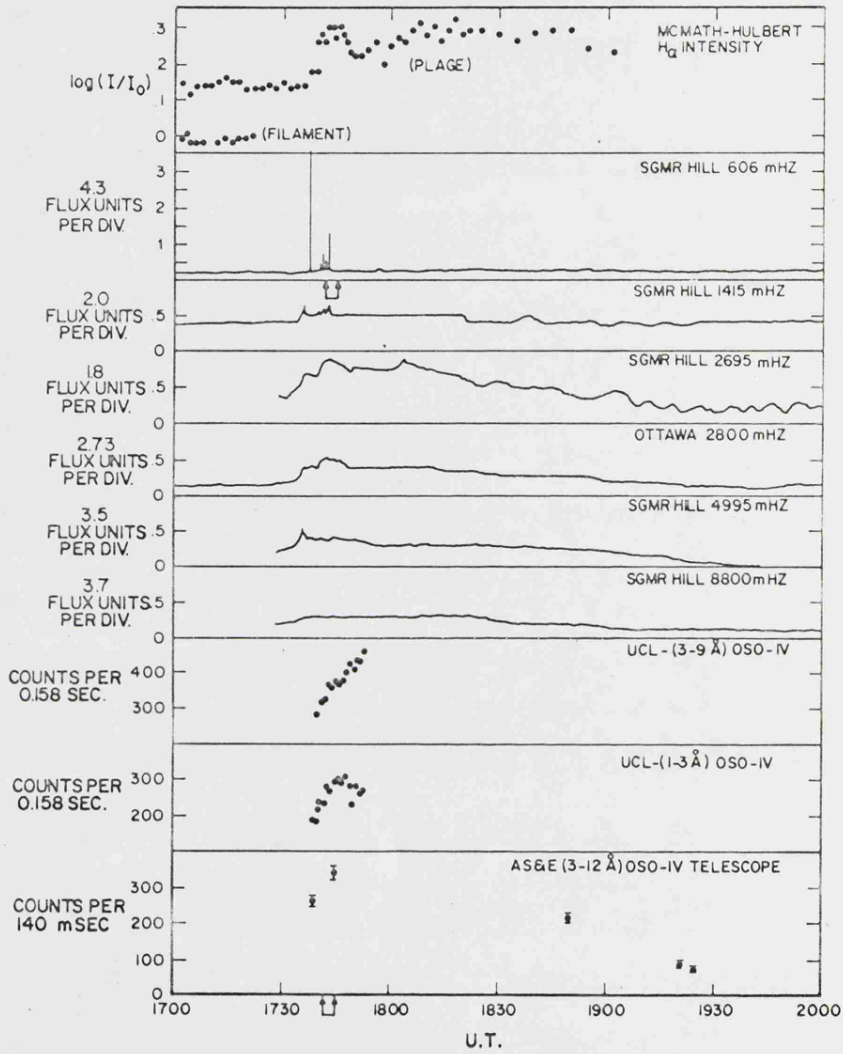


Figure 1.1 Time profile of the 8 June 1968 flare as seen in H α , radio, and x-ray wavelengths. The period of observation of the rocket-borne x-ray telescope is indicated by arrows.

Since these experiments had no time resolution, however, the time profile of active regions and flares could not be compared to similar results in microwave and H alpha regions, a comparison which is of considerable interest in attempts to explain the physical processes involved.

Most of the solar data with good time resolution has been obtained from broadband spectrometers on satellites in particular on the very successful Orbiting Solar Observatory (OSO) series. The importance of good time resolution is demonstrated in fig 1.1 in which radio, H alpha and X-ray fluxes for a flare are shown. An experiment of this type is that flown on OSO-4 by the Leicester/University College, London groups in which proportional counters view the whole of the sun with a time resolution of 15 secs (Culhane et.al.1969).

Other, similar experiments over slightly varying energy ranges have been flown by other groups and are listed in more detail in review papers by Underwood (1968) and Pounds (1969).

Because of the lack of collimation of the detectors in these instruments, confusion can arise in interpretation of the data if more than one active region is visible on the solar disc. The energy information from this type of detector is obviously limited but broad changes in spectra during the onset of flares and short term variations in non-flare X-ray spectra have been observed. The poor energy resolution of these instruments has led to the use

of plane crystal spectrometers enabling line spectra to be resolved.

1.5.3 Plane crystal spectrometers.

With the development of satellites and sounding rockets having good pointing accuracy and stability, grazing incidence diffraction gratings and plane crystal spectrometers have been used extensively for solar studies, the crystal instruments being generally preferred below about 20 Å. The radiation reflected from the crystal is detected using a scanning proportional counter, a complete scan taking about three to five minutes with an energy resolution typically of a few hundred. Thus the time resolution is insufficient to study the development of impulsive flares or bursts.

More use has been made of sounding rockets for this type of experiment, (see for example Batstone et.al. 1970) although several have been incorporated in OSO satellites. Of particular interest is an instrument on OSO-5 flown by the Goddard Space Flight Centre in which the crystal can be commanded to a particular spectral line and the intensity of the line monitored over small time intervals; no results have yet been published.

Data from these experiments allows a measure to be made of the electron density and temperature, and an order of magnitude estimate of the volume of the emitting region obtained from consideration of the relative strengths of identifiable emission lines. Again, as in the case of time resolution studies, confusion can arise if more than one

active region is visible at any one time.

1.5.4 Recent developments in instrumentation.

One of the main disadvantages with early experiments, that of poor spatial resolution, can be overcome by the use of the newly developed grazing incidence telescopes.

Recently, experiments have been flown by the American Science and Engineering group on OSO-4 and by the Leicester group on OSO-5 in which spectroheliograms of the sun with resolutions of one arc minute have been obtained (fuller details of these experiments are given in chapters 2 and 6).

A grazing incidence telescope with a narrow field of view is used, essentially, as a collector of X-ray photons and the sun is scanned by the spacecraft.

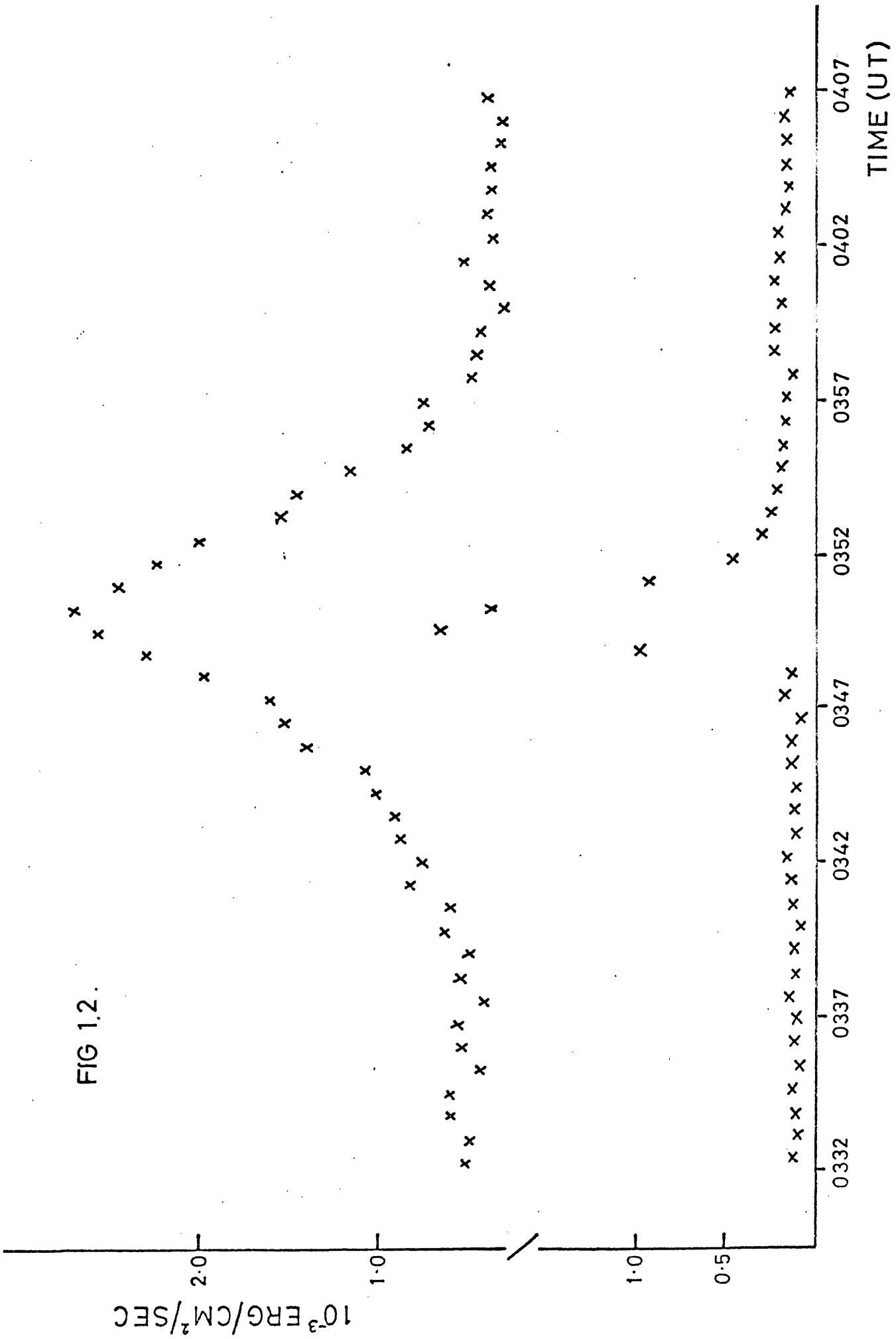
Preliminary results from the OSO-5 experiment have been presented (Pounds 1970) showing small active centres within a larger emitting region. The importance of this type of experiment is clearly demonstrated in fig 1.2 which shows the occurrence of two flares, one on the SE limb and one near the W limb of the sun. The upper peak was associated with a flare observed in H alpha but the lower peak was from a flare giving no detectable emission of H alpha. Clearly, any instrument viewing the whole of the sun would produce results from two flares, while the experimenter would try and analyse the results as if from a single flare.

Spectroheliographs of this type have only moderate time resolution, typically 5 minutes, and the energy resolution is that of the detector and typically 10.

Fig.1.2

Time profiles of flares from different regions of
the solar disc.

FIG 1.2.



The next generation of imaging instruments will make use of improved telescopes giving a true focussing of the radiation and having excellent spatial resolution, improved time resolution and a higher energy resolution.

In a recent flight Vainana (1968) has shown that there is structure in active regions of the order of 2 arc seconds in size using such a telescope with film as a detector. On the same flight two exposures were taken in which a transmission diffraction grating giving an energy resolution of about 100, was interposed between telescope and film. The use of such an instrument on a satellite would obviously ^{be} of considerable value, it being necessary however, to substitute some form of electronic detector for the film for non-recoverable satellites.

Finally in a proposal for flight on an OSO satellite, the Leicester group describe an instrument capable of an energy resolution of over 3000. A grazing incidence mirror is used to focus radiation onto a focussing crystal spectrometer. The detector used is of the form described in chapter 5 and allows the continuous monitoring of a spectral line.

With such a high resolution it is possible to measure the enhanced broadening of a spectral line due to Doppler shifts for temperatures of a few million degrees (Smith 1968). This will allow independent and localised measurements of temperature and by measuring the shift in the line will give values for the velocity in the line of sight of the emitting region.

1.6 A summary of future detector requirements.

In the case of non-solar X-ray astronomy there are two major areas in which improvements in detectors would play a vital part. Although increased energy resolution would be an advantage, the very low flux from most sources makes dispersive systems impracticable at present. Failing this, an increase in the energy range, particularly at long wavelengths, would provide much useful information about energy producing mechanisms in the source.

The second major detector requirement is for an imaging system for use with focussing telescopes. The accurate positioning of sources would enable optical identifications to be made while measurements of size and structure would lead to further knowledge of the emitting region.

In the case of the sun, the principle requirement is for good spectral and temporal resolution of X-ray emission from small active regions in the corona. To achieve this an instrument of the type described in the previous section, again with an imaging detector, is required.

In conclusion, it may be said that the development of good spatial resolution imaging detector will be a key factor in the advancement of X-ray astronomy.

CHAPTER 2. POSITION SENSITIVE PARTICLE AND PHOTON DETECTORS.

2.1 Introduction.

The potential of imaging detectors in solar and non-solar X-ray astronomy has been discussed in chapter 1. This chapter is devoted to a review of current methods of X-ray detection and imaging. A detailed comparison of the sensitivity and spatial resolution of the various types of imaging systems is deferred to a later chapter where the advantages of the system reported in this thesis are discussed.

2.2 The photographic method.

The traditional method of X-ray detection is by the use of photographic film. This technique has been used extensively in X-ray astronomy since Burnight (1949) first reported blackening of a film carried on a sounding rocket, shielded from visible and ultraviolet light. Commercially available film has a protective layer of gelatin over the sensitized surface which has a transmission dependent on the X-ray energy.

Results taken with film without this gelatin layer show a probability that an absorbed X-ray will give a developable silver halide grain of between 0.5 and 1.0 (Atkinson and Pounds, 1964). Because of the non-uniform grain distribution and other sources of film noise however, the information content is less than would be expected from this probability. Giacconi et al. (1969) have defined the 'effective quantum efficiency' of a film as the efficiency that an individual photon detecting device would need to have to give the same intensity error distribution as the film. Defined in this way the efficiency of a film falls an order of magnitude below that

of a typical comparable image dissection device employing scanning techniques (0.01 compared with 0.1).

The cause of this low quantum efficiency^{is} the high background level due to initial fog and the accumulated effect of radiation background^{which} limits the sensitivity of film. The initial fog level varies from film to film but typically can be equivalent to 10^6 photons/cm² which, for sounding rockets, limits the use of film at present to solar studies.

A study of the possible use of film on a satellite by Skelton and DeLoach (1967) has shown that a background of 10^6 photons/cm² can be produced in a film, even with shielding, in a period of a few days, due to particle radiation. Other disadvantages of film are difficulty of retrieval, lack of time resolution and low dynamic range. To counterbalance these disadvantages there are several attractive characteristics of film which have led to its use in some branches of X-ray and ultra-violet astronomy. It has good spatial resolution and a large storage capacity, which can be as high as 10^8 bits/cm², combined with simplicity, reliability of operation and a long period integration capacity. Several pinhole cameras for X-ray observations of the sun have been flown on sounding rockets (see for example Blake et.al. (1965), Russell (1965) and Russell and Pounds (1966)).

More sensitive instruments employing grazing incidence telescopes to increase the collection area without increasing the area of the detector (and hence the background) have been used for solar X-ray studies giving resolutions, limited by the optics, of a few arc seconds. (Underwood et.al. (1967) and Vaiana et.al. (1968)). An interesting development in this field has been in the use of X-ray transmission gratings (Gursky and Zehnpfennig (1966) and

Zehnpfennig (1966)). The gratings, thin replicas of normal optical gratings, positioned in front of the telescope, give a simultaneous recording of the X-ray image and the spectra associated with various features. The dispersion of the gratings is small (about 30 arc seconds per angstrom) but with high resolution X-ray optics a resolving power of (E/dE) of 100 can be achieved. Results taken with such an instrument on a sounding rocket have been reported by Vaiana et.al. (1968).

Film has also been used on the Rowland circle of a grating spectrometer (Jones et. al. 1968) to give simultaneous recording of the ultra-violet spectrum of a solar event. A distributed detector such as film has considerable advantages in such a system over conventional scanning techniques, in particular it's high storage capacity and resolution.

2.3 Gaseous ionisation methods.

2.3.1. Introduction.

In all forms of gas counters the incoming photon is converted into electrons, the number of which depends on the energy deposited by the photon. The efficiency depends, in principle, only on the window thickness and the depth of the gas.

The simplest form of detector is the ionization chamber in which no multiplication occurs. With the present limits on preamplifier noise performance the ionization chamber cannot be used to detect single events. The other two forms of this detector, the Geiger and proportional counters, feature internal multiplication of the initial ionisation to enable individual events to be detected, but as a consequence there is a loss in energy resolution due to the statistics of the avalanche process.

With the Geiger mode of operation , ionizing events are recorded as pulses of uniform amplitude. The Geiger counter was the detector used in the first sounding rocket experiment to detect non-solar X-rays (Giacconi et.al. 1962) and has been used extensively since by this and other groups. In the proportional region the amplitude of the pulse is dependent on the mean number of ion pairs produced by the incoming photon. The amplitude distribution of the pulses about the mean is governed by the statistics of the initial ionization and the multiplication process. Considerable progress has been made recently in increasing the size of such counters. A cosmic X-ray detector with a window area of 3000 cm^2 has been constructed in this department (Pounds 1969) with little loss in resolution, 20% at 5.9 keV , compared to the best resolution so far attained of 14%. (Charles and Cooke 1969). The energy resolution of a typical proportional counter is compared to that of other detectors in Fig. 2.1 which is taken from Aitken (1968).

A reduction by a factor of 80% of the particle induced background can be readily achieved using rise time discrimination techniques , considerably increasing the sensitivity to weak sources. (Mathieson and Sanford 1963 , Gorenstein et.al 1968).

The region of the X-ray spectrum below 1 keV has become increasingly significant , particularly to cosmologists. Detectors having good efficiency at this energy have proved very difficult to construct. Very thin windows , less than $2 \mu\text{m}$ of plastic , are necessary to achieve good efficiency below $\frac{1}{4}$ keV and several methods of forming such windows have been described (see for example Sinha et.al. , 1968 and Caruso et.al.1968).

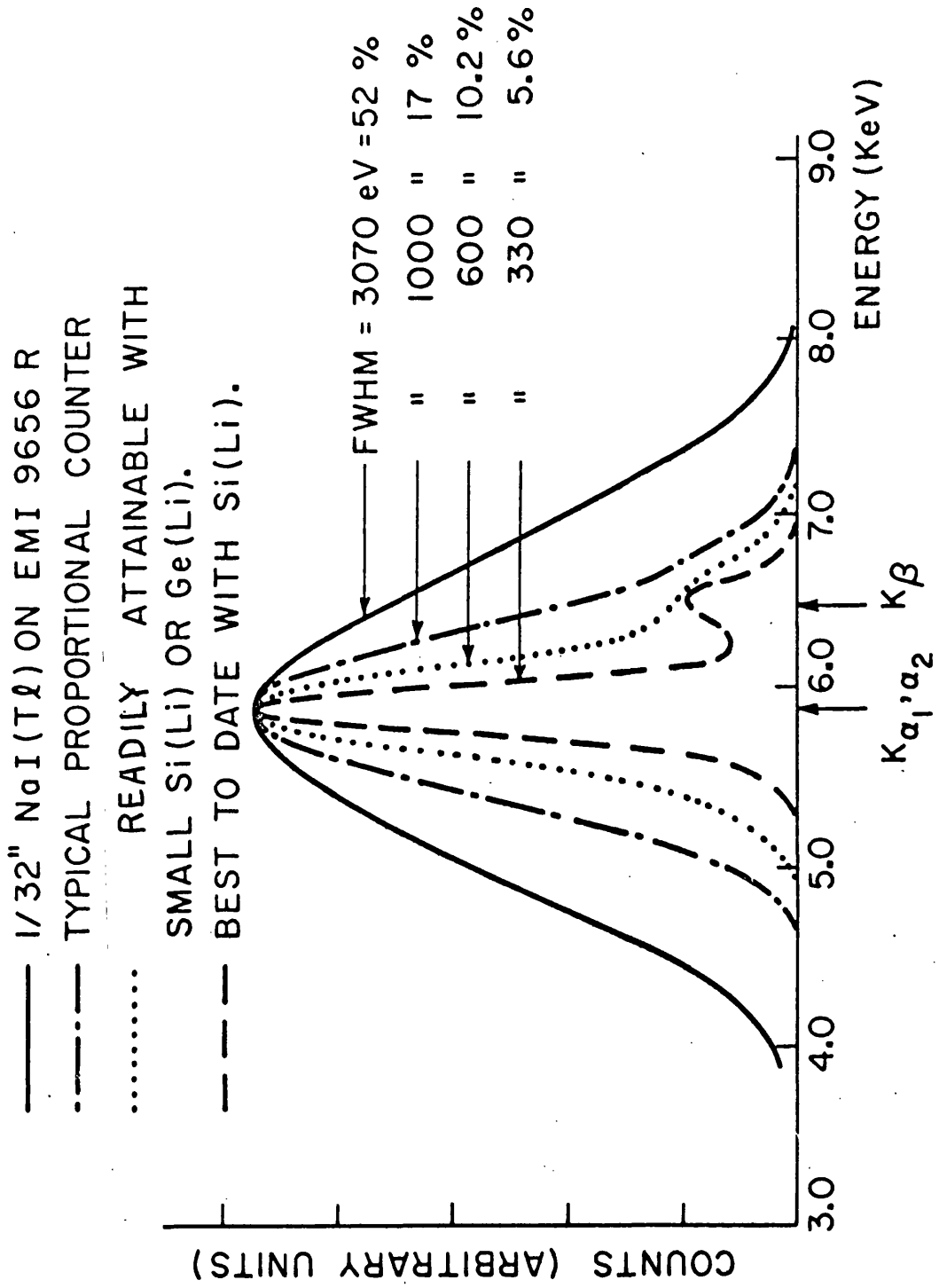
The transmission of thin windows of ' Melinex ' , a

Fig. 2.1.

Energy resolutions of various detectors for 5.9 kev X-rays.

(A very recent value of 200 ev for a Ge detector
has been reported, see text).

FIG 2.1. Fe^{55} X-RAY SPECTRA



typical window material, is shown in fig.2.2. For window thicknesses giving good efficiency at energies below the carbon K edge at 44 \AA , some means of maintaining a constant gas pressure to compensate for leaks is necessary, which increases considerably the complexity of the system. Recently workers at Saclay in Paris have developed a sealed 150 cm^2 detector with a $2 \mu\text{m}$ mica window, but as yet no details have been published.

2.3.2. Imaging detectors.

The proportional counter hodoscope.

A simple type of electronic imaging detector consists of a matrix of separate proportional or Geiger counters, each with its own preamplifier and scalar. On physical grounds alone the best resolution obtainable is of the order of a few cms. Eiben et.al. (1969) constructed a hodoscope from six horizontal layers of proportional counters each composed of twenty rectangular tubes of $5 \times 5 \times 100 \text{ cm}^3$, with the upper and lower layer crossed with respect to the inner four layers. An interesting feature of this device is that each counter consists of an anode wire surrounded by the square section cathode comprising twenty similar wires, allowing the tracks of high energy charged particles to be calculated with little loss in energy of the particles.

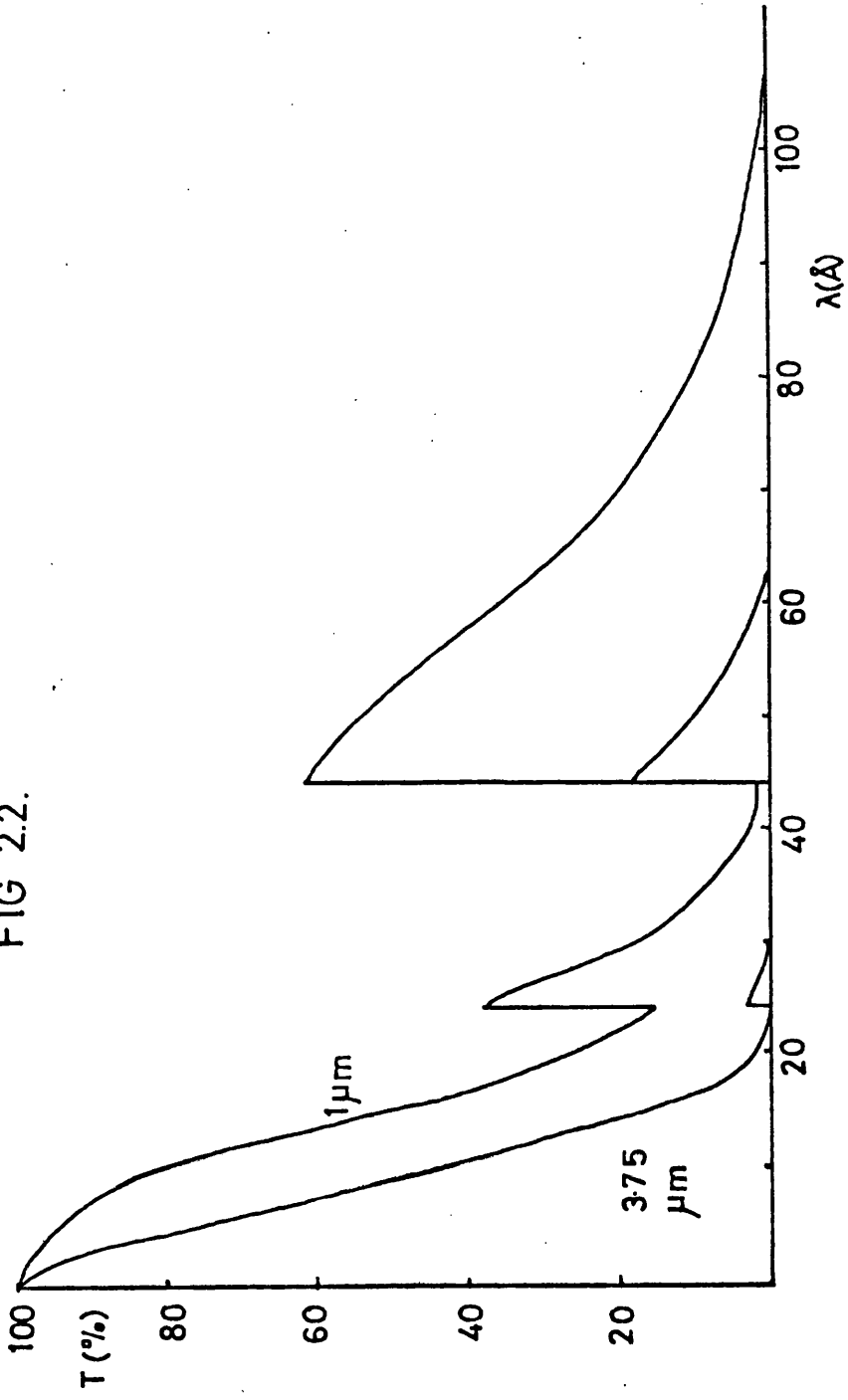
The limit of spatial resolution achieved with such a device is a few mms. at which distance sparking between anode and cathode becomes a problem. Two dimensional dissection can only be performed for high energy particles which will penetrate at least two of the layers.

An interesting use of this type of counter in X-ray astronomy is in background reduction. Since the X-ray pulse avalanche

Fig 2.2

Transmission of 'melinex'.

FIG 2.2.



is very localised, the wires of the counter can be put in anti-coincidence hence eliminating any high energy particle which would give a pulse on more than one wire.

Multi-wire proportional counters- the Charpak chamber.

The use of multi-wire proportional counters to select and localise charged particles and X-rays was first described in detail by Charpak et.al. (1968 a). The detector consists basically of anode wires separated by one mm. or more stretched between the ends of a 'pan' type proportional counter. The counter behaves exactly as a conventional proportional counter since the avalanche region is of the order of 0.1 mm. and energy resolutions of 15% at 5.9 keV were obtained.

The spatial resolution obtainable is restricted by the pitch of the anode wires. However, by consideration of the time taken for a pulse to arrive at the wire, interpolation between wires becomes possible. This is only practicable in the case of high energy particles because of the need for an external time reference for the arrival of the particle at the counter.

In a later paper the same authors (Charpak 1968 b) considered ways of reading out the information from a multi-wire chamber. Several methods were described including the use of inductances between each wire giving a position sensitive delay in the arrival of the pulses at each end of the inductor chain, and resistors between each wire giving a branching of the current pulse also dependent on the position of the activated wire.

Applications of this type of counter, particularly in the field of particle physics have been described by several workers (see for example Koester 1970 and Braid 1970).

A similar counter with two dimensional position sensitivity has been described briefly by Epple et.al. 1967 in which the cathode of the detector consists of isolated strips lying at right angles to the anode wires. No details of its operating characteristics or spatial resolution were given. A similar system has also been described by Kantor (1968) giving a resolution of 1 cm in 'x' and 'y' directions but, again, no details of its operating characteristics were presented. A recent paper (Nunamaker et.al. 1970) describes a pan type counter of asymmetrical geometry in which the anode wires were mounted very close to one cathode plane which again consisted of isolated strips. An improvement in the resolution determined from the cathode strips over that obtained with the anode wires is reported but details of the work have not yet been published. This increase in resolution at the cathode would be expected because, although the avalanche is localised in the region of the anode wire, the pulse which appears on the cathode due to the movement of ions in the high field region near the anode, is not restricted to one strip of the cathode but extends over some distance. The effect of this, if readout was of the current branching type, would be to give the ' centre of gravity ' of the cathode pulse and reduce the effect of the discreteness of the cathode strips. Some interpolation between the strips would then be possible whereas no such effect can be observed at the anode wires.

Counters with resistive anode wires.

Methods involving the branching of the current pulse.

Position sensitive counters utilising the branching of current in a resistive anode wire have been operated successfully giving resolutions down to 1 mm. Following earlier work on semiconductor detectors with resistive rear electrodes, Kuhlmann (1966 a and b) constructed a proportional counter with an anode wire of carbon coated quartz of resistance $1.5 \text{ k}\Omega/\text{cm}$. The current pulses I_1 and I_2 from the ends of the wire were amplified and the quotient $I_1/(I_1+I_2)$ generated electronically. This function is dependent only on the position of incidence of the particle or photon along the wire. With a cylindrical counter 30 cms. in length a resolution of 1.2 mm. was obtained with charged particles. It should be noted that for a minimum ionising particle at an oblique angle to the anode wire the quotient $I_1/(I_1+I_2)$ will represent the central position or 'centre of gravity' of the track.

McDicken (1967) describes a Geiger counter operating on the same principle. The anode wire in this case was of nickel-chrome of resistance $85\Omega/\text{cm}$. Only the first $1.5\mu\text{s}$ of the Geiger pulse was used in the calculation of the position in which time the discharge had travelled 4cms. on either side. This imposed a dead space at each end of the 70cm. long counter and the best resolution obtained was 2cms. f.w.h.m.

Methods involving the risetime of the pulse.

Borkowski and Kopp (1968) have described an ingenious method for determining the position of ionising events by measuring the risetime of output pulses from proportional counters having resistive anode wires. The advantage of this method over the branching

methods is that improved resolution is possible with relatively simple electronic circuitry.

The risetime of a proportional counter pulse for a point ionising event is dependent only on the geometry of the counter and the gas used. For a high energy minimum ionising particle the risetime is then also dependent on the track length and orientation in the counter. (see for example Ricker and Gomes (1969) and Gott and Charles (1969)). The counter used by Borkowski, with an anode wire of resistance $40 \text{ k}\Omega/\text{mm.}$, can be treated as an infinite RC line, the result being that the pulse from the counter has a rise time dependent only on it's location.

The positional sensitivity in the 50 cm. counter was determined to be approximately 30 ns./mm. , thus, even for high energy particles, the variation in rise time due to different track orientations will give an additional uncertainty of no more than one or two mms. This point was not considered by the authors who used only well collimated beams perpendicular to the counter wire.

A reference electrode near the wire of the counter was used as a fast timer and the crossover time of the doubly differentiated pulse, which is dependent only on risetime and not on pulse height, was compared to the start of the pulse obtained from the reference. With 22 keV X-rays a positional uncertainty of 0.5 mms. f.w.h.m. was obtained for a beam 0.1 mm. wide with a counter 400 mm in length, a percentage resolution of better than 0.1%.

In a later paper (Borkowski and Kopp, 1970) a method of two dimensional dissection using a form of the Charpak chamber with resistive wires is described. The resolution along the wires for a 200 mm. counter of 0.4 mm. f.w.h.m. was achieved, the resolution in

the direction perpendicular to the wires, however, is governed by the gap between adjacent wires in a similar way to the multi-wire counters described earlier. The method of image extraction is summarised in fig.2.3. With this system, not only can the position of an event be located in two dimensions, but there is little loss in energy resolution, 6% f.w.h.m. at 22 keV compared to 5% for a typical single wire counter. This system is similar in principle to the one devised for use with channel multiplier arrays described in this thesis.

The gas proportional scintillation counter.

Gas scintillation counters, particularly those using noble gases, are well known for their good time resolution, but in general their energy resolution is poor. The use of a cylindrical geometry electric field has led to the development of the gas proportional scintillation counter. (See for reference Charpak and Renard (1956) and Policarpo (1967)).

The initial scintillation in the rare gas, usually Xenon, is followed by further scintillations in the avalanche region of the counter. The rise time of the light pulse follows the electron drift time which is slow (of the order of 10 μ s) and prohibits the use of the counter for fast coincidence work or for very high count rate applications. Addition of small amounts of quench gas, however, increases the rise time of the pulse, for example, with 2% methane the rise time is 1.5 μ s., but a loss in light output of a factor of three results. (Conde et.al. 1968).

Comparison of the energy resolution of the light pulses with the electron pulses for 5.9 keV X-rays has shown a slight worsening of resolution - from 19% to 21%, due to the statistics

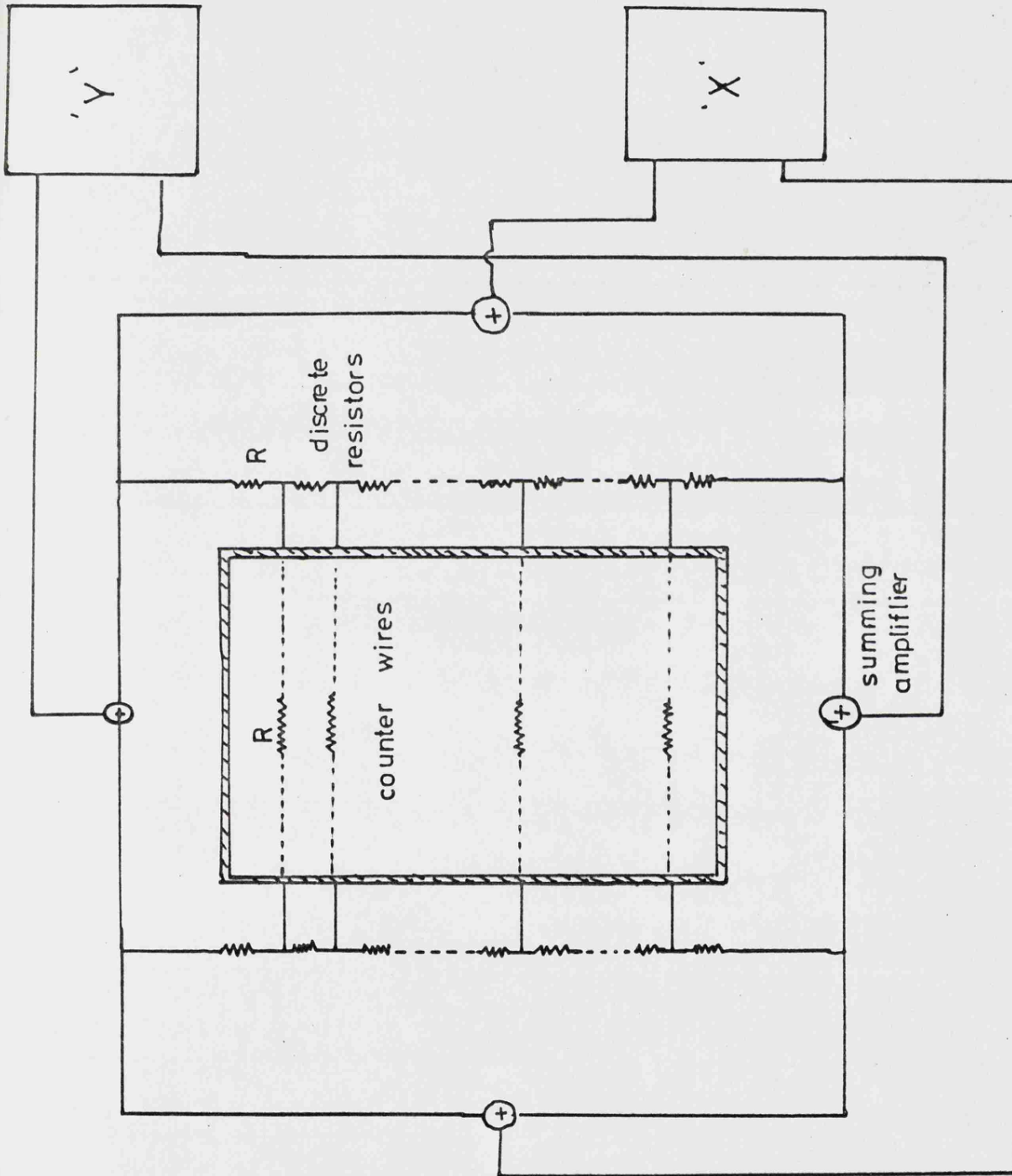
Fig 2.3

Two dimensional position sensitive proportional counter

(after Borkowski).

Discrete resistors, R , between each of the counter wires, resistance R , gives four position signals leading to determination of X and Y co-ordinates of the pulse.

FIG 23.



of the photo-multiplier tube used to view the output (Policarpo 1969).

The fact that the scintillations are localised in the avalanche region near the wire has been utilised by several workers to obtain image information (see for example Lansiaart 1963 and Lansiaart et.al. 1966). The detector used by Lansiaart and his co-workers consists essentially of a pan type counter geometrically bounded by plane, parallel electrodes. The cathode, and window, of the detector is followed by a detection space which is essentially an ionisation chamber bounded by a grid, which is followed immediately by the anode plate leaving a narrow gap with a high electric field. Avalanches occur in this region and a focussing photomultiplier views the scintillations through the anode which consists of a thin conducting layer on a glass plate.

No details of the energy resolution of this type of detector have been published but a spatial resolution of 1mm. for 5.9keV X-rays has been reported (Roux et.al. 1968).

2.4 Scintillation detectors.

The scintillation detector has considerable potential as an imaging device but as yet the range over which its light output is sufficiently high to give reasonable energy resolution is restricted to energies greater than about 1 keV. The exception to this is the gas proportional scintillation counter discussed earlier.

The best energy resolutions obtained so far in X-ray astronomy have been with NaI(Tl) where a resolution of 52% at 5.9 keV. is reported, fig 2.1 (Matsuoka 1966). Serious problems arise at this energy due to the non-linearity of the crystal around its iodine L edge.

The efficiency of a scintillator at this energy had previously been assumed to be 100% but this has been shown to be incorrect (Patla and Kiss 1965). More recent work by McCann and Smith (1968) with NaI(Tl) again estimates the efficiency to be 100% in disagreement with Patla and Kiss. Further measurements of efficiency are needed to resolve this point.

The most promising developments in scintillators arise from reports by Hofstadter et.al. (1964) and Madden et.al.(1968). Hofstadter reports that the use of $\text{CaI}_2(\text{Eu})$ results in a light output of almost twice that of NaI which may be expected to extend the energy range below 1 kev. A similar increase in light output has been discovered by Madden using semiconductor crystals. Tellurium doped CdS in particular showed a very high light output. Unfortunately it appears that at this time difficulties in the manufacture of the crystals have resulted in relatively poor resolutions.

Although the performance of these detectors is generally poorer than proportional gas counters, the robustness and imaging capabilities of scintillators, together with high inherent stability make them possibly useful detectors for some applications in X-ray astronomy. A recent proposal for a satellite soft X-ray spectrometer imaging system using $\text{CaF}_2(\text{Eu})$ crystal as an X-ray image converter is described in the final section.

2.5 Semiconductor detectors.

Within the last few years the technique of construction of thin window silicon and germanium detectors has been exploited commercially and good practical systems have been developed. Lithium drifted silicon and germanium detectors with gold surface barrier contacts

have been produced with effective window thicknesses of $0.1\mu\text{m}$ ('Ortec' Ltd. advertisement). Even thinner windows are theoretically possible with silicon surface barrier detectors and this type may supercede the lithium drifted type for low energy applications. Fig 2.4 demonstrates that the low energy cut-off of a thin window Si detector is defined by the cryostat window, the cut-off of the dead layer window could be as low as 0.25 kev, while the high energy response is governed by the depth of the depletion layer (after Aitken,1968).

The best energy resolution so far reported has been 200ev f.w.h.m. in a small, cooled, Ge(li) detector for 5.9 kev X-rays which represents a considerable improvement over any other type of detector (Walter, 1970, and Nuclear Enterprises Ltd. advertisement 1970).

An alternative method of realizing very thin windows is to irradiate the detector through the side in a direction perpendicular to the electric field (Armantrout 1966). In the soft X-ray region, however, the result of the increased trapping due to the lower electric field in this type of detector, is that the efficiency and resolution fall at energies below about 20 kev.

The choice of detector type, germanium or silicon, depends largely on the operating conditions. For energies below about 50 kev silicon detectors offer the best theoretical resolution and have less sensitivity to high energy background events and spurious noise. If one wishes to extend the observations over a larger energy range the germanium detector is the obvious choice. Both types require operation at reduced temperatures.

For the particular application of semiconductor detectors to X-ray astronomy, larger areas are necessary to give reasonable counting statistics for the generally weak incident fluxes. Considerable

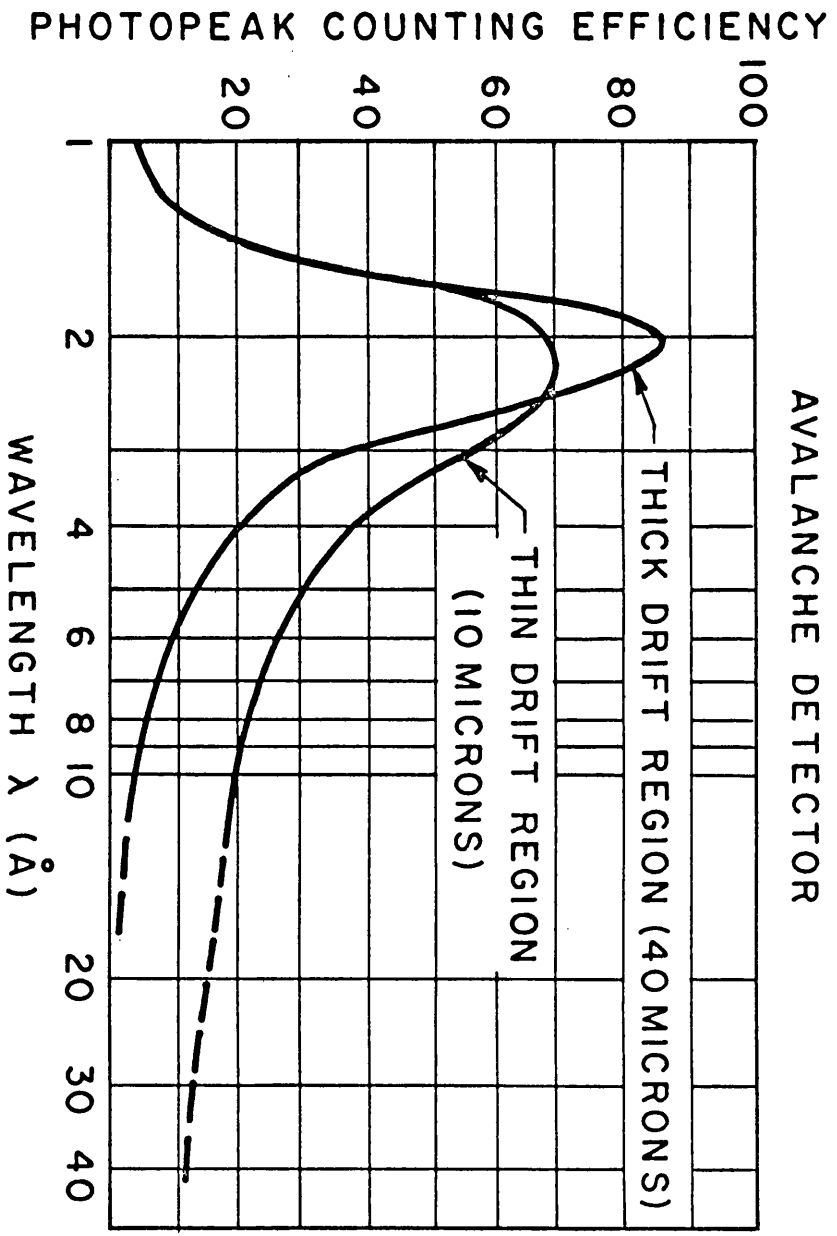


FIG 2.5.

difficulties are associated with large area detectors, not only in the difficulties of manufacture of the crystals, but also in the increased noise due to increased detector capacitance. At present it is found to be preferable to use several smaller detectors in parallel. If the detectors are matched to within 1% a simple technique developed by Saunders and Maxwell, 1968, allows very precise adjustment of the gains by varying the bypass capacitor on the bias of each of the individual elements.

If the advances in detector performance and preamplifier design of the last few years are maintained, a large area detector of practical use in X-ray astronomy may soon become available.

Avalanche detectors.

The practical usefulness of semiconductor detectors at low energies is governed not only by the window but also by the electronic noise. For the present limit on detector performance of 200 ev f.w.h.m for 5.9 kev X-rays, the detector performance at energies below 1 kev becomes inferior in both efficiency and resolution to a good proportional counter.

The attractiveness of obtaining internal multiplication in semiconductor detectors has long been recognised. Theoretical studies of the possible improvement in resolution of an avalanche detector by Haitz and Smitz (1966) and Ogawa (1967) predicted very good resolution. The measured resolution was found to fall short even of the best resolution obtainable with a non-amplifying silicon detector due to frozen in non-uniformities in the resistivity of the material. (see for example Huth et.al.(1964), Huth et.al.(1965), Huth (1966)).

The spectral response of a silicon avalanche detector is shown in fig 2.5. With the the detector operated in the proportional

mode a resolution of 30% f.w.h.m. at 5.9 kev has been reported by Wiza (1967), while in the Geiger mode very fast pulses have been observed and using a tunnel diode preamplifier, pulse rates of 100 mc/s can be handled. This indicates that the device could be very useful as a fast reference timer. A further advantage is that the device may be operated at room temperature.

The disadvantage of the type of detector developed by Huth lies in the very high operating voltage required for multiplication. This inevitably means a large leakage current and hence increased noise. One method of avoiding this problem has been outlined in a recent paper by Gibbons (1968) who adapted an idea of Ruegg (1967) to the fabrication of an RAPD (reach-through avalanche photodiode) for use as a low energy detector. This theoretical work indicates a method of obtaining a high field for multiplication with a low applied voltage. The detecting volume of the device has a low field which sweeps the carriers to a high field region which can be completely buried, thus eliminating much of the problem of leakage currents. No experimental work appears to have been carried out on this type of device.

Position sensitive semiconductor detectors.

Position sensitive detectors utilising the branching of charge on a resistive electrode or surface barrier strip contacts have been described extensively in the literature. (see for example Dodge et.al. 1966 and Laegsaard et.al. 1967). A two dimensional position indication has been obtained by evaporation of mutually orthogonal surface barrier strip contacts on opposite faces of the detector (Hofker et.al. 1966). Resolutions of the order of 0.1 mm

over a distance of a few mms are common.

Because of the method of obtaining the positional information the noise of the electronics must be reduced even further in order that semiconductor detectors can compete with established methods of soft X-ray image dissection. One possible method of readout which does not involve the branching of charge has been described by Brown et.al.(1970) in which a multiple diode array is scanned by an electron beam on the 'picturephone' principle giving resolutions of 50 μm for 1 Mev γ rays.

2.6 Photoelectric detectors.

In principle, photoelectric methods at once remove the need for very low noise electronics and for thin leak tight windows, the main problems in the operation of semiconductor detectors and gas counters at low energies. All types of photoelectric detector depend on the conversion of the incoming photon into electrons which are then detected in some way. At very high counting rates the detector may be an electrometer. For X-ray astronomy, however, it would be desirable that the detector should be capable of detecting single photons.

Most photoelectric detectors have used conventional discrete dynode photomultiplier tubes or channel multipliers. Other methods of detecting the electrons involve acceleration and subsequent detection in Geiger counters (Melhorn and Albridge, 1964), scintillation counters (Schumaker and Grodski, 1965), and semiconductor detectors (Chevalier, 1967 a and b).

The dependence of photoelectric yield on photon energy and type of photocathode has not been investigated in any detail except by workers at Leningrad State University. Measurements in the 1.39

to 13.3 Å region have been made by Rumsh et.al.(1960) and in the 23.6 to 113 Å region by Lukirskii et.al.(1960 and 1964).

Detailed investigations into the use of various photocathodes for X-ray astronomy have been carried out by Smith (1968) and Somer and Graves (1969). In the work of Smith the photocathode material was deposited on the detecting surface of a Mullard channel multiplier which acted as an amplifier for the photoelectrons. Measurements of photon detection efficiency for the device for different wavelengths and photocathode materials showed that MgF₂ had the highest photoelectric yield consistent with long term stability. The values obtained for photoelectric yield were in general agreement with those reported by Lukirskii at wavelengths greater than 16 Å.

The efficiency of the channel multiplier as a function of grazing angle after stabilisation of the photocathode is shown in fig.2.6 and the variation in efficiency over a long period for MgF₂ and LiF in fig.2.7 (after Smith 1968). In a similar experiment Somer and Graves measured the photon detection efficiency of a system consisting of a target of photocathode material, the photoelectrons from which were focussed onto a 'spiraltron' channel multiplier. A comparison of efficiencies for different types of photocathode is shown in fig.2.8. No long term stability checks were carried out by these authors, however.

These photocathodes are of particular interest in the soft X-ray region because of their fairly uniform response, high efficiency and lack of fine structure around absorption edges.

2.7 Electro-imaging detectors.

The basic distinction between the various types of electro-

FIG 26.
MAGNESIUM FLUORIDE
(AFTER STABILISATION)

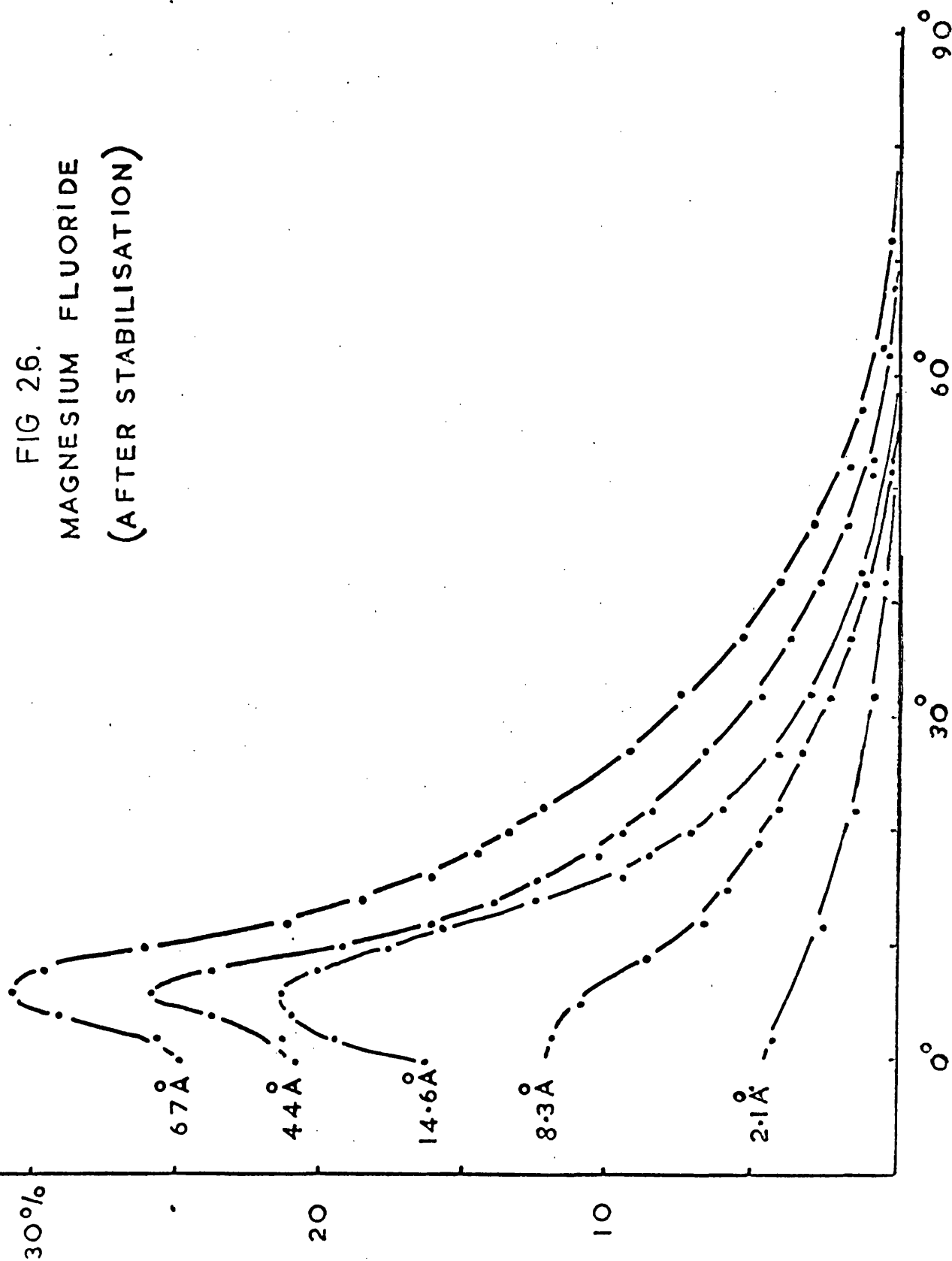


FIG 2.7. PHOTO-EMISSION STABILITY

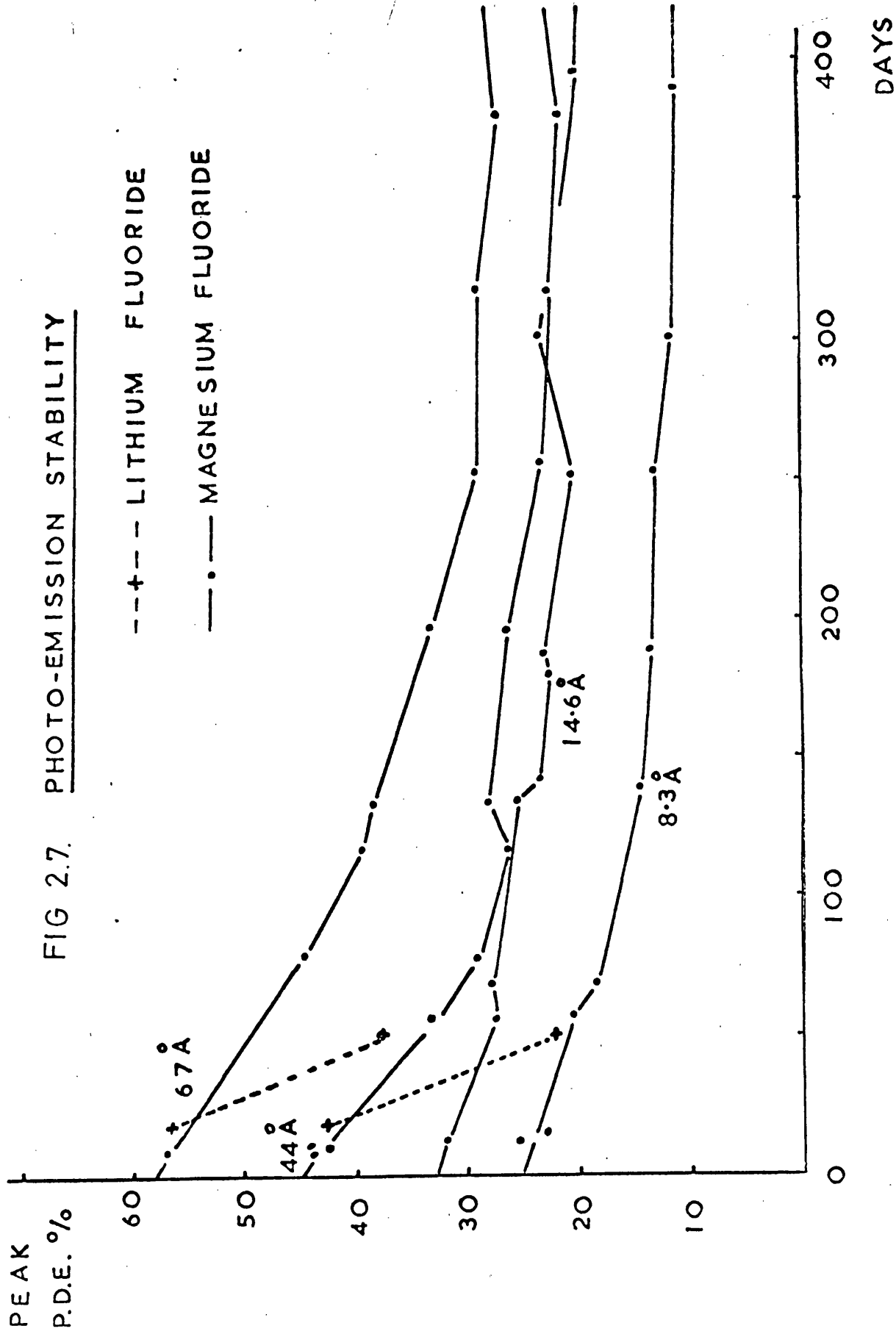
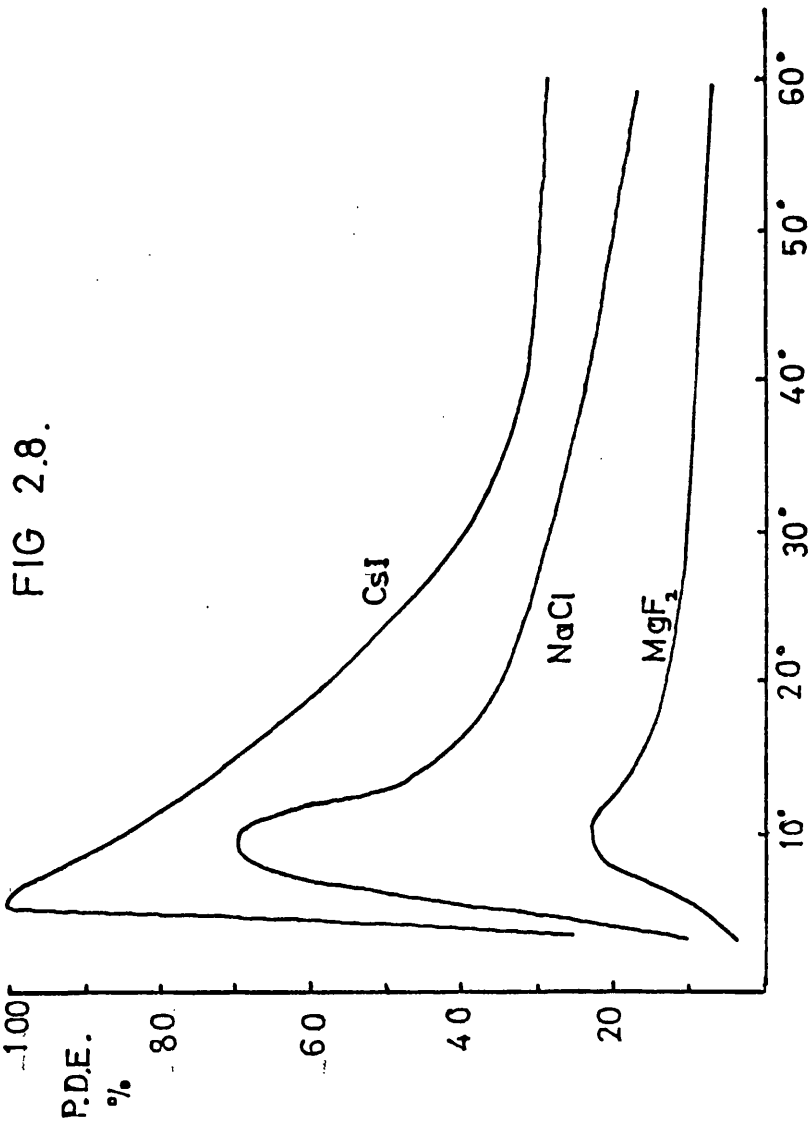


Fig. 2.8.

Measured efficiencies for various photocathodes (after Somer and
Graves).



imaging systems is between integrating and non-integrating devices. In an integrating device photons are recorded and stored, while with a non-integrating system photons can only be recorded if the relevant resolution interval is being scanned.

2.7.1. Integrating detectors.

Other than photographic film, which has been discussed earlier, there are two types of integrating detector. The incoming photon can either be detected and its position recorded directly, or the photon image can be converted to a charge image on an insulator which can then be read out at will.

Into the first category fall the various types of position sensitive proportional and semiconductor counters discussed earlier. The most significant development in this type of detector recently has been the advent of the channel multiplier array.

The single channel multiplier has been used extensively in satellite experiments for the detection of ions, electrons, and UV radiation, although not X-rays to date. (see for example Burrous et.al., 1967, Tetry et.al. 1969). Arrays of single channels have been used in which each channel triggered a bistable thus allowing a limited amount of integration between readouts (Waters, 1964). Recently, however, arrays of straight single channels with a pitch of 50 μm have become available commercially from Mullards Ltd. A similar device has been developed by Bendix Ltd., the 'spiraltron' which has a higher gain but rather poorer spatial resolution.

They have been proposed for use in several forms of scanning type imaging devices which will be discussed later. The object of the work reported here was to investigate the use of such an array as an individual photon detector with the object of producing an

integrating imaging device for soft X-rays.

Channel multiplier arrays have also been used as a means of reducing exposure times for photographic film. The image incident on the array is converted to an electron image at the output of the array with a gain of 10^4 or more. The electrons are then accelerated onto a phosphor in intimate contact with the film. This method has been developed successfully for X-rays by Guest et.al.(1969) and has been incorporated in an increased sensitivity field ion microscope by Turner et.al.(1969).

An alternative method of integration is the conversion of the X-ray image to a charge image on an insulator. The image can then be read out in a number of ways of which the most commonly used is that of electron beam scanning. The charge on the insulator is neutralised by the beam and the information can be extracted either from the scanning beam (as in the vidicon), or the returned beam component, either before stabilisation (image isocon) or after stabilisation (image orthicon). (see for example the review paper by Livingstone,1967.) The spatial resolution of a typical system is about 20 μm with a sensitivity corresponding to about 20 electrons leaving the photocathode.

An alternative method of readout of the stored charge image in one dimension has been reported by Boksenberg et.al.(1968a,b) in which a vibrating reed, positioned just above the surface of the insulator is scanned over the image. The charge on the surface induces a charge on the scanning head at the frequency of vibration of the reed, and the resulting signal is amplified. The major attraction of this device is that the image is not destroyed in the

readout as is the case with the scanning electron beam type. the best spacial resolution obtained was about 60 μm with a sensitivity giving a signal to noise ratio of 3 for a charge of 100 electrons.

The disadvantage of this method lies in its lack of sensiiivity. If the X-ray image is converted using a photocathode and the photoelectrons used directly to form the charge image, the limit of detection of 100 electrons corresponds to about 100 detected photons. This limit may be improved by the use of a scintillator/photocathode rather than the simple photocathode, or an intermediate stage of amplification using, for example, a chennel array.

In any of these methods, the distribution of heights of the charge pulses means that there is some ambiguity in the number of detected counts per picture point. Work on this type of system is being undertaken by Giacconi et.al.(1969) for flight on a proposed ATM (Apollo telescope mount) mission.

2.7.2 Non-integrating detectors.

In a non-integrating detector the X-ray image is scanned by a small aperture detector such that the whole image is recorded. The spatial resolution is governed by the size of the detector aperture while the sensitivity is that of the detector used.

There have been many examples of this type of detector in X-ray astronomy with various types of gas counters, scintillation and photoelectric detectors being used. In particular the Leicester group, in cooperation with University College, London has an exp-

eriment on the OSO-5 satellite consisting of a focussing mirror and small aperture proportional counter. The mirror has a narrow field of view (2 arc minutes) and the spacecraft provides a 'raster' scan of the sun. Further details of this experiment are included in chapter 6 in which the operating characteristics of the proportional counters are described.

Paolini et.al.(1968) have described a similar experiment on the OSO-D satellite in which a grazing incidence telescope focusses the X-rays onto a CsI photocathode. The photoelectrons released are accelerated through 10 kv and detected in a plastic scintillator. One arc minute resolution is obtained using a small aperture and the spacecraft again provides a raster scan of the sun.

A variation on this system has been described by Ballas et.al.(1968) and which is intended for use on future ATM missions. The image formed by the mirror is detected in a $\text{CaF}_2(\text{Eu})$ crystal which is coupled to an electrostatic image dissector by fibre optics. Voltages applied to the focussing plates of the dissector, scan the image across a small aperture, the part of the image transmitted through this aperture being passed to an ^{electron} multiplier tube. A lower limit to sensitivity of 0.4 electrons per incident 8.3A photon has been quoted for the crystal.

A similar device using a channel multiplier rather than a discrete dynode photomultiplier has been described by Abraham et.al. (1967). Channel multiplier arrays have also been proposed for imaging systems of this sort. The X-ray image is converted to an electron image, preserved in the array, and then detected on a phosphor screen viewed by a television camera.(see for example Giacconi et.al.(1968) and Guest et.al.(1969)). No detailed analysis

of the sensitivity of any of these instruments has yet been published.

The principle disadvantage associated with scanning systems is the loss in time resolution. Each scan element must be viewed long enough for adequate counting statistics to be obtained. Reduction in the number of elements in the scan increases the count rate per element and thus improves the time resolution with a consequent loss in spatial resolution. The reason for the popularity of scanning systems, however, is that they are in general easier to construct and operate successfully.

CHAPTER 3. EXPERIMENTAL TECHNIQUES AND APPARATUS.

3.1 Introduction.

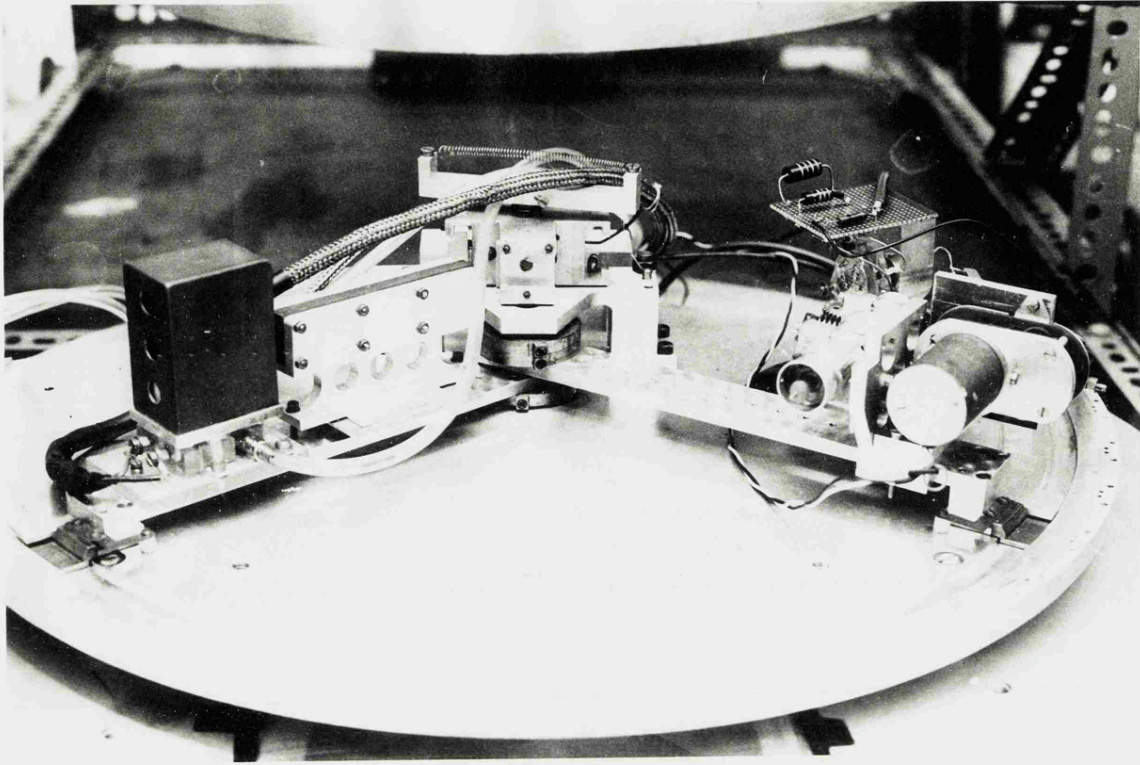
Since channel multipliers will only operate in a vacuum, all the experimental investigations were carried out in one of the three vacuum systems available. Studies of the X-ray response of the channel multiplier array were conducted in a vacuum chamber containing a plane crystal spectrometer and X-ray source, the investigation of the imaging properties in a chamber containing only a source and a means of collimating the beam, and the investigation of long term effects on an array under high vacuum in an ion pumped chamber.

The plane crystal spectrometer was also used in the investigation of the proportional counters subsequently flown on the O.S.O. - 5 satellite and described in Chapter 6.

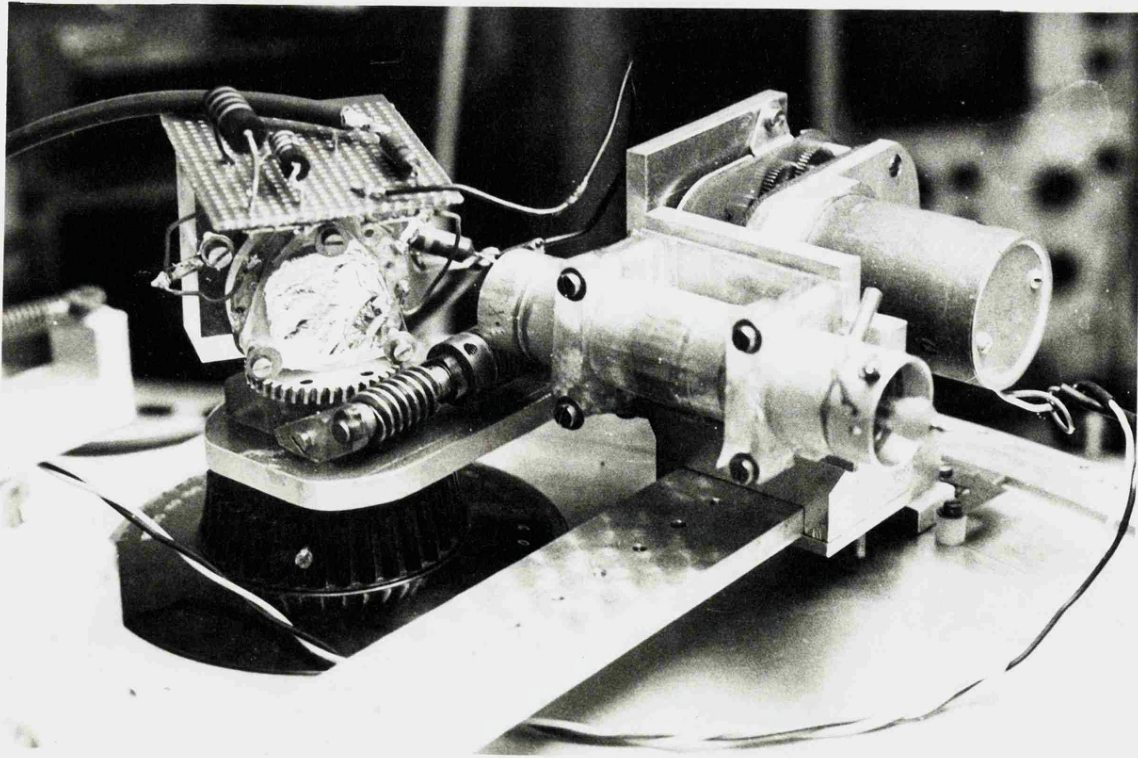
3.2 The plane crystal spectrometer.

A general view of the spectrometer is shown in plate 3.1a. The source consisted of an aluminium anode, on which various materials were placed to give characteristic line emission, bombarded by electrons from a filament. Normally in this type of source the filament is held at a negative potential and the anode is earthed. This has been found to give a high noise level in channel multipliers, due to electrons, and consequently the anode was maintained at a positive potential, the cooling water being pumped round a closed insulated system.

The X-rays were collimated to 10 arc minutes



a



b

PLATE. 3.1

in a horizontal direction using a Soller collimator and allowed to strike a 2 sq. cm. crystal. Provision was made for different crystals to be used, without demounting, in the rotating crystal holder. A potassium acid phtallate crystal, (2d spacing 26.6 Å) was used for short wavelengths, 5 to 15 Å, while a lead stearate crystal, (2d spacing \approx 100 Å), was used for longer wavelengths. The crystals and the collimator could be lined up very easily with an autocollimator.

The vertical spread of the beam was determined by the detector aperture used, typically 1 mm. diameter, which subtended an angle of \approx 16 minutes of arc at the source, after reflection from the crystal. The two arms of the spectrometer could be locked together to provide a manual 'Bragg scan', or could, alternatively, be moved independently. Ports in the baseplate provided access for source cooling water, detector gas and electrical connections. The tank was pumped through a liquid nitrogen trap by a 5 ins. silicon oil diffusion pump to pressures of the order of 10^{-5} torr.

A full description of the spectrometer and of the use of lead stearate crystals for ultra soft X-rays has been given by Charles (1968).

3.2.1 Modification of the detector mount.

During the investigations into the response of the array it was necessary to compare the count rate in the array with that of a monitor proportional counter for a given incident flux of X-rays, and also to rotate the

array about an axis perpendicular to the beam. The unit designed to accomplish this is shown in Plate 3.1b. Once an emission line had been identified, the source arm was locked, and rotation of the detector arm allowed either the proportional counter or the array, positioned at the same distance from the crystal, to be induced into the beam.

No vertical movement was provided for, the height of the proportional counter and the array being adjusted to be at the centre of the beam. A D.C. motor was used to rotate the array about a vertical axis along one of its diameters, and a calibrated scale provided a measurement of angle to better than 0.5° .

3.2.2. The use of characteristic emission lines.

The continuum emission available from a small source such as the one used here is low in intensity, giving a count rate little more than that due to cosmic rays in the proportional counter. The wavelengths used, therefore, were restricted to those obtainable using the characteristic emission lines of light elements.

The physical nature of the target material for maximum intensity was found, by experience, to be different for different materials. Nickel and Molybdenum were used in the form of thin sheet, aluminium, copper, boron and zinc as a powder, while Carbon K radiation could be obtained very readily due to the formation of carbon layers on the target during operation. In addition

2.1 Å X-rays were obtained from an Fe 55 K captive source, the range of wavelengths then extending from 2.1 Å to Boron K radiation at 67 Å. Since these emission lines have well established wavelengths, the geometrical measurement of source and detector arms was not critical.

3.2.3. Measurement of the X-ray flux.

In order to make measurements on the absolute efficiency of a detector, the X-ray flux in the beam must be measured. The technique used for doing this is based on the method described by Smith (1968) for the calibration of proportional counters. The incident flux is measured using a thin window proportional counter whose efficiency can be calculated. The efficiency of such a counter is given by:

$$Z = k \cdot \exp(-\mu_w x) (1 - \exp(-\mu_g x))$$

where 'Z' is the photon detection efficiency, μ is the linear absorption coefficient and 'x' is the path length in the material. The subscripts 'w' and 'g' refer to the window material and the gas. The factor 'k' represents the fraction of the photons which are absorbed in the gas and subsequently detected.

Clearly, for an accurate measurement of flux a high transmission through the window and a high absorption in the gas is desirable and 'k' must be known. For short X-ray wavelengths the window was of 4 µm melinex with 1000 Å of Al. on one surface while for wavelengths longer than 8 Å, 2 µm 'makrofol' with a similar thickness of Al. was used. Since the uniformity of this material was quoted by the

manufacturers to be better than 10%, it was not necessary to measure its transmission. A piece of identical material was placed in the beam in front of the detector under test, attenuating the beam by the same amount as for the monitor counter.

As a filter of some kind is required on the array to eliminate stray ions, electrons and UV, it was convenient to use a window sample for this purpose. The aluminium on the window is placed in intimate contact with the counter body so that charge does not build up on what would otherwise be an insulator, thus destroying the field uniformity in the counter. Under these conditions the factor K is essentially unity.

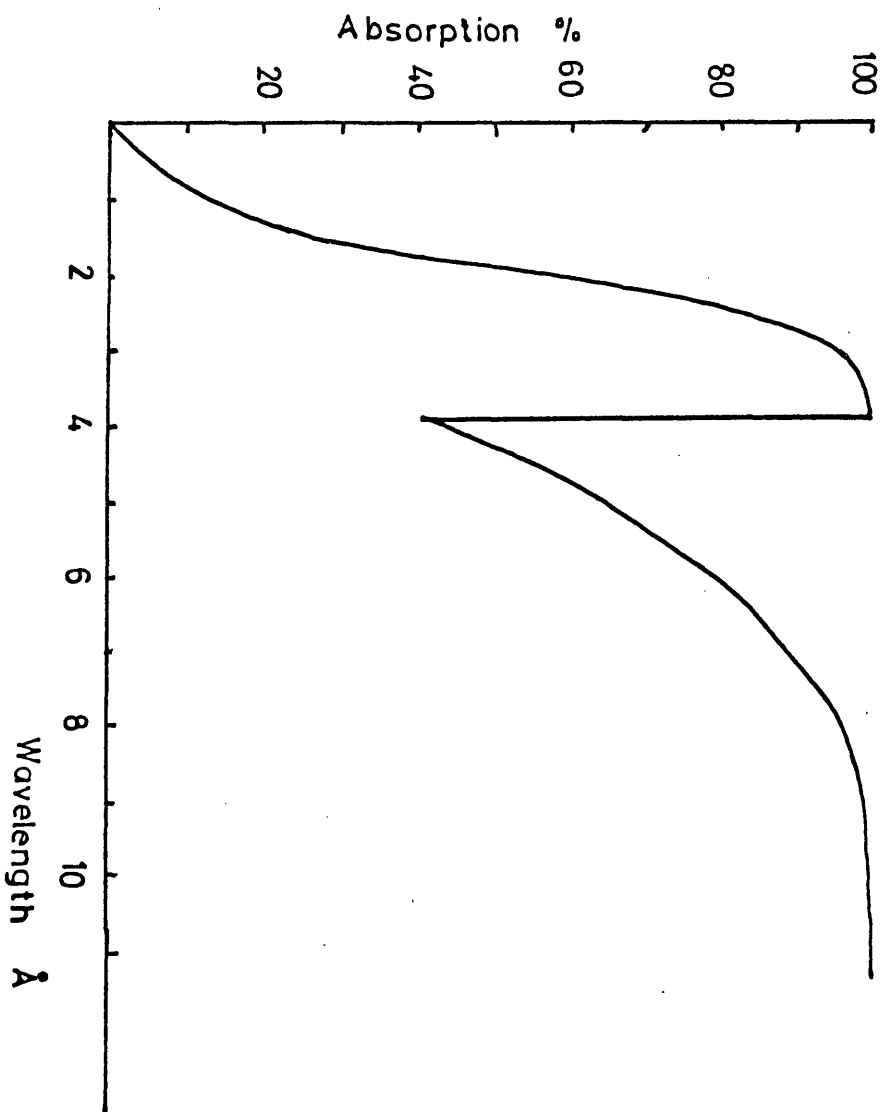
The window material was sandwiched between the body of a cylindrical proportional counter, type PX 28 K* fitted with gas flow tubes, and a piece of 0.004" brass shim in which was drilled a small, accurately measured hole of about 1mm. diameter. This shim was arranged so that the hole coincided with the hole in the counter body and was then glued to it.

The gas used in the detector was normally Argon/Methane 90:10, but at longer wavelengths Argon/Methane 25:75 was used to allow the X-ray to penetrate well into the counter body before interacting with the gas, thus further reducing any window charging effects.

So, from knowledge of the area of the window aperture and the depth of the gas, the flux in the beam,

* " 20th Century Electronics".

FIG 31.



after passing through the window sample, can be calculated.

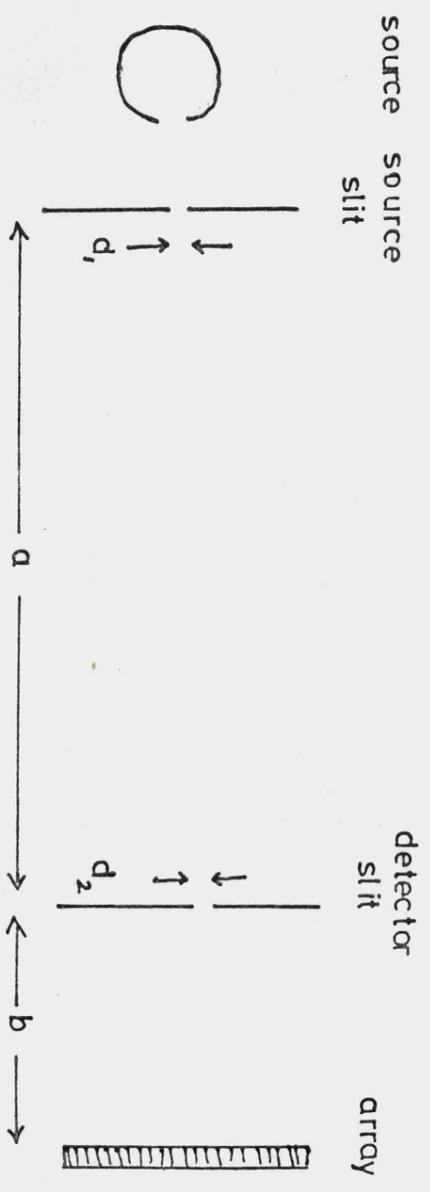
A correction for wavelengths less than 10 \AA had to be applied for the absorption factor in the gas, due to photons at this energy having a non-zero probability of penetrating right through the counter and being absorbed in the wall. This factor is shown in fig 3.1. (Cooke and Stewardson, 1964).

3.3 The collimated X-ray source.

The second of the available vacuum systems is shown in plate 3.2. Originally designed as a focussing crystal spectrometer, the source alone was retained in the chamber and the detector mount completely redesigned. The source, consisting of a copper anode bombarded by electrons from a filament, was used in the same way as that in the plane crystal spectrometer and was of an essentially similar design. Again the anode was maintained at a high potential, the cooling water being pumped round a closed system to prevent leakage to earth through the water. The chamber was evacuated through a nitrogen trap by a 4 ins. silicon oil diffusion pump giving an operating pressure of 10^{-5} torr, which was measured with an ionisation gauge.

X-rays from the source were collimated by two slits positioned in front of the source and detector as shown in plate 3.2 and fig 3.2. The source slit was placed immediately in front of the source and was earthed. The detector slit was separated from the detector carriage on which it was mounted by a perspex spacer, allowing the

FIG 3.2.



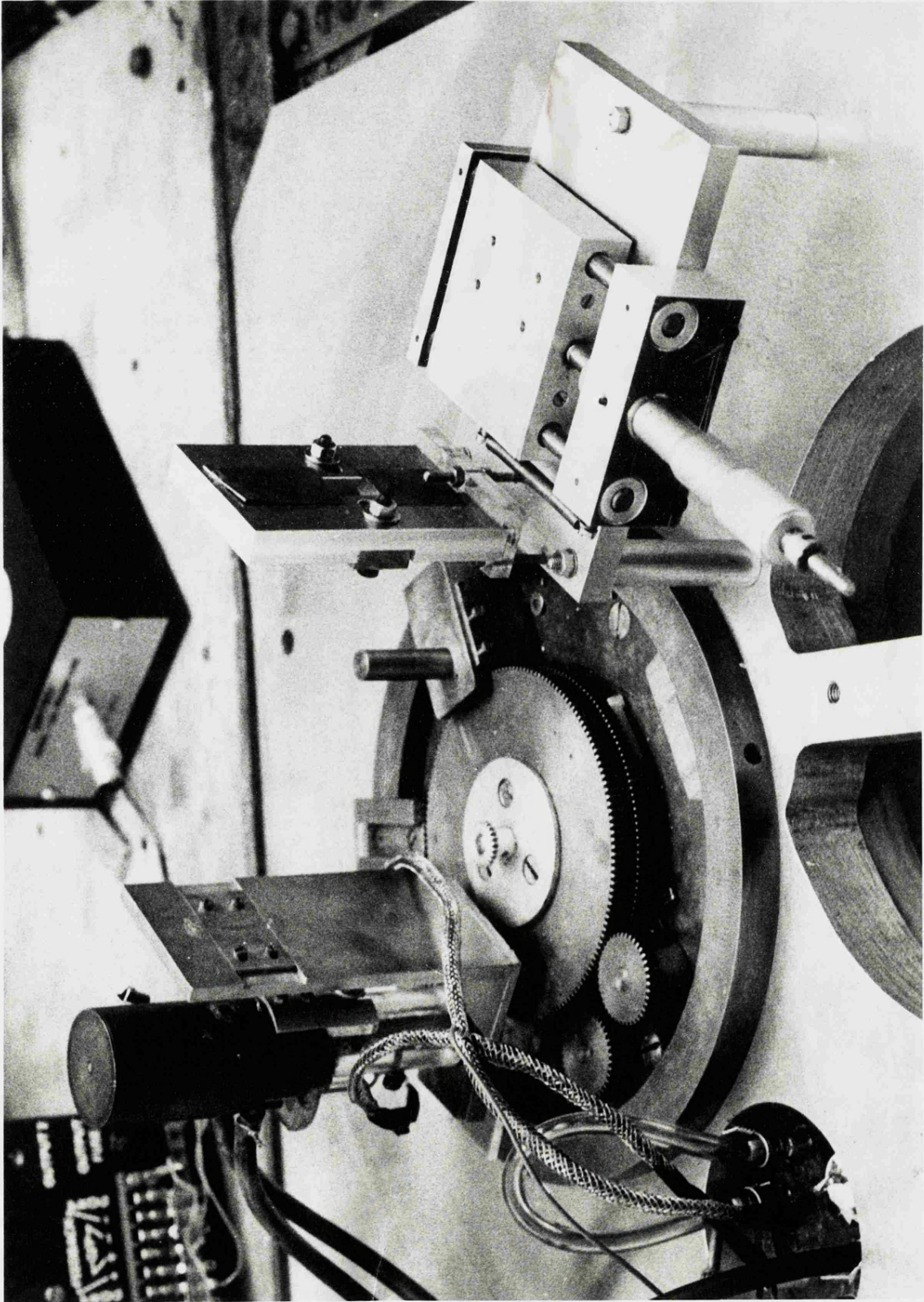


PLATE 3.2

voltage of the slit to be varied to eliminate spurious counts in the detector due to secondary emission.

Referring to figure 3.2 it can be shown, using simple geometry, and assuming a large source area, that the beam width, t , at the detector is given by:

$$t = \left(\frac{a+b}{a} \right) (d_1 + d_2) - d_1$$

where the parameters are those shown in the diagram,

There are several effects which contribute to inaccuracies in the calculation of the beam width.

a) Irregularities in the finish of the slits. This effect is fairly small and has been neglected.

b) Skew in the slits resulting in a wedge-shaped beam. With careful alignment this can be reduced to a negligible amount.

c) Error in measuring the width of the slits.

d) Errors in alignment.

e) Diffraction at the slits. A simple calculation shows that this effect is much smaller than either c or d and consequently has been neglected.

The largest errors are those from c and d, the other effects being negligible in comparison. The slits and detector were aligned optically by viewing a source of light through the array, which has a high optical transmission. In order to do this, however, the slits had to be at least 1 mm wide. To get a narrow beam therefore, the alignment was completed and then the slits narrowed and

their width measured with a feeler gauge; the narrowest slit width that could be measured with any accuracy was 25 μm with an error of 10 μm . With the restrictions imposed by the size of the chamber the narrowest attainable beam width was thus 40 μm which was adequate for most of the investigations. An error of 20 μm was estimated, a check with photographic film showing that the beam width was uniform over its length (approx. 1 cm.) and within the error margin. The vertical spread in the beam was defined by the detector window and gave a beam height of about 1 cm. at the detector, over which distance the intensity was uniform.

3.3.1 The detector mount.

In order to investigate the linear X-ray resolution of the array a method of moving the detector in the narrow beam from the slits to an accuracy of better than 10 μm was devised and is also shown in plate 3.2. The mount consists of a table arranged to be at the correct height on which is mounted the detector slit. A moving platform, mounted on two ball races, is driven against a spring by a micrometer which, in turn, is driven by a flexible drive from outside the chamber.

The detector was mounted on the platform as close as possible to the detector slit. The measurements were all made with the micrometer driving the platform against the spring to avoid sticking.

3.4 The ultra-high vacuum system.

To demonstrate the viability of channel multiplier arrays for use in satellites, continuous operation in high vacuum to simulate satellite conditions is required. The most convenient way of providing a good vacuum over a long period is with an ion-pumped UHV system.

A 2 litre stainless steel chamber with an electrode port and a Bayard-Alpert ionisation gauge was evacuated with an ion pump and, without baking, a pressure of 10^{-8} torr could readily be achieved. Gold wire seals were used throughout and molecular sieve pumps were used to rough out the chamber.

3.5 The electronics.

3.5.1 The pulse handling electronics.

Because of the limited electron gain of the channel multiplier array, a low noise charge sensitive preamplifier is necessary for accurate measurements on pulse height distributions. The initial work was carried out using the amplifier described in section 3.5.2. After the viability of the X-ray imaging method had been established using these preamplifiers, commercial amplifiers with very low noise figures were introduced (Ortec type 118A). These have a quoted noise figure of 175 rms electrons for zero input capacity, with 2 μ s shaping time constants.

On occasions it was necessary to use a high voltage blocking condenser if the detector anode was not earthed. In these cases a Tennelec 100B valve preamplifier was used

because of its insensitivity to transients. Absolute gain measurements were made by the use of a standard pulser, Ortec 204, and a calibrated charge termination.

The pulses from the preamplifier were amplified using a Harwell 2000 series amplifier, 2151, which, with a noise referred to the input of 7 uv rms, contributes a negligible further noise to that of the preamplifier. The pulses could then be fed either via a single channel analyser to a scalar and ratemeter, or to a multichannel analyser. The scalar, Harwell 2117, had a resolving time of 1 μ s, and the multichannel analyser had a maximum of 256 channels, and facilities for coincidence counting and multichannel scaling. The units used in the experimental work are listed in table 3.1.

Table 3.1.

<u>Unit.</u>	<u>Type.</u>
Low noise preamplifier.	Ortec 118A. Tennelec 100B.
Main amplifier.	Harwell 2000 series, 2151.
Single channel analyser.	Harwell 2170.
Scalar.	Harwell 2117.
Ratemeter.	Harwell 2134.
Timing unit.	Harwell 2219.
Precision Pulser.	Ortec 204.
Multi-channel analyser.	Northern Scientific, NS-600 with X-Y plotter.
EHT unit..	Harwell 2147, 0-3 kv.
Oscilloscope.	Advance OS 2100.

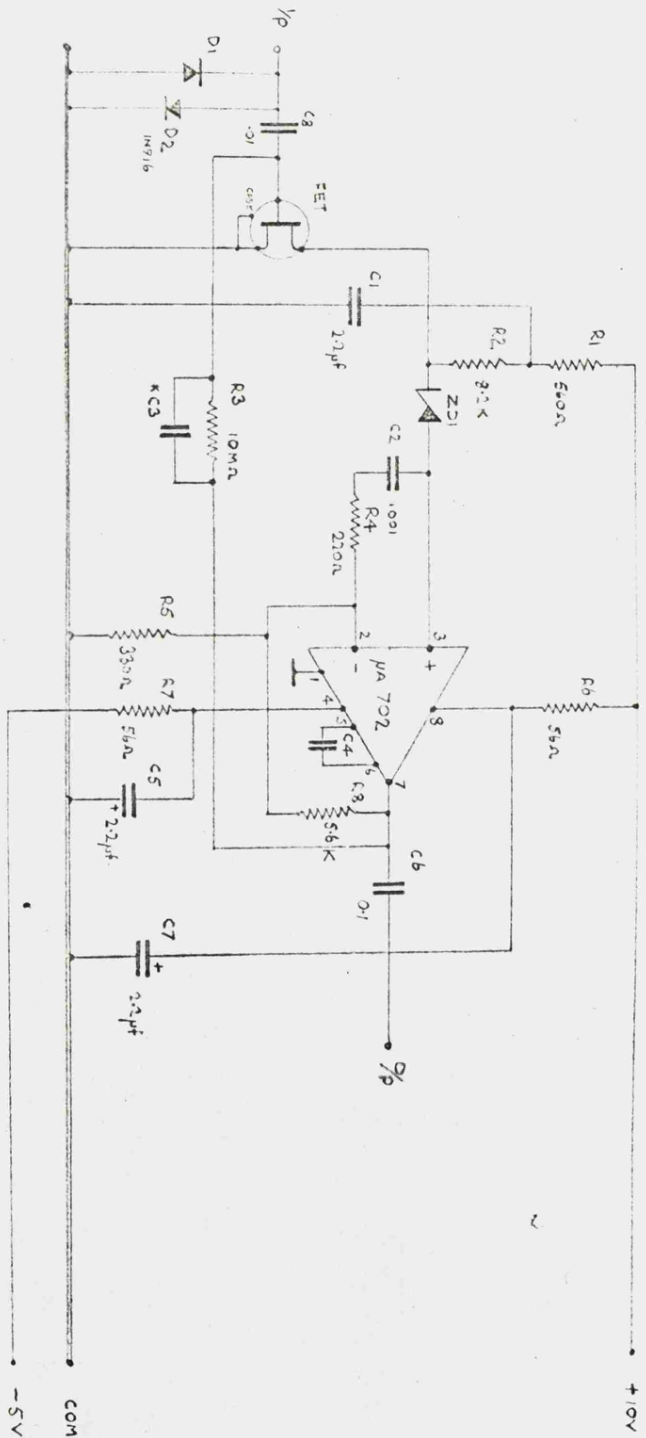


FIG. 33 The preamplifier.

All these units had a quoted stability of better than 1%, and, in addition, the Harwell EHT set could be reset to an accuracy of 1 volt over the range 300 - 3000 volts.

3.5.2. The charge sensitive preamplifier.

In the method of imaging to be discussed in this thesis, it is necessary to have two low noise charge sensitive preamplifiers with fairly well matched gain and input characteristics. For the preliminary investigation of the method a charge sensitive preamplifier was designed, fig 3.3. The input stage consists of a low noise FET, Texas Instruments BFW 56, which provides an initial gain, followed by an integrated circuit amplifier, both enclosed in a feedback loop.

The feedback capacitor, which determines the gain, was the stray capacity of the 10 M Ω resistor in the loop, the resistor also providing the shaping with a fall time for the pulse of about 5 μ s. The noise for zero input capacity was 600 rms electrons and the charge sensitivity approximately 10^{-12} C/volt. An emitter follower, not shown on the diagram, was used to drive the 100 Ω cable to the main amplifier.

3.5.3. Ancillary electronic equipment.

In addition to the units mentioned previously, an X-ray source power supply, designed and built in this department, and giving up to 4 kv anode voltage was used. The emission current was monitored and a servo system stabilised it by varying the filament current. A Telsec 662 pen recorder was available for long term monitoring

of count rate and was particularly useful for investigating the stability of the X-ray source.

A Leybold Elliot ionisation gauge, slightly modified, was used to supply current to a filament which acted as a source of electrons in the UHV system. Low voltage power for the electronics to be described in chapter 5 was provided by Solartron AS 1164-2 double power supplies.

3.6 General experimental techniques.

Before taking measurements using the channel array the pressure in the chamber was allowed to reach $2 \cdot 10^{-5}$ torr or less, thus eliminating any variation in operating characteristics with pressure. (A small variation in pulse height distribution was apparent with a change in pressure from 10^{-5} to 10^{-4} torr).

The X-ray source was allowed to stabilise after switching on, experience having shown that after a ten minute 'burning in ' period, the emission drop^{ped} very slowly over a period of several hours and this slight fall could easily be corrected for. It was found in practice that considerable care had to be taken in shielding cables inside the spectrometer to avoid increased noise in the highly sensitive preamplifier. Operation during times when imperfectly suppressed machinery was in operation was avoided.

An earthed screen of aluminised melinex extending laterally outwards from the crystal in the spectrometer, and the source slit in the the collimated X-ray source ,

was used to prevent electrons, ions and scattered UV from reaching the array. During measurements of gain and pulse height distribution, regular checks were made on the zero level and linearity of the multi-channel analyser using the standard pulser, which in turn was calibrated using a digital voltmeter. Fuller details of experimental techniques applicable to particular sections of the work are given in the relevant chapters.

CHAPTER 4. THE OPERATING CHARACTERISTICS OF CHANNEL MULTIPLIER

ARRAYS.

4.1 Introduction.

In its simplest form, as first described by Wiley and Hende (1962), the channel multiplier is a straight glass tube having a length to diameter ratio of between about 50 and 100, the diameter being anything from less than 0.1 mm to more than 1mm. The inside surface of the tube is coated with a semi-conducting material which has suitable secondary emission characteristics for an electron multiplication process.

With a potential difference applied between the ends of the tube, any secondary electron emitted from the mouth, due for example to an X-ray, will be accelerated, and on striking the wall again will produce other electrons. This process results in a pulse at the exit end of the tube containing between 10^8 and 10^{10} electrons under typical operating conditions. For a straight tube however, ions generated from the residual gas in the final stages of the avalanche can reach the entrance with sufficient energy to liberate a secondary electron, resulting in a second pulse, and this process can continue for up to 4 or 5 avalanches. Thus, the pulse height distribution is very pressure sensitive, but due to a progressive charging up of the channel wall, the distribution becomes saturated giving a peak with a f.w.h.m. of typically 40%.

In a paper in 1965, Evans described a curved channel multiplier in which the ions cannot travel a sufficient distance before striking the wall to gain enough energy to liberate a secondary electron. Curved channels are thus insensitive to pressure but give a slightly lower gain with a f.w.h.m. of 50%. Because of their

insensitivity to variations in pressure, curved channels have superseded straight ones in most applications. Considerable evidence concerning the nature of the pulse height distribution and efficiency of the curved channel multiplier for ions, electrons and X-rays has accumulated since 1965. (see for example Schmidt and Hendee (1966), Adams and Manley (1966), Egidi et.al.(1969), Smith (1968)).

In 1968 the first published work appeared on the channel multiplier array (Smith, 1968,b). Early arrays were manufactured from lead or soda glass and had a pitch of between 50 and 200 μ m. These experimental devices have now been replaced by commercially available arrays marketed by Mullards Ltd.. Both types consist of an array of straight channels with a length to diameter ratio of between 20 and 100, the channels being very regularly spaced in the later types (Guest et.al. 1969).

Work along similar lines by Bendix Ltd. has resulted in the 'Spiraltron' channel array, similar in principle to the Mullard device, but in which the individual channels are in the form of a spiral. Although the spiraltron has the advantage of giving a considerably higher mean gain and a peaked pulse height distribution rather than the exponential of the straight channel array, the spatial resolution is only about 1 mm compared to the 40 μ m of the Mullard array.(Somers and Graves, 1969).

In this chapter the operating characteristics of the Mullard channel array are described, and in particular its response to X-rays. Two arrays, both of lead glass, loaned from Mullards, were available for the work. Array A was an experimental type G 20 in the form of a circular disc of diameter 2 cms. Precise details of the pitch of this array were not available from the manufacturer but measurements indicate that the bore of the channels is 40 μ m or less.

The length to diameter ratio was about 50. Contact to each face of the array was made by an evaporated gold layer, the resistance between faces being about 100 M Ω .

Array B was a commercially available type, G 40, of 2.7 cms. diameter, the pitch of the channels being 50 μm and the bore 40 μm . The disc was 1.6 mms deep giving a length to diameter ratio of 40. The total resistance between the faces of the disc was 100 M Ω indicating a resistance per channel of about $2.10^{13}\Omega$. Contact to the faces of the array was made via a deposited layer of nichrome.

While the individual channels in array A were perpendicular to the face, in array B they were inclined at about 13° to the normal.

Since the object of the work was to investigate the properties of an array for use as an imaging X-ray detector, it was decided to use array A, the non-standard one, for the imaging and life testing work, while array B was used for a more careful study of response to various types and energies of radiation. Neither the imaging properties or the operational lifetime would be expected to be critically dependent on the dimensions of the array.

All the experimental work reported in this chapter was carried out in the plane crystal spectrometer, with the exception of that described in sections 4.5 and 4.6 in which the collimated X-ray source and the ultra-high vacuum system were used .

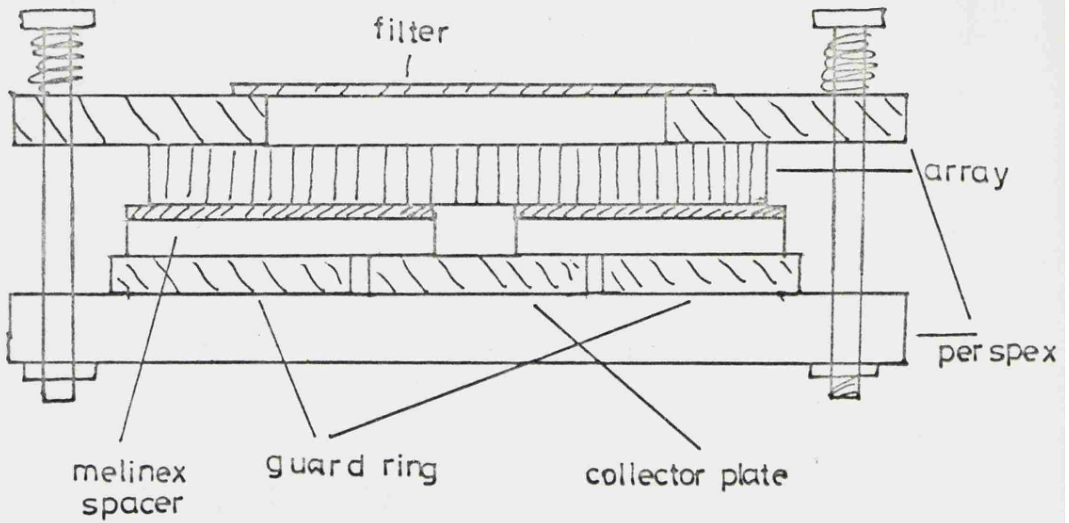
4.2 The detector mounts.

Array A.

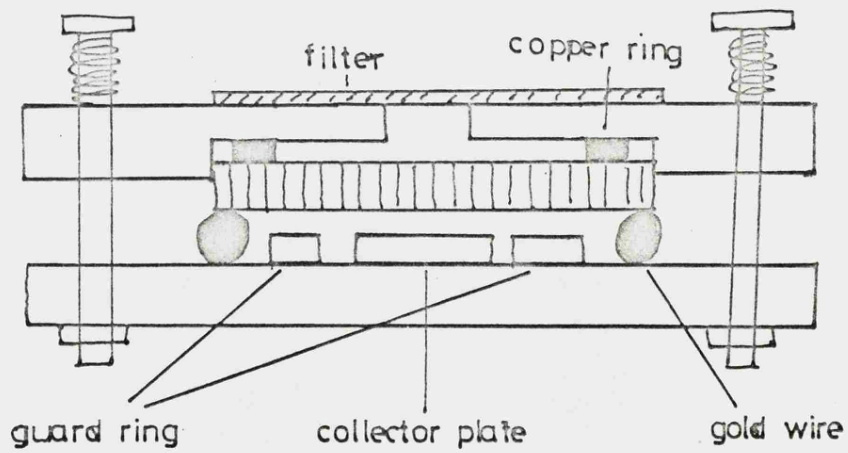
Contact to the faces of the array could be made quite easily and several different methods were used. For most of the

FIG 4.1.

A



B



work, however, the array was glued in position over a hole in a perspex plate using a rubber solution. The contact to the front face consisted of a thin piece of copper shim lightly sprung onto the array. The back contact in the imaging work was made using the aluminised surface of a piece of 12 μm melinex. A sheet of this material with a suitable hole in it provided not only the contact, but also a means of spacing the array from the collector plate by a constant and known distance. Fig 4.1.a.

Array B.

Considerable difficulty was encountered in making a noise free contact to the nichrome faces of the array. Originally a method similar to that used for array A was used but it was found that, after periods of operation varying between minutes and hours, noise pulses began to appear, often in bursts, giving count rates in the electronics of up to 10^4 s^{-1} . These pulses, from their shape, were clearly due to a bad contact.

The most successful arrangement is shown in fig 4.1.b in which contact to the faces was made using metal strips, copper at the front and gold wire at the back, held against the array by light springs. This mounting was not entirely free from spurious pulses and considerable care had to be taken to avoid counting the noise and getting invalid results.

This contact difficulty may be explained by the fact that the array provided by Mullards was imperfect in surface finish compared to later ones, although its detection ability was unimpaired. Another difficulty encountered in correctly lining up the array was due to the 13° angle the channels made to the normal to the face. To determine the response of the array as a function of angle of incidence it was necessary to make the individual channels horizontal.

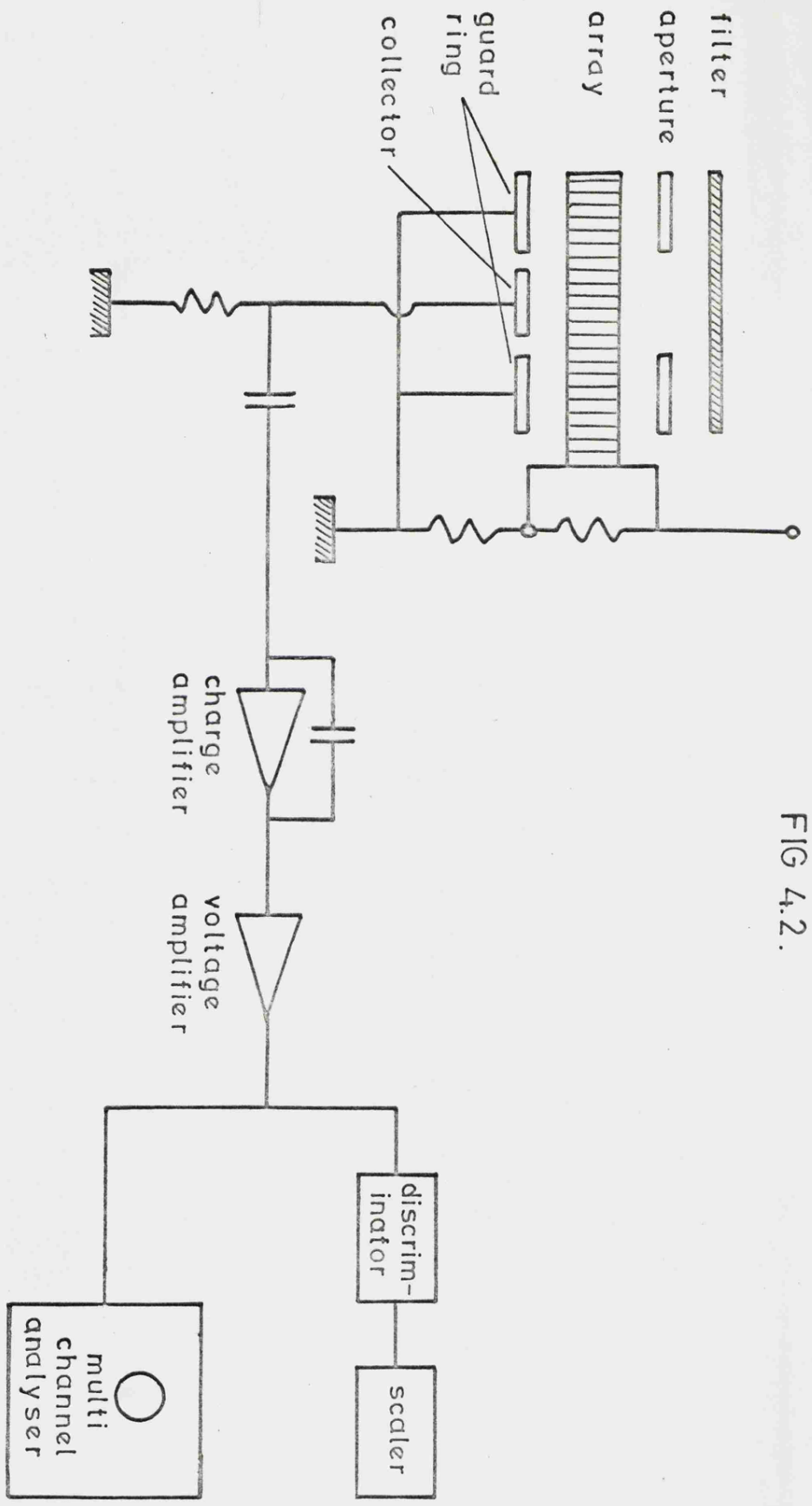


FIG 4.2.

This was achieved by viewing an optical source of parallel light through the array which was rotated until the transmission was a maximum. In this way the channels could be lined up to within only about 2° due to diffraction effects in the array.

For both arrays a thin plastic filter could be positioned over the entrance aperture, thus eliminating any stray electrons or ions.

4.3 The pulse height distributions of the arrays.

4.3.1 Array A.

Before proceeding with the experimental imaging work a brief investigation of the operating characteristics of this array was carried out. The pulses from the centre of the array were collected on a copper plate, surrounded by a guard ring to maintain uniformity of field across the gap, and fed into the Ortec 118 charge sensitive preamplifier. The electrical connections and subsequent electronics are shown in fig 4.2.

The cathode of the array was maintained at a negative potential, the potential divider R_1 , R_2 providing an accelerating voltage across the gap between array and collector. A plastic filter excluded particles and UV radiation.

The pulse height distributions for 8.3 \AA X-rays at various applied voltages are shown in fig 4.3. The voltage across the $300 \mu\text{m}$ gap was found not to be critical but had to be more than about 30 volts for complete collection of the pulses. The upper limit on the voltage on the array is determined by Joule heating, particularly at the contact, and the manufacturers recommended limit was not exceeded. The practical lower limit is the voltage at which most of the pulses

FIG 4.3. PULSE HEIGHT DISTRIBUTIONS FOR ARRAY A

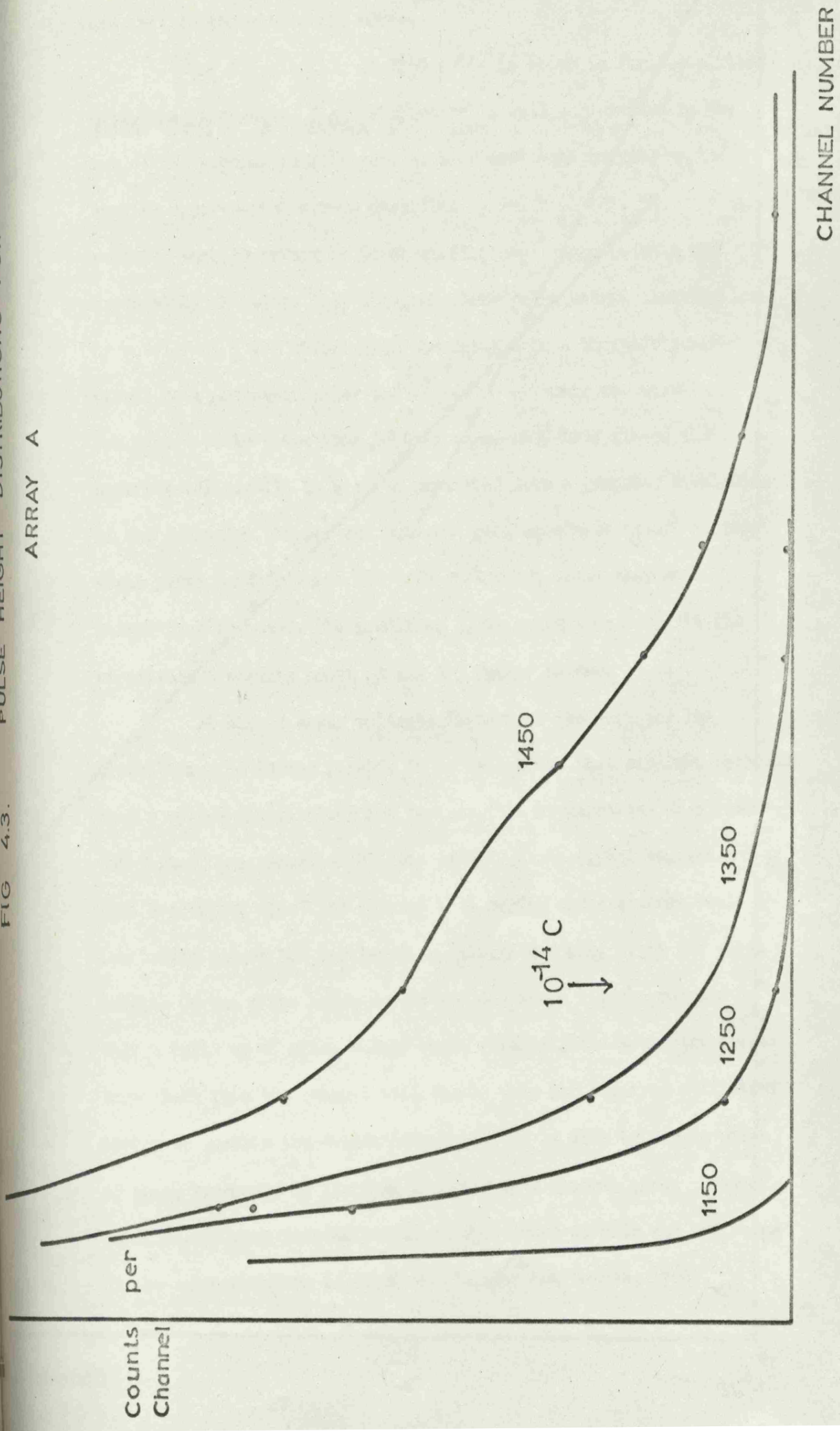
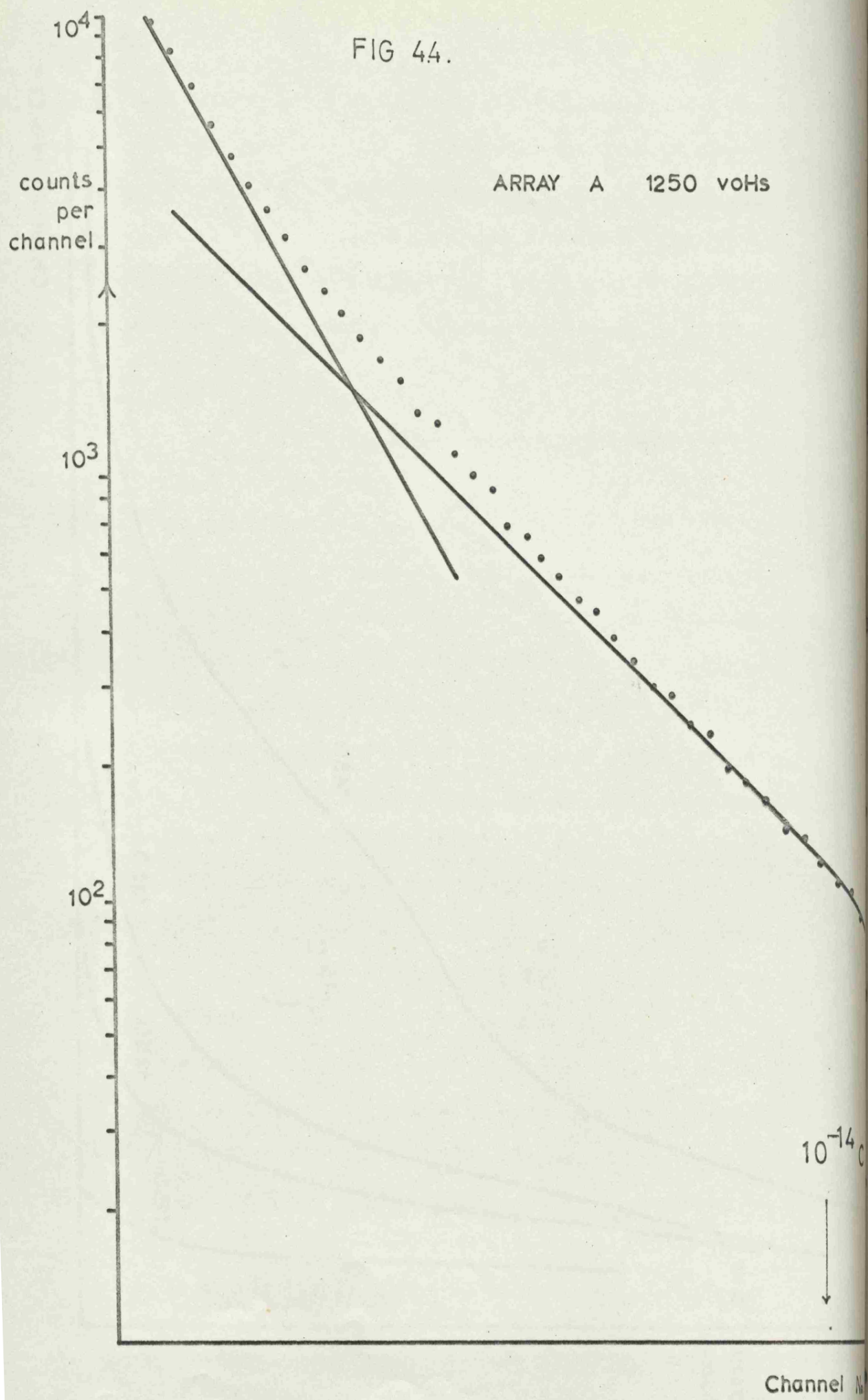


FIG 44.

ARRAY A 1250 voHs



are lost in the electronic noise.

The distribution at 1250 volts is shown in fig 4.4 plotted semi-logarithmically. The distribution is well represented by the sum of two exponentials, in general agreement with results on the earlier experimental arrays described by Smith (1968). The only other reported work on arrays by Guest et.al.(1969) suggests only one exponential function. They obtained their pulse height distributions by accelerating the pulses from the array onto a phosphor screen viewed by a photomultiplier and their sensitivity was considerably worse than in this work. They have fitted their experimental results to a curve predicted from a computer simulation of the avalanche process and obtained good agreement except at very small pulse heights, where the predicted curve shows many more pulses than observed. The predicted curve would appear to fit the experimental results shown in fig 4.3 rather better.

At higher array voltages there is a tendency for the distribution to become peaked. It is well known that straight channels show a peaked distribution and two possible explanations have been put forward in explanation of this effect. Evans (1965) suggested that a charging up of the channel wall during the avalanche would eventually reduce the accelerating voltage and thus limit the pulse height. On the other hand, Bryant and Johnstone (1965) proposed that a build up of space charge would repel emitted secondary electrons back into the channel wall before they had acquired sufficient energy to sustain the avalanche process. To be able to decide which of these processes is limiting the gain in a channel array, however, considerably more information about the spread in gain and the shape of the current pulses is required (Schmidt and Hendee, 1966).

4.3.2 Array B.

The pulse height distributions for array B are very similar to those of array A, but have a lower charge output for the same voltage and do not show a tendency to peak for high voltages. This lower gain is due to the greater length to diameter ratio of array A. A typical distribution is shown in fig 4.5 for a voltage of 1200 volts. The 8.3 Å X-ray distribution is also shown semi-logarithmically in fig 4.6 again demonstrating the double exponential curve.

Each exponential can be represented by an expression of the form:

$$n = N \cdot \exp(-q/\bar{q})$$

where n is the number of pulses of height q , and

N is the number of pulses of zero height.

The factor \bar{q} can conveniently be used to describe the gain and is the statistical mean of the distribution. It can be either by plotting the distribution semi-logarithmically as in fig 4.6 in which \bar{q} is the value of q at which $n = N/e$ or, alternatively, by counting the number of pulses, n_1 and n_2 above two discriminator levels, q_1 and q_2 in which case:

$$\bar{q} = (q_2 - q_1) / \ln(n_1/n_2)$$

The second method was the most convenient way of measuring \bar{q} . The variation of \bar{q} with applied voltage for X-rays for the upper exponential for both arrays is shown in fig 4.7. Results for the steeper, low gain exponential showed no systematic change with voltage. The occurrence of the sporadic noise bursts mentioned earlier, particularly in the low pulse heights where it was not so apparent, was the principle cause of the inconsistent results.

The effect of different exciting radiations on the pulse

FIG 4.5.

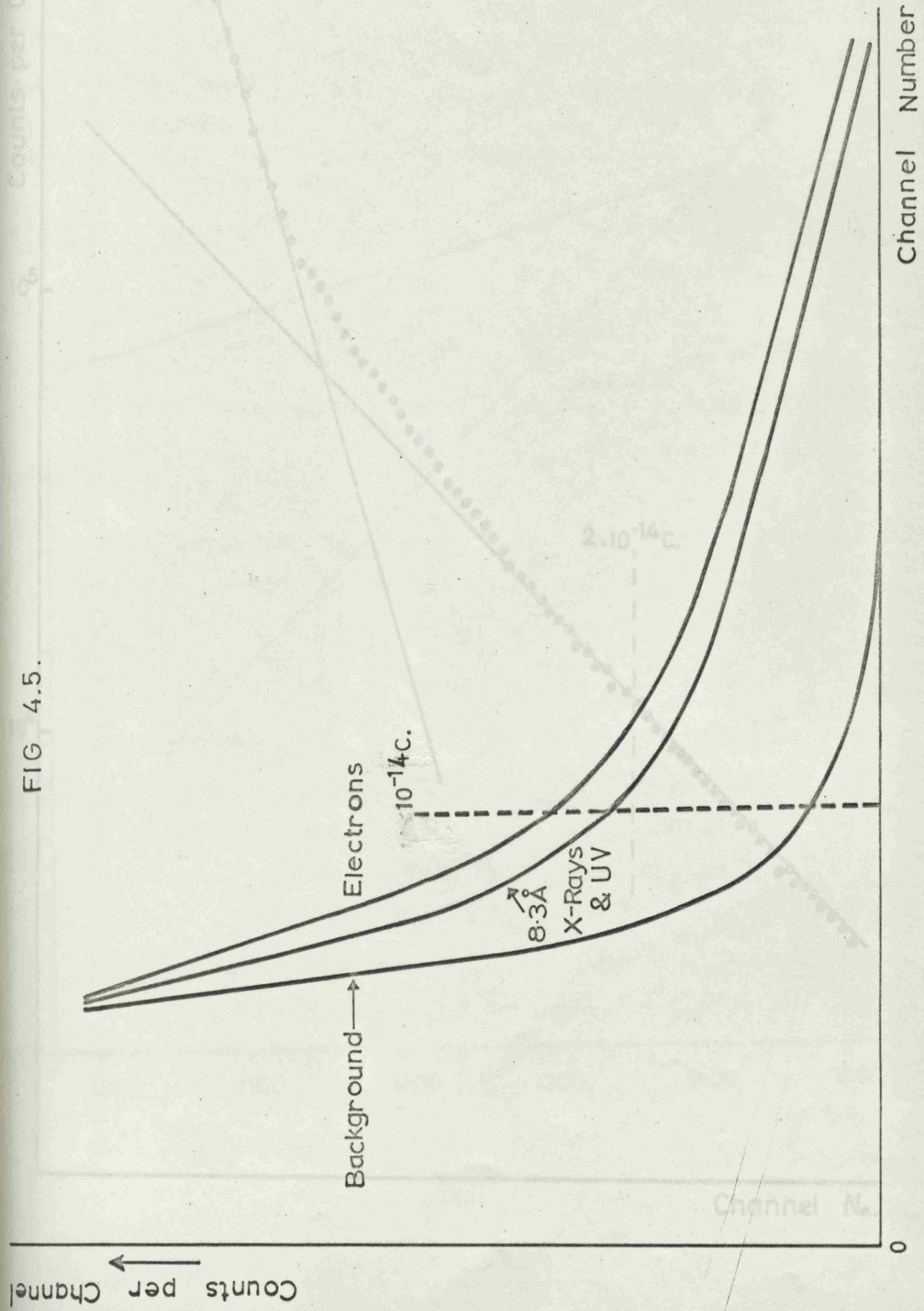
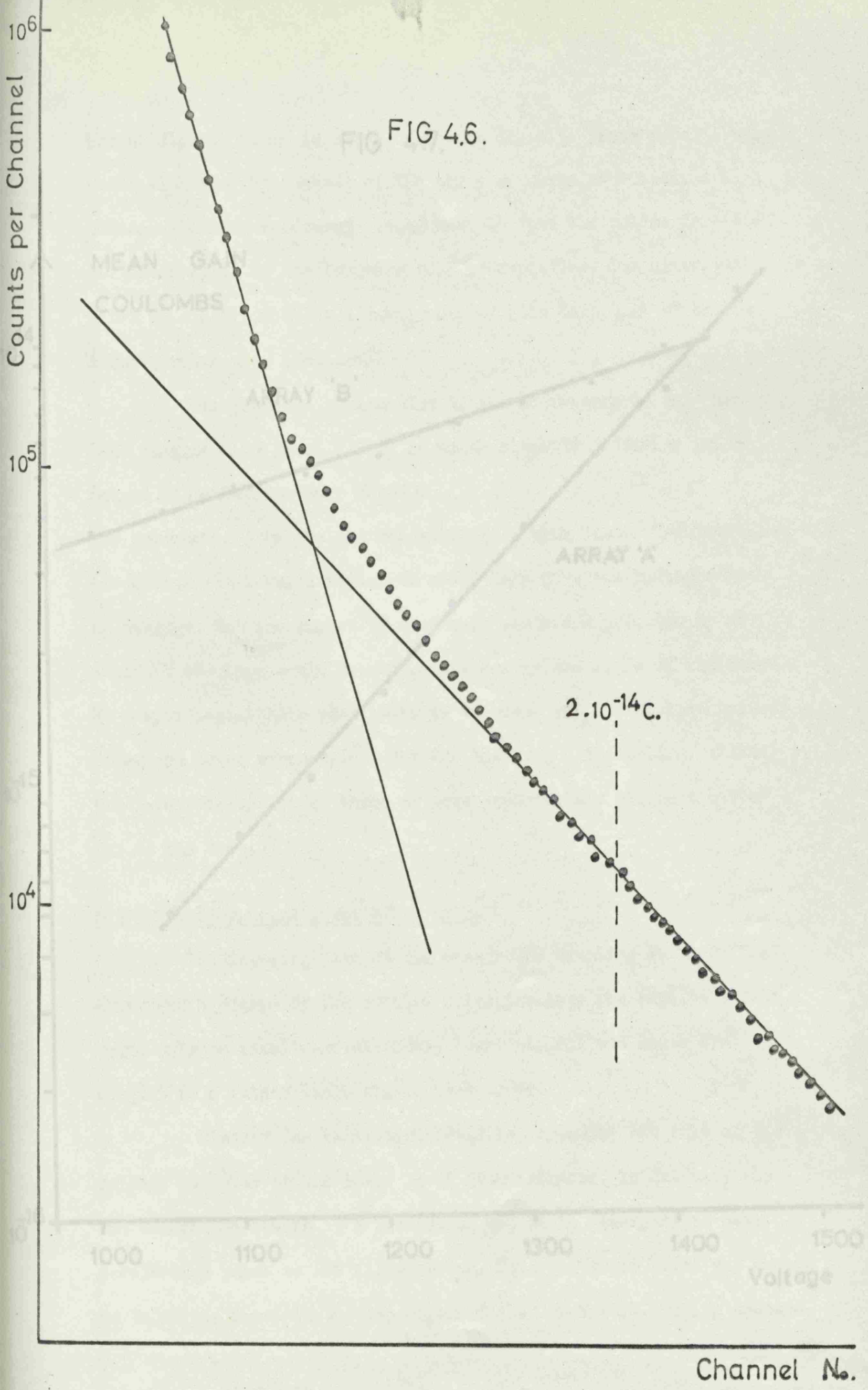


FIG 4.6.



height distribution is FIG 4.7. In Fig 4.5. These results were

taken with the type cathode of the array at earth potential, a high voltage blocking condenser being used to feed the pulses from the given by electrons had a slightly higher gain than that of UV and X-rays, which were identical.

One possible explanation of the difference in gain has been suggested by Ousef (1967) in which slightly differing pulse height distributions were found

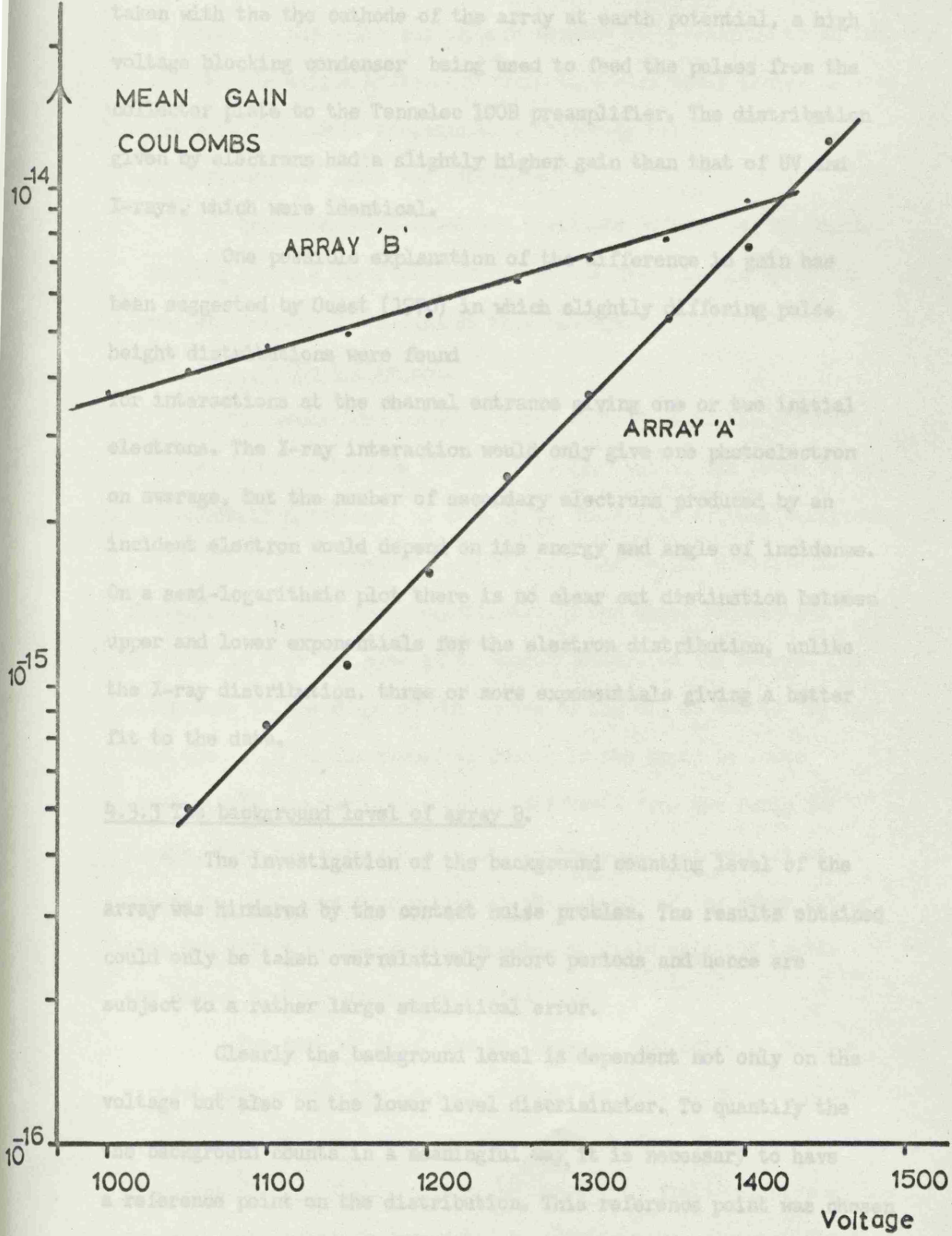
for interactions at the channel entrance giving one or two initial electrons. The X-ray interaction would only give one photoelectron on average, but the number of secondary electrons produced by an incident electron would depend on its energy and angle of incidence.

On a semi-logarithmic plot there is no clear cut distinction between upper and lower exponentials for the electron distribution, unlike the X-ray distribution, three or more exponentials giving a better fit to the data.

5.3.1. Background level of array B.

The investigation of the background counting level of the array was hindered by the contact noise problem. The results obtained could only be taken over relatively short periods and hence are subject to a rather large statistical error.

Clearly the background level is dependent not only on the voltage but also on the lower level discriminator. To quantify the



height distribution is shown, also, in fig 4.5. These results were taken with the the cathode of the array at earth potential, a high voltage blocking condenser being used to feed the pulses from the collector plate to the Tennelec 100B preamplifier. The distribution given by electrons had a slightly higher gain than that of UV and X-rays, which were identical.

One possible explanation of the difference in gain has been suggested by Guest (1970) in which slightly differing pulse height distributions were found for interactions at the channel entrance giving one or two initial electrons. The X-ray interaction would only give one photoelectron on average, but the number of secondary electrons produced by an incident electron would depend on its energy and angle of incidence. On a semi-logarithmic plot there is no clear cut distinction between upper and lower exponentials for the electron distribution, unlike the X-ray distribution, three or more exponentials giving a better fit to the data.

4.3.3 The background level of array B.

The investigation of the background counting level of the array was hindered by the contact noise problem. The results obtained could only be taken over relatively short periods and hence are subject to a rather large statistical error.

Clearly the background level is dependent not only on the voltage but also on the lower level discriminator. To quantify the the background counts in a meaningful way, it is necessary to have a reference point on the distribution. This reference point was chosen to be at the break in the two exponentials for X-rays. During measure-

ments of absolute detection efficiency, it became clear that if all the pulses in the distribution were assumed to correspond to an incident X-ray, the detection efficiency would be unreasonably large, in some cases more than 100%. Consequently, following Smith (1968), the upper exponential alone was considered.

The background level was therefore defined as the counts occurring above a discriminator set at the break in the upper and lower exponentials for X-rays, at that voltage.

The origin of the background.

The background counting rate, defined as in the previous section, for a voltage on the array of 1200 volts, was found to be approximately $5/\text{cm}^2/\text{sec}$. A clue as to the origin of this background can be found from consideration of its pulse height distribution, fig 4.5. If plotted semi-logarithmically the upper exponential is found to have the same gain, approximately, as for X-rays. The difference in the shape of the curves of fig 4.5 is due to the fact that the ratio of the number of counts in the upper to lower exponentials for the background is different from the ratio for X-rays. Thus the background counts in the upper exponential would appear to be pulses originating at the cathode of the array, rather than the effect of thermionic emission or field emission inside the channels which would give a lower gain.

The rate of $5/\text{cm}^2/\text{sec}$ is, however, too large to be consistent with cosmic ray induced counts. The most probable explanation is that scratches or imperfections in the surface finish on the cathode give rise to high field regions, and consequent field emission at the surface. This theory is supported by results taken by Guest (1970) in which the background of an array was studied by drawing the pulses

onto a phosphor and film. Dark areas on the film can be correlated with scratches and imperfections on the array resulting in 'switched on channels', that is, channels which have a very high spontaneous count rate.

The cause of the lower exponential in both background and X-ray distributions is not known. Very careful measurements with high statistical accuracy are needed to determine its origin and relationship to the upper exponential. This was not possible with this array owing to the contact problem.

4.4 Absolute detection efficiencies for array B.

As the pulse height distribution is exponential, it is clear that the detection efficiency is dependent on the position on the distribution of the lower level discriminator. If the pulses in the upper exponential distribution are produced by X-rays while those in the lower are not, then the detection efficiency should be determined from the total number of counts, down to near zero pulse height, in the upper exponential. This clearly will not give a practical value of efficiency. The only practical way of defining efficiency is to consider the total number of pulses in the upper exponential which occur above the crossover point in the two curves.

Thus, with the array voltage fixed at 1200 volts, the distribution was obtained on a semilogarithmic plot and the discriminator set at the crossover, at which value it was maintained throughout the measurements and checked regularly.

The method used for determining the efficiency was that described in chapter 3. The window material of the proportional counter was mounted on a piece of brass shim in which was drilled a hole

of about 1 mm diameter as described earlier. A second piece of window material was mounted over an identical hole in another piece of shim and fixed over the cathode of the array. The diameter of each of the holes was measured with an accurate travelling microscope. Thus the effect of the window thickness on the monitor counter was compensated for by the filter necessary to exclude stray ions and UV radiation.

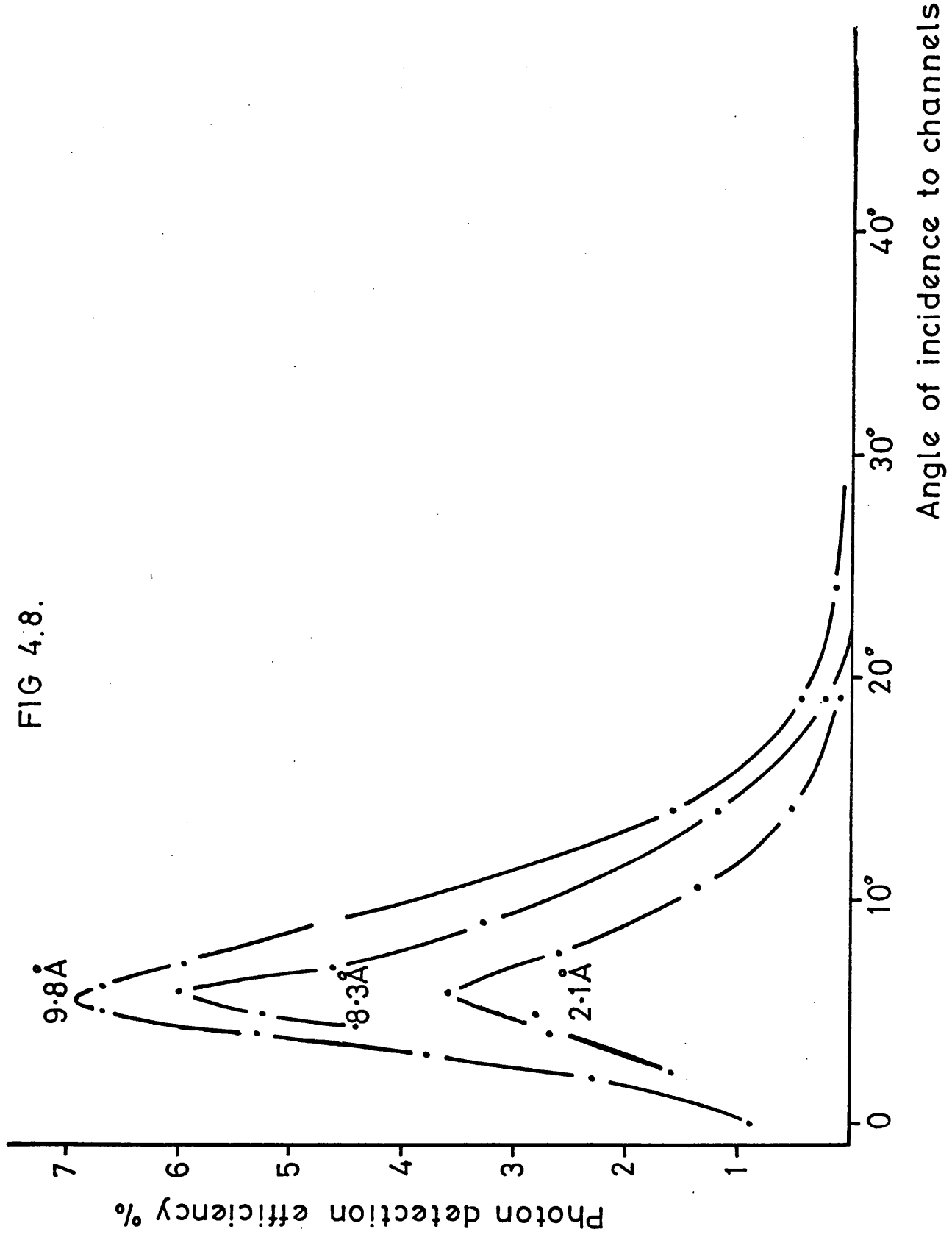
The array was mounted on the modified detector mount described in chapter 3 and adjusted so that rotation of the array resulted in no lateral motion of the cathode face with respect to the beam. Having identified an emission line using the monitor proportional counter, the rate at the maximum of the line was measured. The array was then positioned at this maximum, and since the detector apertures were of identical size, the profile of the X-ray beam at the detectors was not important.

The background rate was measured with the array positioned first on the high, and then on the low wavelength side of the line, an average of these being subtracted from the rate when on the line. Thus a simple comparison of count rates in the array and monitor counter, after correction for gas absorption, gave values for the detection efficiency of the array at a number of wavelengths.

The detection efficiency is shown in figs 4.8 and 4.9 plotted as a function of angle of incidence. At near normal incidence there is a drop in the efficiency due to X-rays penetrating well down the channel before hitting the wall, giving a lower gain and fewer pulses above the discriminator. At angles θ other than normal incidence, the area of the beam actually striking the array is reduced by a factor $\cos\theta$, but the area of the array illuminated remains constant.

These curves can be compared to those for single channel

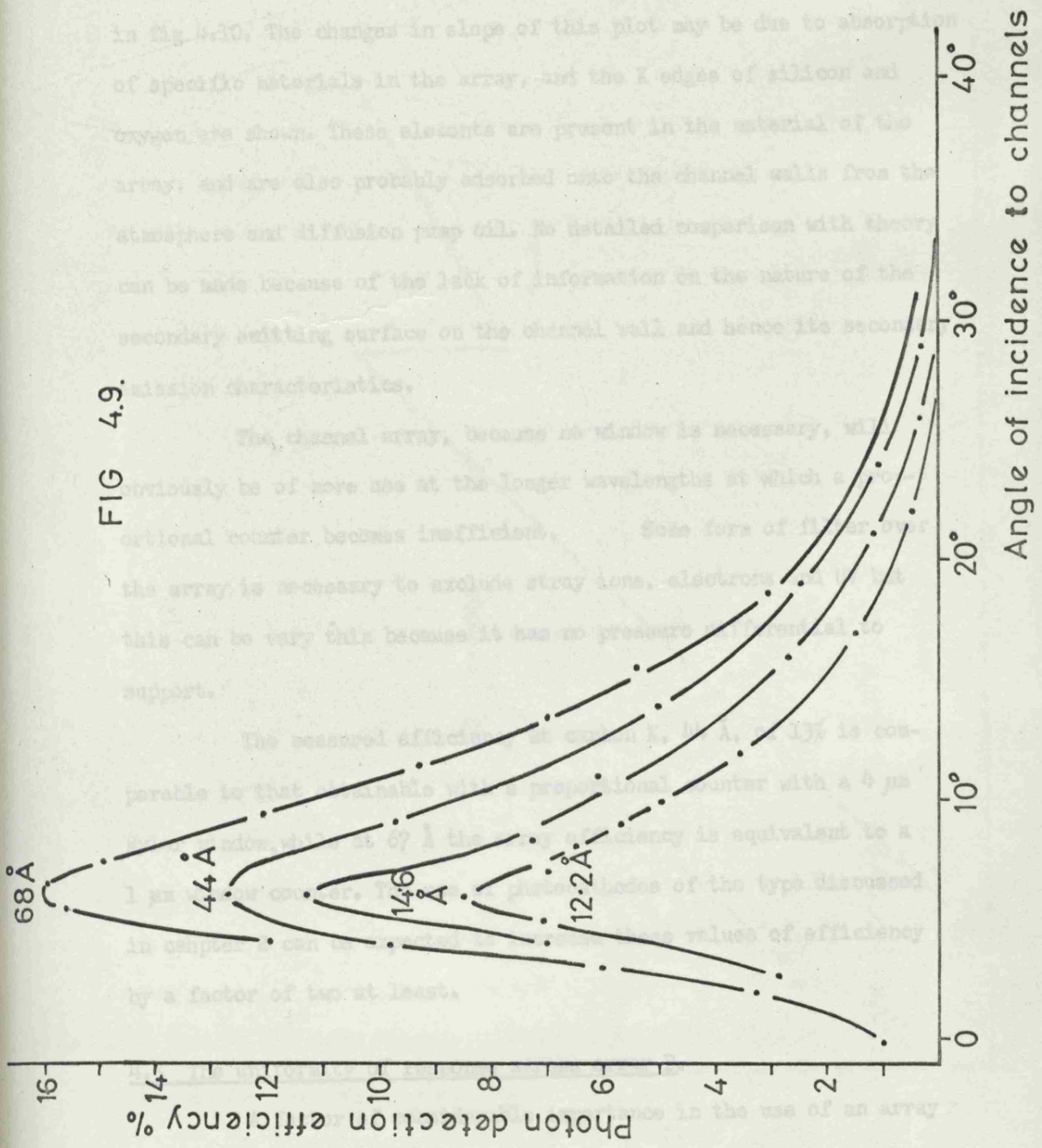
FIG 4.8.



multipliers (Smith 1966) which show a very similar response, but a rather lower detection efficiency. The error measurements was estimated to be 20%, due principally to variation in window thickness and rather arbitrary choice of detection threshold.

The peak efficiency is plotted as a function of wavelength in Fig. 4.9. The changes in slope of this plot may be due to absorption of specific materials in the array, and the K edges of silicon and oxygen are shown. These elements are present in the material of the array, and are also probably adsorbed onto the channel walls from the atmosphere and diffusion jump till. No detailed comparison with theory can be made because of the lack of information on the nature of the secondary emitting surface on the channel wall and hence its secondary emission characteristics.

FIG 4.9.



multipliers (Smith 1968) which show a very similar response, but a rather lower detection efficiency. The error ^{in the} measurements was estimated to be 20%, due principally to variation in window thickness and rather arbitrary choice of detection threshold.

The peak efficiency is plotted as a function of wavelength in fig 4.10. The changes in slope of this plot may be due to absorption of specific materials in the array, and the K edges of silicon and oxygen are shown. These elements are present in the material of the array, and are also probably adsorbed onto the channel walls from the atmosphere and diffusion pump oil. No detailed comparison with theory can be made because of the lack of information on the nature of the secondary emitting surface on the channel wall and hence its secondary emission characteristics.

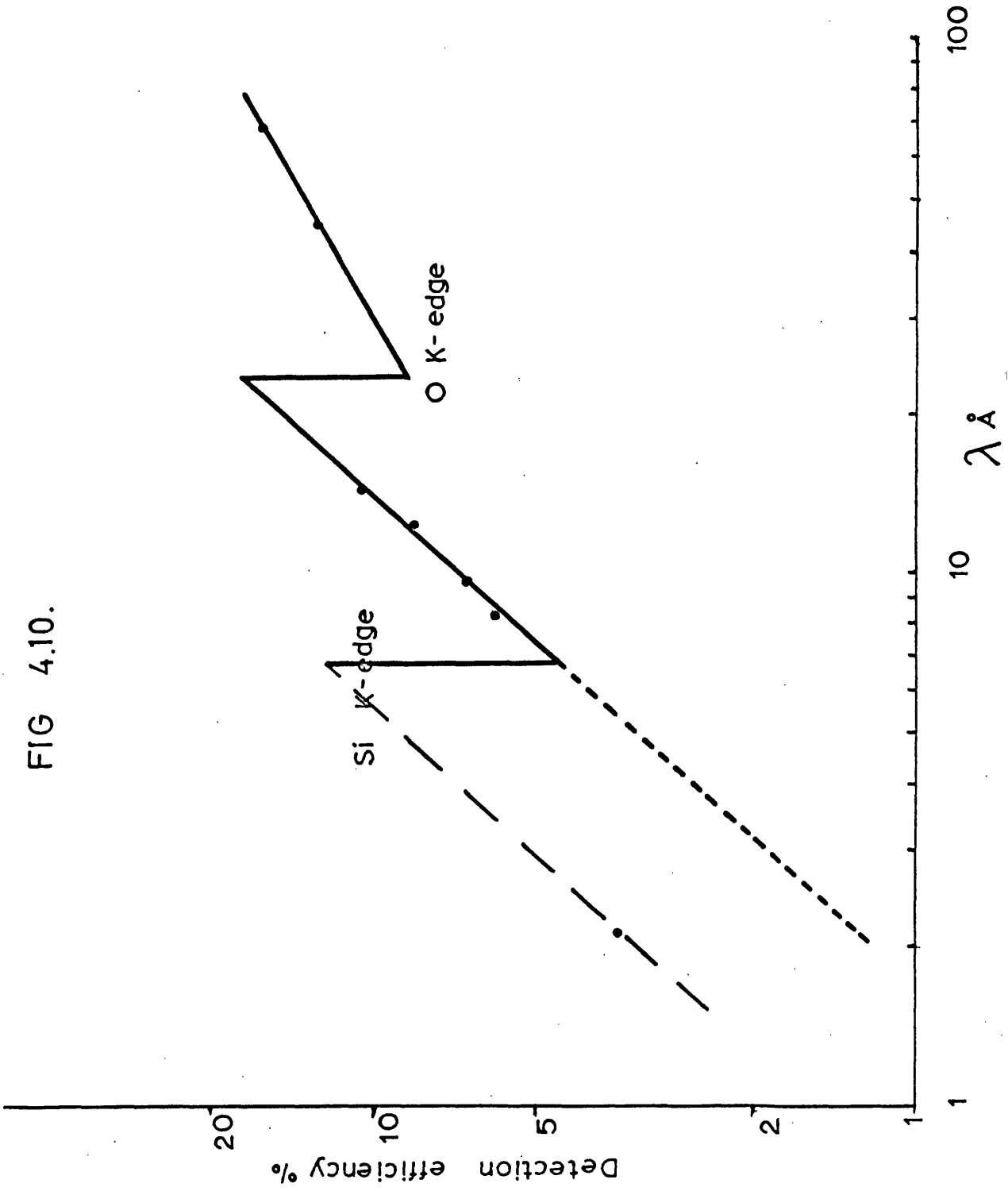
The channel array, because no window is necessary, will obviously be of more use at the longer wavelengths at which a proportional counter becomes inefficient. Some form of filter over the array is necessary to exclude stray ions, electrons and UV but this can be very thin because it has no pressure differential to support.

The measured efficiency at carbon K, 44 \AA , of 13% is comparable to that obtainable with a proportional counter with a 4 \mu m mylar window, while at 67 \AA the array efficiency is equivalent to a 1 \mu m window counter. The use of photocathodes of the type discussed in chapter 2 can be expected to increase these values of efficiency by a factor of two at least.

4.5 The uniformity of response across array B.

A factor of considerable importance in the use of an array

FIG 4.10.



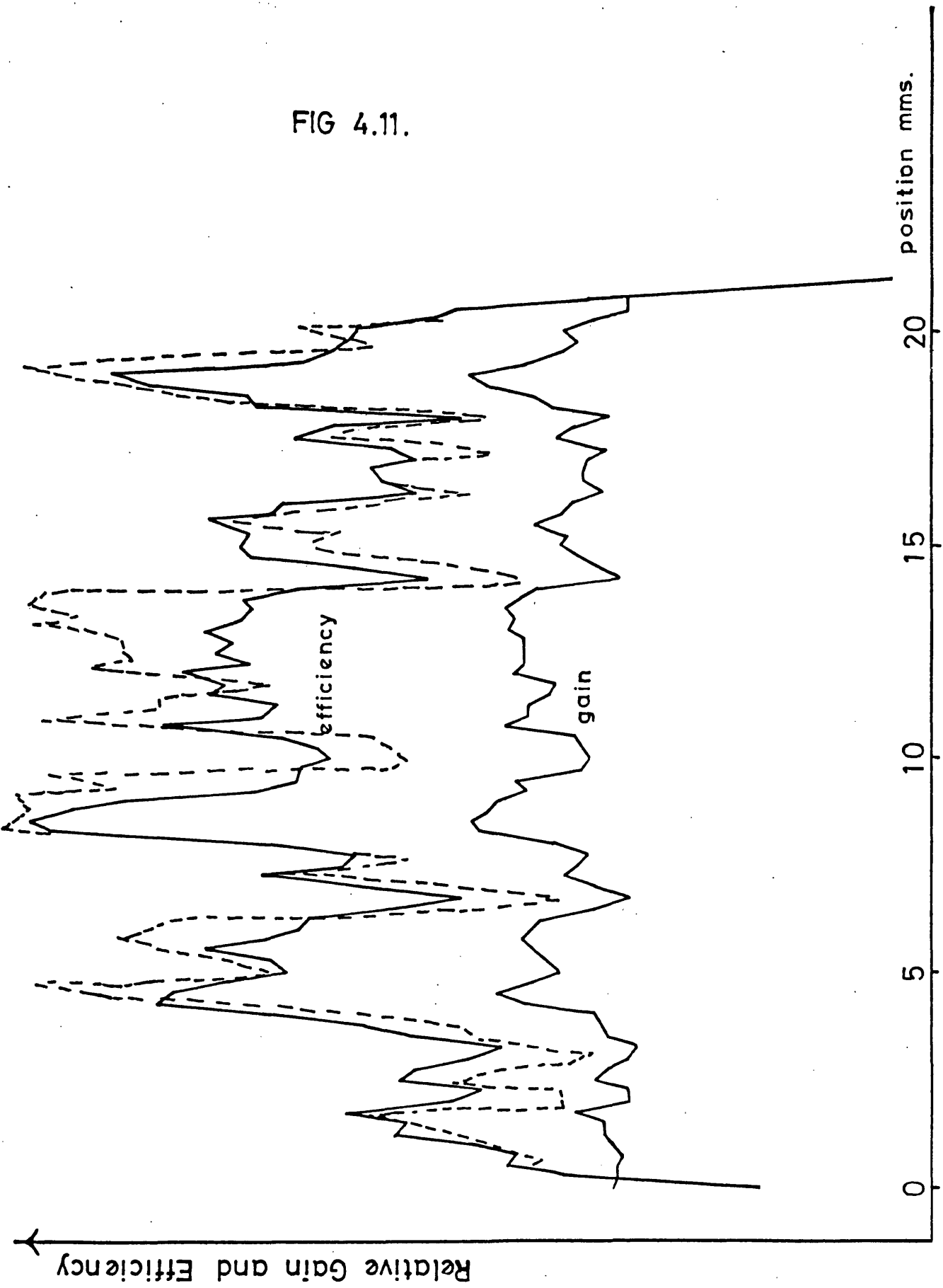
as an imaging device is the uniformity of response, particularly efficiency, across the cathode face. This was investigated by scanning the array with a pencil beam of X-rays and monitoring the count rate, again over two discriminators, enabling a comparison of efficiency and gain with position to be made for the upper exponential.

The array was mounted on the micrometer drive of the X-ray collimator, the slits being temporarily removed and replaced by a piece of copper shim with a 0.5 mm diameter hole and filter. The X-ray source was to ^{allowed} reach a stable condition and the intensity of it monitored before and after the measurements to allow for any variation in emission. The count rates above the two discriminators were measured simultaneously by feeding the pulses into the single channel analyser and scalar, and also into the multichannel analyser, used essentially as a discriminator, and ratemeter. A digital readout was obtained from the ratemeter for increased accuracy and ease of reading, by monitoring the voltage with a digital voltmeter.

The pencil beam was stepped across the array in 0.25 mm steps, the middle centimetre of the array only being investigated. This was repeated until a one cm. square in the centre of the array had been mapped. A typical variation of count rate and gain is shown in fig 4.11. The count rate was such that the error due to counting statistics was small.

Clearly there is a striking similarity between gain and count rate fluctuations. The count rate above such a discriminator is a function of the photoelectric conversion efficiency at the cathode and also of the gain. In order to assess the extent to which the varying gain can account for the observed count rate profile the expected count rate was calculated for each value fo gain.

FIG 4.11.



Taking the upper exponential only, the pulse height distribution can be represented by:

$$n = N \cdot \exp(-q/\bar{q}) \text{ as discussed earlier.}$$

The count rate integrated over a discriminator at q_1 is then:

$$n_1 = \int_{q_1}^{\infty} N \cdot \exp(-q/\bar{q})$$

\bar{q} has been determined from count rates over the two discriminators and is independent of any variation in photo-electric conversion efficiency.

By considering the value of \bar{q} and n_1 at some position, a, on fig 4.11, the expected count rate at any other position, b, can be calculated:

For position a,

$$n_a = \bar{q}_a \cdot N \cdot \exp(-q_1/\bar{q}_a)$$

and for position b,

$$n_b = \bar{q}_b \cdot N \cdot \exp(-q_1/\bar{q}_b)$$

$$\text{and by division } n_b = n_a \cdot (\bar{q}_b/\bar{q}_a) \cdot \exp(q_1/\bar{q}_a - q_1/\bar{q}_b)$$

The value of n_b is shown as the broken line in fig 4.11. The fluctuation in gain will account for the varying count rate to within 20%, which is within the error set on the calculation of 30%. This large error is due to the exponential term which contains the difference of two quantities, q_1/\bar{q}_a and q_1/\bar{q}_b , of comparable size.

Thus it can be said that the variation in photoelectric conversion efficiency is less than 20% over a one cm. square of the array. Examination of the variation in gain reveals a periodicity with dimensions of the order of 1 mm. This can be explained by the fact that the array is constructed of hexagonal channels, approximately 0.8 mm across, cemented together. Since the bundles can originate from different sections of the original, some variation in gain is

Relative Efficiency

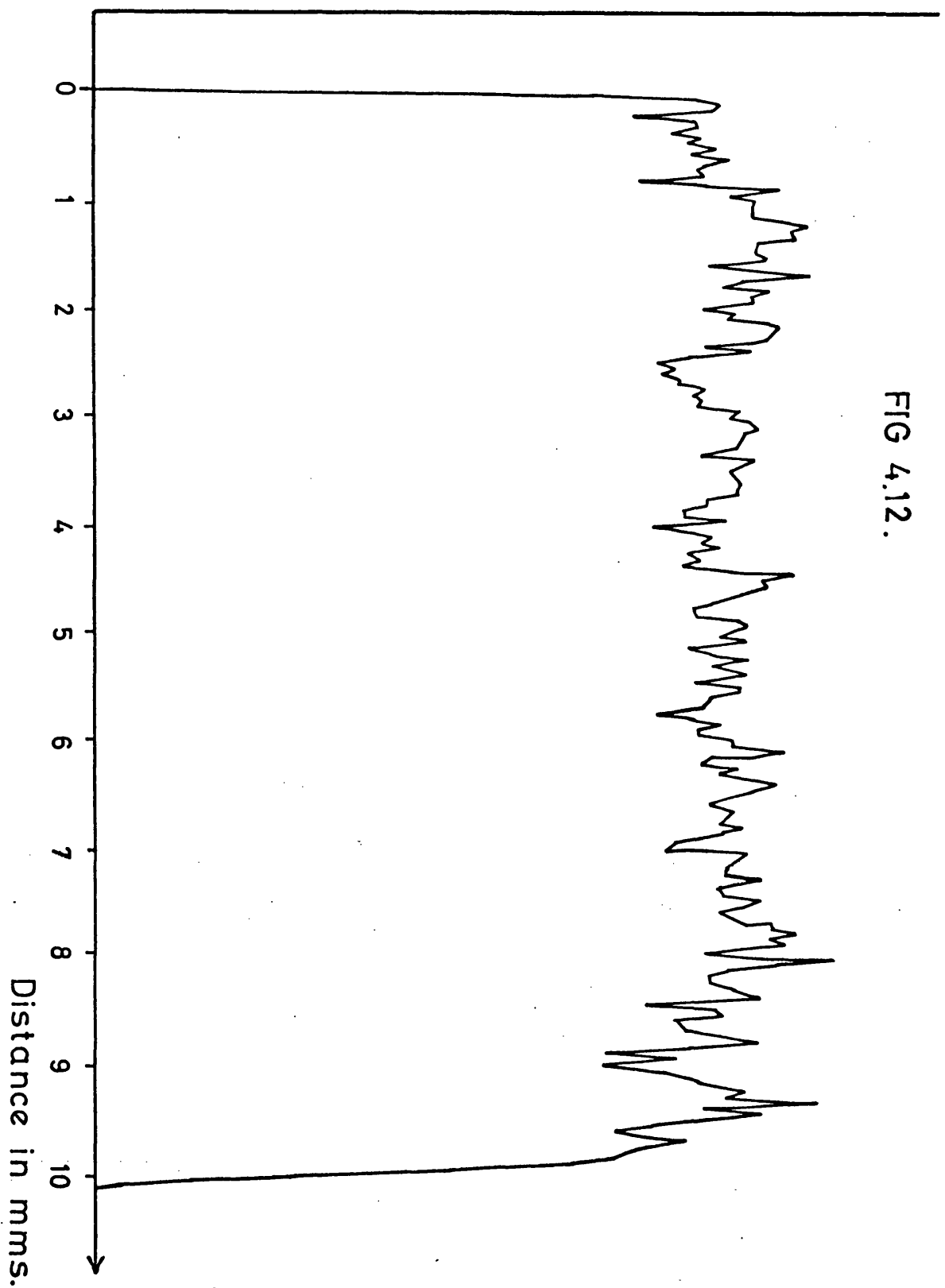


FIG 4.12.

Typical variation in efficiency using a slit beam 75 μ wide and 1/2 cm high stepped in 50 μ intervals.

to be expected. Although the variation in count rate of fig 4.11 would be a serious problem in the use of the array as an imaging device, considerable improvements in manufacturing techniques can be expected.

Another projected use of the array is in a high resolution spectrometer, discussed in chapter 1. The image would in this case be a narrow slit and the effect of the hexagonal bundles would be expected to be reduced. To verify this, the slits were replaced and a beam 5 mm high and 75 μm wide was scanned across the array. The variation in count rate is shown in fig 4.12. Although the area of the beam is comparable to the area of the pencil beam used earlier, the count rate profile is much smoother and supports the above theory. For use in this type of one dimensional imaging application, the array response, even at this early stage of development, would be adequate.

4.6 Lifetests of array A in high vacuum conditions.

The non-standard array was used in this work because of the length of time of the measurements, no significant difference in the life of different arrays being expected. The array was split into three pieces, one of which was used in this measurement and the others in the imaging work. Initially, the array was mounted as described earlier, and in fig 4.1.a. After several days in the UHV system, however, noise similar to that of array B was observed. The array was then remounted as in fig 4.1.b which, after an initial noisy period, was found to be satisfactory.

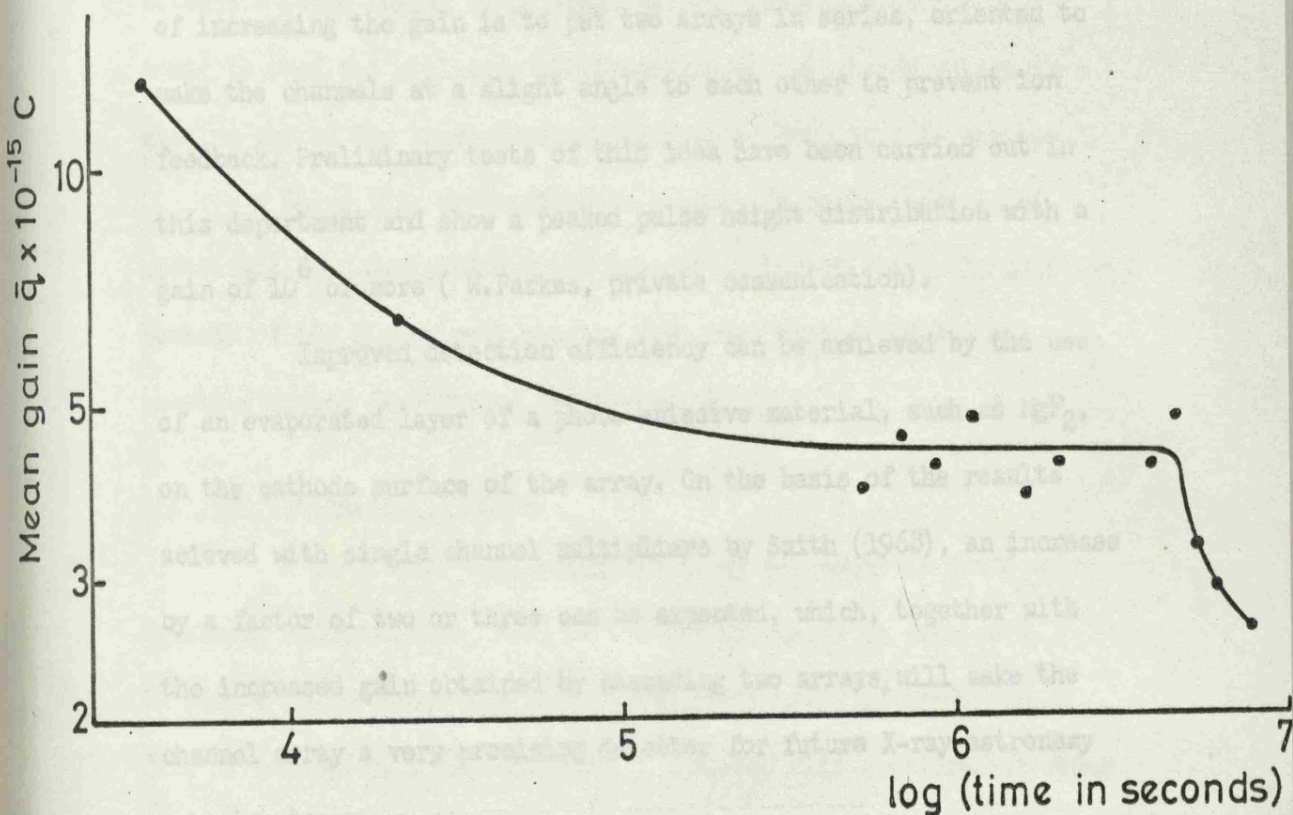
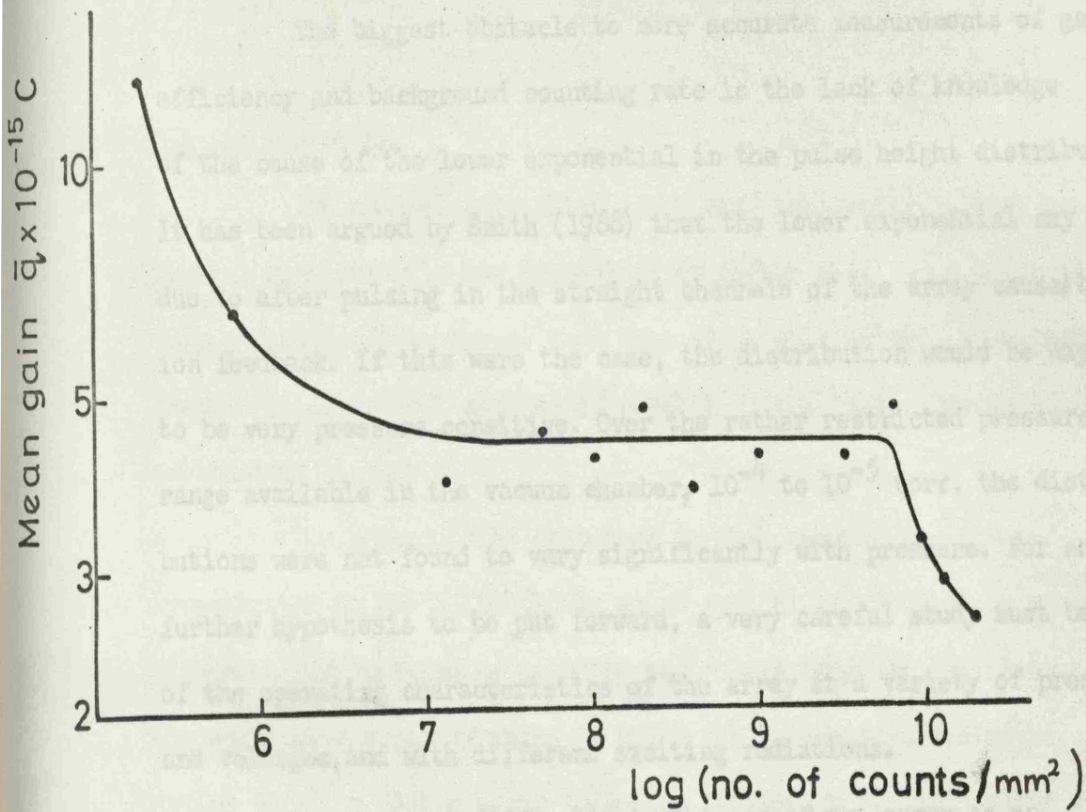
The pressure in the UHV system was allowed to reach 10^{-8} torr before switching the EHT on. No baking was attempted because of the unknown effect of high temperatures on the array. The array was set at 1450 volts and left on for three months. Initially, a low

count rate was obtained from an Fe 55 source so that the array could be conveniently examined in the early stages. The pulse height discriminator was again set at the break in the distribution and the gain recorded. The count rate was then increased to 3000 /sec ^{/mm²} using electrons emitted from the filament of the ionisation gauge. The noise increased over the period of the experiment making accurate gain measurements difficult. The noise of the preamplifier showed no variation however, indicating a general deterioration in the condition of the array.

The mean gain of the upper exponential is shown as a function of the number of integrated counts and of time under vacuum in fig. 4.13. The experiment was stopped after 10^{10} had been accumulated in three months, by which time most of the pulses were below the discriminator level.

The results are similar to those obtained for single channel multipliers, within the accuracy of the measurements (see for example Timothy et.al.1969). The considerable number of lifetests carried out on single channels so far, has not led to any definite conclusions as to the cause of the fatiguing. The most likely explanation so far advanced is that adsorbed gas on the wall is cleaned off with continuous operation in high vacuum resulting in a wall with a lower secondary emission coefficient and lower gain.

FIG 4.13.



4.7 Further work.

The biggest obstacle to more accurate measurements of gain, efficiency and background counting rate is the lack of knowledge of the cause of the lower exponential in the pulse height distribution. It has been argued by Smith (1968) that the lower exponential may be due to after pulsing in the straight channels of the array caused by ion feedback. If this were the case, the distribution would be expected to be very pressure sensitive. Over the rather restricted pressure range available in the vacuum chamber, 10^{-4} to 10^{-5} torr, the distributions were not found to vary significantly with pressure. For any further hypothesis to be put forward, a very careful study must be made of the operating characteristics of the array at a variety of pressures and voltages, and with different exciting radiations.

A practical difficulty in the use of the array as an individual photon detector is in its low gain. One possible method of increasing the gain is to put two arrays in series, oriented to make the channels at a slight angle to each other to prevent ion feedback. Preliminary tests of this idea have been carried out in this department and show a peaked pulse height distribution with a gain of 10^8 or more (W.Parkes, private communication).

Improved detection efficiency can be achieved by the use of an evaporated layer of a photo-emissive material, such as MgF_2 , on the cathode surface of the array. On the basis of the results achieved with single channel multipliers by Smith (1968), an increase by a factor of two or three can be expected, which, together with the increased gain obtained by cascading two arrays, will make the channel array a very promising detector for future X-ray astronomy experiments.

CHAPTER 5. THE USE OF THE CHANNEL MULTIPLIER ARRAY AS AN
IMAGING DETECTOR.

5.1 Introduction.

The channel multiplier array has, inherently, a very good spatial resolution in two dimensions of better than 50 μm , which is only a factor of two worse than that obtainable using a fast photographic film. Several methods of readout of the image have been outlined in chapter 2.

The method to be described in this chapter was first investigated by Smith (1968), in which spatial information in one dimension was obtained by scanning the charge image at the anode of the array with a narrow strip on which the pulses were collected. Having verified that a strip collector provided a suitable means of image dissection, it was suggested that by capacitative coupling between a large number of adjacent strips, the whole of the image could be read out utilising the branching of the charge pulses in a similar way to the current branching methods described in chapter 2.

Using this proposition as a basis, a fully operational system has been designed and its properties investigated. In addition methods of two dimensional readout have been considered and one possible system constructed and tested.

5.2 One dimensional imaging.

A particular application in X-ray astronomy is found with focussing spectrometers, such as the one discussed in chapter 1. In such a spectrometer the image is conventionally recorded on film or scanned by a detector having a narrow slit aperture. In order

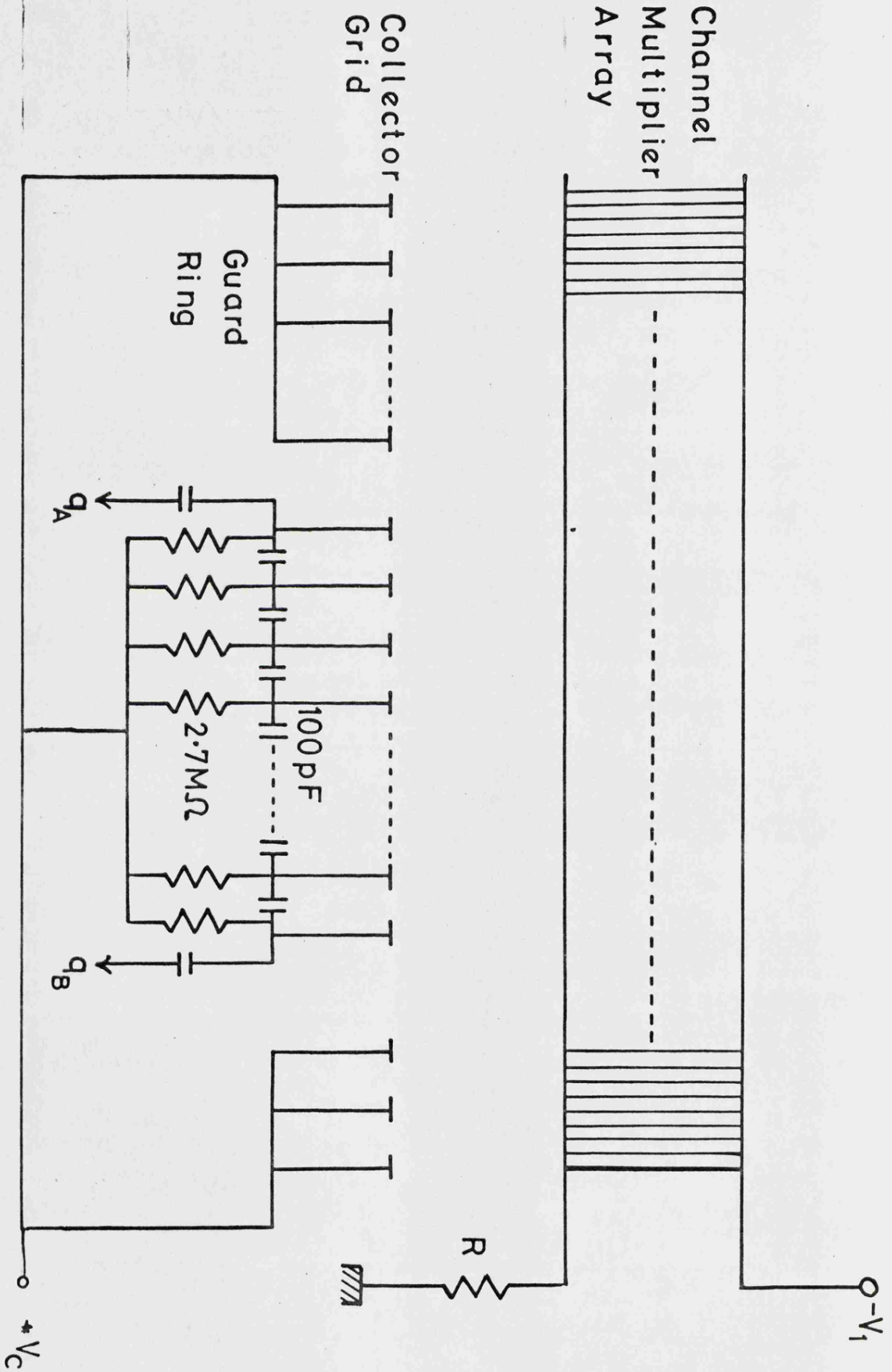


FIG. 5.1 Channel multiplier array and collector subsystem.

to utilise fully the properties of an array in such a system, the pulses are collected on a number of parallel strips rather than the simple collector plate, enabling the image to be read out directly without scanning.

There are two approaches to reading out the information; either the pulses on any strip can be amplified using a separate amplifier for each strip or, by using a charge branching process, the position of the strip at which the pulse arrives can be computed. The first approach is most useful for high count rate applications or cases where fast timing is essential, for example in some nuclear physics experiments. The second is a simpler method and has adequate count rate capabilities for the type of experiments envisaged in X-ray astronomy.

The method adopted in this work was to use fine tungsten wires as the collector strips, each wire being capacitatively coupled to its neighbour by discrete, equal value condensers. A charge arriving at any of these wires is then divided across the capacitative network to virtual earths at each end as shown in fig 5.1.

For a grid of N wires, a pulse q incident at wire n will give charge pulses q_a and q_b at each end of the condenser network of

$$q_a = ((N - n)/N) \cdot q$$

$$\text{and } q_b = (n/N) \cdot q$$

The function $q_b/(q_a + q_b)$ is then:

$$\frac{q_b}{q_a + q_b} = \frac{n}{N} \quad \text{which is independent of}$$

the initial charge q , and is a linear function of n , the position of incidence of the pulse on the grid.

5.2.1 The analogue pulse electronics.

Initially, in order to generate the function $q_a/(q_a + q_b)$, the pulses q_a and q_b were amplified using the charge sensitive preamplifiers described in chapter 3, followed by voltage amplification using two Harwell 2000 series amplifiers. The voltage pulses V_a and V_b were summed and fed into the single channel analyser set to a 4 volt threshold and a very narrow window, about 0.1 volt. For pulses $V_a + V_b$ which were in this window, the multichannel analyser was enabled using the co-incidence inputs and the V_a pulse allowed to record.

Clearly this is an inefficient way of obtaining the position pulse because of the very narrow window required to simulate a narrow pulse height distribution from the array. Once the viability of the method had been tested in this way, therefore, the Ortec 118A low noise charge sensitive preamplifiers were obtained, and the requisite electronics to allow registration of every pulse was designed and constructed and is shown in block diagram form in fig 5.2.

Pulses were accepted only if over a certain height and if both V_a and V_b were present, stretched to 15 μ s and summed. An inhibit of 30 μ s from the arrival of the pulse allowed the processing to be carried out. The stretched pulses were fed into an analogue divider, Burr Brown type 4112, which had an accuracy of 1% of full scale for inputs of 5 to 10 volts. For smaller pulses it was found that the accuracy fell off very sharply, and to avoid this the summed pulse $V_a + V_b$ was fed into the single channel analyser set to accept pulses between 5 and 10 volts. It was also necessary to allow about 10 μ s for the output of the divider to stabilise before allowing the pulse into the multichannel analyser. The circuit diagram of the stretcher card is shown in fig 5.3. The gain of the two pulse channels could be adjusted

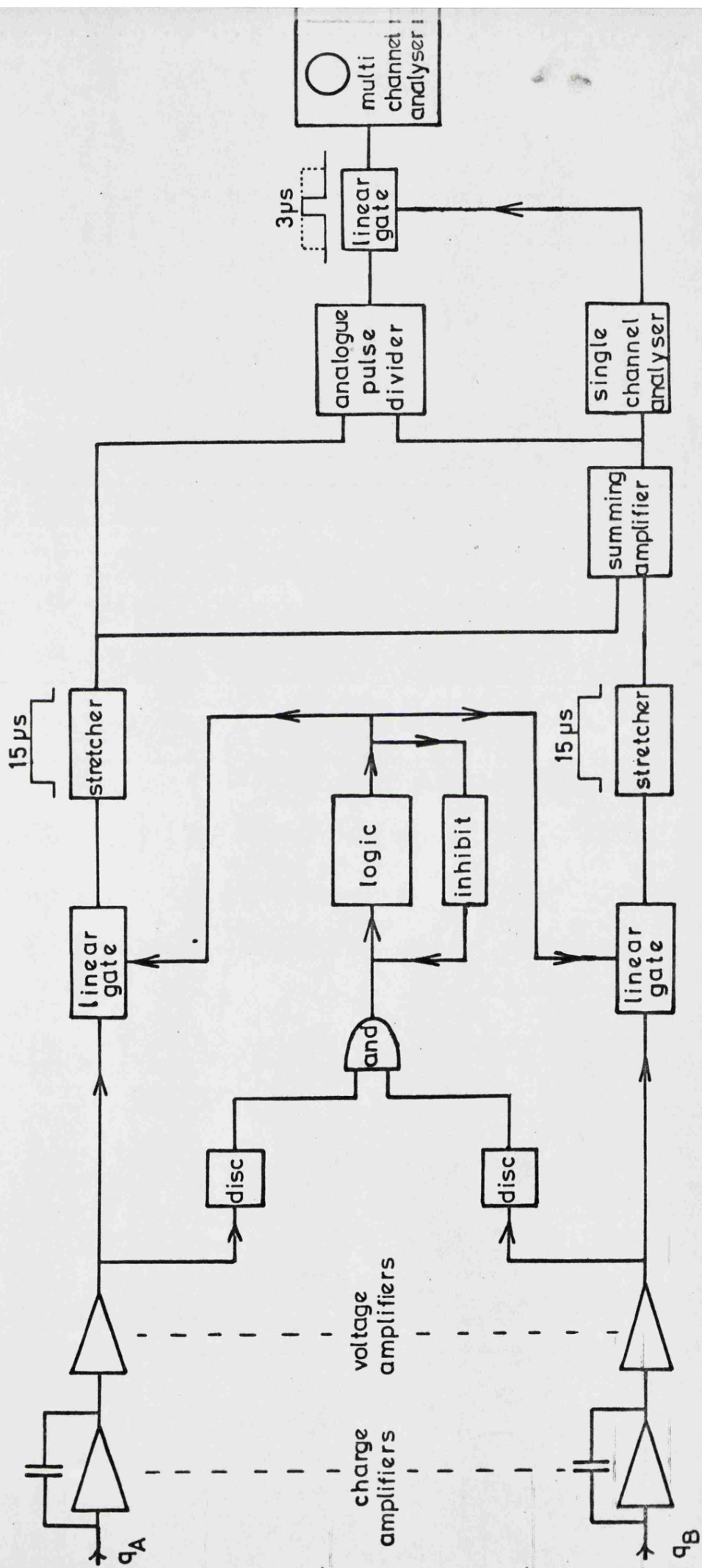


FIG. 5.2
Block diagram of electronics.

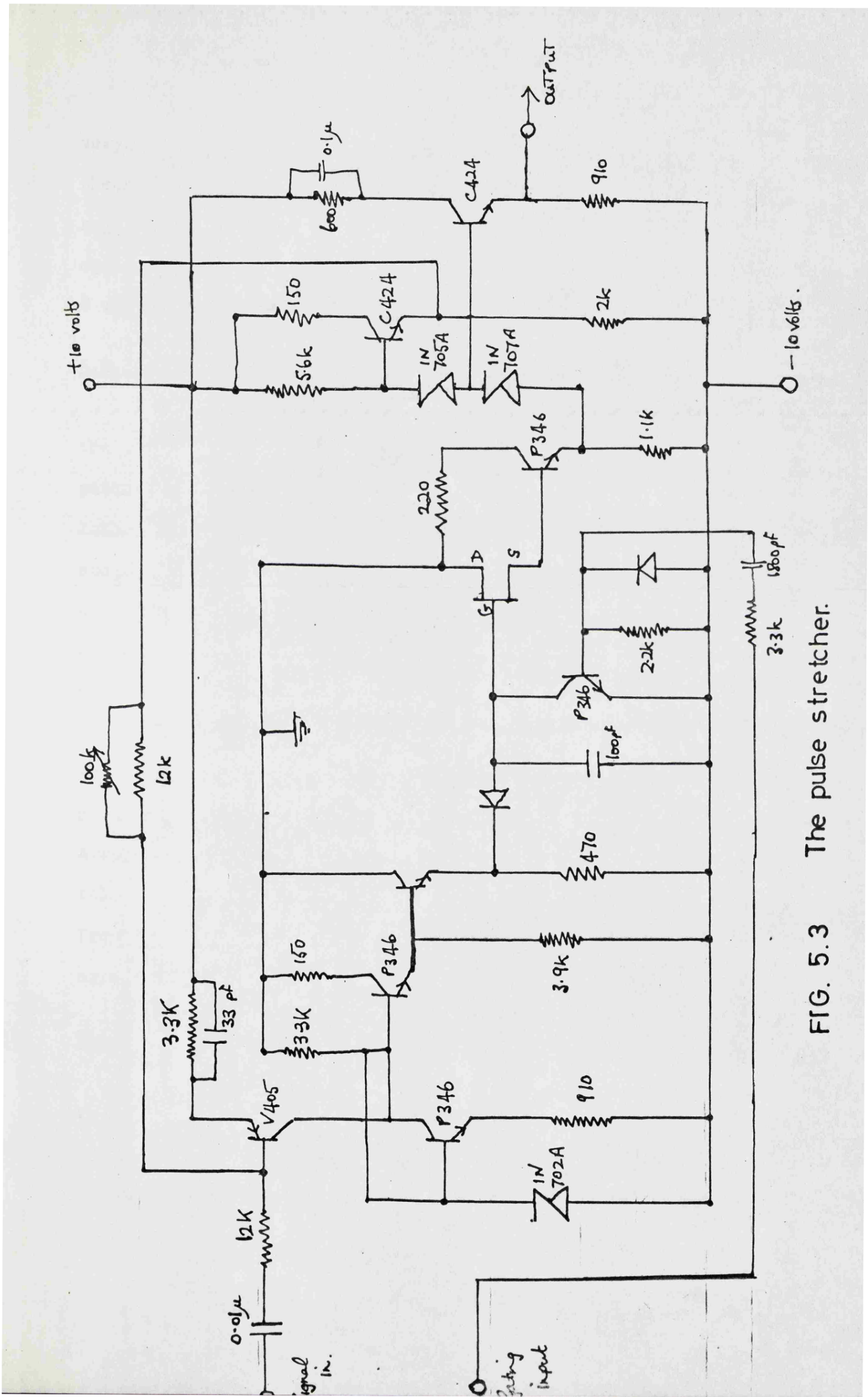


FIG. 5.3 The pulse stretcher.

very accurately and the linearity and temperature stability was checked carefully. Subsequently, the gain adjustments were repeated regularly during the experimental work. The position pulse height equivalent to one end of the grid was adjusted to be just less than 8 volts to make full use of the 256 channels available in the analyser.

5.2.2 The experimental procedure and results.

The grid of wires used as a collector of the pulses from the array was constructed from 45, 100 μm tungsten wires at 200 μm pitch. The wire was wound onto a former using the feed screw of a lathe to an accuracy of about 10 μm and then glued to a glass microscope slide. The wires at one end were cut away, while at the other end were spot welded to short lengths of copper wire soldered into the condenser board. The completed grid is shown in plate 5.1.a and a close up of the wires in plate 5.1.b.

Twenty wires from the centre of the grid were used while the rest of the wires on either side were connected together to form guard strips to maintain continuity of the field in the gap between array and collector. The condensers used were silvered mica 1% tolerance and 2.7 M Ω resistors on each wire provided a leakage path. Provision was made to vary the collecting voltage between grid and array. (fig 5.1).

The calibration of the grid.

It was shown earlier that the position pulse $V_a/(V_a + V_b)$ is a linear function of the position on the grid. This is only true, however, if the capacity between adjacent wires is large compared to the stray capacity to earth. For low value condensers the electronic noise is small but the stray capacity to earth becomes comparable to

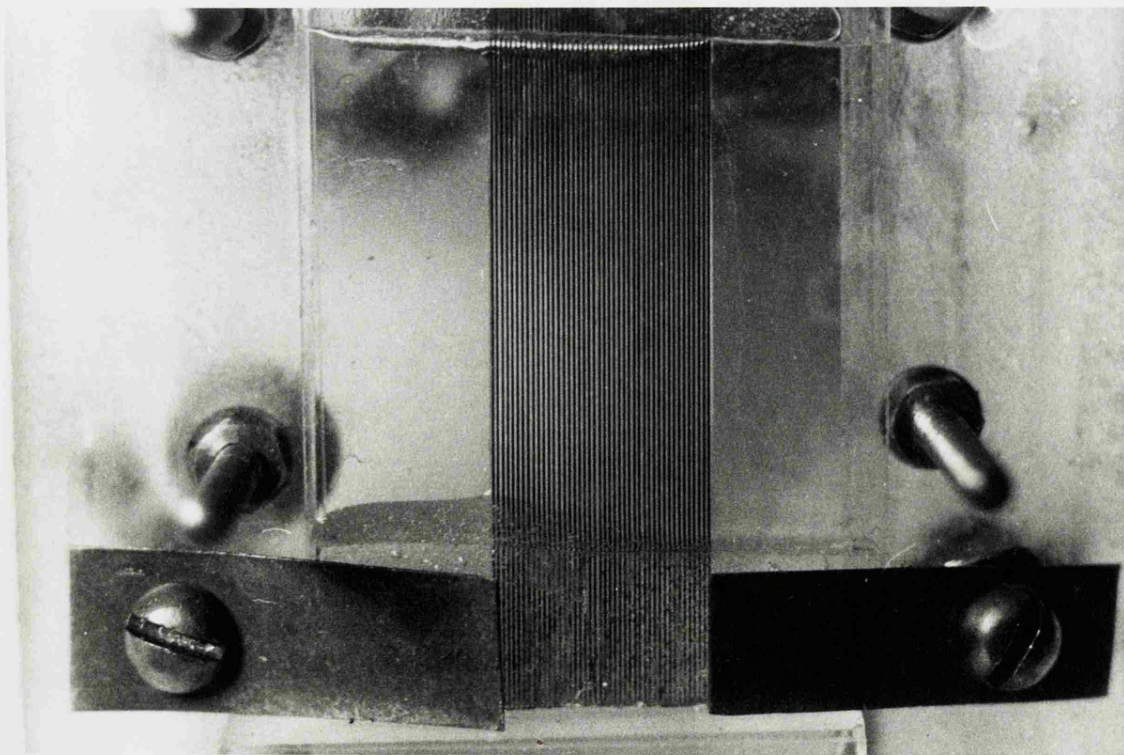
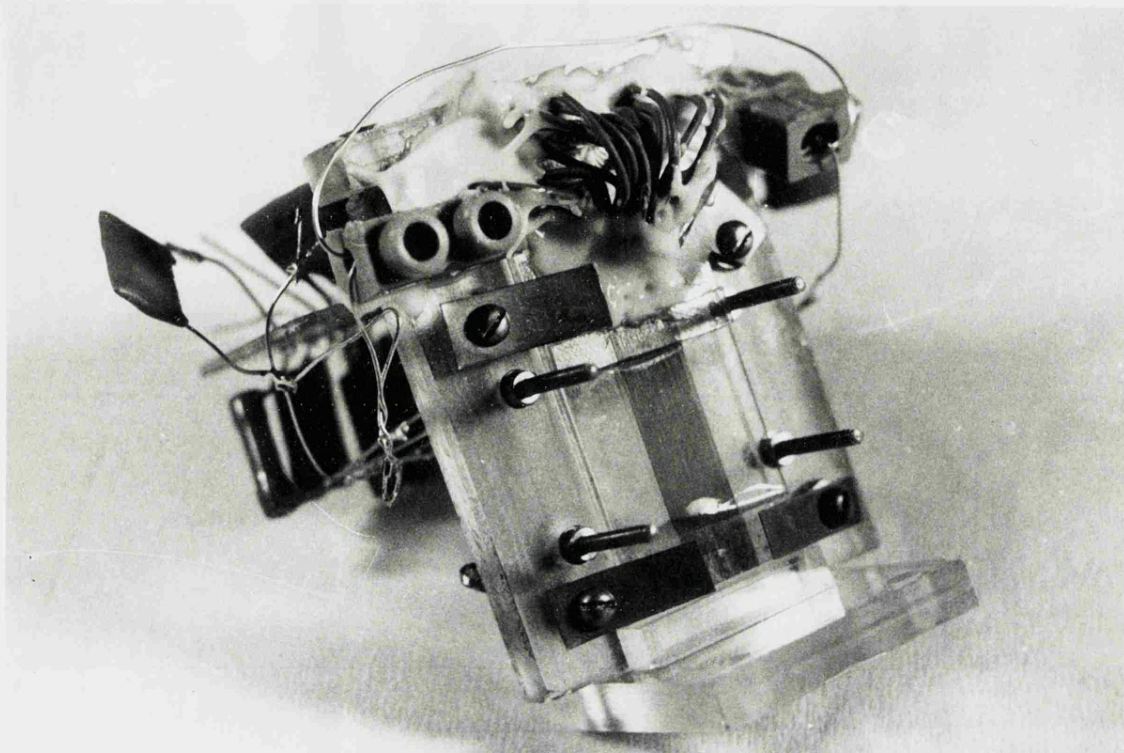


PLATE 5.1

the capacity to the preamplifiers, especially towards the centre of the grid. The choice of the condenser value is therefore a compromise between the conflicting requirements of low noise and linearity. Several values were tried and two of the curves obtained for values of 100 pF and 2000 pF are shown in figs 5.4 and 5.5. Although the 100 pF curve is slightly non-linear, the considerable improvement in noise performance over larger values outweighs this effect and a value of 100 pF was used for the remainder of the work.

The possibility of using the capacity between adjacent wires of the grid was also investigated. The curves for V_a , $V_a + V_b$, and $V_a / (V_a + V_b)$ are shown in figs 5.6 and 5.7. Although the capacity is small, the position pulse height does not show any great non-linearity, although there is considerable scatter from wire to wire due to variation in inter-wire capacitance across the grid. The greater loss of signal to earth gives an increased noise on the position pulse, but this approach may become useful for a larger grid more carefully constructed.

Having decided on the network values, a method of checking the grid and electronics was devised and subsequently used before any experimental work. A charge pulse from the standard pulser was injected onto each of the active wires of the grid in turn, and the height of the position pulse recorded on the multi-channel analyser. In addition to a check on the connections and stability of the electronics, the wire positions could be fixed in terms of given pulse heights and the f.w.h.m. of the electronic noise ^{each} at ~~the~~ wire position determined. As would be expected, there is a slight increase in noise towards the edge of the grid. The superimposed distributions from each of the wires in turn is shown in fig 5.8.

FIG. 5.4

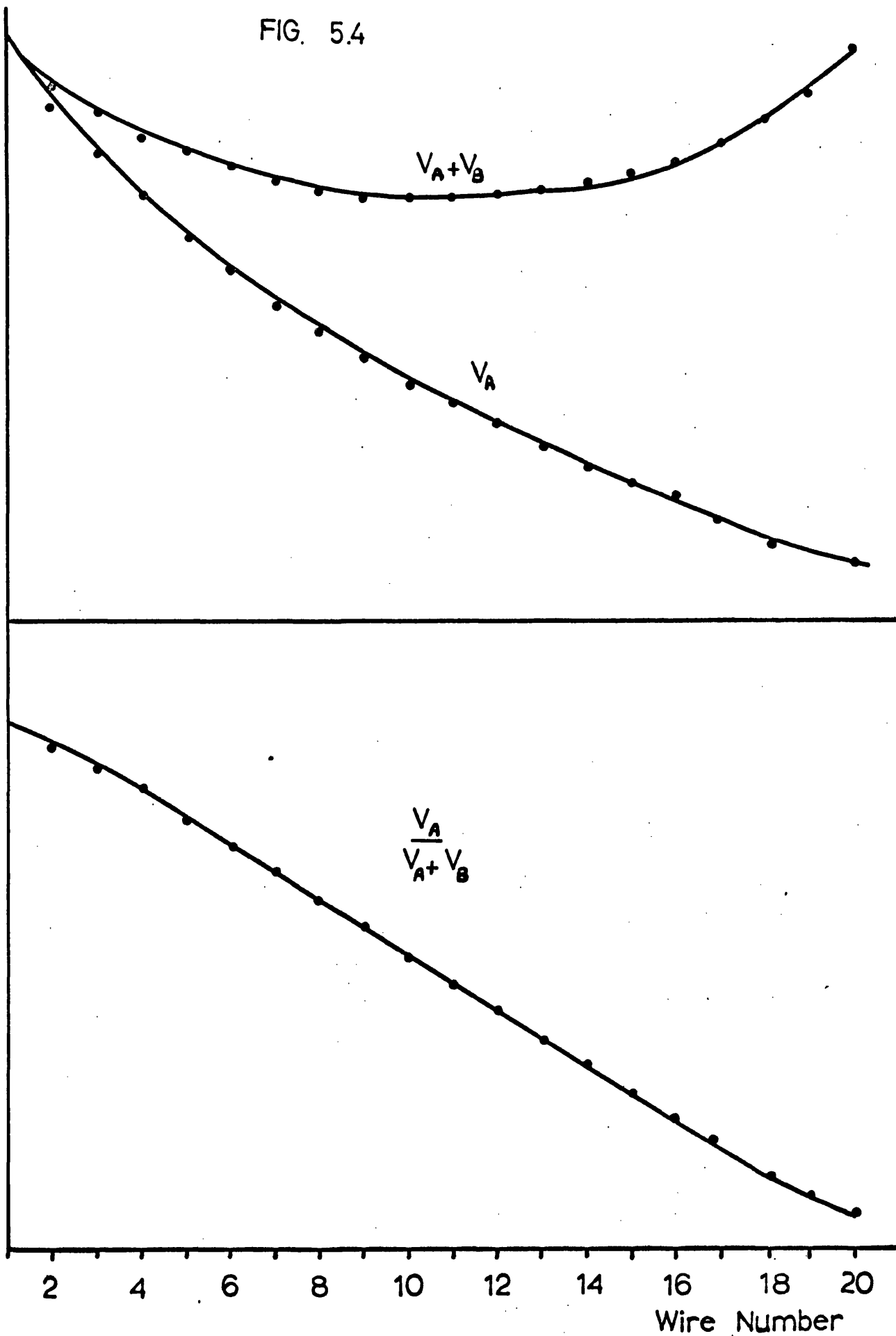
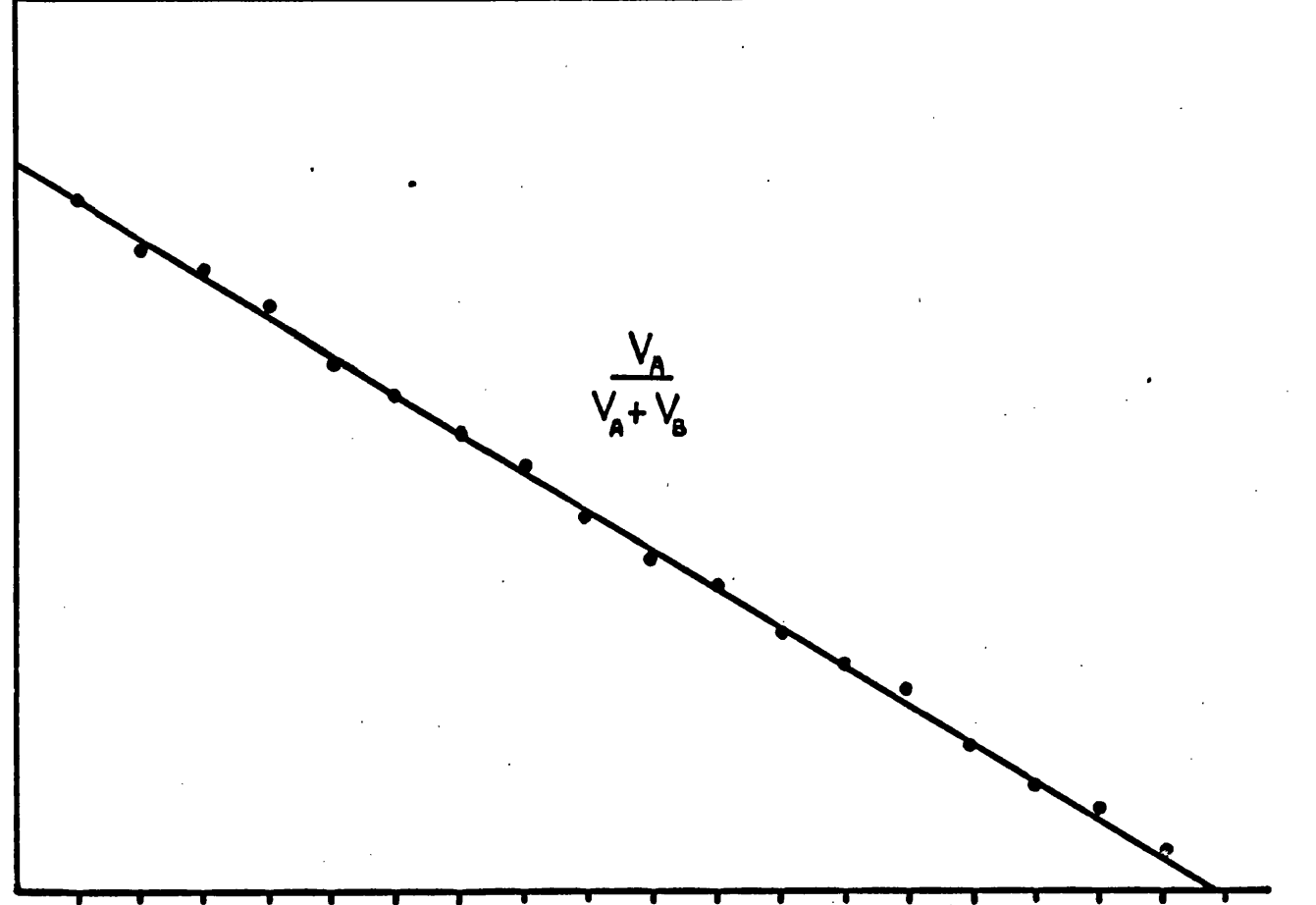
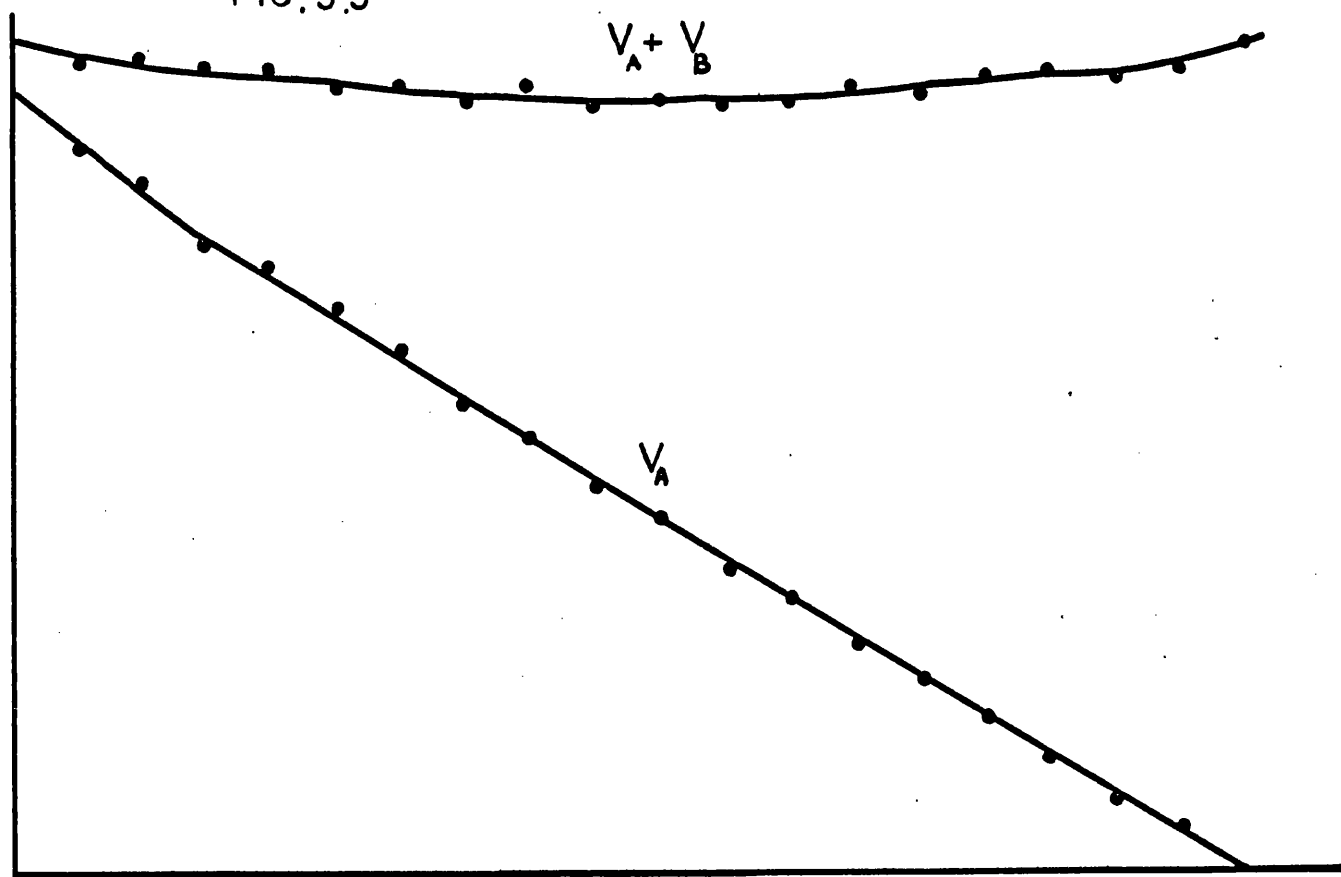


FIG. 5.5



2 4 6 8 10 12 14 16 18 20

Wire Number

FIG. 5.6

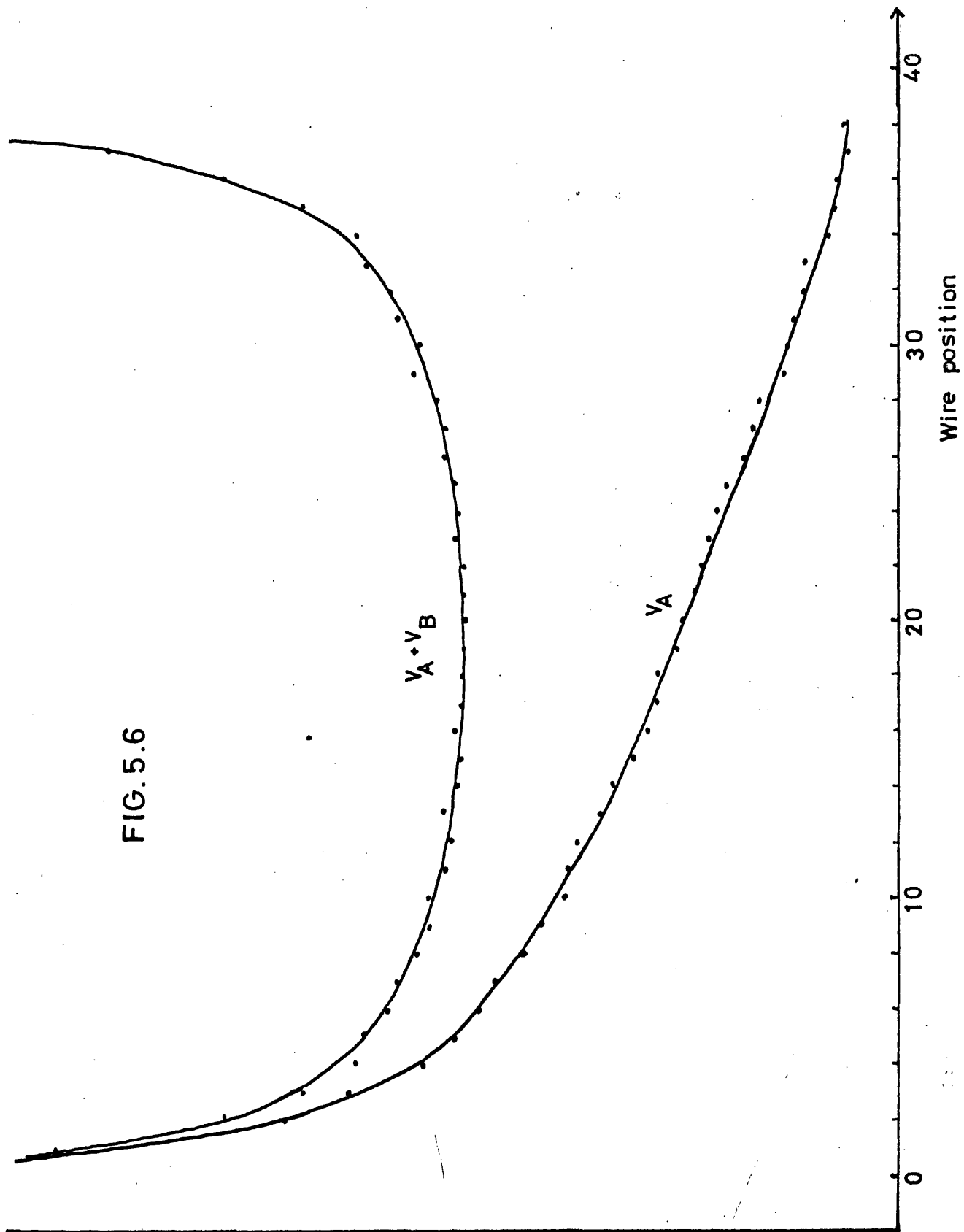


FIG. 5.7

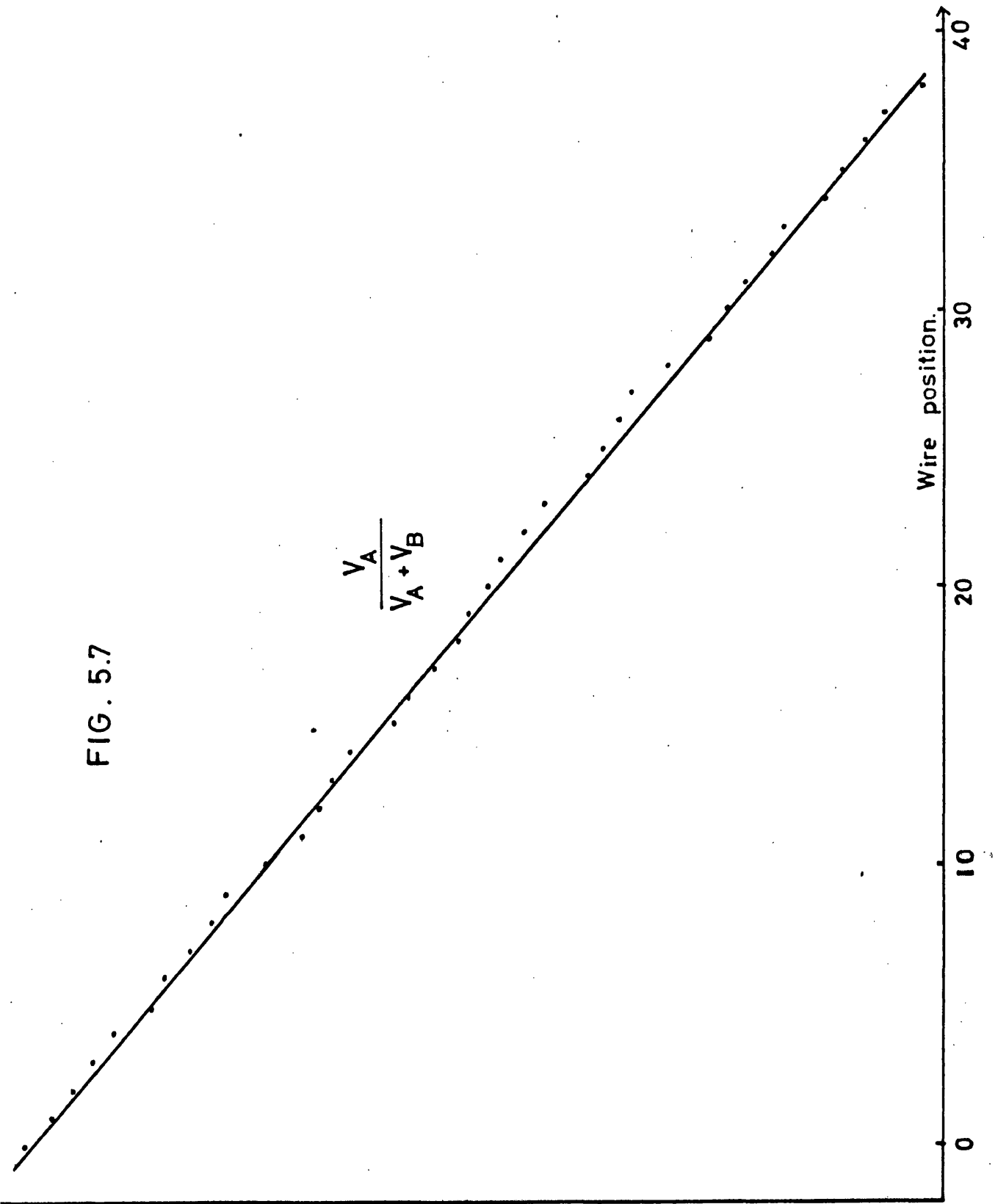
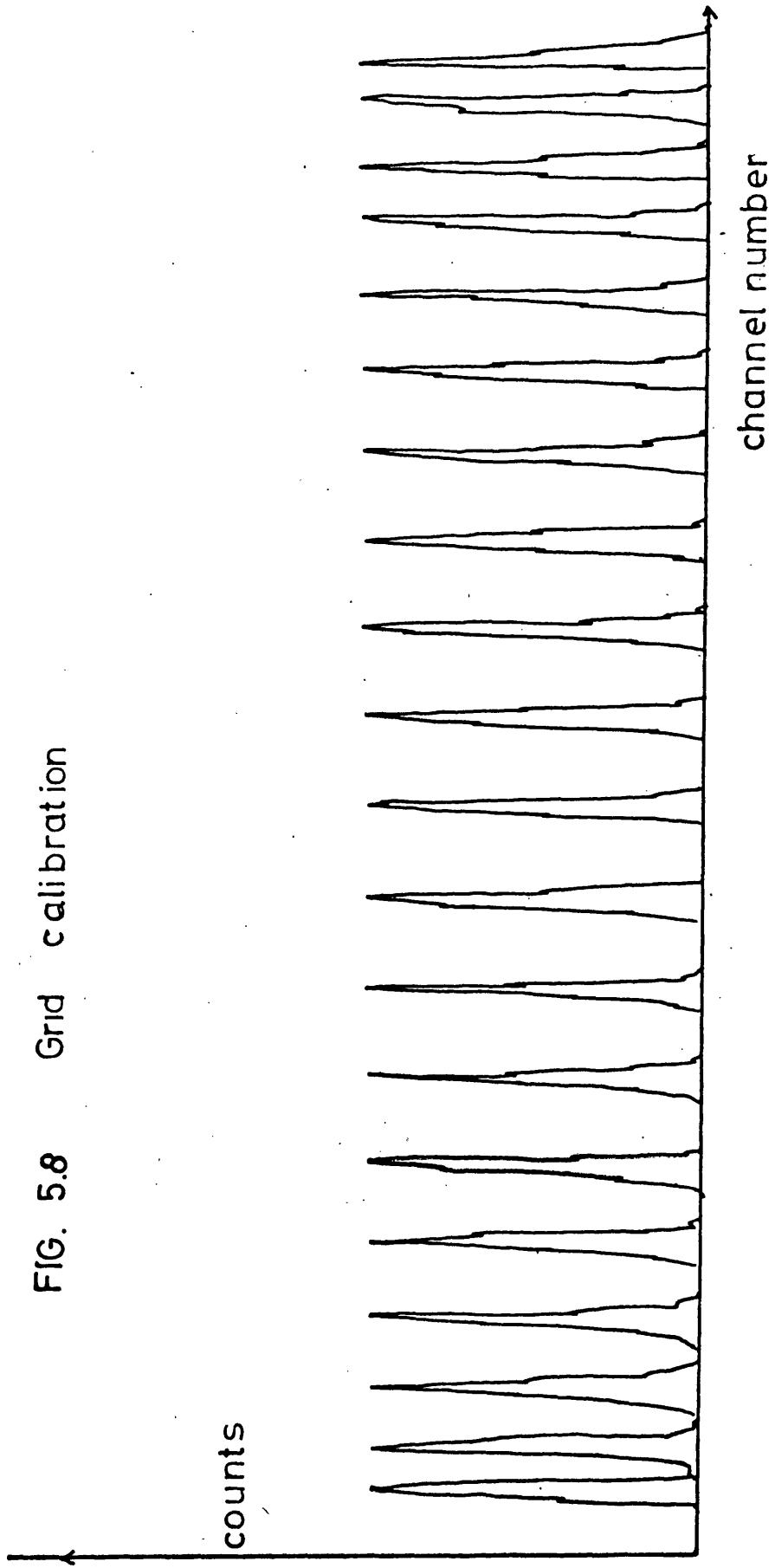


FIG. 5.8 Grid calibration



Using this calibration, the difference in pulse heights between adjacent wires can be found, and hence the known beam width of the X-rays at the array can be expressed as a difference in pulse height, or channel number. A $40\ \mu\text{m}$ beam is thus equivalent to about $2\frac{1}{2}$ channels of the 256 channel analyser.

The distribution of the position pulse height under uniform illumination.

The grid was positioned $300\ \mu\text{m}$ from the array using melinex spacers as described in chapter 4. The array was operated at 1.4 kv and this voltage was fixed for the remainder of the work. $8.3\ \text{\AA}$ X-rays from the X-ray source were allowed to uniformly illuminate the array and the position pulse height distribution investigated.

This distribution was found to vary considerably with the collecting voltage between the array and grid. For low voltages, below about 30 volts, the pulses were not collected efficiently and the distribution showed anomalous peaking effects. At voltages of between 30 and 60 volts the distribution was smooth, but showed a general rise towards the edges of the grid, and at voltages greater than 60 volts the distribution became non-linear with peaking at each wire, fig 5.9.

The linearity of the position pulse with distance.

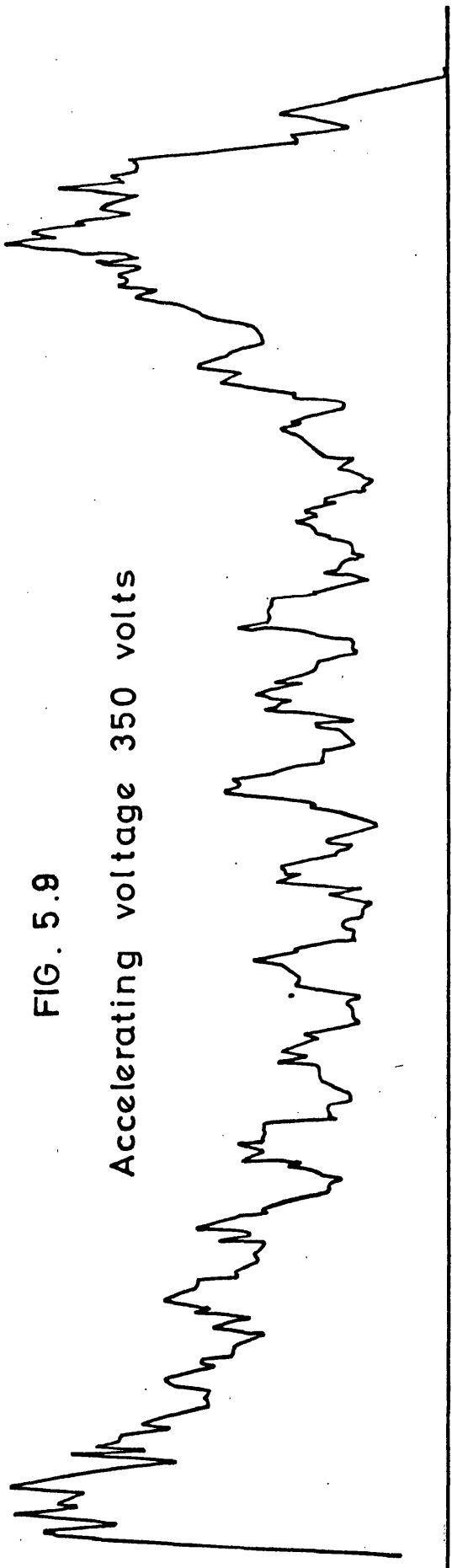
In order to investigate further the distributions obtained under uniform illumination, the slits in the X-ray collimator were aligned to be parallel, both to each other and to the grid wires, and the response to a narrow beam of X-rays investigated. Because of the relatively high optical transmission of the array, it was found to be possible to achieve this alignment quite accurately, to within $10\ \mu\text{m}$ or so, with the grid and array in position.

A narrow beam of X-rays, approximately $40\ \mu\text{m}$ wide at the

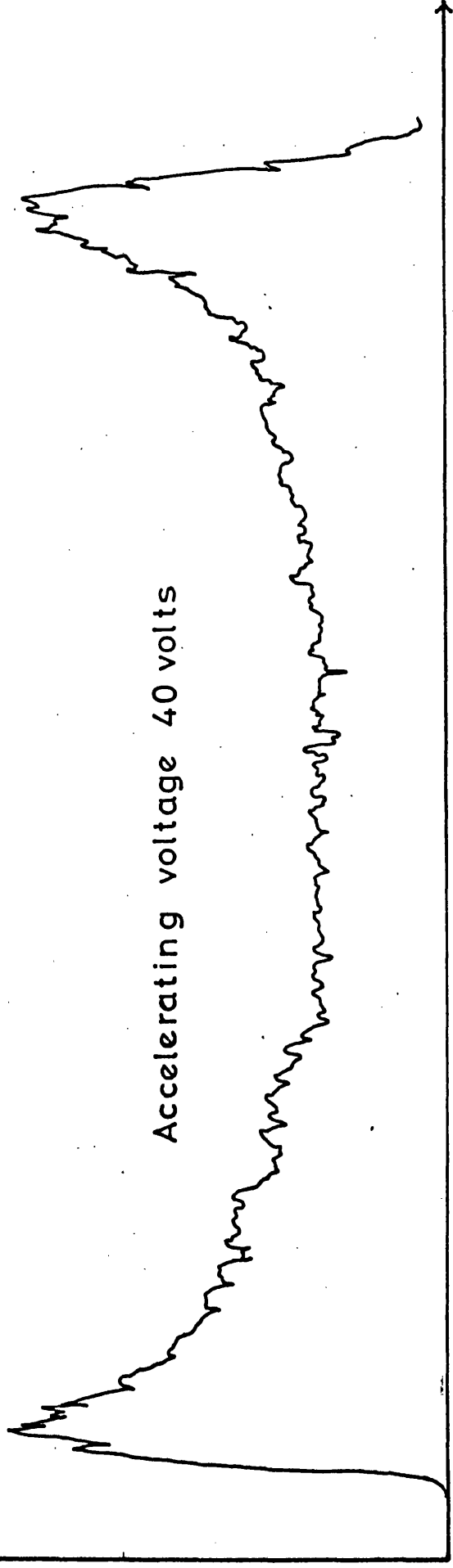
Counts per Channel

FIG. 5.9

Accelerating voltage 350 volts



Accelerating voltage 40 volts



Channel Number

array, was obtained and the grid scanned across it using the micro-meter driven table discussed earlier. For any position of the beam the position pulse height distribution was approximately gaussian made up of contributions from the width of the beam and the electronic noise. A full analysis of the spatial resolution is given in a following section.

The array was scanned across the beam in steps of $100\ \mu\text{m}$ and the peak of the position pulse height distribution recorded. The most linear response was obtained with a collecting voltage of 40 volts and is shown in fig 5.10 compared to that obtained with the standard pulser. The measured curve agrees well with the predicted curve obtained from the pulser except at the ends of the grid, where an additional loss in linearity is apparent. A check over the centre part of the grid with a narrow beam, approximately $20\ \mu\text{m}$ wide moved in steps of $20\ \mu\text{m}$ is shown in fig 5.11.

In fig 5.12 the response for a collecting voltage of 350 volts is shown, the flat regions in the distribution corresponding to the wire positions obtained from the pulser calibration.

Discussion.

As the linearity curves are clearly closely related to the distributions under uniform illumination, the discussion will be restricted mainly to the latter. The shape of these distributions is dependent on the field conditions in the gap; for low collecting voltages, below about 20 volts, the distribution is peaked around the wire positions but does not go to zero at intermediate positions, for a voltage of about 40 volts very little irregularity is evident at wire positions as shown in fig 5.11, while for higher voltages the distribution again becomes peaked at wire positions, fig 5.9.

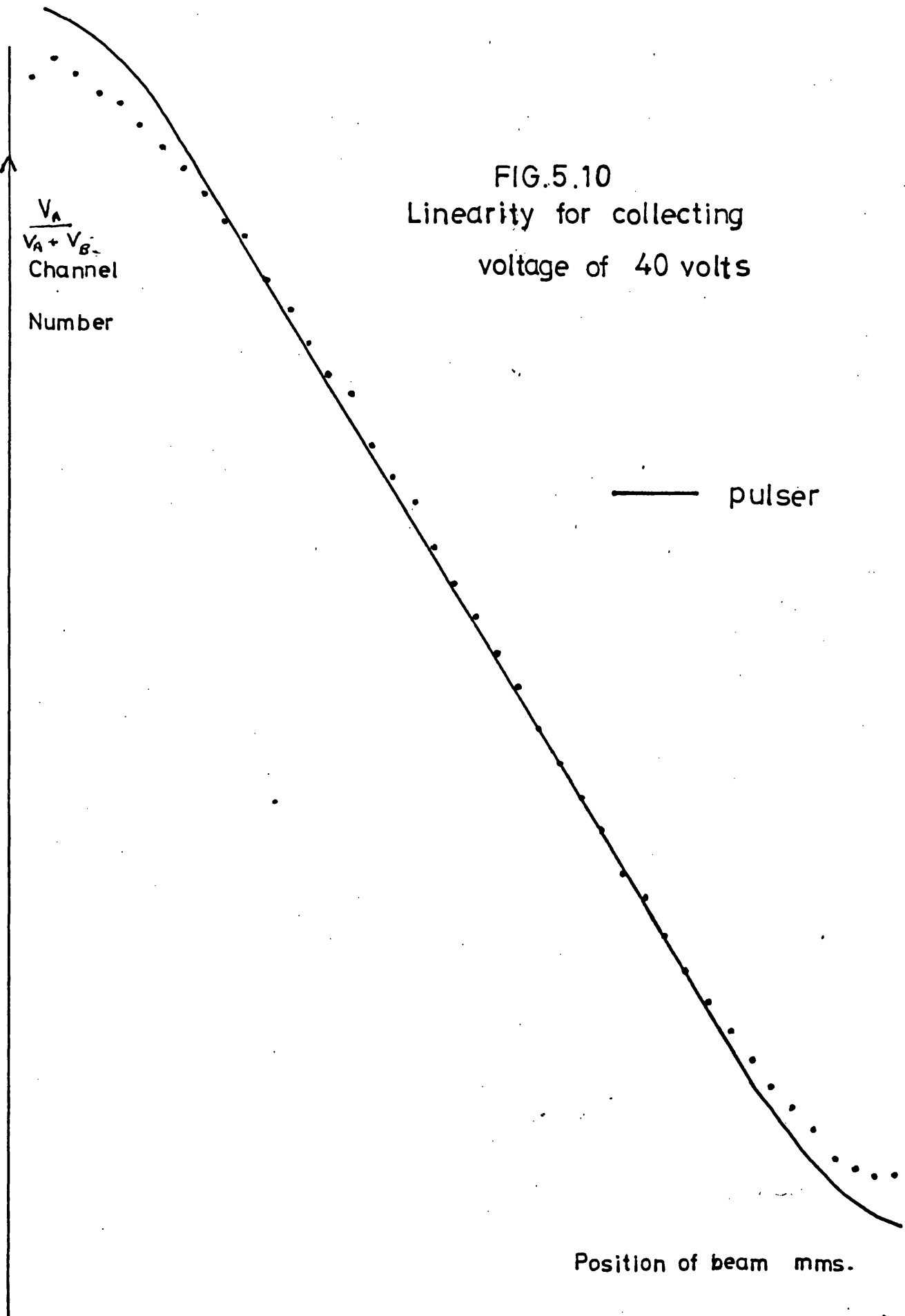
FIG.5.10
Linearity for collecting
voltage of 40 volts

$\frac{V_A}{V_A + V_B}$
Channel
Number

— pulser

Position of beam mms.

14 15 16 17 18



$$\frac{V_A}{V_A + V_G}$$

Channel number

FIG. 5.11

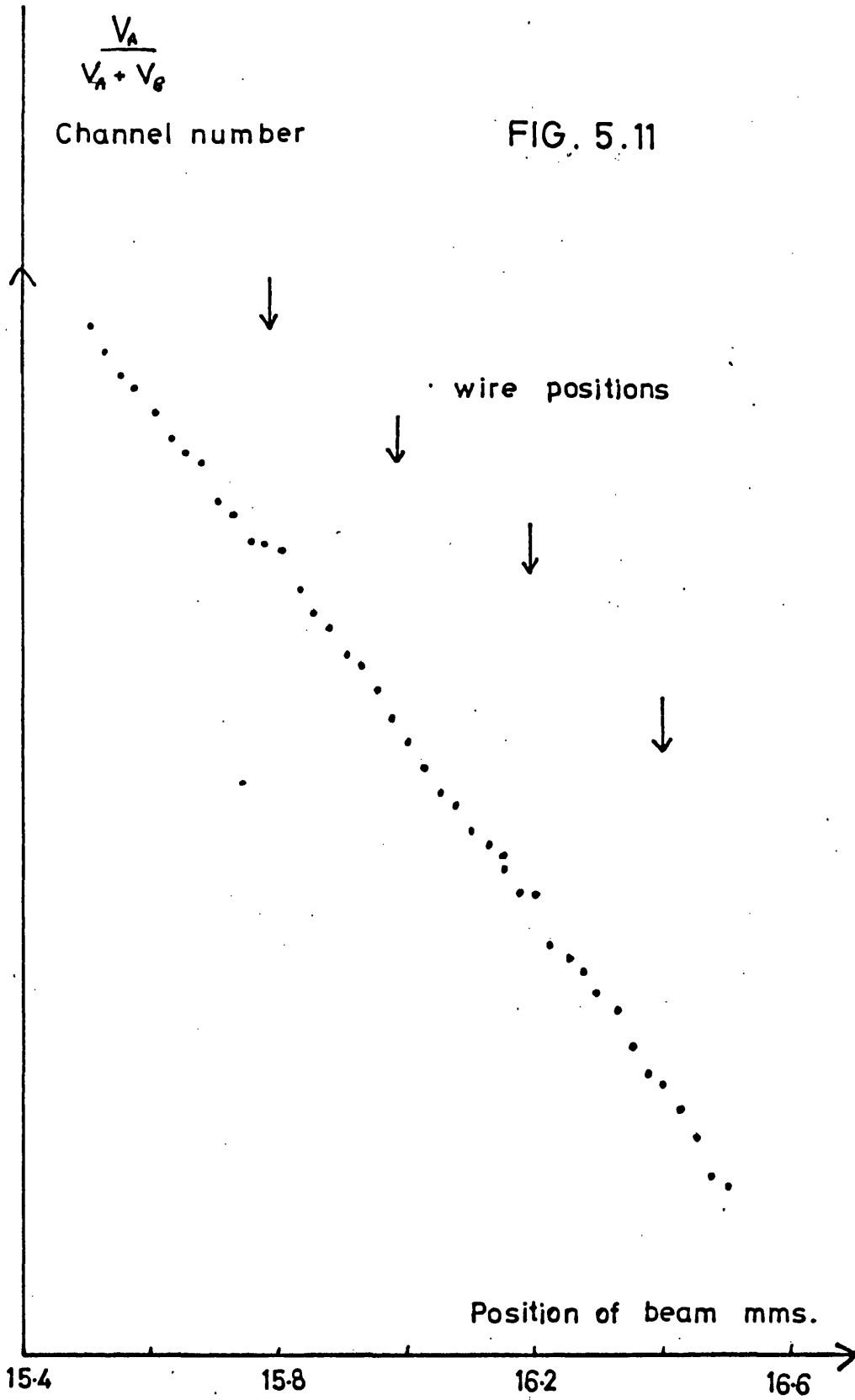


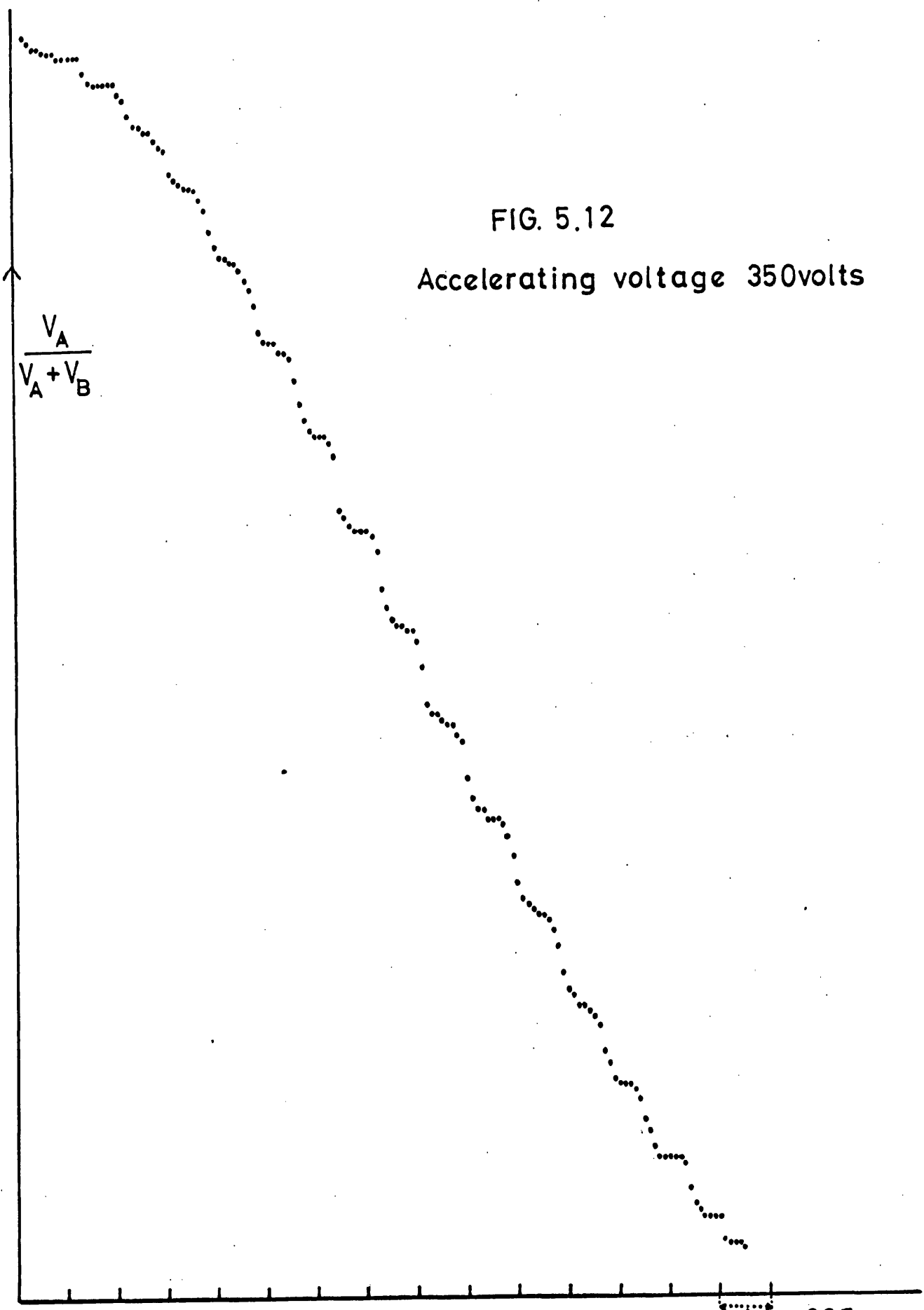
FIG. 5.12

Accelerating voltage 350volts

$$\frac{V_A}{V_A + V_B}$$

0.25 mm.

Position of beam



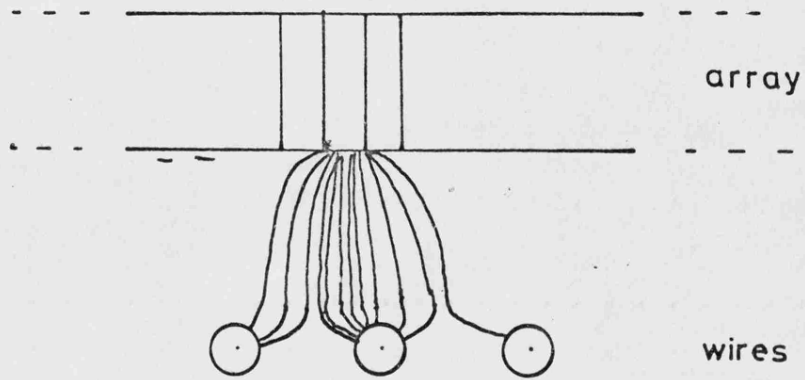
(The distribution for low voltages, not shown, is very similar to that for high voltages, although the change in the distribution is a gradual transition.)

The only effect on the pulse of the field strength is in the energy of the electrons on arrival at the grid and hence their time of flight, which in turn determines to what extent ballistic effects are important. Before making any further attempt at analysis, therefore, some qualitative idea at least of the energy distribution of the electrons in the pulse and the field conditions in the gap is required.

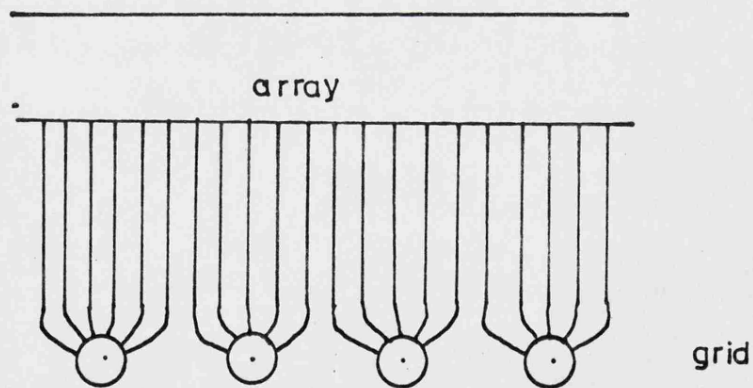
Guest (1970) has obtained values for the number of electrons having an energy within certain ranges and also the retarding potential required to stop electrons of given energies. Using these figures it is possible to estimate the energy and directional distribution of the electrons in the pulse. A qualitative picture of the pulse is shown in fig 5.13.a. A significant fraction of the pulse has a considerable velocity perpendicular to the channel. Although the figures obtained by Guest are not directly applicable to this array at this voltage, a total energy of 12.5 eV with an energy along the channel axis of 10 eV for about 20% of the pulse can be estimated. Assuming a uniform field between array and grid, the spread in the electron pulse could be as much as 200 μm , or one wire pitch, depending on the field strength.

In order to evaluate the field a solution of Laplace's equation must be found. A simplified solution for parallel, infinitely narrow wires is given in many text books, (see for example, Methods of Theoretical Physics, Morse and Feshbach, 1953, p 1236) and this simplified solution was used to estimate the field conditions in the gap for a 40 volt collecting voltage, fig 5.13.b.

FIG. 5.13



A. The electron pulse.



B. The field in the gap.

Low collecting voltages.

For voltages below about 20 volts the spread in the electron pulse due to ballistic effects will be most pronounced. If this spread covered two or more wires, it can be shown that the position pulse height represents the 'centre of gravity' of the discrete amounts of charge collected by each of the wires (see appendix).

Clearly then, if this spread is sufficiently extensive and uniform, the position pulse height will represent the position of arrival of the pulse and the distribution under uniform illumination should be a smooth curve. Conversely, if no spreading occurs, the distribution will go to zero at positions between wires.

The observed distribution is a mixture of these two effects indicating that the spread is insufficient for the position pulse to accurately reflect the origin of the electron pulse.

A collecting voltage of about 40 volts.

For collecting voltages greater than about 20 volts, the electrons in the pulse will have sufficient energy to liberate secondary electrons. Because of the field configuration these electrons do not need much energy to cross the field lines and be collected by adjacent wires.

The net effect of this is to increase the effective spread of the pulse. It is important to note however, that this additional spreading only gives a position pulse of the centre of gravity of the pulse because the secondary emission reflects the spread in the pulse due to ballistic effects.

The effective spread in the pulse, including the effect of secondary emission, was measured using a single wire of the grid for a collecting voltage of 40 volts, a scan across the beam giving a value for the spread of about 350 μm f.w.h.m., in general agreement with the above argument and with the previous observations.

The distribution under uniform illumination is now a smooth curve, but the linearity curve of fig 5.11 shows that there is still a small effect at the position of the wires. The additional loss in linearity towards the edge of the grid noted in fig 5.10 can be attributed to the spreading of the pulse. The loss occurs within about one or two wire pitches of the edge of the grid and is consistent with part of the pulse spreading and being collected by the guard strips. The position pulse will then be weighted towards the centre of the grid in agreement with the observations.

High collecting voltages.

As the collecting voltage is increased beyond 40 volts the distribution becomes peaked, the extent of the peaking depending on the field. This is caused by a reduction in the spread of the pulse which is due to two factors.

The increased energy of the pulse decreases the time of flight and hence the ballistic spread. Also the field lines in the gap become stretched and although the secondary emission yield is increased, there is no increase, to a first approximation, in the energy of the electrons, and the number of electrons capable of crossing the field line is reduced. The position pulse will then tend to peak.

The distribution under uniform illumination follows the

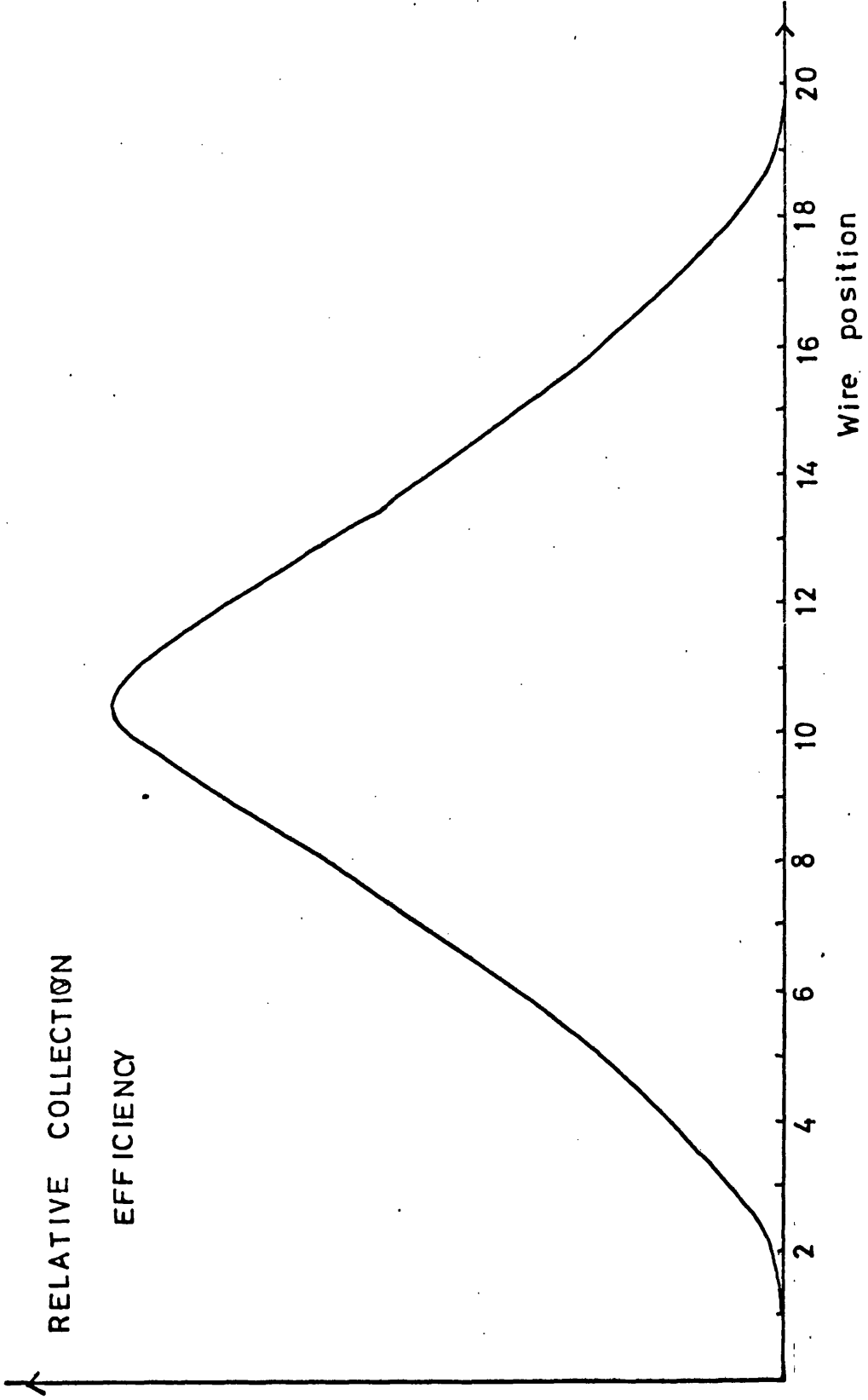
predicted distribution from the linearity curve very well, the former being approximately the mathematical derivative of the latter. However this would not necessarily be expected because ^{large enough} pulses λ to make both q_a and q_b occur above the discriminator in the centre of the grid may not do so at the edges, due to the attenuation of the network. As a result of this and the fact that the array pulse height distribution is exponential, the efficiency, defined as the number of pulses giving rise to a position pulse, as a function of distance along the grid should have a maximum value at the centre. In fig 5.14 the predicted efficiency is shown for discriminator settings of $2 \cdot 10^{-14} C$ and an array gain of $7 \cdot 10^{-14} C$, typical values for this array and electronics. The fact that this does not occur in the distributions shown earlier can be explained by the requirement that $V_a + V_b$ should be between 5 and 10 volts stipulated for accuracy in the divider. A pulse $V_a + V_b$ of 5 volts is equivalent to an input charge sufficiently large for the attenuation of the network never to make either q_a or q_b fall below the discriminator.

Clearly, for most applications a uniform response across the grid is essential and this requirement leads to a fall in effective efficiency. The restriction on pulse heights can be reduced by only using the centre part of the grid as the detecting area, and under these circumstances there will be a net reduction in effective efficiency by a factor of about two.

The linear resolution of the system.

In order to investigate the spatial resolution, the collimator slits and the grid were realigned very carefully and the slits adjusted to the narrowest measurable width giving a beam width at the array of $40 \pm 20 \mu m$. The array and grid were stepped across the beam and a

FIG. 5.14



distribution collected at each point. The results for a collecting voltage of 40 volts are shown, superimposed, in fig 5.15 where it can be seen that positions 150 μm apart are well resolved over most of the grid except at the edges. This is due to the loss in linearity discussed earlier. The effect on the f.w.h.m. of these distributions for an increased collector voltage is shown in fig 5.16 where the distributions for positions 25 μm apart over a distance of one wire pitch are plotted for a collecting voltage of 350 volts. The tendency of the position pulse to hold on a wire position is very clearly demonstrated. A similar plot for 40 volts collecting voltage revealed no measurable change in f.w.h.m.

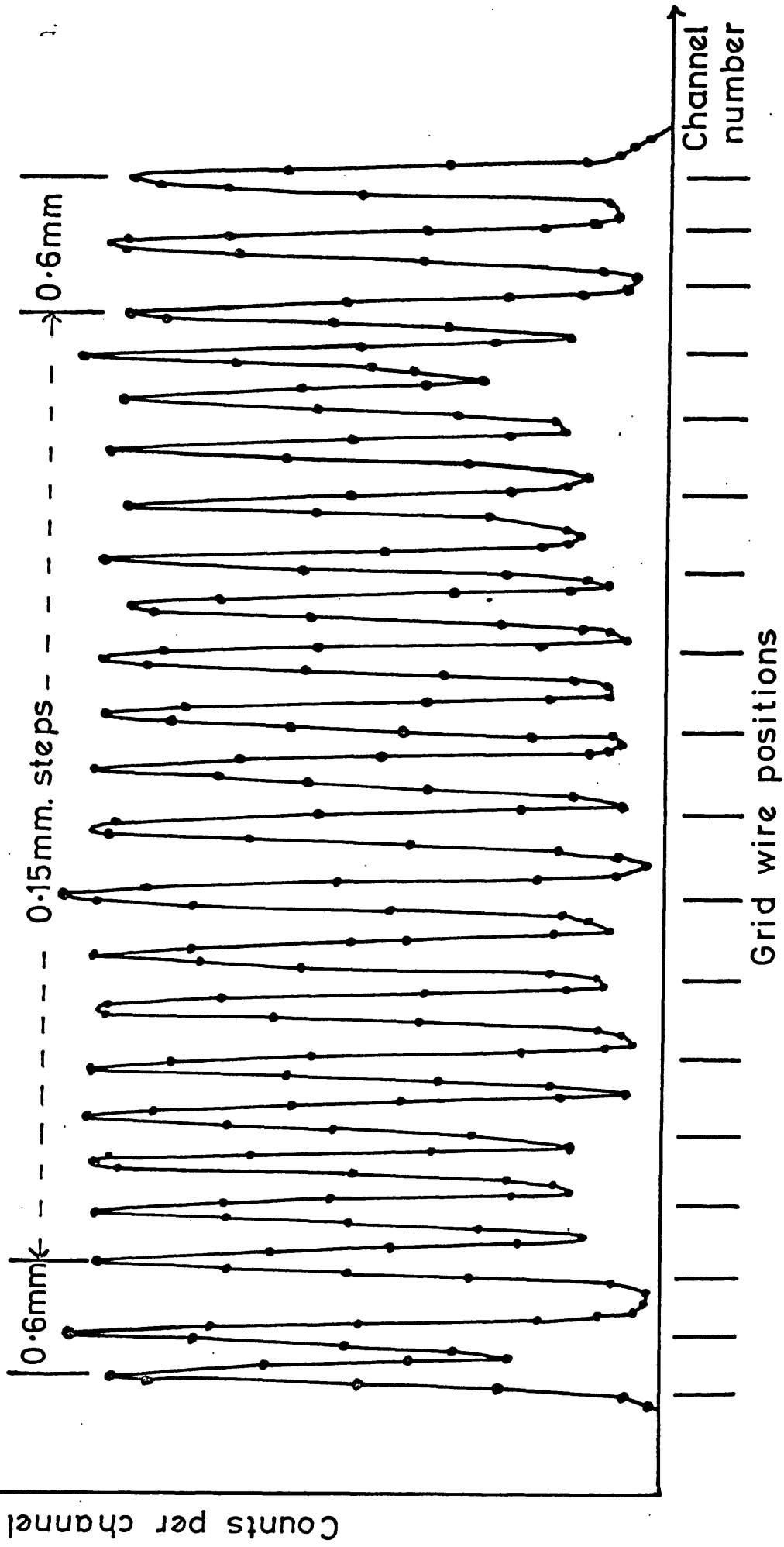
To assess the ultimate resolution of the grid it is necessary to compare the f.w.h.m. of the distribution obtained experimentally with the predicted width determined from the electronic noise and the beam width. The contribution due to electronic noise may be found using the standard pulser and the beam width may be expressed in channel numbers as a difference in pulse heights as mentioned earlier.

Using the zero offset facility on the multi-channel analyser effectively giving it 2048 channels, the distributions for two of the wires in the centre of the grid were obtained using the pulser. The X-ray beam was allowed to fall at two positions giving distributions centred approximately on the wires as shown in fig 5.17. The f.w.h.m. of the electronic noise was 17 channels and the beam width of 40 μm is equivalent to 22 channels. Thus the predicted f.w.h.m. can be calculated as the quadratic sum of these two contributions, that is:

$$\sqrt{17^2 + 22^2} = 28.$$

The error on the measurement of the beam width was 50%

FIG. 5.15



Position Pulse $\frac{V_A}{V_A + V_B}$ for steps of 0.15mm of X-ray beam for 200 μ m grid.

FIG. 5.16

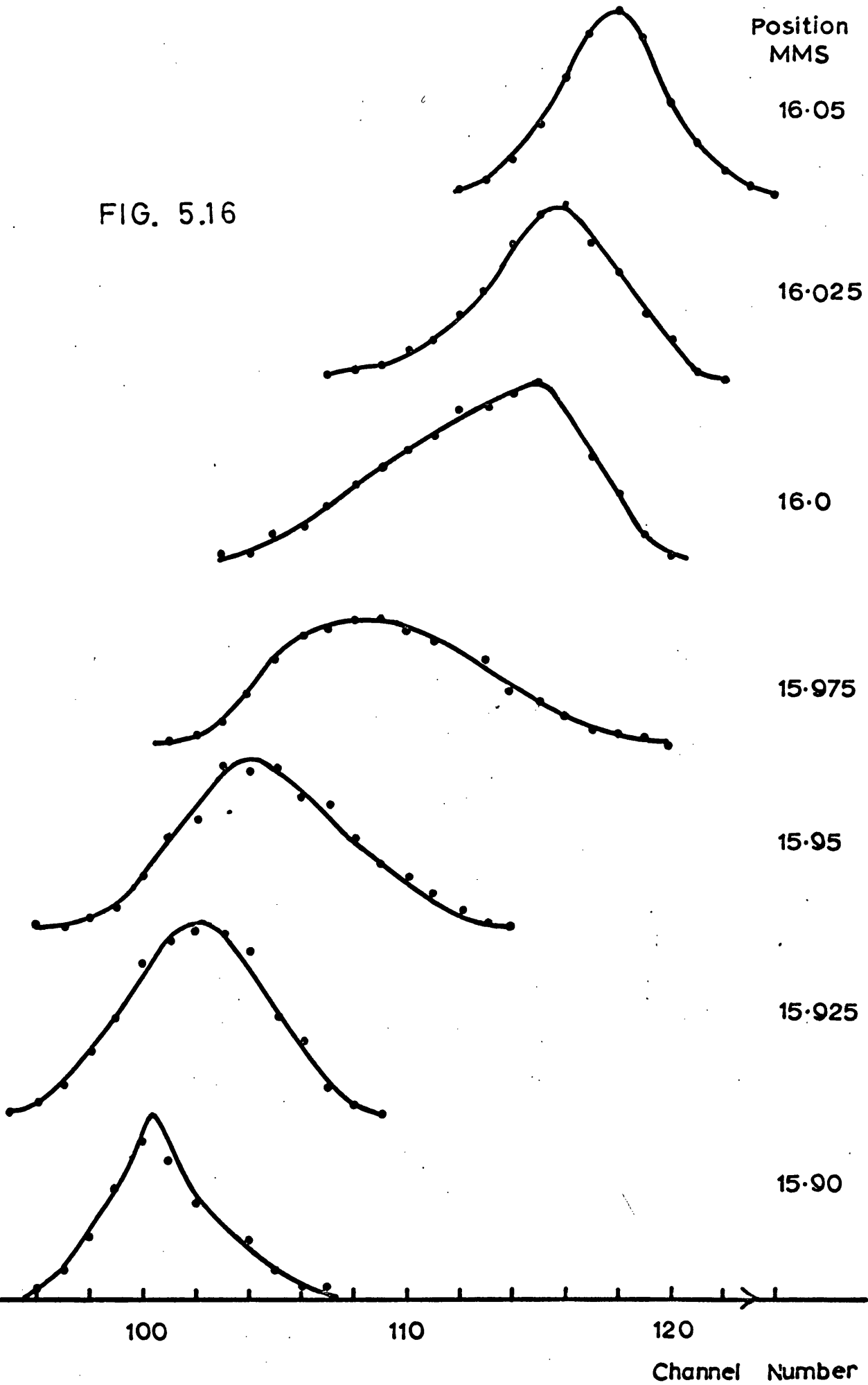
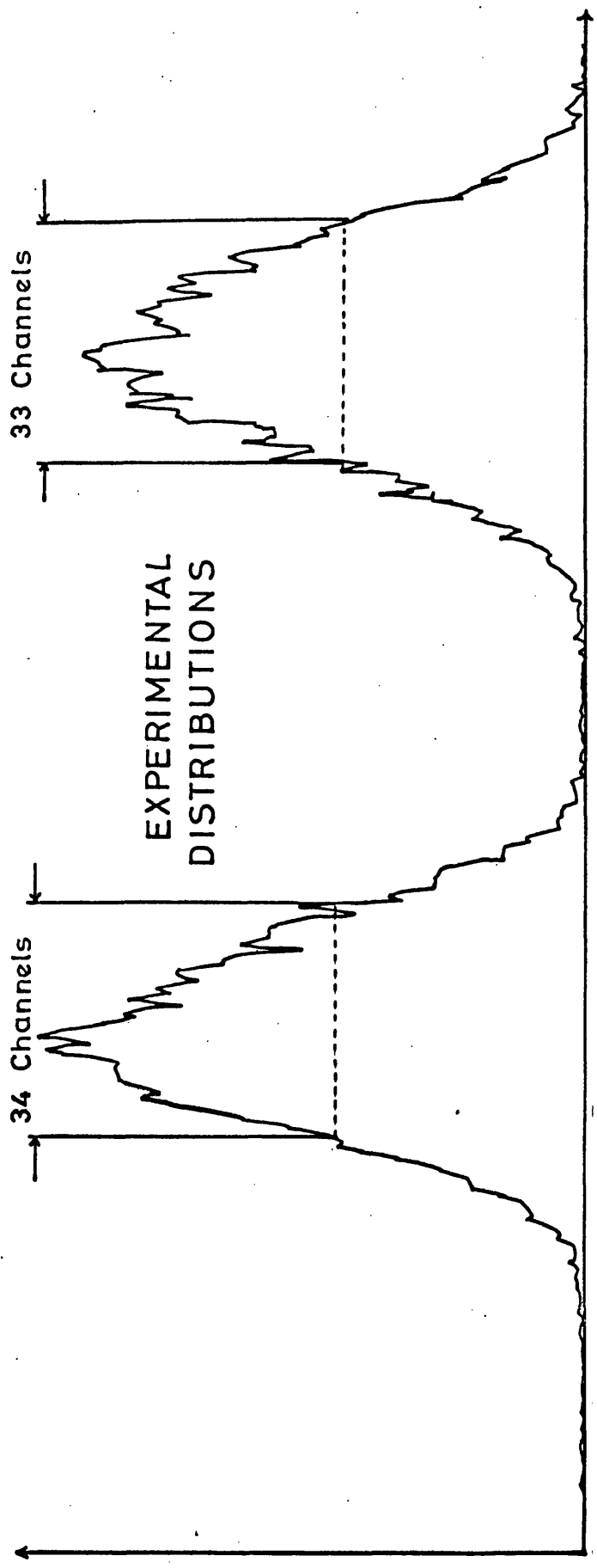
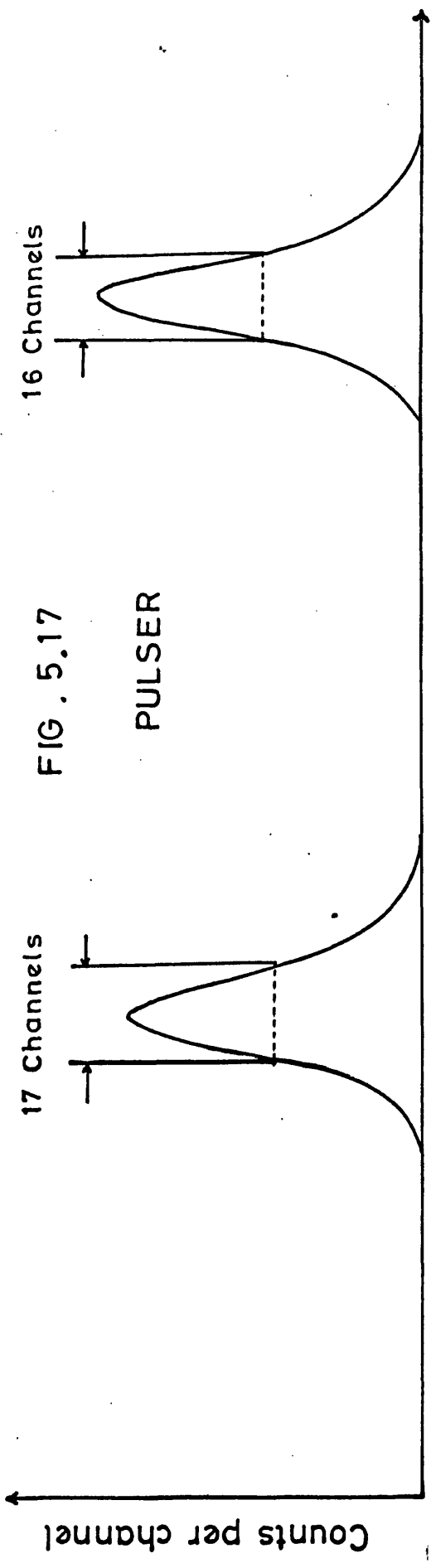


FIG. 5.17

PULSER



giving an error on the experimental width of ± 8 channels. The measured value of 34 channels falls within the error in the prediction.

The effect of the individual channels in the array has not so far been considered but only an estimate can be made of this effect because of lack of knowledge of the pitch and bore of the array. For a pitch of $40 \mu\text{m}$ an extra contribution to the predicted width of $40 \mu\text{m}$, or 22 channels of the analyser, would be expected, assuming the beam is randomly aligned to the array. Thus the measured f.w.h.m. can be well accounted for in terms of the noise, beam width and channel diameter. Under these circumstances the ultimate resolution, or positional uncertainty, of the system defined as the f.w.h.m. of the distribution, is $60 \mu\text{m}$.

An improvement in spatial resolution can be achieved by reducing the number of wires, since the noise is a fixed fraction of the dynamic range of the position pulse. To investigate this possibility the number of wires was reduced to four and the above measurements repeated. The distribution under uniform illumination is shown in fig 5.18, again clearly demonstrating the effect of loss of part of the pulse to the guard strips. The distribution is no longer a uniform curve but has peaks associated with the residual non-linearity, which is now enhanced due to the reduction in electronic noise.

In fig 5.19 the narrow beam distributions for positions $150 \mu\text{m}$ apart are shown using the 2048 channel position on the analyser. The linearity curve is shown in fig 5.20 showing that the non-linear region now extends over a considerable part of the grid. The f.w.h.m. of the noise is still only 22 channels but the beam width of $40 \mu\text{m}$ is now equivalent to 80 channels. The predicted

FIG. 5.18

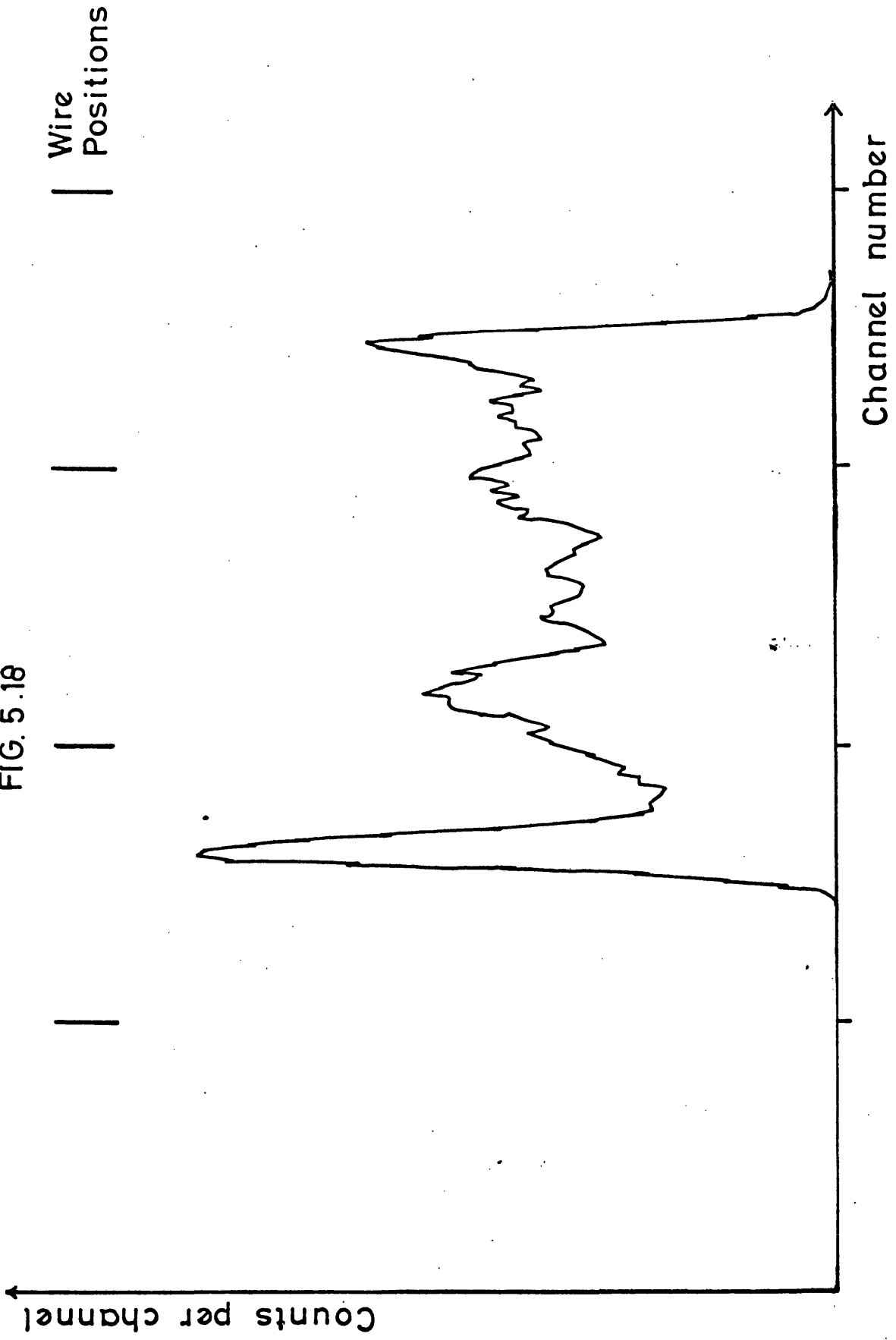


FIG. 5.19

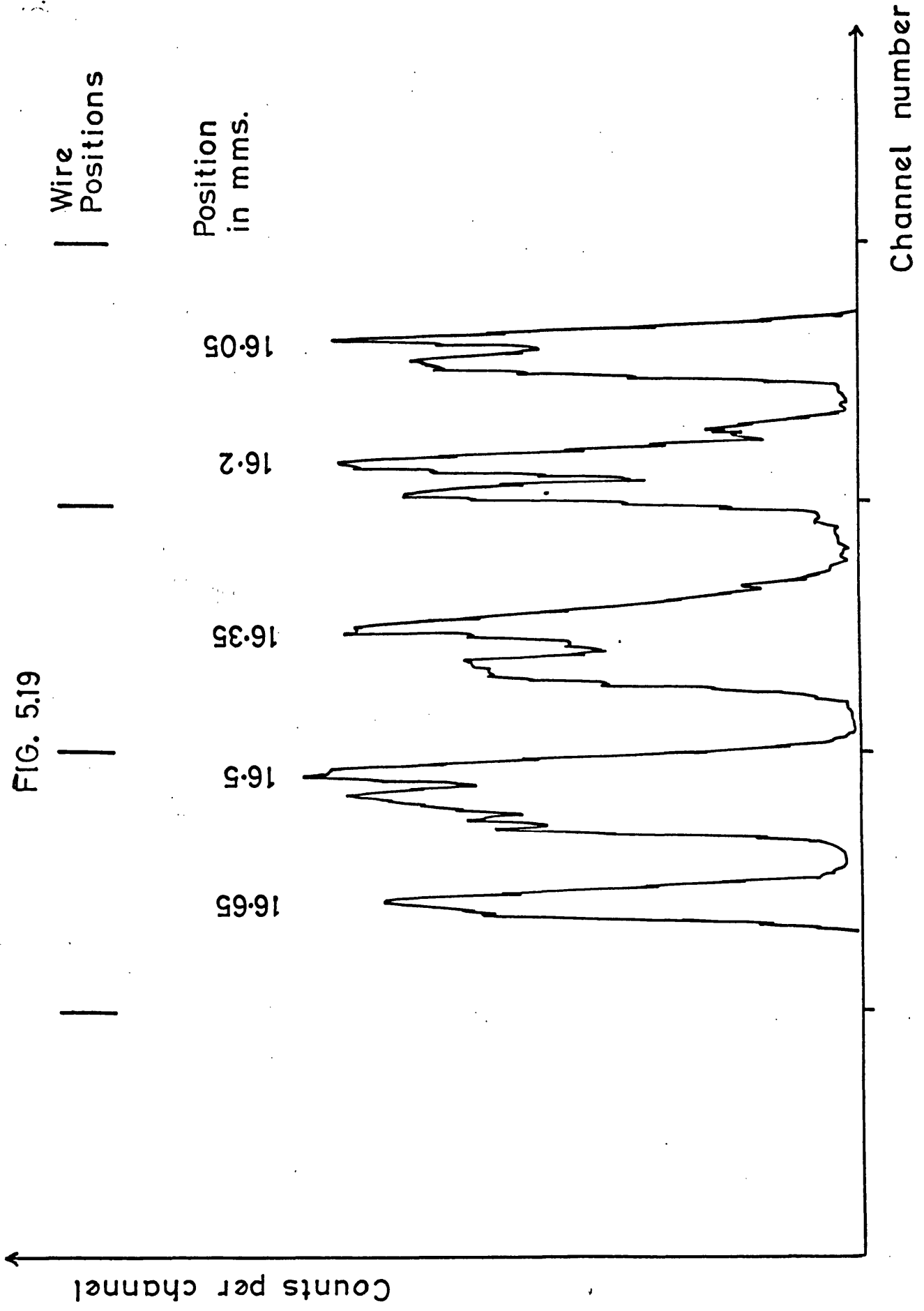
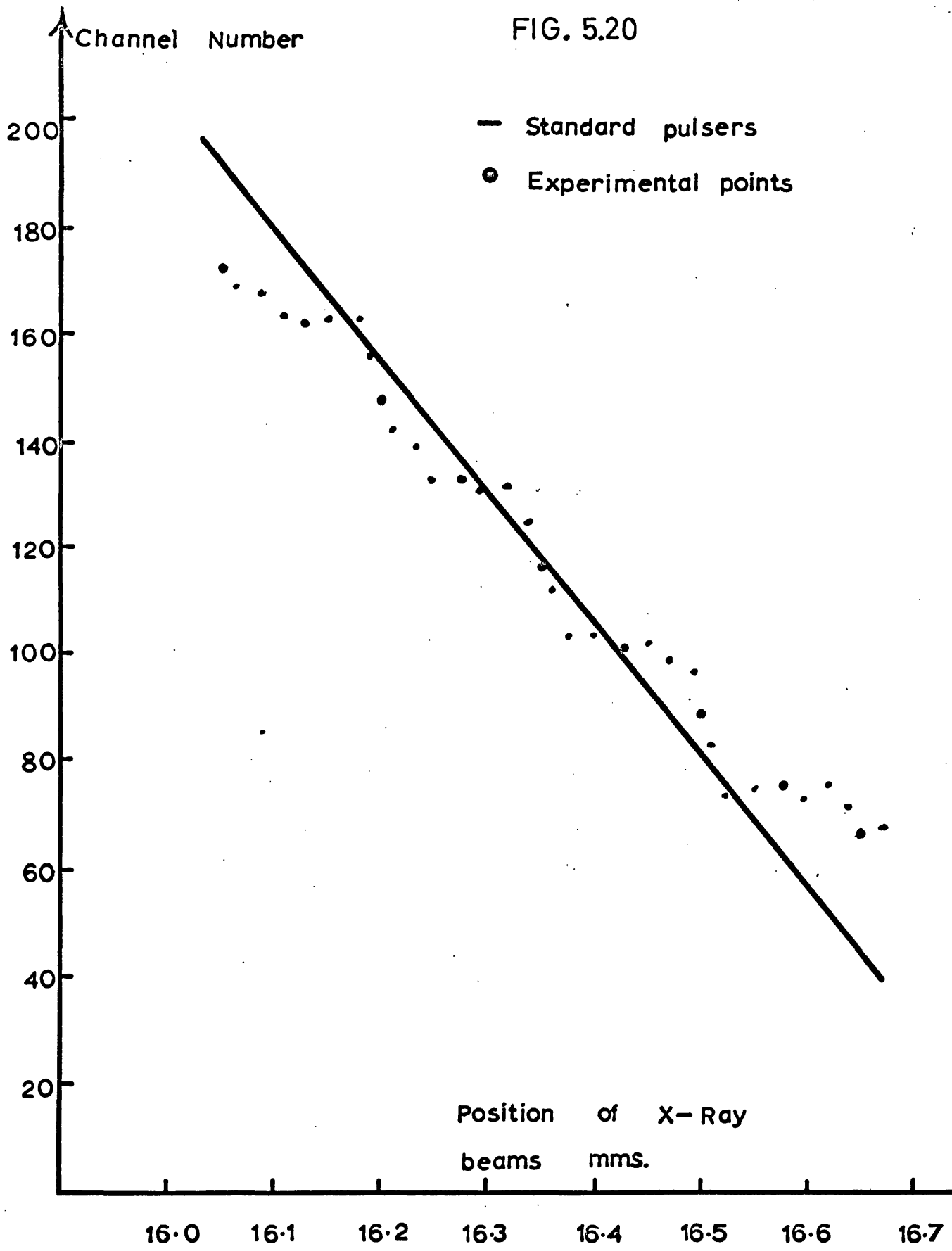


FIG. 5.20



experimental f.w.h.m. should thus be $(80^2 + 22^2)^{\frac{1}{2}} = 86$ channels. The measured f.w.h.m. varies from 80 to 160 and can be correlated with the position of the beam relative to the grid wires indicating that the effect is due to local non-linearities near the wires.

In conclusion it can be said that there is a local non-linearity in the position pulse height correlated with the wire positions. With the twenty wire grid this effect is smoothed out by the noise width, which is comparable to the scale of the non-linearity. For accurate reproduction of the X-ray image, therefore, it is not sufficient only that the spatial resolution be adequate, but the linearity over this distance, and hence the accuracy of reconstruction of the image profile should be maintained. In practice, with the present technology, this means that the pitch of the grid should be less than the distance over which small scale variations in linearity can be tolerated.

Improvement in spatial resolution using a finer grid.

From the above discussion it is clear that the improvements in resolution can best be obtained by using a grid of finer pitch. For wire of less than 100 μm diameter, the previous method of construction using the feed screw of a lathe was found to give poor results, wires tending to overlap. Consequently a winding machine capable of winding grids with 20 μm wire at 40 μm pitch was constructed and is shown in plate 5.2.

The wire is drawn from the spool and passed over a guide pulley, both of which are on a moving table. The frame onto which the wire is wound is rotated slowly using a small DC motor and a cog wheel fastened to the frame is used to pulse a stepping motor via a micro-switch. The number of cogs on the wheel determines the number of pulses per revolution from the microswitch and these pulses are

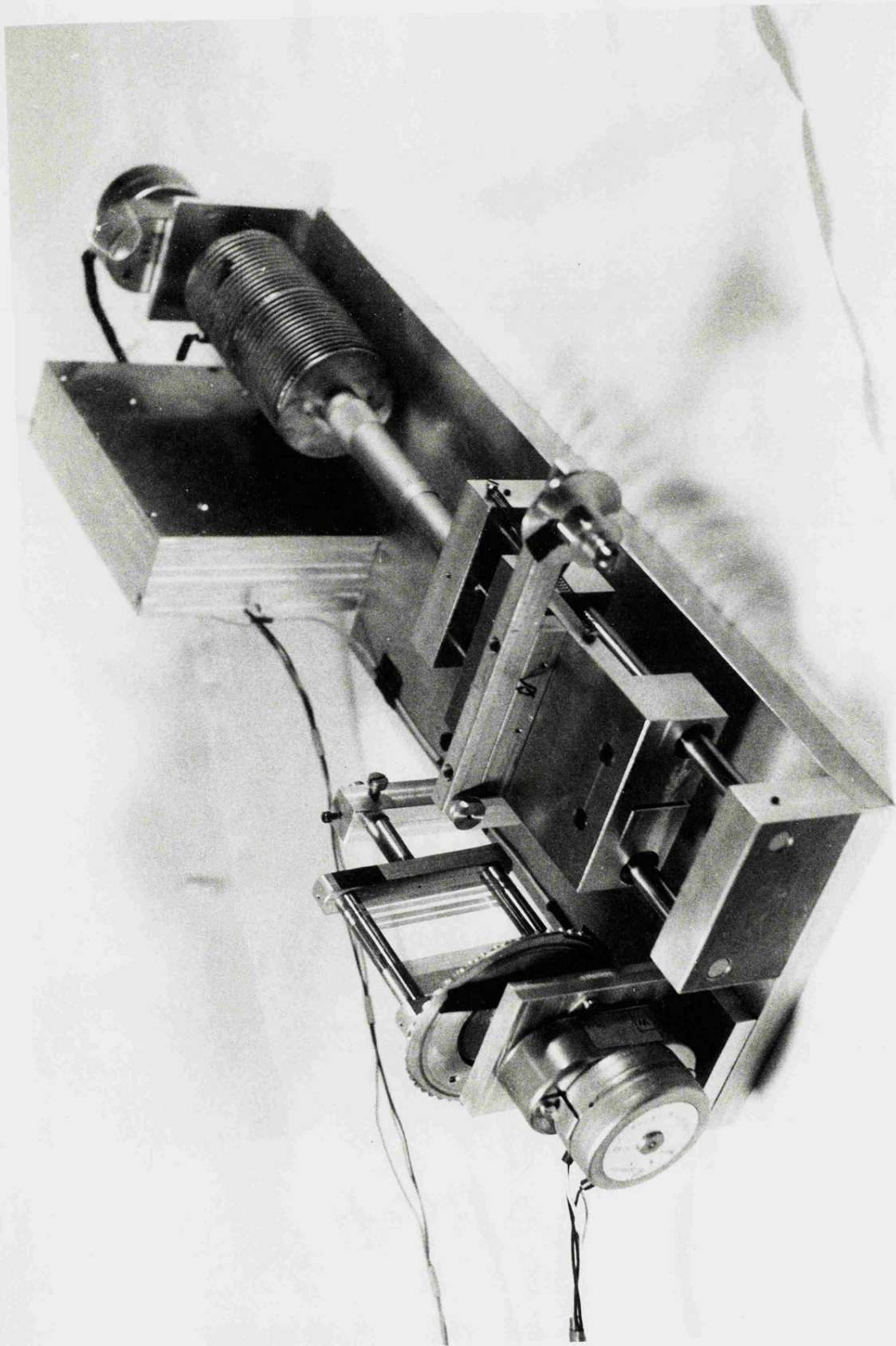


PLATE 5.2

used to drive the stepping motor, via suitable electronics, and hence a micrometer which advances the table. Considerable care had to be taken to achieve a highly polished frame and clean wire, but having taken these precautions a grid of 25 μm wire at 50 μm pitch was wound and transferred to a glass slide as before. The wire used in this case was gold plated tungsten, thus enabling simple solder connections to be made to the condenser network. The completed grid, again of twenty wires and guard strips, is shown in plate 5.3.a and a closeup of the wires in plate 5.3.b. It is apparent from this plate that there are imperfections in the grid produced during the transfer of the wire to the glass plate and subsequent glueing.

The field conditions in the gap were optimised as before using uniform illumination, the best position now being at 75 μm from the array with a collecting voltage of 40 volts. The distribution under uniform illumination was found to be very similar to that for the coarser grid, showing no fluctuations from a smooth curve within the statistical accuracy of the measurement.

The 40 μm X-ray beam was then scanned across the array, again in steps of 150 μm , and the resulting superimposed distributions and the linearity are shown in figs 5.21 and 5.22. The predicted width of the distributions can again be obtained from the electronic noise of 22 channels and the beam width, in this case, of 66 channels giving; $(66^2 + 22^2)^{\frac{1}{2}} = 69$ channels.

The measured f.w.h.m.'s varied considerably over the grid, from 60 to 150 channels. Also, the shape of the distribution should be a smooth curve from the convolution of a rectangular distribution from the beam and the Gaussian of the noise. These large discrepancies in the width and shape of the distributions, especially noticeable

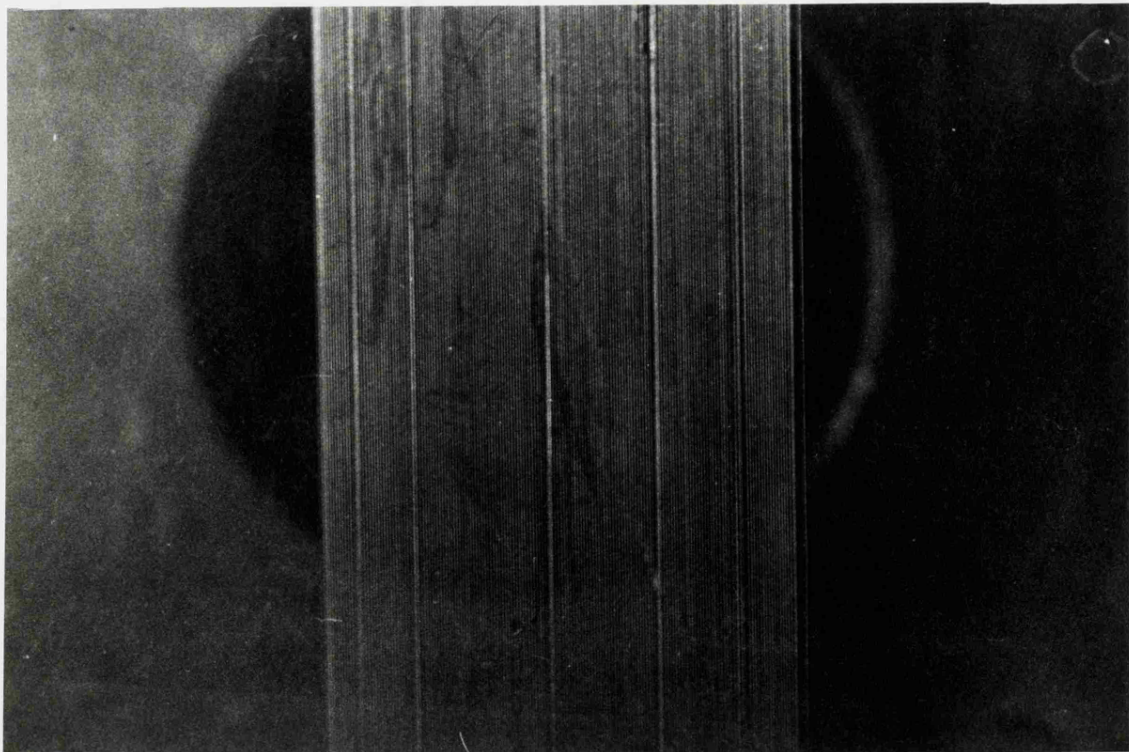
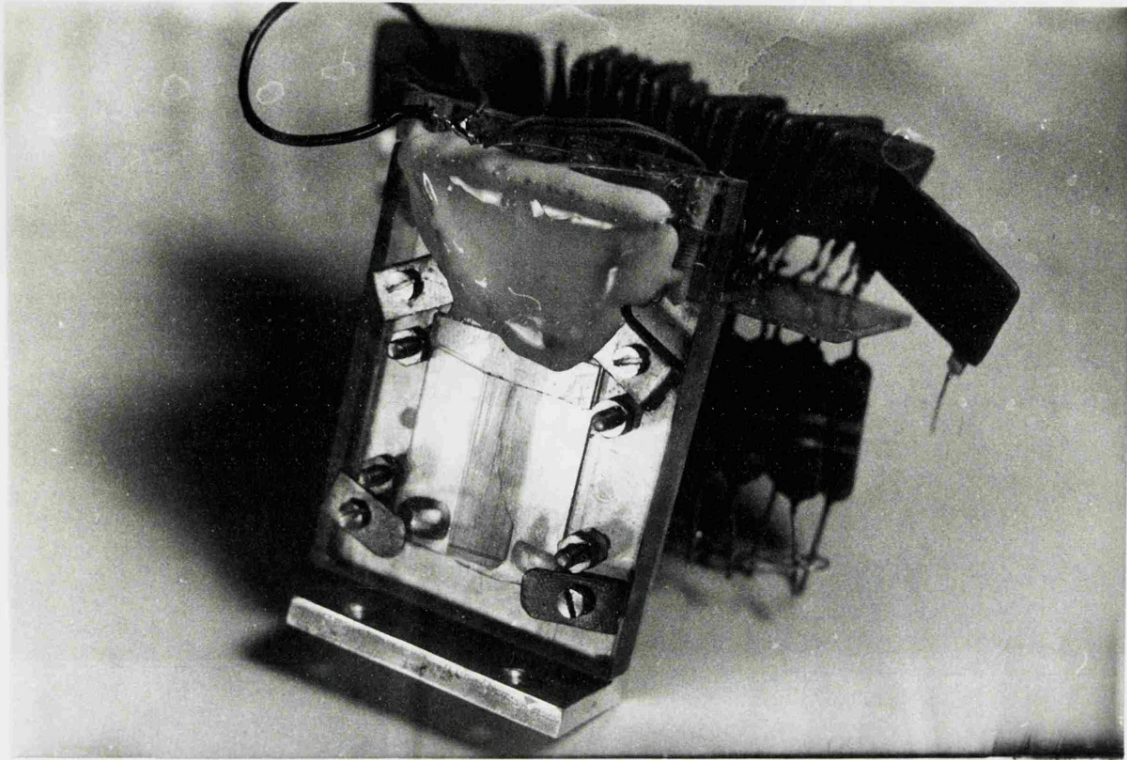
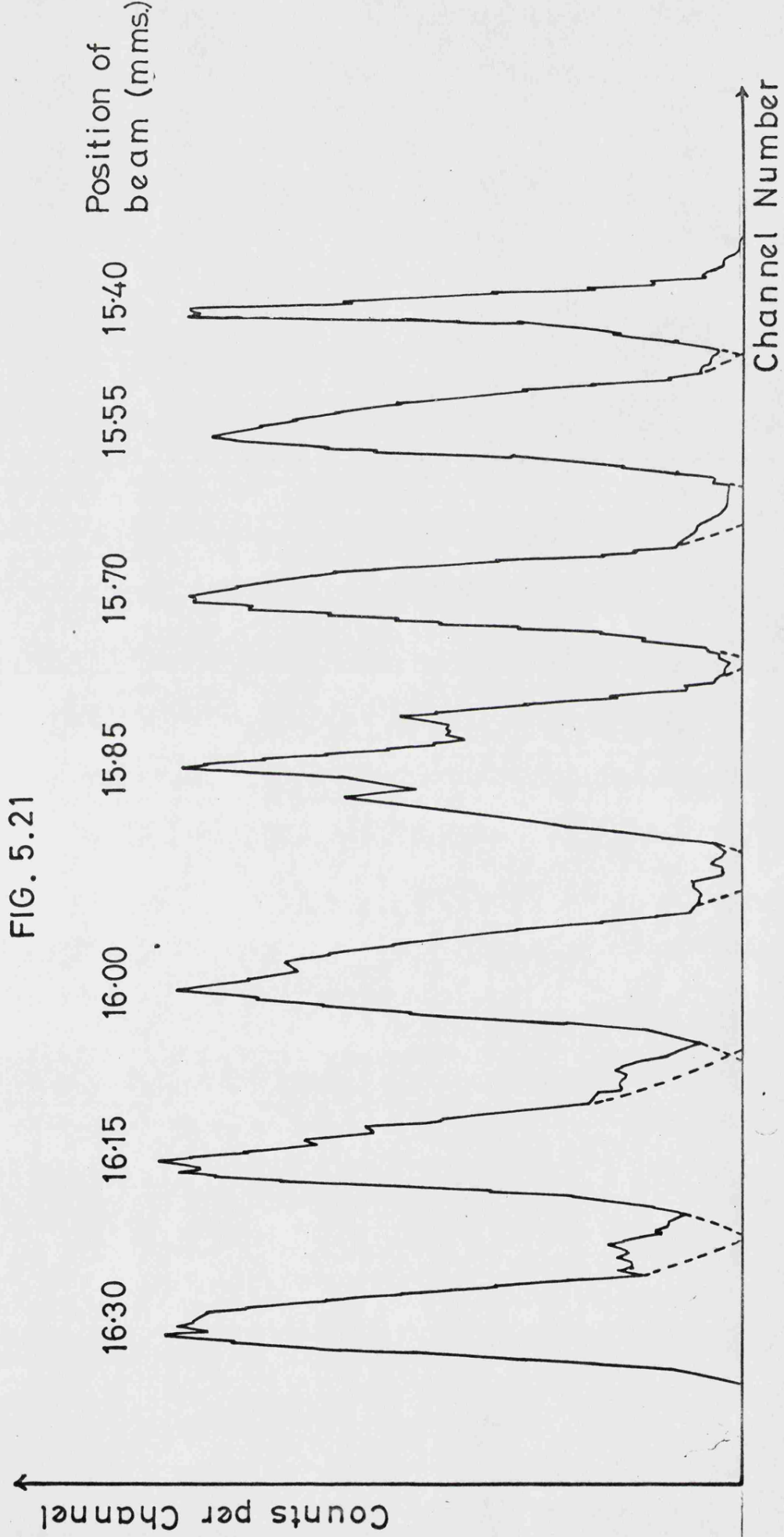
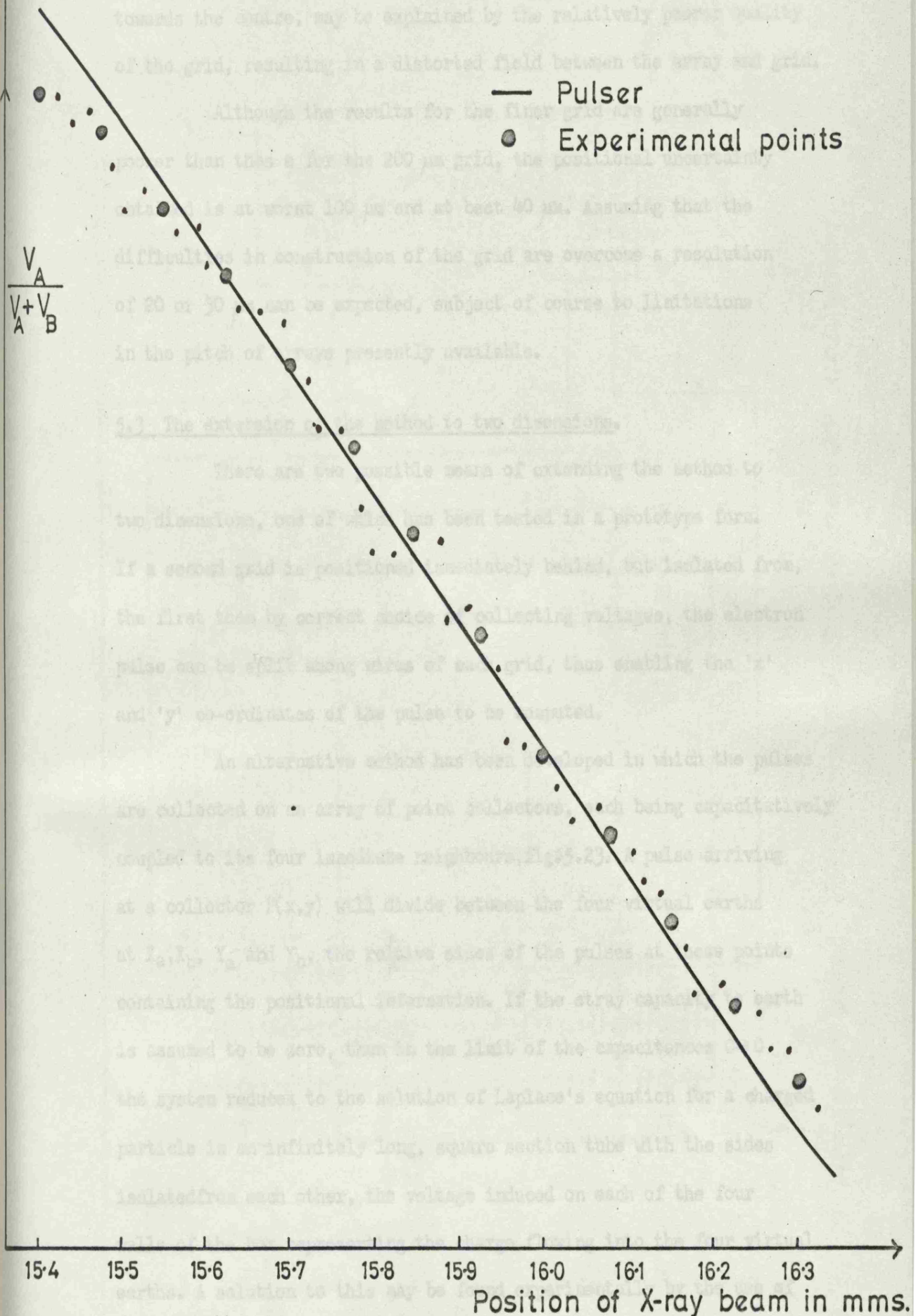


PLATE 5.3



Position pulse $\frac{V_A}{V_A + V_B}$ for steps of 0.15 mm. of X ray beam for 50 μ m. grid.

FIG. 5.22



Variation of $\frac{V_A}{V_A + V_B}$ with position of beam for 50 μm . grid.

towards the centre, may be explained by the relatively poorer quality of the grid, resulting in a distorted field between the array and grid.

Although the results for the finer grid are generally poorer than those for the 200 μm grid, the positional uncertainty obtained is at worst 100 μm and at best 40 μm . Assuming that the difficulties in construction of the grid are overcome a resolution of 20 or 30 μm can be expected, subject of course to limitations in the pitch of arrays presently available.

5.3 The extension of the method to two dimensions.

There are two possible means of extending the method to two dimensions, one of which has been tested in a prototype form. If a second grid is positioned immediately behind, but isolated from, the first then by correct choice of collecting voltages, the electron pulse can be split among wires of each grid, thus enabling the 'x' and 'y' co-ordinates of the pulse to be computed.

An alternative method has been developed in which the pulses are collected on an array of point collectors, each being capacitatively coupled to its four immediate neighbours, fig 5.23. A pulse arriving at a collector $P(x,y)$ will divide between the four virtual earths at X_a, X_b, Y_a and Y_b , the relative sizes of the pulses at these points containing the positional information. If the stray capacity to earth is assumed to be zero, then in the limit of the capacitances $C \rightarrow 0$ the system reduces to the solution of Laplace's equation for a charged particle in an infinitely long, square section tube with the sides isolated from each other, the voltage induced on each of the four walls of the box representing the charge flowing into the four virtual earths. A solution to this may be found experimentally by the use of either discrete resistors or a resistive medium such as an electrolyte

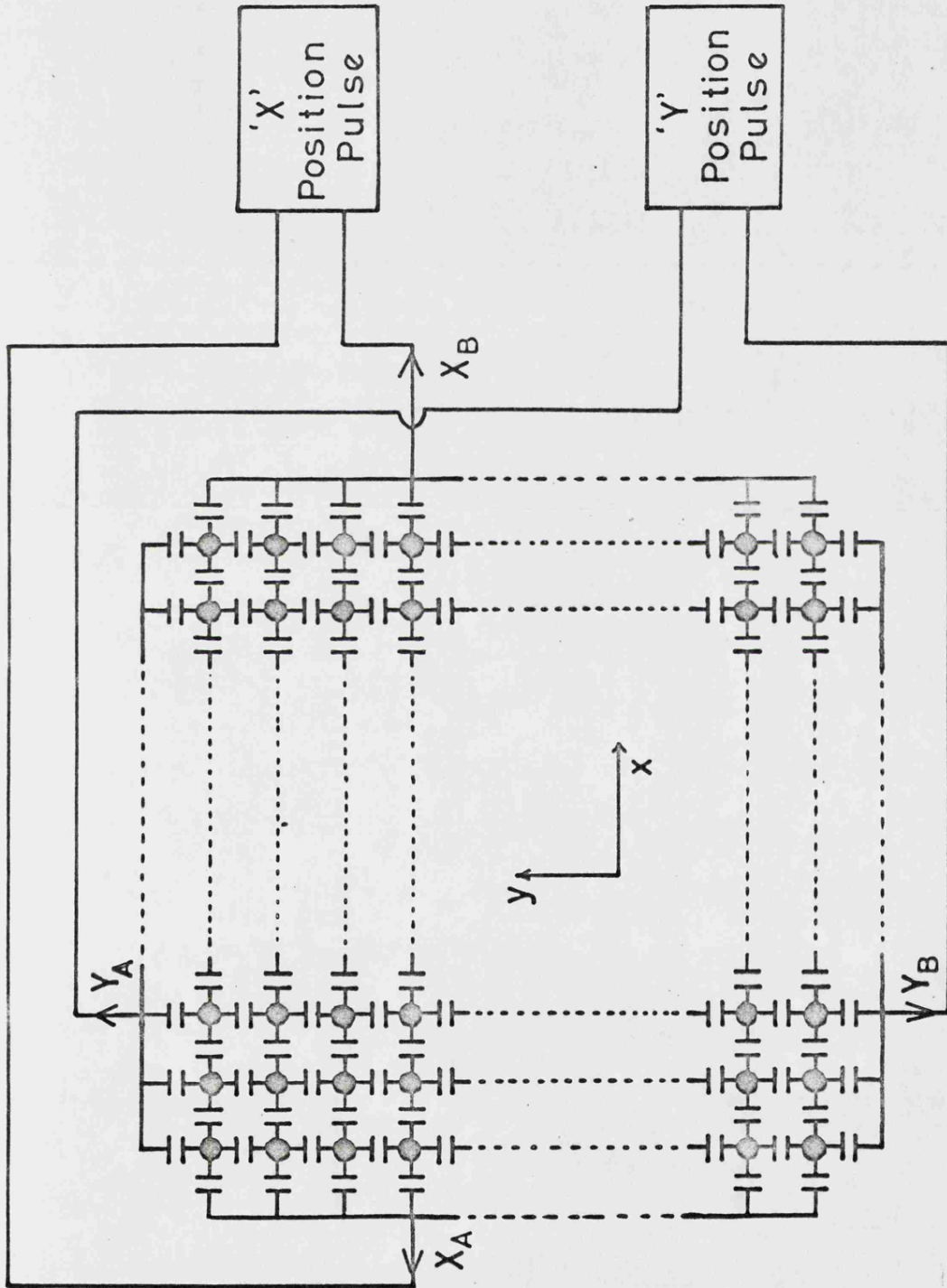


FIG. 5.23

Array of point collectors for 2 dimensional analysis

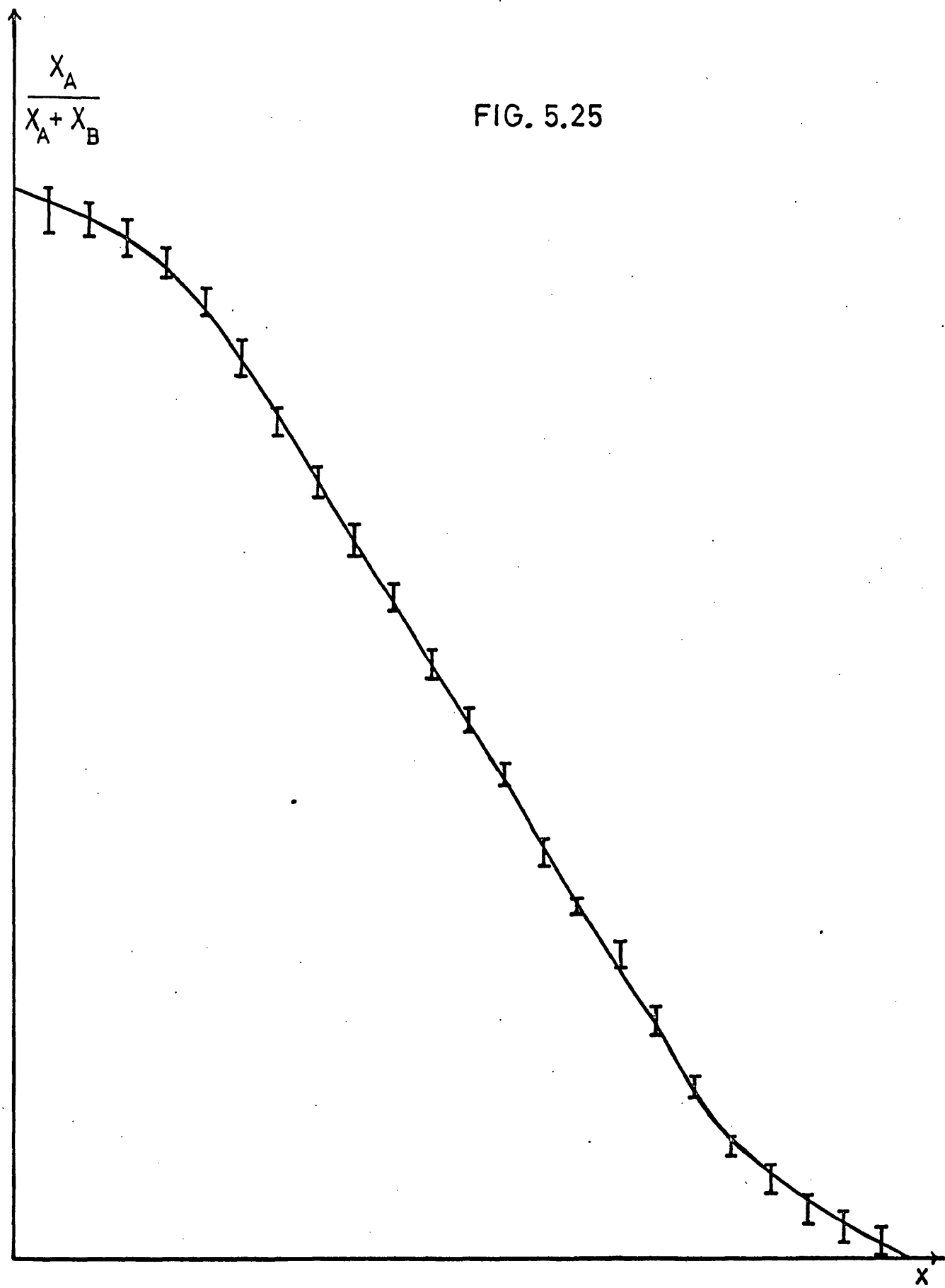
or graphite paper.

An initial check on the idea was made by replacing the condensers shown in fig 5.23 by discrete resistors to build up a 5 x 5 point array. The current flowing from the sides of the array when a probe at a different potential was applied to any point was measured, this current being analagous to the charge branching process in a condenser network. In fig 5.24 the position pulse $X_a/(X_a+X_b)$ is shown as a function of x , y being held constant, for a strip contact to all the resistors forming a side of the array and for a point contact in the centre of each side. The different values of $X_a/(X_a+X_b)$ for a particular value of x are those obtained when y is varied. Clearly, for a point contact there is a wide variation in position pulse height for different values of y , while the variation for a strip contact is within experimental error.

After this preliminary check had established that strip contacts were necessary, a more comprehensive check was made using a resistive graphite sheet. The position pulse height is shown in fig 5.25, the error bars having the same significance as for fig 5.24. Using this technique it became clear that determination of $X_a/(X_a+X_b)$ and $Y_a/(Y_a+Y_b)$ would give the x and y co-ordinates of the position of arrival of each pulse.

In order to test this method experimentally a grid of 7 x 7 points was constructed using 125 μm 'Lumex' insulated wire by stretching the wires, fixed in a square array on two sheets of 'vero-board' and twisting one of the sheets through 180° bringing the wires in the centre together to form a closely packed square array. The wires were then glued and sawn off, the end being polished and the resulting grid potted in a non-conducting epoxy. Each of the

FIG. 5.25



Simulated collector position

wires was then soldered into a discrete condenser network, the completed assembly and a close-up of the grid being shown in plate 5.4.

Because of the large number of components and the limited amount of space in the vacuum chamber, no leak resistors were used and since the potting material was non-conducting the guard ring could not be earthed. As a consequence, the grid and guard ring charged up fairly rapidly under uniform illumination, but using a narrow beam of radiation the count rate was sufficiently low for the charge to leak away and give fairly stable operation. Because of this charging of the grid under uniform illumination, it was not possible to optimise the collecting voltage very accurately experimentally and this was predicted on the basis of the previous results with the one-dimensional grid.

The grid was checked using charge pulses from the standard pulser and the curves for X_a , $X_a + X_b$ and $X_a / (X_a + X_b)$ are shown in fig 5.26. The narrow beam of X-rays, 40 μm wide, in the x direction and covering the whole array in the y direction, was aligned to fall along the y axis of the grid, and stepped along the grid as before. The resulting distributions are shown in fig 5.27. The beam width, which is equivalent to 100 channels, together with the f.w.h.m. of the electronic noise of 45 channels, gives an expected experimental f.w.h.m. of 110 channels. The measured width varies from 70 to 150 channels and can be correlated with the position of the beam relative to the wire positions indicating that the discrepancy is due to residual non-linearity.

This was confirmed by a careful linearity check which is shown in fig 5.28 in which the 'staircase' effect is clearly demonstrated. The two dimensional grid described here has obvious disadvantages due

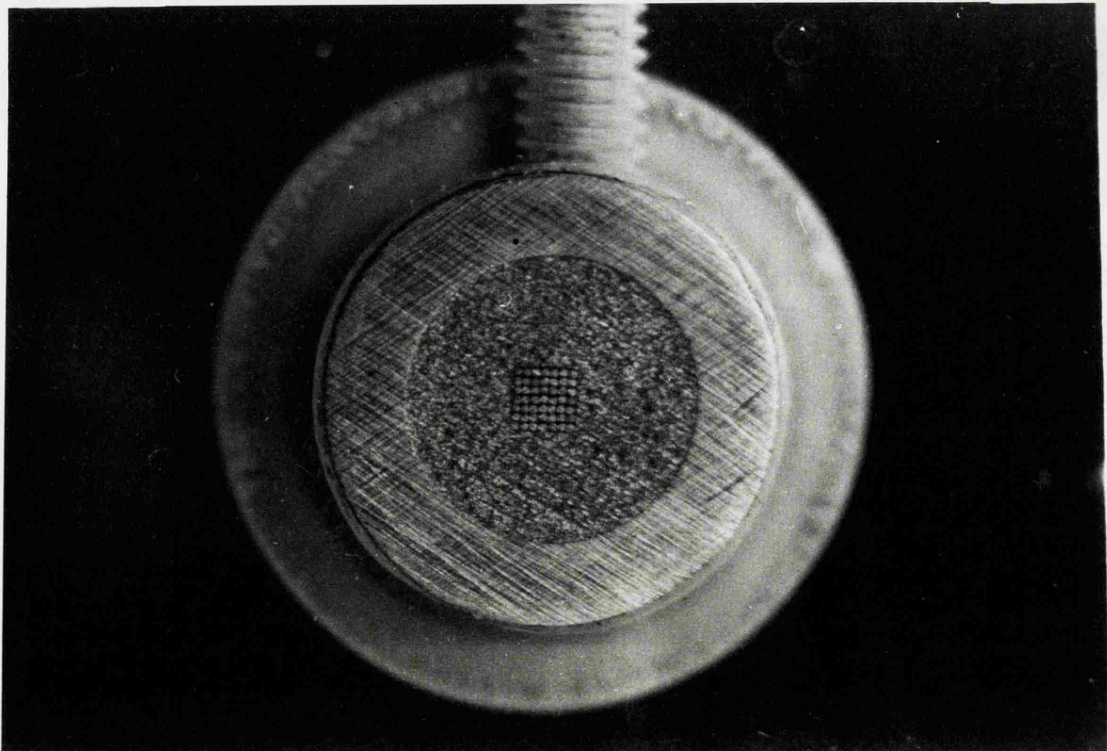
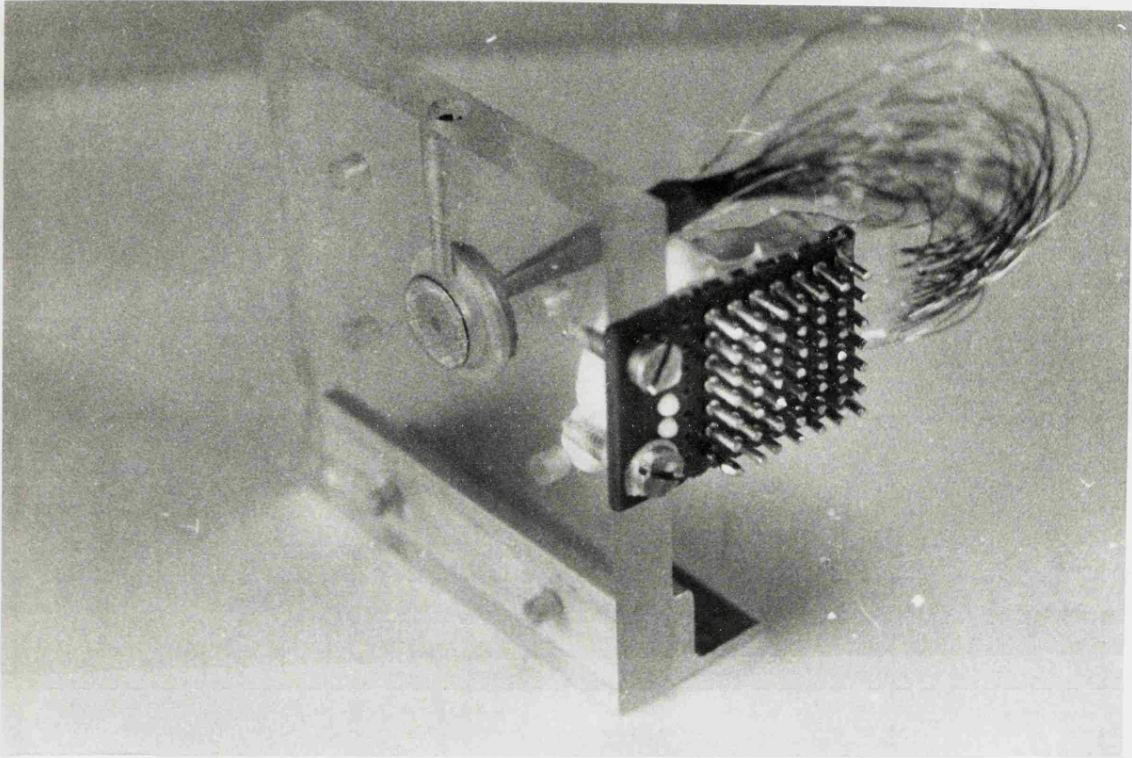


PLATE 5.4

FIG. 5.26

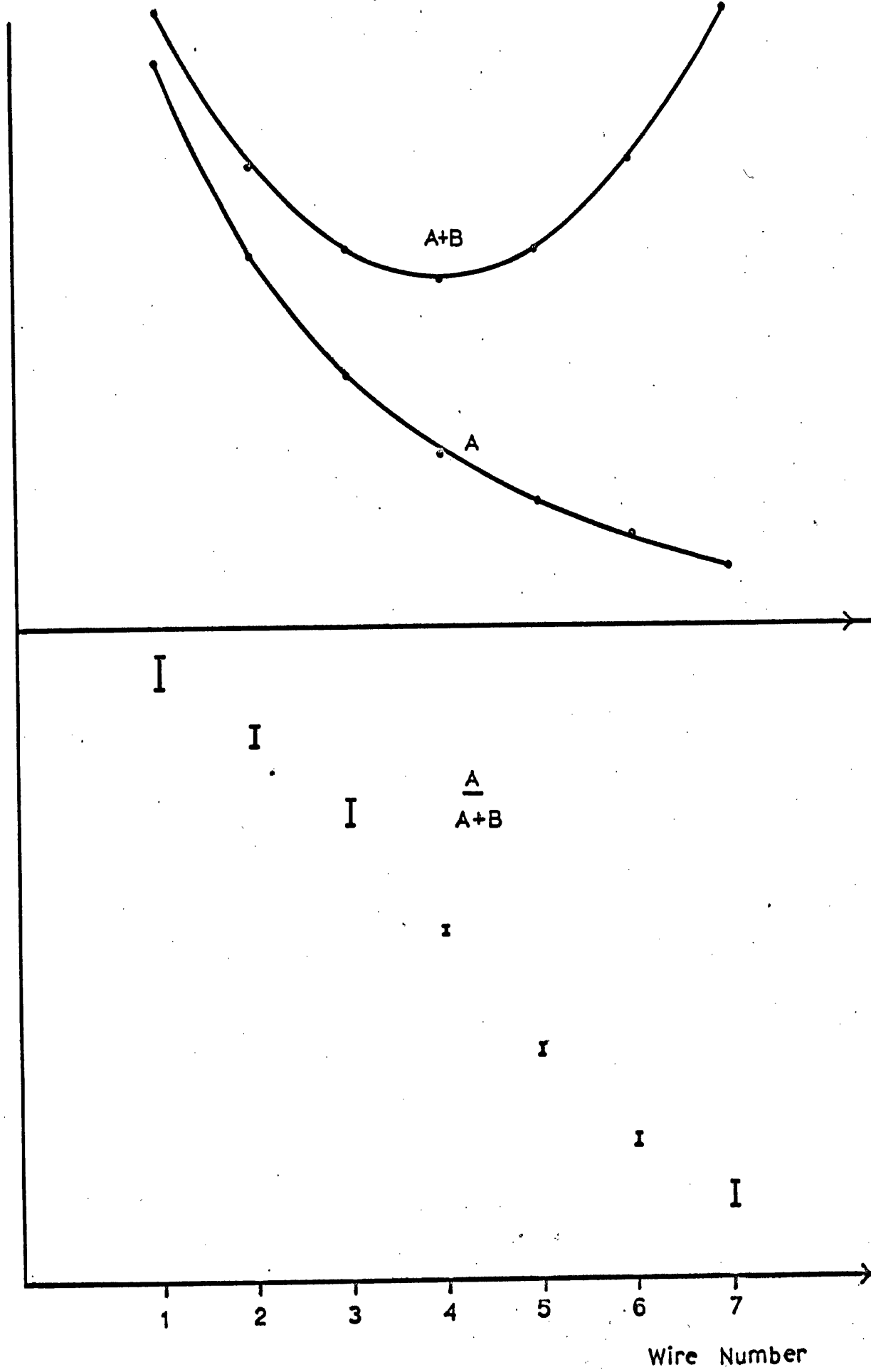


FIG. 5.27

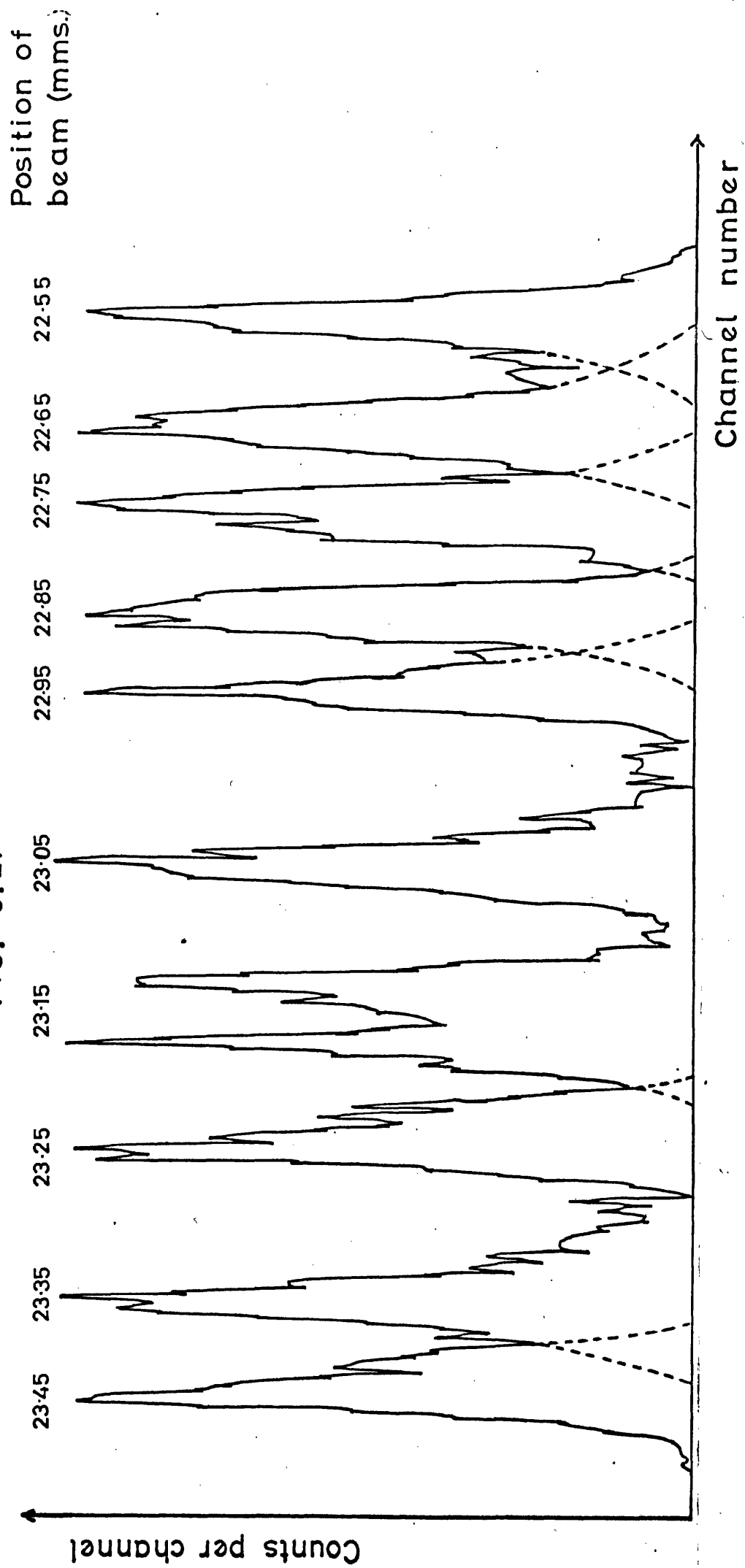
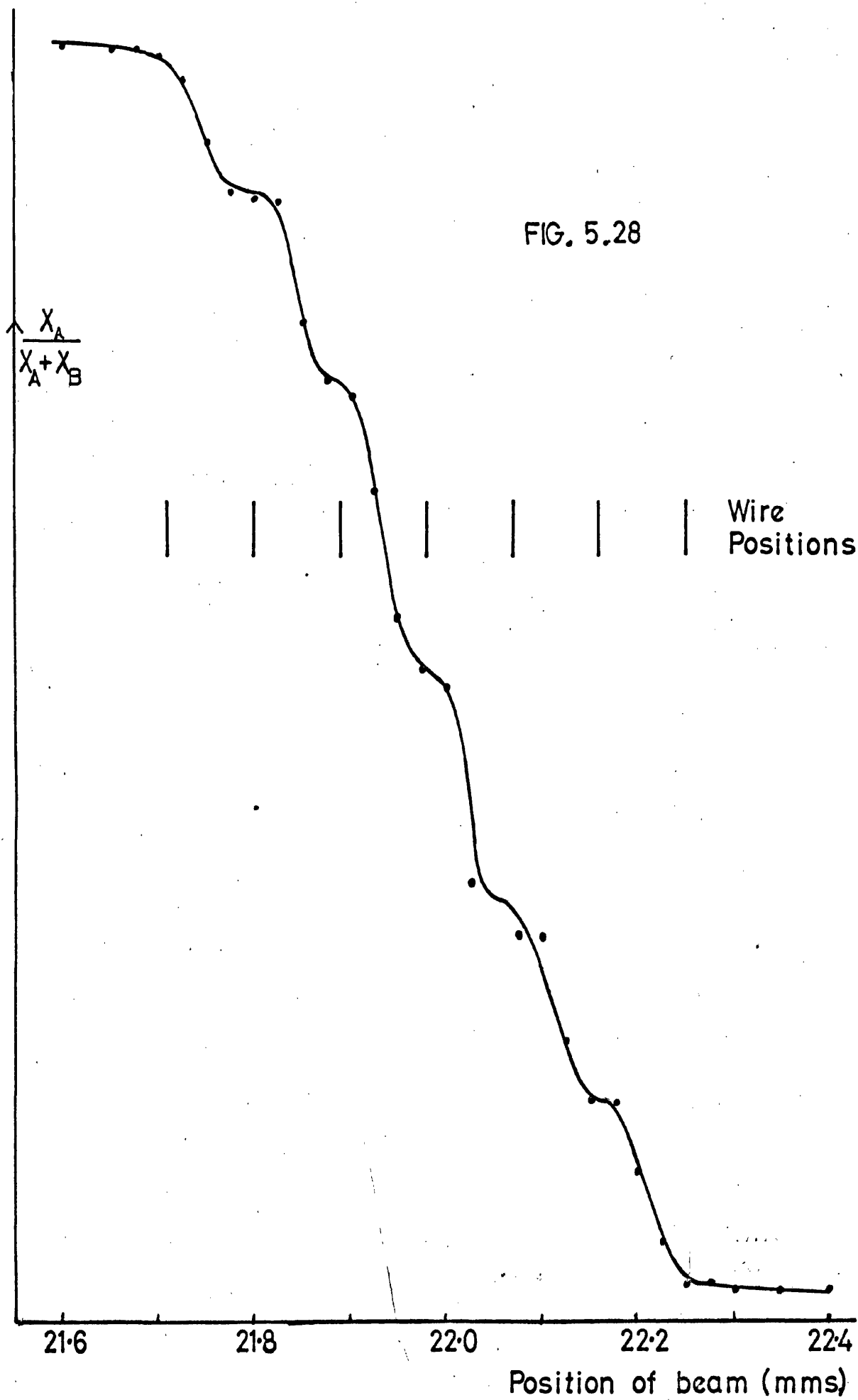


FIG. 5.28



to difficulties in construction. Comparison of the results obtained in one dimension with four ^{wires} of the 200 μm grid, with these in two dimensions, shows that there are notable similarities in the resolution obtained and in the observed non-linearity. By analogy, therefore, it would be expected that a larger two dimensional grid would have capabilities similar to that of the 200 μm grid. Use of dummy condensers would enable the active collectors to be confined to the linear part of the curve, thus making the image easier to extract from the experimental results. The considerable number of discrete components required suggests that thin film techniques may be used in the construction of larger grids.

5.4 A comparison with other imaging detectors.

5.4.1. One dimensional dissection.

There are several different types of imaging detector which have been described in Chapter 2, but of these photographic film and image dissection, using a proportional counter for example, have been more widely used, and the discussion will be limited to these types.

The experiment designed by the Leicester group and described briefly in Chapter 1 consists of a grazing incidence collecting mirror, a 10 cm^2 crystal, and a detector which must have a spatial resolution in one dimension of $20\ \mu\text{m}$ in order not to degrade the spectral resolution. Recently, the increased size of the OSO satellite has relaxed this requirement to $50\ \mu\text{m}$.

The simplest form of detector to meet these requirements is photographic film which has a spatial resolution of between 2

and 20 μm depending on the speed of the film. However, since it is required to monitor spectral lines with good time resolution, film cannot be used. The alternative methods are to use a proportional counter or other detector with a 50 μm wide aperture, scanned across the image, or to use a channel multiplier array, and an estimate will be given of their suitability for this application.

The background counting rate for the array, on the basis of the results of chapter 4, is 5/sec/cm². This will give a rate per picture point, area 10 cm x 50 μm , of about 0.25/sec. A proportional counter of a suitable size, together with an anti-coincidence guard counter, will give a background rate of about 0.5/sec.

Using the form of readout described in this work, the effective efficiency of the detection system would be of the order of 1 or 2% at 8 \AA , the projected wavelength region of the spectrometer, but using suitable photo-emissive coatings an efficiency of 6 to 10% should be obtainable. The efficiency of a typical proportional counter at this wavelength is of the order of 20 or 30% depending on the window material.

For an emission line of strength, say 10^{-5} erg/cm²/sec, a typical figure for an active region at this wavelength (Batstone et.al. 1970), the total counting rate in the array, assuming values for the reflection of the mirror and crystal of 10%, and a 10 cm² collecting area, would be 20 counts/sec, and 60 /sec in the proportional counter. If the emission line is to be dissected into 10 picture points then a signal to noise ratio of 4 would be obtained in the array in one second, while the time taken to scan the image with the proportional counter to give the same signal to noise would be 5 seconds.

For the emission line to be displaced or broadened to 50%

more than the instrument resolution, the solar region responsible would need to produce bulk transport velocities of about 150 km/sec or an ion temperature of the order of $10^6 M$ (where M is the mass of the ion giving the emission line).

In addition to the obvious advantages of the array in terms of time resolution, there are further advantages in ease of construction, since the array, once positioned on a line, need not be moved to monitor the line, whereas the scanning detector would need a precision drive mechanism. In addition to this, windowless detectors can be used at long wavelengths. For example, the important O VIII resonance emission at 21.6 \AA would be difficult to record in a conventional gas counter.

5.4.2 Two dimensional dissection.

With the present techniques of construction of focussing mirrors, the limit of resolution is 2 arc seconds (Vaiana et.al.1968) which for a focal length of 6 metres, gives a spatial resolution requirement at the detector of $50 \mu\text{m}$. The use of a focussing mirror in solar or non-solar X-ray astronomy requires different types of detector. For solar studies the high X-ray flux means that time resolution is required in order to study the changes in small features in the corona. The detector requirements for this type of system are similar to those for the one dimensional system.

For non-solar studies, the flux is low and time resolution becomes of secondary importance. Of more importance in this application is the long term integration capacity and the sensitivity of the detector. Film is no longer ruled out, but its low sensitivity, high initial background fogging and difficulty of retrieval make the use of an electronic detector more attractive.

The most promising technique is the use of the channel multiplier array and, besides the system described here, an integrating readout system has been described by Giacconi et.al.(1969). Since the detector characteristics will be identical for both methods, it is only necessary to compare the spatial resolution and sensitivity attainable.

In the method described by Giacconi, the pulses from the array are collected on an insulator and the charge image stored for a scanning readout. Several methods of scanning the charge image are available, all of which are capable of detecting a charge of 200 electrons, which is well below the charge in the electron pulse. The detection efficiency of the electron pulses is thus 100% and the integration capacity is limited only by the storage capacity of the electronics. A severe limitation of this method, and one not mentioned by the authors, is that because there is such a large spread in pulse heights from the array, then the scan rate of the charge image must be such that there is ^{little} _^ chance of two pulses being collected in a resolution element between readouts. This is necessary in the interpretation of the count rate and essentially limits the use of the method to non-solar X-ray astronomy. The spatial resolution obtainable using the scanning vidicon technique is about 20 μm .

The spatial resolution obtainable using the method described here is already better than ^{100 μm} and can be expected to be reduced to 50 μm or better using more sophisticated constructional techniques for the grids. The sensitivity is slightly less than the Giacconi method by a factor of about two due to the attenuation of the condenser network and the integration capacity is again only limited by the electronics. These two methods clearly have very similar operational

characteristics, the principle advantage of the charge branching method lying in its simplicity.

As an illustration of the performance that can be expected from such a detector using the focussing mirrors which will be available within the next few years, the observing time required to obtain an X-ray image of the extra-galactic source believed to be associated with the radio galaxy M-87 will be estimated. The galaxy M-87, or Virgo A, is a peculiar galaxy consisting of a small core 2 arc seconds across and a jet of material extending about 20 arc seconds from its centre, presumed to be the result of an explosion. Of considerable interest is the determination of which part of the jet or core is emitting the observed flux of X-rays.

The flux at the earth in the energy range 1 to 4 keV is about 0.1 ph./cm²/sec. A mirror having a collecting area of 50 cm² and a reflection efficiency of 20% will give a flux at the detector of 1 ph/sec. Assuming a detection efficiency of 10% this will give a count of 0.1/sec. If the X-rays are being emitted from a region less than two arc seconds across they will all be focussed into one picture point.

The background rate in such a resolution element will be very small and can be neglected. The cosmic X-ray background flux is about 15 ph/cm²/sec/sr. which gives a negligible count rate per resolution element. Clearly the position of the source can then be fixed in a few seconds and the strength determined to a high statistical accuracy in of the order of 10⁴ seconds.

Finally, further improvements in telescopes will enable sources such as the Crab to be detected in any of the local group of galaxies and the coronal emission of nearby main sequence stars studied.

5.5 Further work.

There is considerable scope for improvement in both the one and two dimensional systems, particularly the latter which, with the large number of discrete components required, is not a practical system at this time. The use of thin film techniques for the fabrication of the two dimensional grid has already been mentioned, and work on the alternative of a crossed grid system is in the planning stages in this department.

The use of two arrays in cascade would considerably increase the spatial resolution in both one and two dimensions, the very large pulses obtained decreasing the electronic noise by a large factor. Work already carried out on cascaded arrays indicates that there is a significant spread in the electron pulse between the arrays, but because of the method of readout, this should not affect the spatial resolution (W.Parkes , private communication).

With this increased pulse height, the possibility of large one dimensional arrays using the capacitance between wires becomes feasible. If the wires are mounted on an earthed metal sheet but separated from it by a thin semiconducting layer to drain off the charge, the whole grid would be self contained, having only two connections for the q_a and q_b pulses. If this can be achieved, then the complete detector could be reduced to a very simple 'plug-in' module.

CHAPTER 6. THE LEICESTER EXPERIMENT ON THE OSO-5 SATELLITE.

6.1 Introduction.

The need for spatial, as well as spectral and temporal resolution, in solar X-ray experiments has been discussed in chapter 1. The experiment designed by the Leicester and University College, London, groups makes use of a non-focussing grazing incidence telescope to define a narrow field of view, a raster scan 40 arc minutes square of the sun being provided by the motion of the whole instrument. The static field of view of the mirror is 1.66 arc minutes in diameter and the collecting area 0.7 sq.cm.

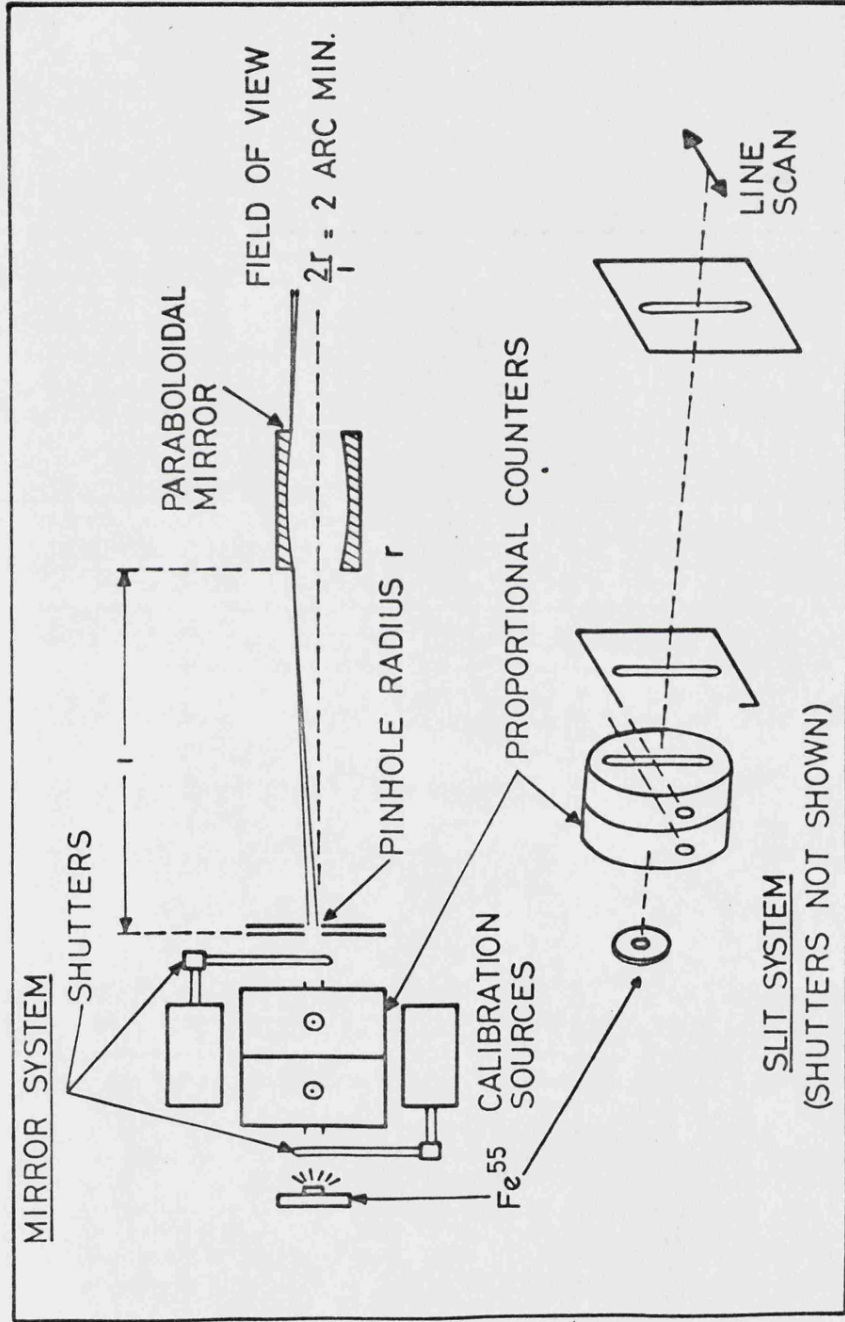
In addition a slit system having a field of view of 2 arc minutes, in one direction only, gives improved time resolution for flare events. A sketch of the two systems is shown in fig. 6.1 (after Herring et.al.).

Spectral information is obtained from proportional counters at the exit apertures of the slit and mirror systems, the wavelength region covered being 3-9 Å and 8-14 Å respectively. The instrument can either be held pointing at the sun, in which case the slit system is used giving a time resolution of 0.64 sec. or commanded to perform a raster scan of 40 lines in a period of 5 minutes, 7.2 seconds. Either system may be used alone, or an alternating mode can be selected in which the slit system operates on every third line.

A fuller description of the instrument has been given by Negus et.al.(1970) and Herring et.al.(1970), my personal responsibility being only in the design and testing of the proportional counters.

FIG. 61

OSO-5 U.C.L./LEICESTER INSTRUMENT



6.2 The proportional counters.

6.2.1 Design criteria.

Because of the limitations on the size of the counters due to the small volume of the spacecraft, the counters were of necessity rather small and, for optimum utilisation of the available space, were of a double pill box design. An exploded view of the counter for mirror system is shown in plate 6.1.a, the diameter and depth both being $1\frac{1}{2}$ ins.

The front half of the counter is used as the solar X-ray detector and has a small pinhole window, offset from the centre, for the mirror counter, and a slit window along a diameter for the slit system. The rear half of the counters is separated by a blanking plate from the front portion, the gas supply being common, and is used as a calibration counter enabling any deterioration of the counter performance due to escape or contamination of the gas to be monitored.

The calibration counter could be irradiated on command with 2.1 \AA X-rays from an Fe 55 source. In order that the pulses from this counter could be processed using the electronics of the solar counter, the anode wire was of a slightly different diameter, thus reducing the gas gain sufficiently for the pulse height distribution to be centred within the seven channel analyser. The completed detectors sealed, ready for flight, are shown in plate 6.1.b.

The mirror counter was required to have a spectral response limited to the range $8\text{--}14 \text{ \AA}$. This was achieved by the use of an aluminium window which gives a high transmission to wavelengths longer than the 7.9 \AA Al absorption edge. Wavelengths shorter than this were rejected using pulse height discrimination. The gas used was

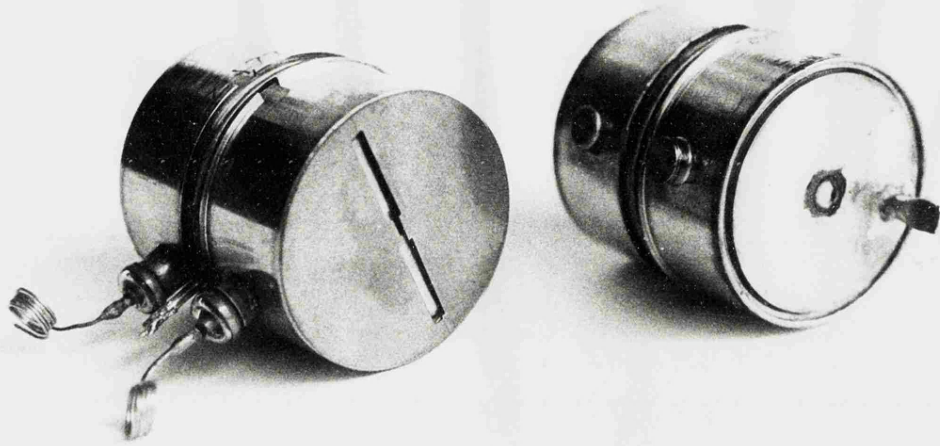


PLATE 6.1

Argon: CO₂ (90%, 10%) which ^{has} adequate absorption for the counter dimensions.

The response of the slit counter was limited to the range 3-9 Å by the use of a beryllium window. Krypton was chosen instead of argon because of its higher absorption and freedom from absorption edges in this wavelength range. The spectral response of the counters is discussed in more detail in a later section.

6.2.2 The calibration of the proportional counters.

Using emission lines isolated in the plane crystal spectrometer, the modal charge output (q), the f.w.h.m. (f), and the efficiency (z) were measured for a number of wavelengths. The method used was that described in chapter 2. The accuracy in the measurement of the modal charge output is determined principally by the statistics of the pulse height distribution and the noise present in the calibration pulse from the standard pulser, and leads to an accuracy of 2%. This of course is only a relative accuracy, the measured value of q being in error by as much as 50% of the absolute value due to the effect of differing risetimes of the counter pulse and the standard pulser (Gott and Charles, 1969). The error in the measurement of the f.w.h.m. of the distribution is governed by the statistical errors present as a result of counting the channels of the multichannel analyser and is about 3%. The error in the efficiency measurements is determined by the error in the determination of the diameters of the apertures on monitor and test counters, and by any variation in the thickness of the window material used on the monitor counter and also used as a compensator for the test counter. An estimate of this error leads to a value of 10% as a typical figure. This, of course, does not apply

to measurements of the transmission of window material in which the count rate in the detector with and without the sample in the beam is compared. The error is then only due to any variation in the transmission of the sample and the ^{counting} statistics.

Measurements are described for four counters, two of each type. The two prototype counters (slit: ZF 628, mirror: ZC 136) were the ones originally intended for flight. The window materials were nominally 5 μm Al for the mirror, and 75 μm Be for the slit, at pressures in the counters of 46.8 cm. and 38.4 cm. respectively. During final testing of the satellite however, these counters failed and were replaced. The flight counters had windows of 15 μm Al and 75 μm Be at pressures of 46.8 and 38.4 cm. Due to lack of time, these counters could not be tested in any detail and further tests were carried out using counters from the same batch, and samples of window material taken from identical sheets. Results are given for two of the replacement batch of counters. (reference numbers, slit: ZH 771, mirror: ZH 772). All the measurements were taken at an anode voltage of 1615 volts, the operating voltage in flight.

For a counter operating in the proportional region, the charge output q is related to the wavelength of the incident radiation by the equation:

$$q = A. \lambda^{-b} \quad \text{where } b \approx 1.$$

Any departure from proportionality can thus be determined by measurement of b .

The f.w.h.m. is related to the energy of the radiation by the expression:

$$f = \frac{2.36.k}{E^m} \quad \text{where } m \approx 0.5 \text{ and } k \text{ depends on } F,$$

Table 6.1.

Reference number.		Wavelength A				
		2.1	5.4	8.3	9.8	
ZF 628 slit.						
b	1.03	$q \cdot 10^{-13} C.$	3.14	1.18	0.76	0.63
m	0.50	$q_{cal} \cdot 10^{-13} C$	2.85			
k	0.184	f %	17.5	28.3	35.0	38.4
ZH 771 slit.						
b	0.98	q	5.46	2.10	1.43	1.21
m	0.48	q_{cal}	3.12			
k	0.207	f	22.0	31.9	39.0	43.8
ZC 136 mirror.						
b	1.01	q	13.4	5.35	3.15	2.71
m	0.49	q_{cal}	2.75			
k	0.204	f	22.1	32.0	40.2	43.1
ZH 772 mirror.						
b	1.00	q	11.5	4.32	2.71	2.42
m	0.48	q_{cal}	2.48			
k	0.221	f	23.6	37.0	44.5	47.2

the Fano factor, and the variance of the 'single electron' distribution. The measured values of q, f, b, k and m are presented in table 6.1 and the spectral variations in q and f in figs 6.2 to 6.5.

The errors in the measurement of b and m of 3% and 5%, obtained from the graphs, indicate that there are no significant variations from the expected values of 1 and 0.5.

The resolution R , of the pulse height distribution of a proportional counter is given by:

$$R = (F/n_0 + \sigma^2/n_0)^{\frac{1}{2}}$$

where F/n_0 is the variance of the n_0 initial ion pairs and F is the Fano factor, and σ^2 is the variance of the multiplication process, that is, the single electron distribution.

This may be rewritten as:

$$R = (Fw/E + \sigma^2w/E)^{\frac{1}{2}}$$

where w is the mean energy per ion pair,

and E is the photon energy.

and hence $k = (w.(F + \sigma^2))^{\frac{1}{2}}$.

The factor σ^2 has been restricted theoretically to the range 0.61 to 1.0 by Byrne (1962). F , the Fano factor has been measured to be 0.2 for Argon by Alkhozov et.al.(1967) and although no measurements have been made on krypton, values much larger than 0.2 would not be expected. Using these values and putting $w = 26.5$ ev (Melton et.al. 1954) then k is limited to the range 0.146 to 0.178.

The measured values are considerably worse than the highest predicted value of k . The restricted geometry of the counter giving spreads in gas gain due to variations in cathode geometry is the probable cause of these discrepancies. This is supported by the fact

FIG. 6.2

SLIT COUNTER

Charge output
Coulombs

ZH 771

ZF 628

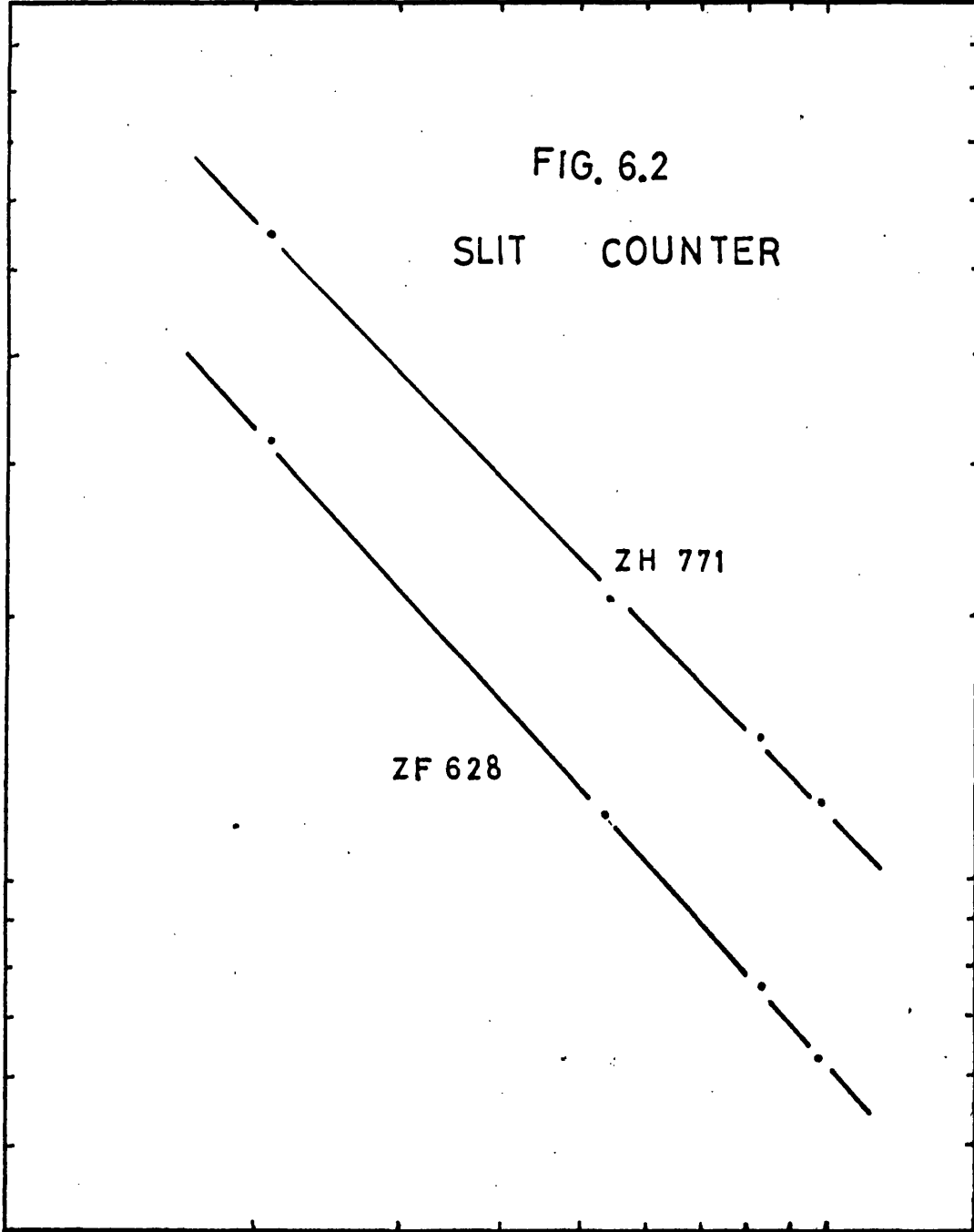
10^{-12}

10^{-13}

1Å

10Å

Wavelength



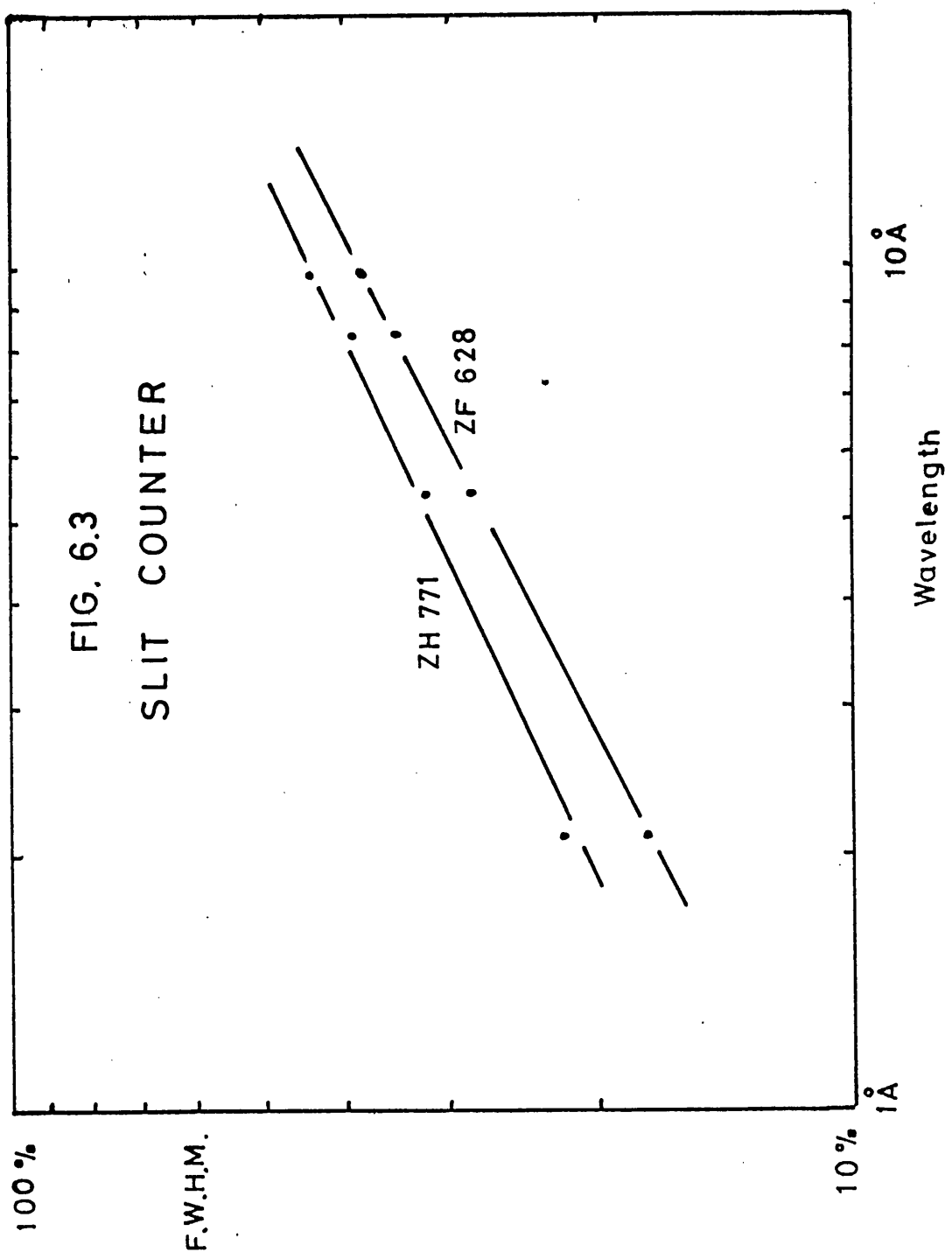


FIG. 6.4

MIRROR COUNTER

10^{-12}

Charge
output.
Coulombs.

10^{-13}

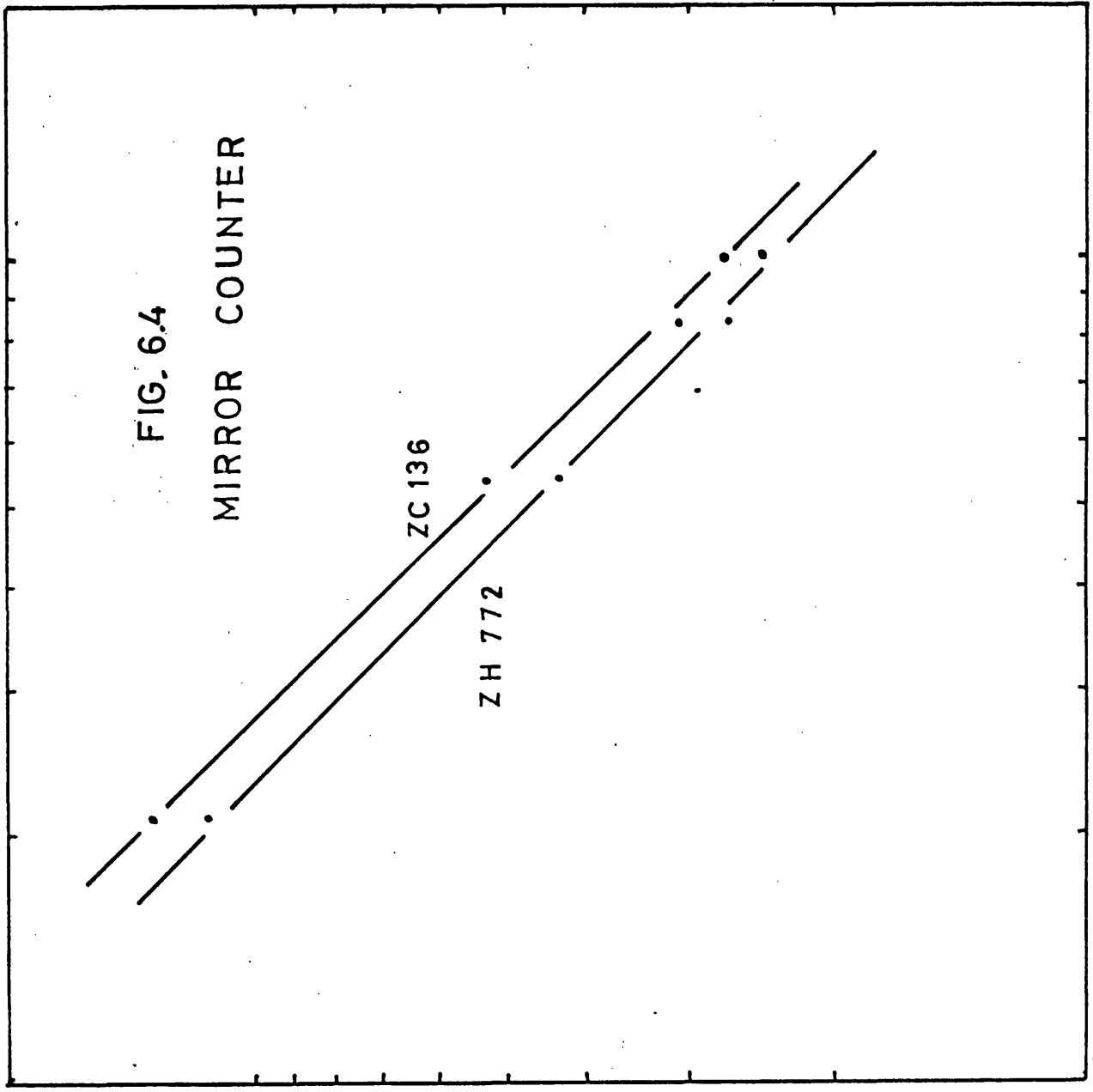
ZC 136

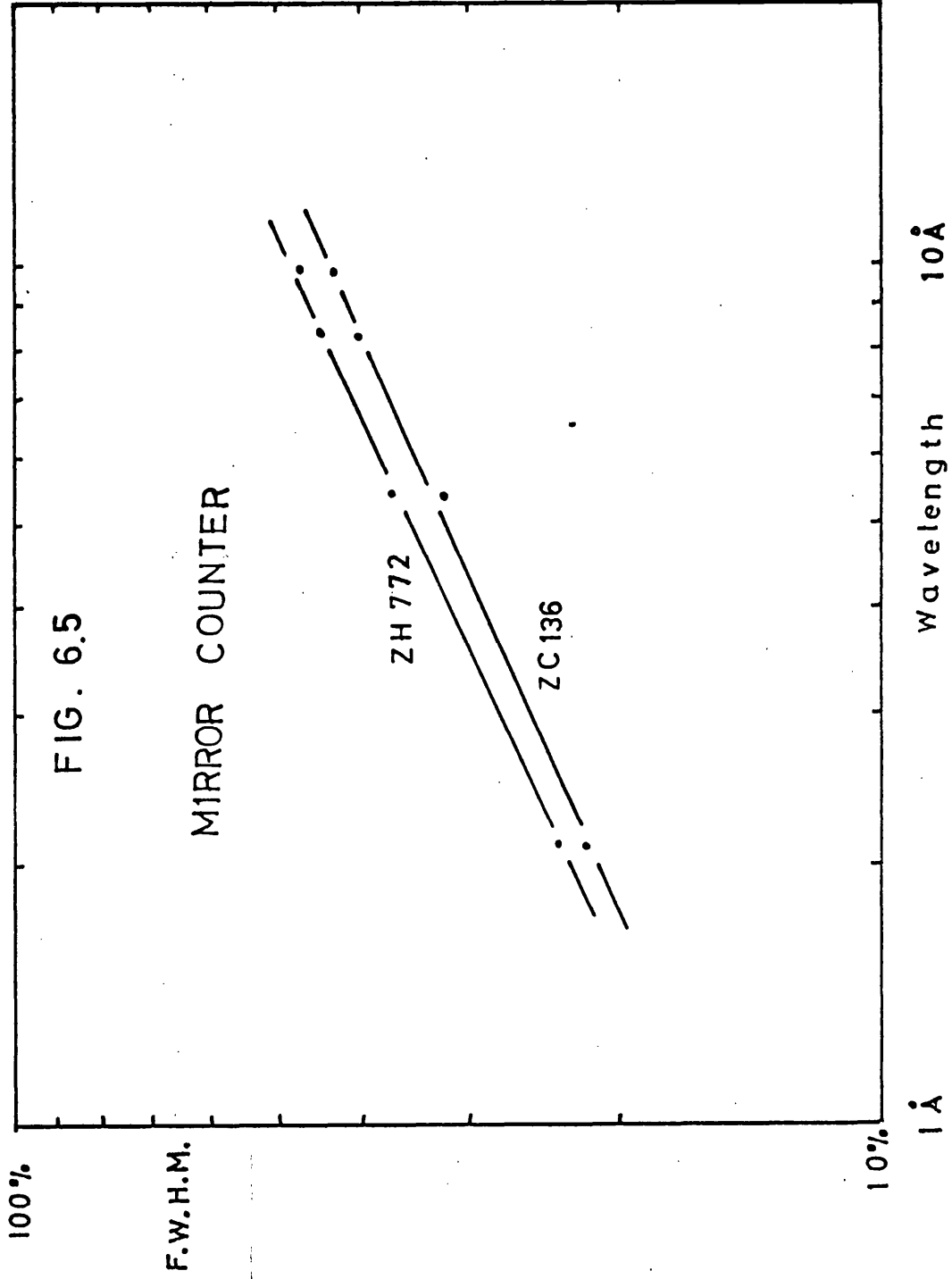
ZH 772

1 Å

Wavelength

10 Å





that the results for the mirror counter, in which the detector aperture is well removed from the anode wire, are significantly worse than for the slit counter, in which the field at the window is more uniform. The counter efficiencies.

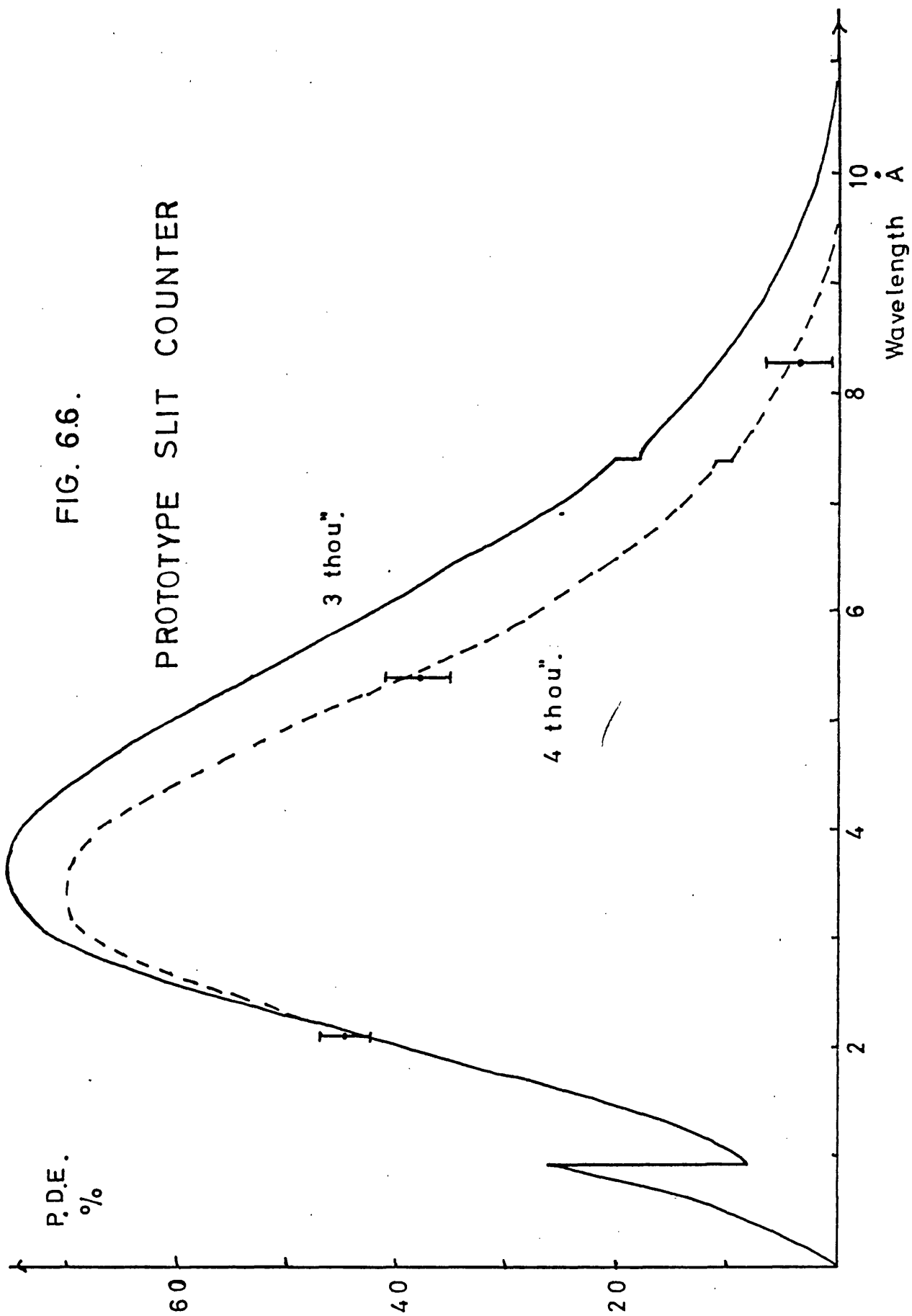
The efficiencies of the two prototype counters were measured using the method described in chapter 2, at wavelengths of 2.1, 5.4, 8.3, and 9.8 Å, and the results are shown in figs 6.6 and 6.7. The solid line represents the calculated efficiency for the nominal window thickness and absorption length (values obtained from published results of Cooke and Stewardson, 1964).

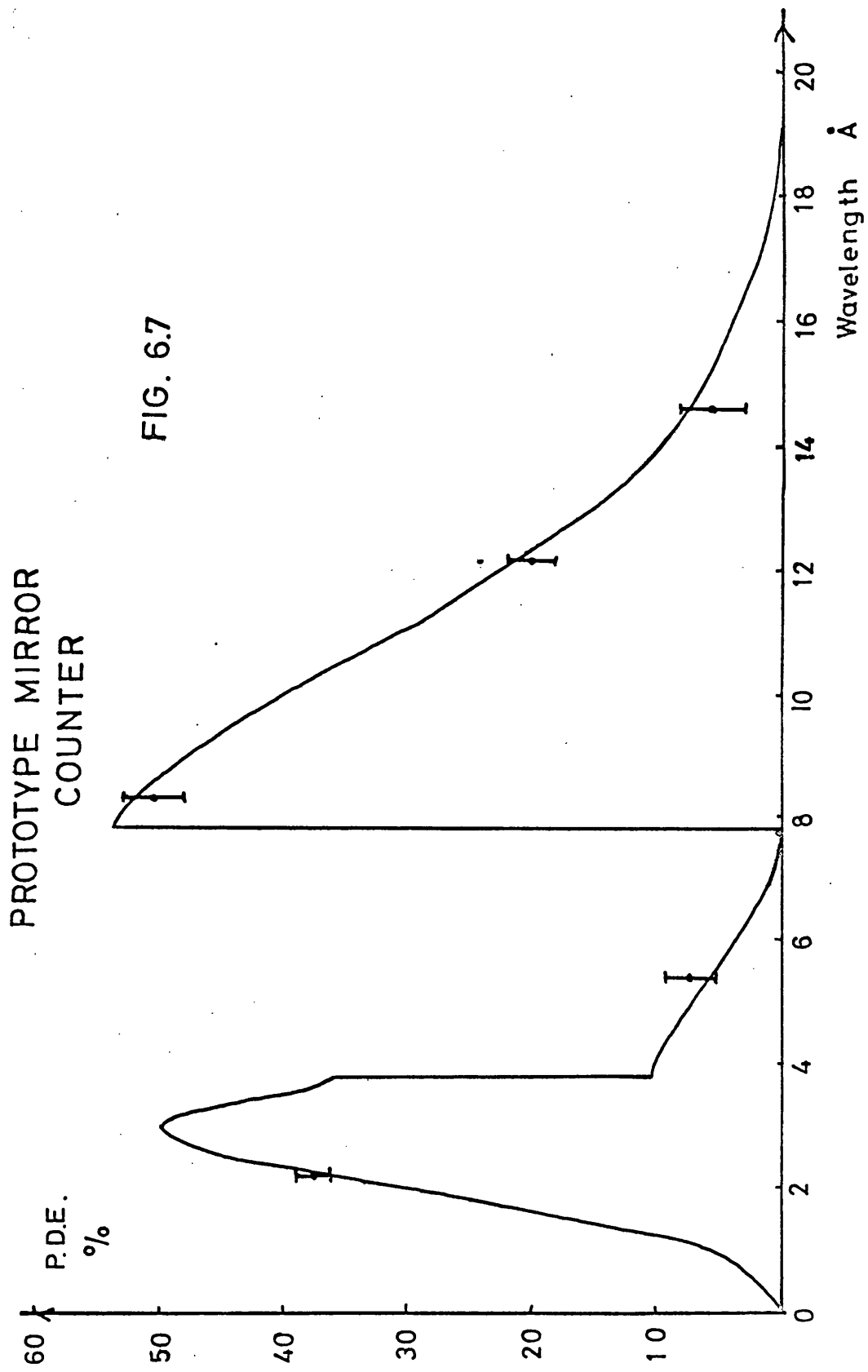
For the mirror counter the results agree well with the calculated curve but the slit counter shows a lower efficiency at longer wavelengths. The broken line in fig 6.7 represents the calculated efficiency for a window thickness of 100 μm rather than the nominal 75 μm. It is unlikely that the thickness is so much in error, but a small amount of contaminant free of edges in this region could also give a lower efficiency. The most likely source of contamination is BeO of which a mass fraction of 4% would be needed to give the observed results.

As mentioned earlier, the efficiencies of the flight counters could not be measured directly due to lack of time. However, from the previous work it is unlikely that the efficiency is very dependent on the particular counter, but rather on the window transmission. Therefore, to obtain an estimate of the expected efficiencies, the transmission of samples of window material taken from identical sheets to those on the flight counters, was measured and the efficiencies calculated using these transmissions and the gas absorption curves of Cooke and Stewardson.

FIG. 6.6.

PROTOTYPE SLIT COUNTER





The results are presented in figs 6.8 and 6.9. The solid line again represents calculated efficiencies for the nominal window thicknesses. In this case there is no significant discrepancy between the measured and predicted values.

The Be used in the prototype counters was quoted by the manufacturers as having a mass fraction of BeO of 2%, not appreciably less than that required to give the observed results. In the case of the flight counters, however, the Be. was supplied by a different manufacturer and had a quoted BeO content of 0.12%, supporting the suggestion that BeO is responsible for the discrepancies in the results for the prototype counters.

High count rate effects.

The changes occurring in the counter pulse height distributions at high X-ray fluxes were measured for the counters ZH 771 and 772. The counters were illuminated by the X-ray source directly and the radiation isolated by the use of filters where necessary. The electronics system was checked for base line shifts and found not to contribute significantly to the results at count rates below 10^5 c.p.s. The results are shown in figs 6.10 to 6.12.

The results are consistent with a space charge effect such as that described by Culhane et.al.(1966) in which the the shift in the modal charge is dependent on the energy of the radiation and hence the size of the avalanche.

6.3 Some results.

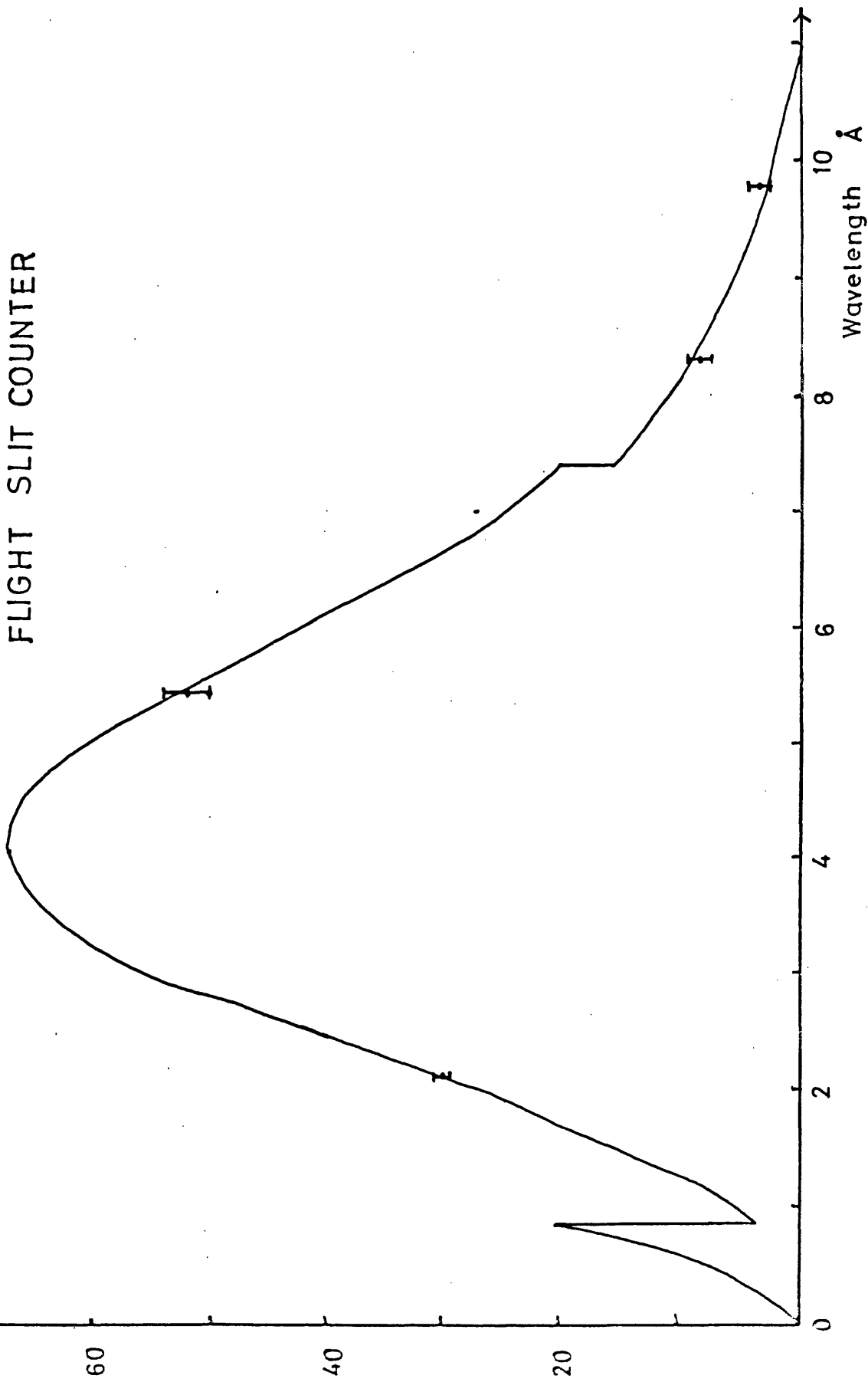
The staellite was launched on 15 Jan. 1969 and has been operating correctly since then with no deterioration in the performance of the proportional counters. The 440 element matrix of data points

P.D.E.

%

FIG. 6.8

FLIGHT SLIT COUNTER



FLIGHT MIRROR COUNTER

FIG. 6.9

P.D.E.
%

Wavelength Å

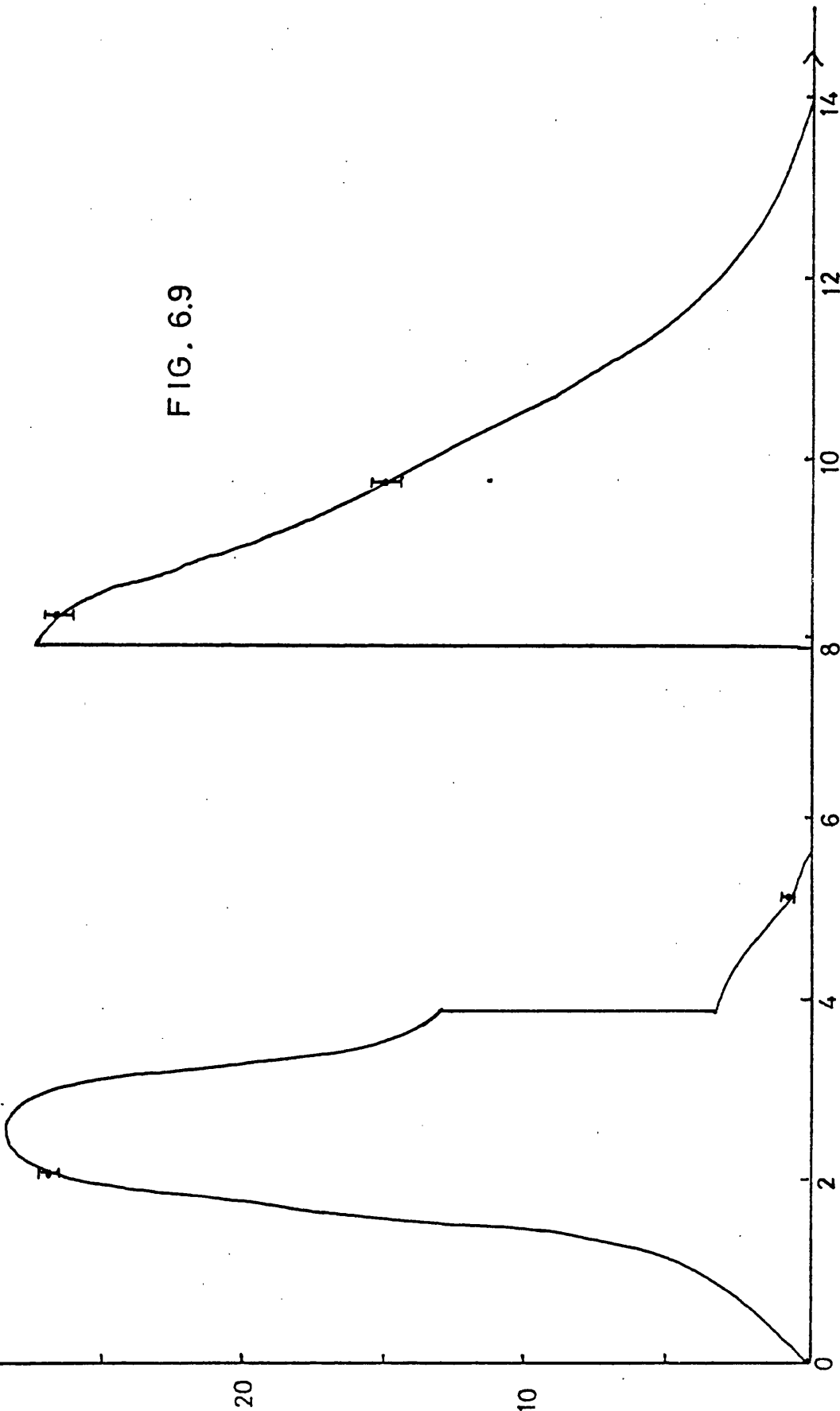


FIG. 6.10 SLIT COUNTER 8.3Å

ZH 7 71

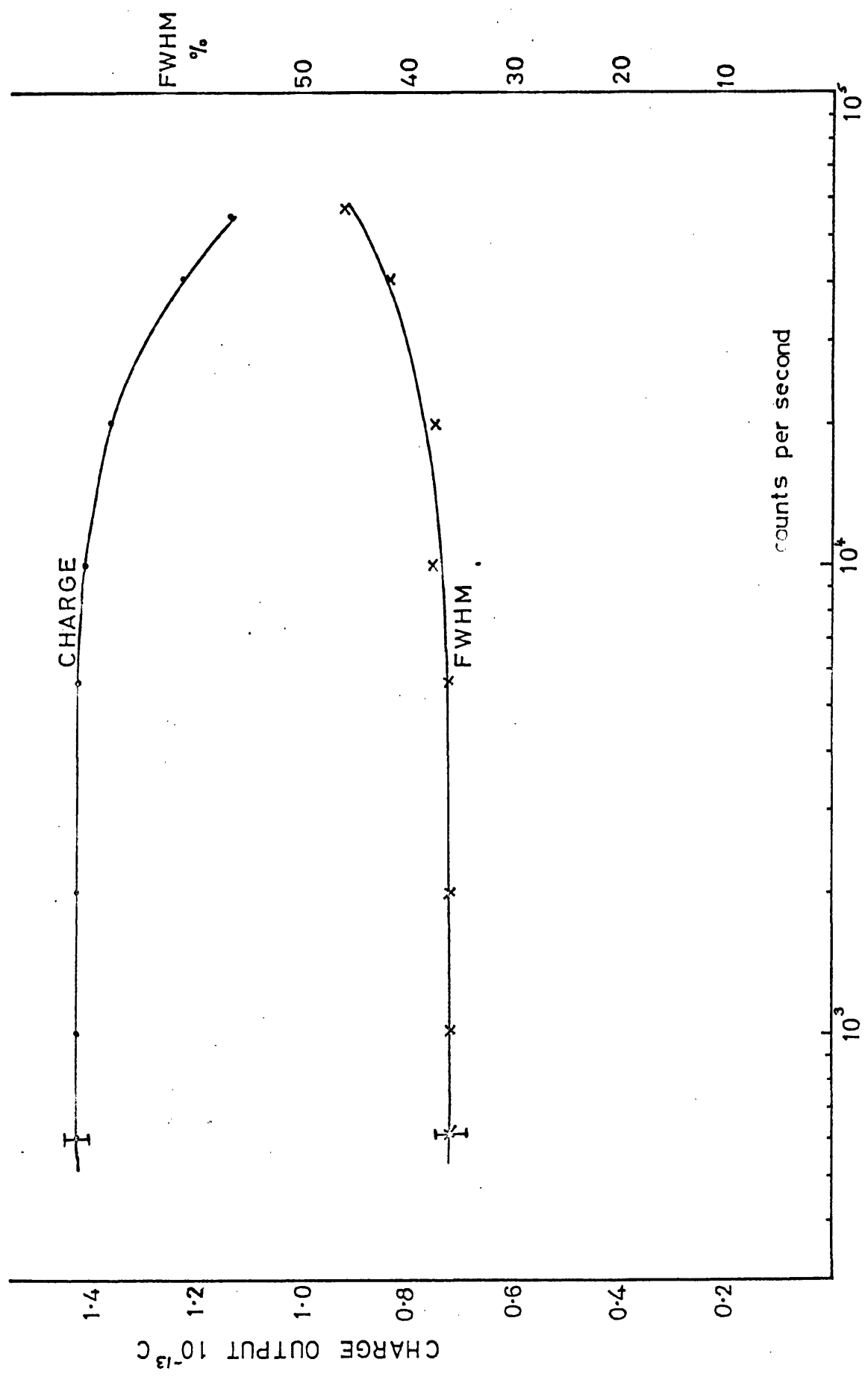


FIG. 6.11 SLIT COUNTER 5.4 Å

ZH 771

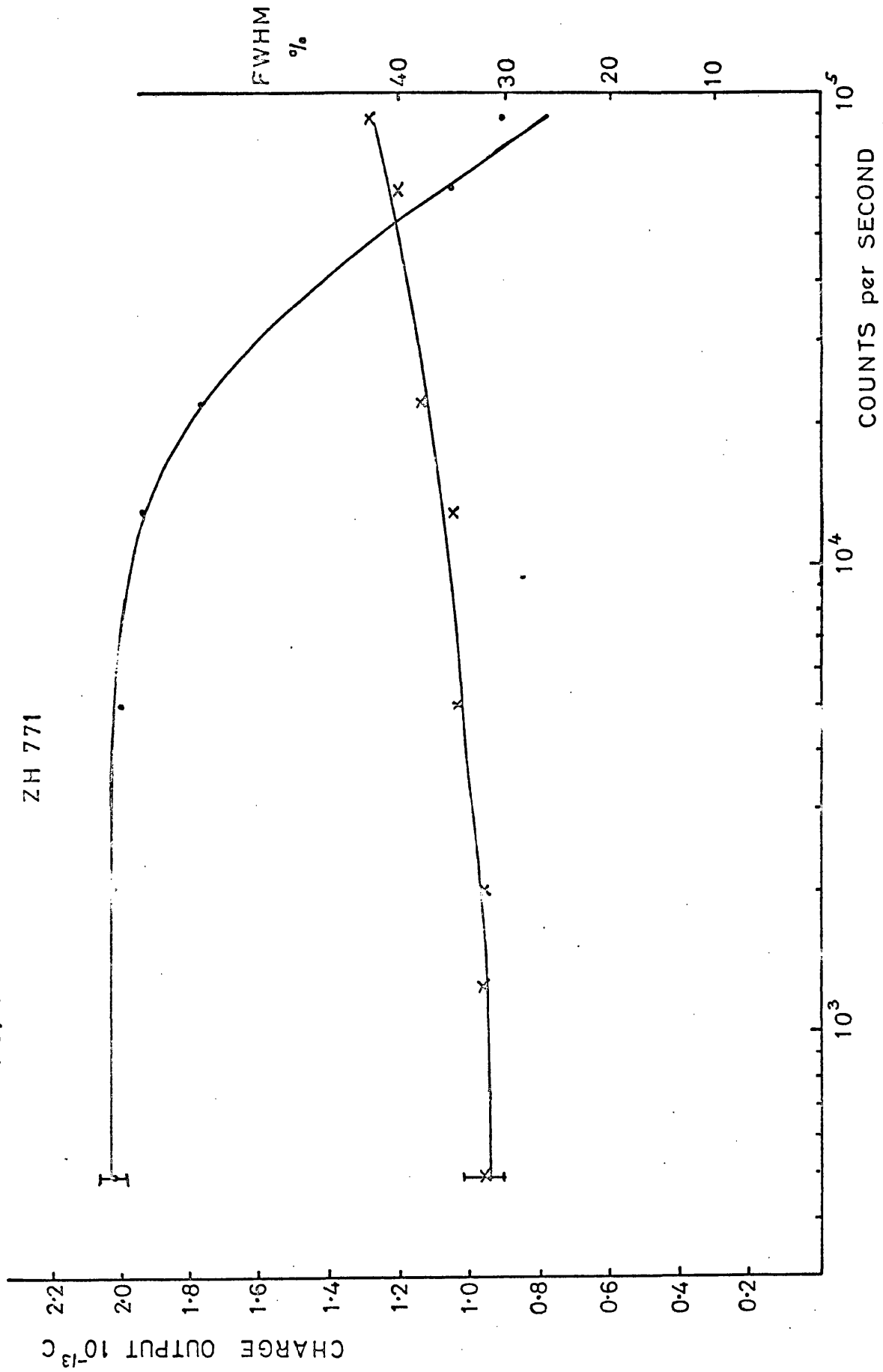
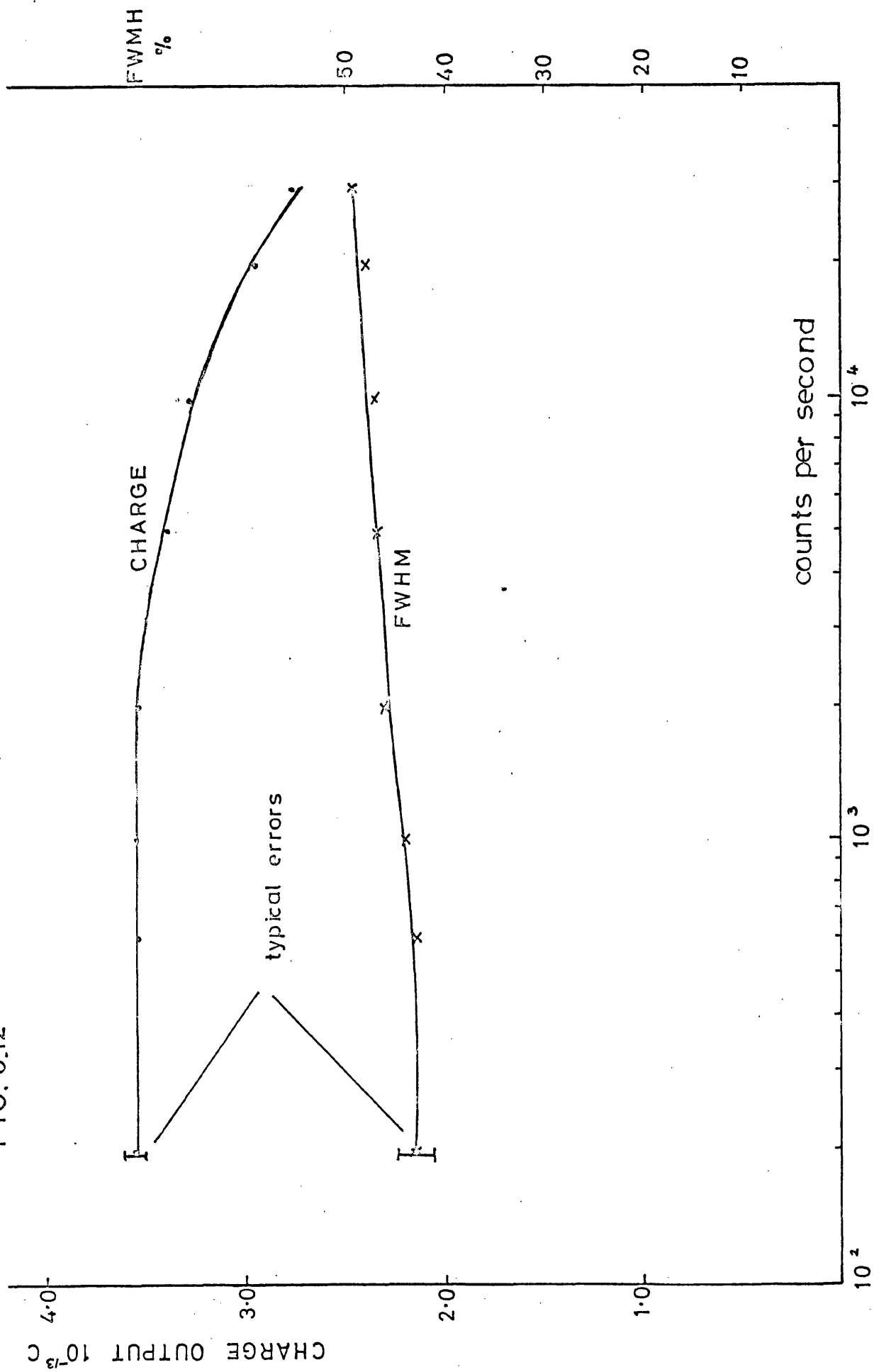


FIG. 6.12



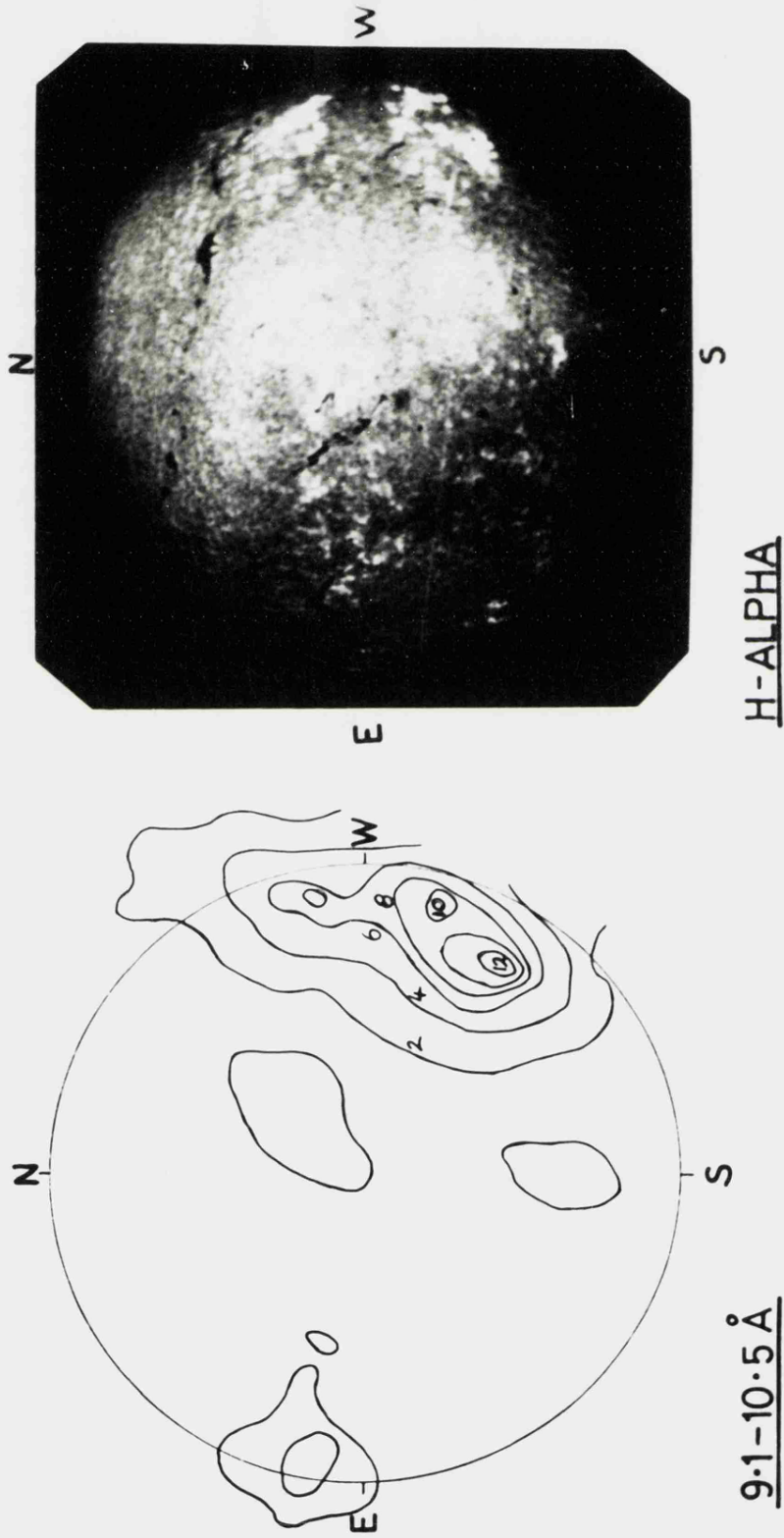
provided in the raster scan mode of the instrument has been used to give contour maps of the intensity of the X-ray emission from the sun. Daily maps are published in the ESSA monthly solar geophysical data bulletins.

A typical map obtained using the 9.1 to 10.5 Å channel of the mirror counter is shown in fig 6.13 and can be compared with the photograph of the sun taken in H alpha. In fig 6.14 a series of daily maps shows the development and movement of an active region across the disc, clearly demonstrating the potential of spectroheliographs of this type.

In fig 6.15 the time profile of an impulsive flare is shown in which the instrument is locked in the pointed mode giving a time resolution of 0.64 sec. in the slit counter. No correction has been made for the counter efficiency. The highest count rate occurs in the lowest energy channel and the rate in the subsequent channels decreases with increasing energy.

At the time of writing, little detailed work on the energy spectra of events has been done due to absence of other than 'quick look' data. These few results, nevertheless, show quite clearly the importance of spatial and temporal resolution and represent a significant advance in the study of solar X-ray emission and the general physical processes occurring in the corona.

FIG. 6.13



10 - 8 - 69

FIG. 6.14 (courtesy J. Parkinson, Leicester U.)

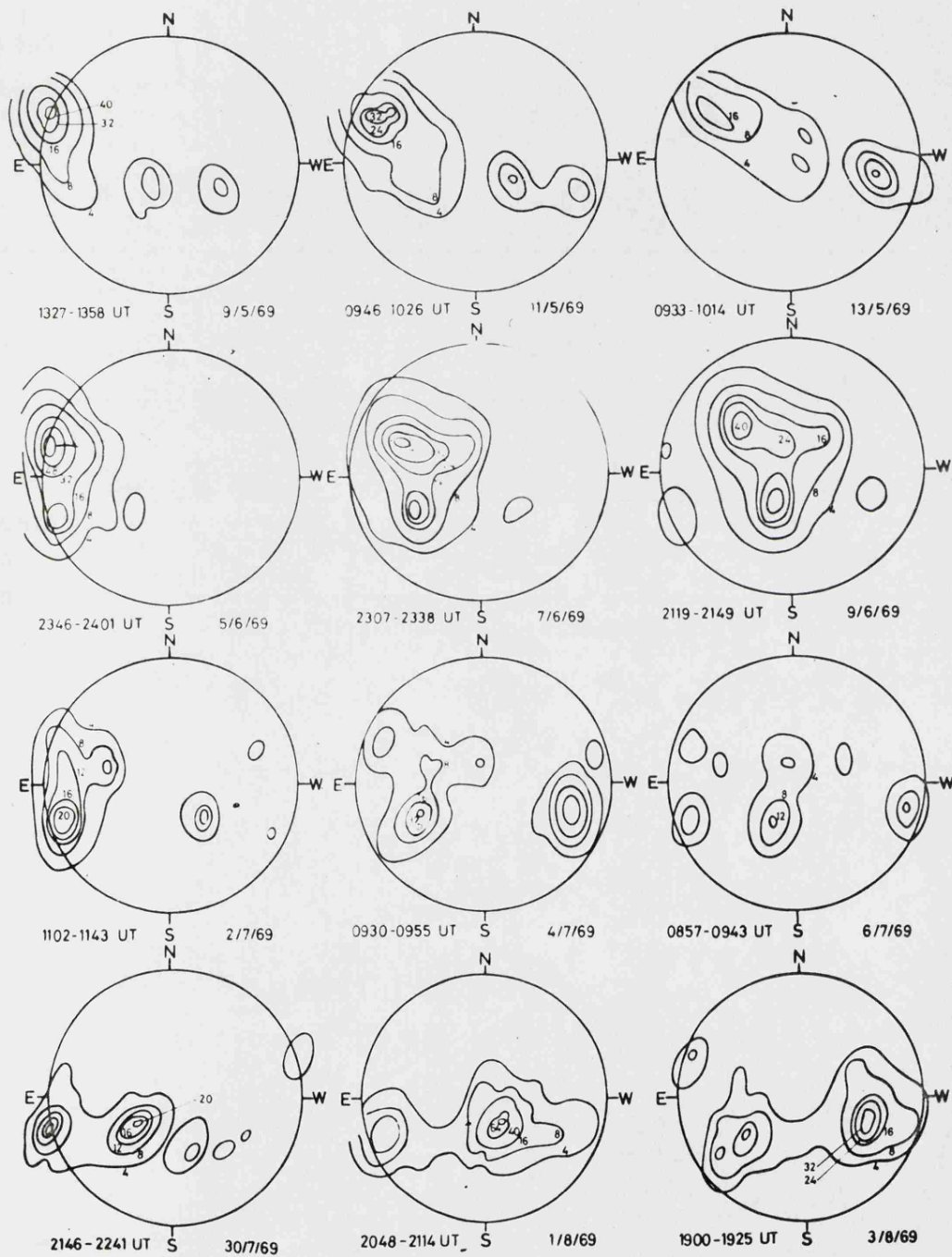
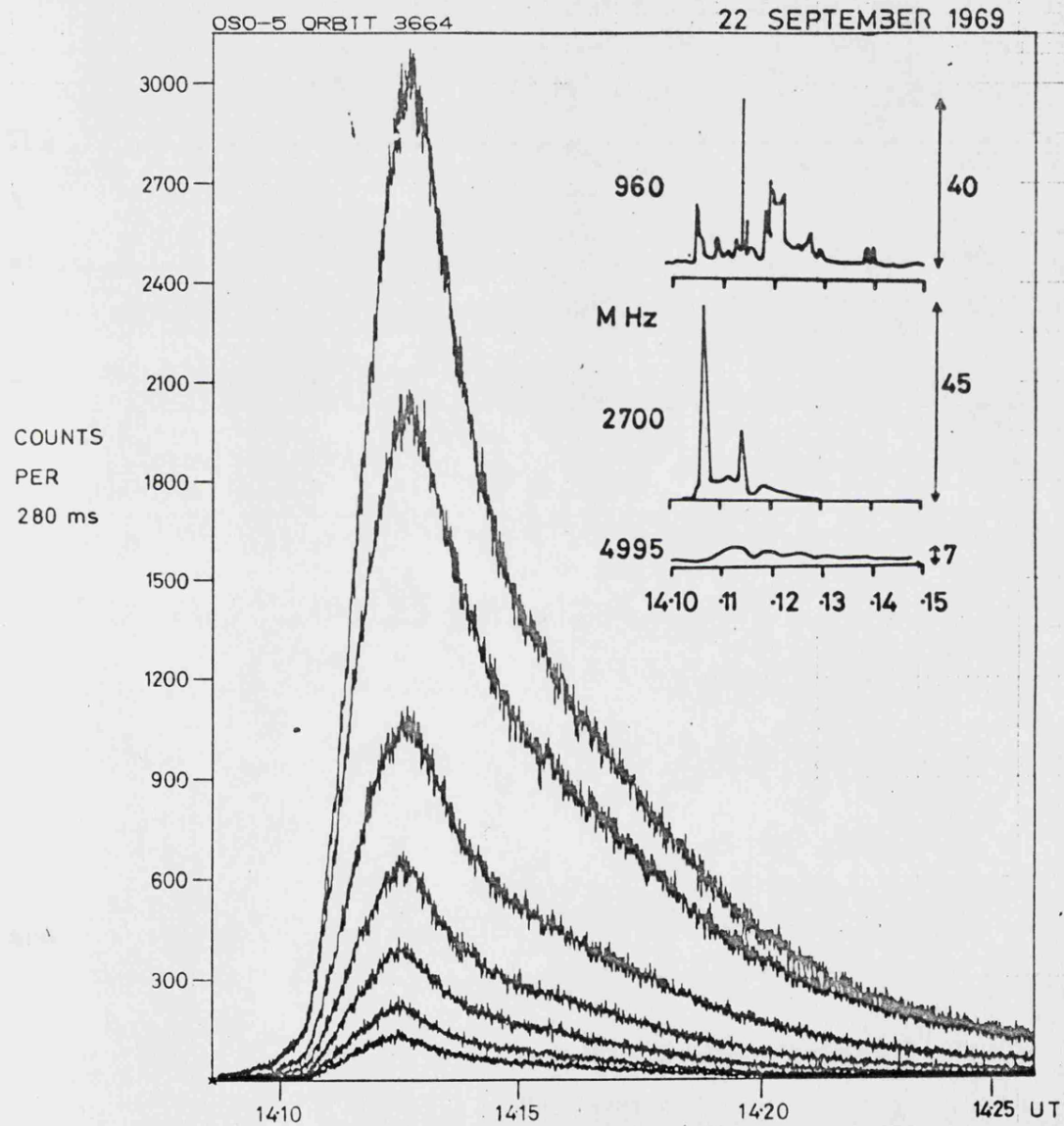


FIG. 6.15 (courtesy J. Parkinson, Leicester U.)



APPENDIX.

Consider a pulse q arriving at a grid of N wires and spreading over $k+1$ wires, each wire $n, n+1, \dots, n+k$ collecting a charge $q_n, q_{n+1}, \dots, q_{n+k}$ where

$$\sum_{i=0}^k q_{n+i} = q$$

The pulse will divide across the condenser network to give a pulse, A and B , at each end, each pulse being the sum of the contributions at A and B from the parts q_{n+i} of the original pulse.

The pulse at A and B due to q_n arriving at wire n will be $q_n \cdot (N-n)/N$ and $q_n \cdot n/N$ respectively, or in general:

$$A = \sum_{i=0}^k q_{n+i} \left[\frac{N - (n+i)}{N} \right]$$

$$B = \sum_{i=0}^k q_{n+i} \cdot \frac{(n+i)}{N}$$

The position pulse $B/(A+B)$ is then;

$$\frac{\sum_{i=0}^k (n+i) \cdot q_{n+i}}{\sum_{i=0}^k (n+i) \cdot q_{n+i} + \sum_{i=0}^k [N - (n+i)] \cdot q_{n+i}}$$

and since $\sum_{i=0}^k q_{n+i} = q$ then

$$\frac{B}{A+B} = \frac{\sum_{i=0}^k (n+i) \cdot q_{n+i}}{Nq}$$

This expression for the position pulse is of a similar form to that obtained as a solution for the centre of gravity of a number of discrete masses. Thus the position pulse represents the centre of gravity of the charges arriving at the separate wires, that is, the point on the array at which the pulse originated.

REFERENCES.

- Abraham, J.M., Catchpole, C.E. and Goodrich, G.W. (1967). 12th S.P. I.E. Technical Symposium.
- Adams, J. and Manley, B.W. (1965). I.E.E.E. Trans. NS-13,3, 88-89.
- Aitken, D.W. (1968). I.E.E.E. Trans. NS-15, June, 10-46.
- Alkhazov, G.D., Komar, A.P. and Vorob'ev, A.A. (1967). Nucl. Instr. and Meth. 48, 1-12.
- Anderton, H. (1966). advances in electronics and electron physics, 22B, 919-925.
- Armantrout, G.A. (1966). I.E.E.E. Trans. NS-13, 328.
- Atkinson, P.A. and Pounds, K.A. (1964). J. Phot. Sci. 12, 302.
- Ballas, J., Knapp, G., Wiza, J. and Zehnpfennig, T. (1968). I.E.E.E. Trans. NS-15, 551-555.
- Batstone, R.M., Evans, K., Parkinson, J.H. and Pounds, K.A. (1970). Preprint of a paper submitted to Solar Physics.
- Beyer, R.R., Green, M. and Goetze, G.W. (1966). Advances in electronics and electron physics. 22A, 251-60.
- Blake, R.L., Kunkel, W., Hiltner, W.A., Lynga, G., Bradt, H., Clark, G., Naranan, S Rappaport, S., and Spada, G. (1968). Astrophys. J. 152, 1015.
- Boksenberg, A., Boyd, R.L.F. and Jones, J.C. (1968a). Nature, 220, 556.
- Boksenberg, A. and Newton, A.C. (1968b). Adv. in elec. and elec. phys. 28A, 297
- Borkowski, C.J. and Kopp, M.K. (1968). Rev. Sci. Instr. 39, 1515-22.
- Borkowski, C.J. and Kopp, M.K. (1970). Paper read at I.E.E.E. Symposium no. 12, March 1970.
- Bowyer, C.S., Byram, E.T., Chubb, T.A. and Friedman, H. (1964). Science 146, 912.
- Bowyer, C.S., Field, G.B. and Mack, J.E. (1968) Nature 217, 32.
- Boyd, R.L.F. (1969). Proc. Roy. Soc. A. 313, 381-93.

- Braid, T.H., Rush, C.J., Lieb, R.J., Himes, J. and Becker, J. (1970).
Paper read at I.E.E.E. symposium no. 12 March 1970.
- Brown, W.L., Buck, T.M., Gibson, W.M., Kerr, R.W. and Lie, N.P. (1970).
Paper read at I.E.E.E. symposium no. 12 March 1970.
- Bryant, D.A., and Johnstone, A.D. (1965). Rev.Sci.Instr.36,1662.
- Burbidge, G. (1969). Proc.Roy.Soc.A.313,331-48.
- Burnight, T.R. (1949). Phys.Rev.76,165.
- Burrous, C.N., Lieber, A.J. and Zaviantseff, V.T. (1967).
Rev.Sci.Instr.38,1477.
- Byrne, J. (1962). Proc.Roy.Soc.Ed.66A,33-51.
- Caruso, A.J. (1968). Rev.Sci.Instr.39,1059.
- Charpak, G. and Renard, G.A. (1956). J.Phys.Radium 17,585.
- Charpak, G., Bouclier, R., Bressani, T., Favier, J. and Zupancic, C.
(1968). Nucl.Instr. and Meth.62,262-268.
- Charpak, G., Bouclier, R., Bressani, T., Favier, J. and Zupancic, C.
(1968). Nucl.Instr. and Meth.65,217-20.
- Charles, M.W. (1968). Thesis, Leicester University.
- Charles, M.W. and Cooke, B.A. (1968). Nucl.Instr. and Meth.61.31.
- Chevalier, P. and Nussli, J. (1967). Comptes Rendus.B,264,462-6.
- Chevalier, P. (1967). Nucl.Instr.and Meth.50,346-8.
- Conde, C.A.N., Policarpo, A.J.P.L. and Alves, M.A.F. (1968).
I.E.E.E. Trans. N.S.15,84-94.
- Cooke, B.A. and Stewardson, E.A. (1964). Brit.J.Appl.Phys.
15,1315-19.
- Cooke, B.A., Griffiths, R.E. and Pounds, K.A. (1969). Nature
224,5215,134-7.
- Culhane, J.L., Sanford, P.W., Shaw, M.L., Phillips, K.J.H., Willmore, A.P.,
Bowen, P.J., Pounds, K.A., and Smith, D.G. (1969). Mon.
Not.R.Astr.Soc.145,435.

- Dodge, W.R., Coleman, J.A., Domen, S.R. and Whittaker, J.K. (1966).
Rev.Sci.Instr.37,1151.
- Egidi, A., Marconero, R., Pizzella, G. and Sperli, F. (1969). Rev.Sci.
Instr.40,88.
- Eiben, B., Faissner, H., Holder, M., Konig, J., Krisor, K., and Umbach, H.
(1969). Nucl.Instr. and Meth.73,83-88.
- Epple, E., Decker, D. and Hornung, F. (1967). Phys. Letters.
25A,391.
- Evans, D.S. (1965). I.E.E.E. Trans, N.S.-12,34-8
- Friedman, H. (1969). Proc.Roy.Soc.A.313,301-15.
- Fritz, G., Meekins, J.F., Henry, R.C., Byram, E.T. and Friedman, H. (1968).
Astrophys.J.Lett.153,1199.
- Giacconi, R. and Rossi, B. (1960). J.Geophys.Res.65,773.
- Giacconi, R., Gursky, H., Paolini, F.R., Rossi, B.B. (1962). Phys.Rev.
Letters.9,11,439-43.
- Giacconi, R., Pounds, K.A. and Clark, G.W. (1968). Proposal sub-
mitted to N.A.S.A. for second solar A.T.M.
- Giacconi, R., Reidy, W.P., Vaiana, G.S., Van Speybroeck, L.P., and
Zehnfennig, T.F. (1969). Space Science Reviews.3.57.
- Gibbons, P.E. (1968). U.K.A.E.A. internal report no.A.E.R.E.
M2025.
- Gorenstein, P. and Mickrewicz, S., (1968). Rev.Sci.Instr.39,816.
- Gott, R. and Charles, M.W. (1969). Nucl.Instr. and Meth.72,157.
- Griffiths, R.E. (1970). Leicester University - Private
communication.
- Guest, A., Holmshaw, R.T. and Manley, B.W. (1969). Mullard Tech.
Communications 10,97,210.
- Guest, A. (1970). Private Communication.

- Gursky, H., Giacconi, R., Gorenstein, P., Waters, J. R., Oda, M., Bradt, G.,
Garmire, G. and Sreekantan, B. V. (1966). Astro. Phys.
J. 144, 1249.
- Gursky, H. and Zehnpfennig, T. (1966). Appl. Opt. 5, 875.
- Haitz, R. H. and Smitz, F. M. I. E. E. E. Trans. N. S. - 13, 198.
- Henry, R. C., Fritz, G., Meekins, J. F., Friedman, H. and Byram, E. T. (1968).
Astro. Phys. J. 153, L11.
- Hofker, W. K., Oosthoek, D. P., Hoeberechts, A. M. E., van Dantzig, R., Mulder, K.
Oberski, J. E. J., Koerts, L. A., Dieperink, J. N. Kok, E. and
Rumphorst, R. F. (1966). I. E. E. E. Trans. N. S. no. 3, 208.
- Huth, G. C. Trice, J. B., and McKinney, R. A. (1964). Rev. Sci. Instr.
35, 1220.
- Huth, G. C. Trice, J. B., Shannon, J. A. and McKinney, R. A. (1965).
I. E. E. E. Trans. N. S. - 12 no. 1, 275.
- Huth, G. C. (1966). I. E. E. E. Trans. N. S. - 13 no. 1, 36.
- Kantor, F. W. (1968). Paper presented at the New York Academy
of Sciences, May, 1968.
- Koester, L. J. (1970). Paper read at I. E. E. E. symposium no. 12.
March 1970.
- Kuhlmann, W. R., Lauterjung, K. H. and Schimmer, B. (1966). Nucl.
Instr. and Meth. 40, 109-12.
- Kuhlmann, W. R., Lauterjung, K. H., Schimmer, B. and Sistemich, K. (1966).
Nucl. Instr. and Meth. 40, 118 - 20.
- Laegsaard, E., Martin, F. W. and Gibson, W. M. (1967). Nucl. Instr.
and Meth. 60, 24 - 26.
- Lansiart, A. and Leloup, J. (1963). Compte rendu du Colloque
International sur l'Electronique Nucleaire. Paris. 1963.
- Lansiart, A., Morucci, J. P., Roux, G., and Leloup, J. (1966). Nucl.
Instr. and Meth. 44, 45.

- Livingston, W.C. (1963). Advances in Electronics and Electron
Physics p.1967.
- Lubirskii, A.P., Rumsh, M.A. and Smirnov, L.A. (1960). Optics
and Spectroscopy 9, 265-7.
- Lubirskii, A.P., Brytov, I.A. and Zimkina, T.M. (1964). Optics
and Spectroscopy 17, 234-7.
- Madden, T.C., Merz, J.L., Miller, G.L. and Thomas, D.G. (1968).
I.E.E.E. Trans. N.S. - 15, 47.
- Mathieson, E. and Sanford, P.W. (1963). Proc. Int. Symp. on
Nuclear Electronics, Paris.
- Matsuoka, M. (1966). Jap. J. Appl. Phys. 5, 671-88.
- McCann, M.F. and Smith, K.M. (1968). Nucl. Instr. And Meth. 65,
173-7.
- McDicken, W.N. (1967). Nucl Instr. and Meth. 54, 157.
- Melhorn, W. and Albridge, R.G. (1964). Nucl. Instr. and Meth.
26, 37-41.
- Melton, C.E., Hurst, G.S., Bortner, T.E. (1954). Phys. Rev. 96, 3, 643-5.
- Negus, C.R., Glencross, W.M. and Pounds, K.A. (1970). Preprint.
- Nunemaker, T.A. and Neumann, M.J. (1970). Paper read at I.E.E.E.
symposium no. 12 March 1970.
- Oda, M. (1965). Appl. Opt. 4, 143.
- Oda, M., Bradt, H., Garmire, G., Spada, G., Sreekantan, B.V., Gursky, H.,
Giacconi, R., Gorenstein, P., and Waters, J.R. (1967).
Astr. Phys. J. 148, L5.
- Oda, M. (1968), Space Science Rev. 8, 507.
- Ogawa, I. (1967). Nucl. Instr. and Meth. 49, 325.
- Policarpo, A.J.P.L., Alves, M.A.F. and Conde, C.A.N. (1967). Nucl.
Instr. and Meth. 55, 105.

- Policarpo, A.J.P.L. (1969). Nucl.Instr. and Meth. 77,309-14.
- Paolini, F.R., Giacconi, R., Manley, O., Reidy, W.P., Vaiana, G.S., and
Zehnpfennig, T. (1968). Meeting of A.A.S. on Solar
Astronomy, Tucson, Feb. 1968.
- Patla, N. and Kiss, A.E. (1965). Brit.J.Appl.Phys. 16, 1871.
- Pounds, K.A. (1969). Proc.Roy.Soc. 313, 367-380.
- Pounds, K.A. (1969, a). Paper read at I.A.G.A. symposium on
Aeronomic Ionisation Processes, Sept. 1969.
- Pounds, K.A. (1970). Discussion meeting on Solar Physics at
the Royal Society, April 1970.
- Ricker, G.R. and Gomes, J.J. (1969). Rev.Sci.Instr. 40, 227.
- Roux, G., Gaucher, J.C., Leloup, J., Morucci, J.P. and Lansart, A.
(1968). I.E.E.E. Trans. N.S. 15, 67.
- Ruegg, H.W. (1967). I.E.E.E. Trans. ED. 14 No. 5, 239.
- Rumsh, M.A., Lukirskii, A.P., Karpovich, I.A. and Schemelelev, V.N.
(1960). Instr.Exp.Tech. 5, 755-61.
- Russell, P.C. (1965). Nature 205, 4972.
- Russell, P.C. and Pounds, K.A. (1966). Nature 209, 5022, 490.
- Sartori, L. and Morrison, P. (1967). Astrophys.J. 150, 385.
- Saunders, E.W. and Maxwell, C.J. (1968). I.E.E.E. Trans. N.S. - 15
423.
- Schmidt, K.C. and Hendee, C.F. (1966). I.E.E.E. Trans. N.S. - 13.
3, 100 - 111.
- Schumacher, B.W. and Grodski, J.J. (1965). Brit.Pat.No. 945.
- Sciama, D.W. (1969). Proc.Roy.Soc.A. 313, 349-55.
- Seward, F., Chodil, G., Mark, H., Swift, C. and Toor, A. (1967).
Astrophys.J. 150, 845.
- Shivanandan, K., Hauck, J.R. and Harwitt, M.O. (1968). phys.Rev.
Lett. 21, 1460.
- Sinha, B.K. (1968). Nucl.Instr. and Meth. 64, 107.

- Skelton, R.D. and DeLoach, A.C. (1967). N.A.S.A. Report. T.M.
X - 5366.
- Smith, D.G. (1967). J.Sci.Instr. 44, 12, 1053-5.
- Smith, D.G. (1968). Thesis, Leicester University.
- Smith, D.G. and Pounds, K.A. (1968). I.E.E.E. Trans. N.S. - 16,
541.
- Somer, T.A. and Graves, P.W. (1969). I.E.E.E. Trans. N.S. - 16
no. 1. 376.
- Tatry, B. Bosqued, J.M. and Reme, H. (1969). Nucl. Instr. And Meth.
69, 254.
- Timothy, A.F. and Timothy, J.G. (1969). J.Sci.Instr. 2, 2, 825.
- Turner, P.J., Cartwright, P., Southon, M.J. van Oostrom, A. and Manly, B.W.
(1969). J.Sci.Instr. 2, 2, 731.
- Underwood, J.H. and Muney, W.S. (1967). Solar Physics. 1, 129.
- Underwood, J.H. (1968). Science, 159, 3813.
- Vaiana, G.S., Reidy, W.P., Zehnpfennig, T., van Speybroeck, L. and Giacconi
R. (1968). Science 161, 564.
- Walter, F.J. (1970). Paper read at I.E.E.E. symposium no. 12
March 1970.
- Waters, J.R. (1964). Nucl. Instr. and Meth. 30, 336-40.
- Wiley, W.C. and Hendee, C.F. (1962). I.R.E. Trans. N.S. -9, 103.
- Wiza, J. (1969). Private Communication.
- Zehnpfennig, T. (1966). Appl. Opt. 5, 1855.